UNIVERSITY OF SOUTHAMPTON

FACULTY OF ENGINEERING AND THE ENVIRONMENT

Civil and Environmental Engineering

Experimental analysis of the influence of proximity to channel boundaries and blockage ratio on far field hydrodynamic effects and performance of rows of tidal turbines

Tim Daly

Supervisors: Dr. Luke Myers and Prof. AbuBakr Bahaj

Thesis for the degree of Doctor of Philosophy in Civil Engineering

March 2015

UNIVERSITY OF SOUTHAMPTON

ABSTRACT

Tidal energy is now the subject of an extensive amount of research. Several studies have demonstrated the significant potential contribution to low carbon electricity production which the tides are capable of. An inevitable transition in this technology is from single turbines to groups of turbines in suitable channels. This is necessary to help reduce the cost of generation, which are still considerably higher than established renewable technologies such as wind power, and also more conventional power generation sources such as coal. However much is still to be learned about the effects tidal technology have on their surrounding flow environment. Changing the specific position of a row of turbines with respect to flow boundaries and the level of blockage of a channel are two particular areas where large gaps in current knowledge have been identified.

This work outlines the results of research carried out with the aim of filling some of these gaps in the knowledge. Experimental methods have been used to examine both the flow field and non-dimensional performance of tidal turbines when proximity to flow boundaries and blockage ratios are altered. Specific flow effects which have been examined include changes to the wake region of tidal turbine rows, the constraining of flow in certain localized regions of the flow domain and changes to volumetric flow rate distribution in split tidal channels.

Results have demonstrated that changes to both the position and blockage ratio of a tidal turbine row in an open channel can cause considerable changes. Locating rows of turbines closer to flow boundaries, and increasing blockage ratio, results in increases to wake velocity deficit and turbulence intensity, and a simultaneous decrease in Reynolds shear stresses. In split tidal channels, it has been shown that locating towards the rear of a split in the direction of flow reduces the volumetric flow through impeded sub channels. This is significant in the context of previous research which has shown the imbalance in volumetric flow rate between sub channels to be directly related to the maximum extractable power of such channels. It is expected that the results of this research will ensure that tidal developers can make more informed choices when examining the optimum size and position of tidal turbine rows in any future tidal energy projects.

FACULTY OF ENGINEERING AND THE ENVIRONMENT

Civil and Environmental Engineering

Doctor of Philosophy

EXPERIMENTAL ANALYSIS OF THE INFLUENCE OF PROXIMITY TO CHANNEL BOUNDARIES AND BLOCKAGE RATIO ON FAR FIELD HYDRODYNAMIC EFFECTS AND PERFORMANCE OF ROWS OF TIDAL TURBINES

By Tim Daly

Nomenclature

ABBREVIATIONS

ADCP	Acoustic Doppler Current Profiler
ADV	Acoustic Doppler Velocimeter
EDF	Électricité de France
EU	European Union
GW	Gigawatts
KW	Kilowatts
LDV	Laser Doppler Velocimeter
MW	Megawatts
RANS	Reynolds Averaged Navier Stokes
SNR	Signal to Noise Ratio
TW	Terawatts

CAPITAL SYMBOLS

A	Area (m^2)
B	Channel width (m)
C_z	Chezy friction coefficient ($m^{\frac{1}{2}}/s$)
C_d	Drag coefficient
D_c	Critical depth (m)
E	Specific Energy (m)
Fr	Froude number
L	Length (m)
M	Number of rows of turbines

N	Total number of data points
P_{er}	Wetted perimeter (m)
P	Power (watts)
Q	Volumetric flow rate (m^3/s)
Re	Reynolds number
RE	Electrical Resistance (Ohms)
R	Hydraulic radius (m)
S_f	Friction slope
S	Fractional change in volumetric flow rate
TI	Turbulence intensity
$U_{deficit}$	Velocity deficit
U	Flow velocity magnitude in x direction(m/s)
VI	Voltage (V)
V	Flow velocity magnitude in y direction(m/s)
W	Flow velocity magnitude in z direction(m/s)
X	Number of units along x axis
Y	Number of units along y axis
ZI	Impedance (ohms)
Z	Number of units along z axis

GREEK SYMBOLS

η	Turbine extraction efficiency
ω	Angular frequency (rad/s)
ρ	Density (kg/m^3)
σ	Standard deviation
ζ	Extraction efficiency
α	Energy coefficient
ϵ	Blockage ratio
$\triangle\iota$	Change in water surface elevation (m)

λ	Friction
μ	Dynamic Viscosity (kg /ms)
ν	Kinematic viscosity (m^2/s)
ψ	Phase of water level difference
ψ	Viscous Shear stress (N/m^2)
τ	Shear stress (N/m^2)
Θ	Angle (radians)
φ	Reynolds Shear stress (N/m^2)
ϑ	Ratio of wake to upstream undisturbed velocity

LOWER CASE SYMBOLS

b	Coefficient of linear fit
d	Turbine diameter (m)
f	Botton roughness coefficient
g	Acceleration due to gravity (m/s^2)
h	Head (m)
k	Resistance coefficient
l	Characteristic length (m)
$\dot{m}$	Mass flow rate (kg/s)
m	Coefficient of linear fit
n	Mannings coefficient ($s/m^{\frac{1}{3}}$)
p	Pressure (N/m^2)
q	Head loss coefficient
rd	Background frictional drag (N)
r	Fraction of overall volumetric flow
s	Inter device spacing (m)
s	Tidal amplitude (m)
t	time (s)
u'	Fluctuation from mean velocity in x direction (m/s)

v'	Fluctuation from mean velocity in y direction (m/s)
w'	Fluctuation from mean velocity in z direction (m/s)

SUBSCRIPTS

D	Downstream value
en	Channel entrance
ex	Channel exit
f	free channel value
I	Impeded channel
tide	Associated with tide across entire channel
t	Associated with turbine
u	Upstream value
∞	Natural Freestream value

Contents

List of Figures

List of Tables

Declaration of authorship

I, Tim Daly, declare that the thesis entitled

"Experimental analysis of the influence of proximity to channel boundaries and blockage ratio on far field hydrodynamic effects and performance of tidal turbine rows"

and the work presented in this thesis are both my own, and have been generated by me as the result of my own original research. I can confirm that:

- This work was doing wholly while in candidature for a research degree at this University.
- Where any part of this thesis has previously been submitted for a degree or any other qualification at this University or any other institution, this has been clearly stated.
- Where I have consulted the published work of others, this is always clearly attributed.
- Where I have quoted from the work of others, the source is always given. With the exception of such quotations, this thesis is entirely my own work.
- I have acknowledged all main sources of help.
- Where the thesis is based on work done by myself jointly with others, I have made clear exactly what was done by others and what I have contributed myself.
- Parts of this work has been published previously as in the following publications:

T. Daly, L.E. Myers, and A.S. Bahaj. Experimental analysis of the local flow effects around single row tidal turbine rows. In International Conference on Ocean Energy, Bilbao, Spain, 6th - 8th October 2010.

T. Daly, L.E. Myers, and A.S. Bahaj. Numerical analysis of the acceleration and wake effects resulting from changes in tidal turbine row position in a channel. In European Wave and Tidal Energy Conference, Southampton, UK, 5th - 9th September 2011a.

T. Daly, L.E. Myers, and A.S. Bahaj. Experimental investigation of the effects of the presence and operation of tidal turbine rows in a split tidal channel. In World Renewable Energy Congress, Linkoping, Sweden., 8th - 13th May 2011b.

T. Daly, L.E. Myers, and A.S. Bahaj. Modelling of the flow field surrounding tidal turbine rows for varying positions in a channel. Philosophical transactions of the Royal Society A: Mathematical, Physical and Engineering Sciences, 371 (1985):118, 2013.

Signed:.....Date: .....

Acknowledgements

First of all I would like to thank both my supervisors Dr. Luke Myers and Prof. AbuBakr Bahaj, who have both demonstrated outstanding professional support and technical expertise throughout this entire process. Despite their very busy schedules, both Dr. Myers and Prof. Bahaj have always given outstanding guidance on the direction of my research and its final contents, and for this I am extremely grateful.

I would also like to thank my many colleagues in the Faculty of Engineering and Environment, who have also been of great support from both a professional and personal perspective. A particular mention should go to Dr. Matt Harrison for his assistance with Matlab and CFD, Nick Linton for his assistance with sourcing material for experimental equipment, and to Bradley Keogh and Khilan Shah for their assistance with experimental work in the Chilworth hydraulics laboratory.

I would like to thank Ms. Fleur Loveridge, a fellow PhD researcher in the Faculty of Engineering and the Environment. Ms. Loveridge has used her status as a chartered civil engineer to help me in fulfilling and signing off on the development objectives required for chartership with the Institution of Civil Engineers. This assistance has greatly aided my professional development and is greatly appreciated.

I would like to thank Ms. Sheila Stickland, personal assistant to Professor AbuBakr Bahaj. Throughout my studies she has given me great support in organising travel to conferences and many other administration tasks. Her assistance in this is acknowledged and greatly appreciated.

I would like to thank the technical staff in the Faculty of Engineering and Environment for their help and support throughout the project. A particular mention should go to Mike Rose, Dave Lynock and Rhys Jenkins for their help with training on workshop facilities, Earl Peters and Mike Street for their help with machining, and Karl Scammell for all his assistance with the use of the Chilworth hydraulics laboratory.

I would like to thank all the members of Southampton University Hillwalking Club for giving me a great distraction from PhD study and some very fond and happy memories over the last three years. A particular heartfelt thanks should go to those I served on committee with, such as Jennifer Warhurst, Alex Robinson, Rachael Evans, Josh Price, Chris Wood and Danielle Waters. Many thanks to you all and best of luck for the future.

Last but by no means least, I would like to thank all my family for their love and support, without which I would not have been able to get through some really tough days. To my sister Irene, her husband and daughter Lee and Virginia, my brother Aidan and his wife Siobhan and to my father and his partner Josephine, I say thanks ever so much for all your

previous and continued love and support.

Chapter 1

Introduction

1.1 Tidal energy and its potential

The renewable energy industry has grown significantly in the past decade due to a number of factors. Among these are the volatility of prices of conventional fossil fuels such as crude oil and gas. The price fluctuations are largely driven by higher demand in emerging economies, seasonal variations throughout the year, and concerns over political instability and potential military conflicts in oil producing nations. Another major driver is the knowledge of the harmful effects on the environment and future generations of the greenhouse gas emissions which accompany the use of fossil fuels. These issues have led to the implementation of policies which strongly encourage the development clean and sustainable energy sources. From a European perspective, arguably the most important of these is the EU renewables directive. This requires all EU member states to source 20% of all their energy requirements from renewable sources by the year 2020 (European Renewable Energy Council 2008). Some of the more established technologies providing Europe with renewable energy at present include hydroelectricity, wind energy and solar PV. Hydroelectricity has been used since as far back as the early part of the 20th century, although the number of new installations in recent times has been limited by concerns over environmental effects. Wind energy, both onshore and offshore, has seen major growth in the past decade, which is set to continue in the coming years. According to Renewable UK, offshore wind alone currently has 3.8GW of capacity under construction in the UK, with a further 7.8GW in the planning stages. According to the UK government, solar PV experienced a five and a half fold increase in installed capacity to 1.4GW in the 12 month period to June 2012, largely driven by falling material and component costs. However both of these technologies are not without their challenges. Wind energy is a relatively intermittent and unpredictable source of energy, and many wind farm developments are the subject of major public opposition due to the associated visual impact. Solar PV is also intermittent and unpredictable, and much research is still being carried out to improve the efficiency of solar PV devices and to allow the use of cheaper materials. Therefore it is clear that no single technology can be relied on to provide all of the energy required from renewable sources, and that a large mix of sources is required. For the UK government, tidal stream energy represents one of the greatest potential energy sources which will help contribute to this mix.

Tidal stream energy involves harnessing the kinetic energy available in tidal flows to generate electricity. This immediately gives tidal energy a distinct advantage over other renewable sources such as wind. The tides of the earth are driven by the gravitational pull of the moon and the sun on the earth. This means tidal is a much more predictable resource than other forms of renewable energy such as solar and wind. Tidal stream differs greatly from barrage schemes which require the construction of a large dam which alters the natural environment and can cause detrimental environmental effects. Some other advantages of tidal stream include the similarity of technology to wind turbines, and the less obvious visual impact on the natural landscape. The exact potential power available has been the subject of numerous studies over the past 15 to 20 years. An assessment by Black and Veatch [2005] estimated a UK power potential of 18Twh/yr, or approximately 5% of total UK electricity demand in 2005. However much of the assumptions and methods used in this analysis have since been disputed. Iyer et al. [2009] cites other conflicting estimates from other authors, such as 96TWh/yr by MacKay [2008] and 25TWh/yr for Scotland alone by Snodin [2001].

Tidal turbine technology itself has been the subject of much prototype and laboratory scale testing over the last decade. It was only in 2008 that the world's first commercially operating turbine was installed and connected into the electrical grid. This project was carried out by the Bristol based company Marine Current Turbines Ltd, in Strangford Lough in Northern Ireland. Since then numerous more tidal developers have emerged in the UK and worldwide, and several tidal energy projects are planned for the remainder of this decade. Similarly like wind energy before it, the next major development in tidal turbine technology is undoubtedly going to be the installation of multiple devices in tidal arrays or farms.

1.2 Considerations when examining potential tidal sites

1.2.1 Flow velocity in tidal sites

A number of sites worldwide have been identified as having the potential for tidal turbines to generate considerable amounts of useable electricity for local and national grids. While a number of parameters need to be taken into account when examining tidal site potential, the first consideration is undoubtedly both spring and neap tide flow velocities in these sites. This is due to the cubic relationship between power and flow velocity associated with turbines. For any turbine of any given sized rotor area, the kinetic energy flux is given by:

$$P = \frac{1}{2}\rho U^3 \tag{1.1}$$

The values for minimum velocities required in tidal sites are not universally agreed upon, and will be dependent on specific device design. However some observers claim that commercially viable tidal power installations require spring tide flow velocities of at least 2.5m/s (Ireland [2006]). One of the earliest studies on the available UK tidal energy resource was by Black and Veatch (2005). Of the sites identified in this study, the vast majority were estimated to have mean spring peak velocity of between 1.5 and 2.5 m/s. Some notables exceptions included:

- The Pentland Firth in Scotland, which had flow velocities of between 3.5m/s and 5.5m/s, and even exceeding 5.5m/s, in certain areas.
- The Severn estuary, with flow velocities between 2.5m/s and 3.5m/s.
- Areas around the Isle of Wight with flow velocities between 2.5m/s and 3.5m/s.
- Areas around some of the Channel Islands such as Guernsey and Sark, with flow velocities between 2.5m/s and 3.5m/s.

Outside of the UK, one of the most promising tidal energy sites is the Bay of Fundy in Canada. This site has specific locations where tidal current flow velocity exceeds 5m/s (Hasegawa et al. [2011]), and is currently the subject of extensive research in both academia and industry.

It is very clear from the aforementioned studies that the power performance of tidal turbines, and hence commercial viability of tidal installations, is highly dependent on flow

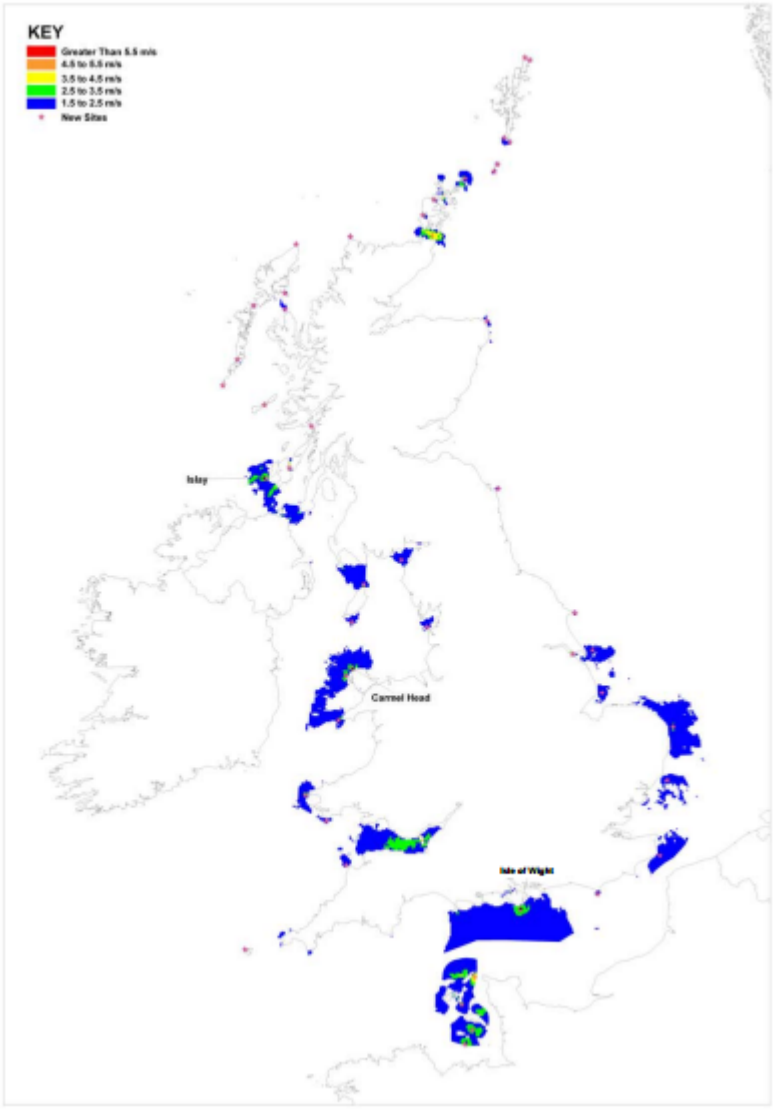

Figure 1.1: UK tidal stream mean spring peak velocities as identified by Black and Veatch [2005]

velocity throughout the tidal cycle. This high dependence on flow velocity has also prompted a large amount of research to be carried out on the effect of the installation of tidal turbines on the surrounding flow regime. Where multiple installations in a given flow domain are proposed, the extraction of power by one installation influences the far field flow domain dynamics, thereby directly affecting the performance of other installations and hence the overall commercial viability of any tidal project. However, the implications of far field flow domain changes associated with tidal power extraction are not confined to the performance of other installations. A number of natural processes, such as sediment transport and fish migration, are also likely to be affected by changes to the flow regime. It is for these reasons that tidal turbine installations require an extensive environmental impact assessment before approval by relevant authorities. Flow changes are also likely to have impacts on shipping activities in the areas surrounding proposed sites. These shipping activities can be of critical importance in the local economies of some isolated areas. Hence the socio-economic impacts of tidal installations and the changes to the surrounding natural environment are also considered before planning approval.

1.2.2 Depth and blockage

Another natural characteristic of tidal channels which is examined in resource assessment studies is the flow depth. This is because flow depth directly affects the size of the turbines themselves which can be installed in any site. As well the cubic relationship with flow velocity, there is also a directly proportional relationship between power and tidal turbine rotor area. As with flow velocity, there is no universally agreed minimum depth required for a tidal site. But it is worth noting that, in the aforementioned Black and Veatch study, many of the sites around the UK identified as most promising had average flow depth of between 25m and 40m. Flow depth is also important for tidal developers as it can impact on the following factors:

- Due to hydrostatic pressure, the flow depth will directly impact on the required strength of tidal turbine support structures as well as the rotors themselves.
- Flow depth will have implications for the installation of the device at the start of its life. Deeper sites are likely to represent a more challenging and expensive installation process, thus directly affecting the viability of any installation.
- Flow depth may also affect maintenance procedures. Some turbines, such as the Hammerfest Strom installation, require divers to carry out regular maintenance. A deeper site will undoubtedly present a more challenging procedure for maintenance personnel. Other systems where a turbine is lifted out of water for maintenance, such as the marine current turbines seagen installation, will have to design their lifting mechanism in accordance with the depth of the channel in which it is installed.

As will be demonstrated later in the literature review, the different flow effects associated with installing at different flow depths is now being examined by many scientific studies.

Depth of a tidal site is also an important consideration as it can directly affect the lateral and vertical blockage of a turbine or row of turbines. If developers decide that a certain

amount of turbines need to be installed to ensure commercial viability of a project, the extent to which these turbines block a channel laterally and vertically will be fixed. Both lateral and vertical blockage are two parameters which can have a direct effect on the flow regime, with the consequent results outlined in the previous section. Shipping is also not only affected by the flow effects associated with different blockages, but also simply by the space occupied by turbines in a given channel. Tidal turbines could restrict the physical space available for ships to pass through in a bounded channel, thereby having a direct effect on local industries with specific shipping requirements.

1.2.3 Position of turbines with respect to shorelines

Another major consideration in any tidal turbine installation is the distance of the proposed site from the nearest point where electricity generated can be placed directly into the electricity grid. This is said to be one major drawback of many proposed tidal energy sites, such as the Pentland Firth in Scotland. The offshore distance of the power generation point means underwater cables are required to transfer the electricity to the onshore grid. As well as adding extra cost to installation, these cables are also responsible for power losses, with longer cables resulting in larger energy losses. The ideal situation therefore is for these cables to be as short as possible, and hence for tidal turbines to be installed as close as possible to the electricity plug in point.

Onshore sediment processes are also likely to be affected by the positioning of tidal turbines. The movement of sediment onshore, and hence the formation and structure of beaches and shorelines, is affected directly by the water flow out at sea. Therefore any changes to the overall hydrodynamic processes of a tidal site directly associated with tidal power extraction (which in themselves are likely to be directly affected by the distance from the shoreline of installation) will affect the build-up of sediment on the shore, which may in turn affect local wildlife and flora.

1.3 Tidal turbine rows

As tidal turbine technology is in its infancy and operating in a challenging environment, the cost of energy is not yet on par with other renewables. According to Fraenkel [2007], the total capital cost of the aforementioned 1.2MW Seagen turbine was £10 million, representing a capital cost per of £8.3 million per MW installed capacity. This is much greater than offshore wind, with estimates for capital cost ranging from £2.5 million/MW (Stallard et al. [2013]) to £3.7million/MW (Kaiser and Snyder [2012]). This can largely be attributed to the much greater size of offshore wind turbines compared to tidal turbines. While improving the design of individual devices themselves is pivotal in reducing these costs, the installation of multiple devices in farms and arrays is also a major potential contributor. A proposed tidal energy farm in Skerries in North Wales by Marine Current Turbines is planned to have 10MW of installed capacity at a total cost of £70 million. Separately, a proposed 398MW capacity tidal farm in the Pentland Firth in Scotland by the Meygen consortium is targeted to have a final capital cost of approximately £5 million/MW.

Because of these potential cost benefits, tidal turbine rows are now the subject of extensive research. Among the most important and widely examined aspects of these is the influence their presence and operation has on their surrounding flow environment. As they are extracting energy from moving water, the flow regime in any given tidal site will be altered as a result. This has implications for tidal farm layout and design in any given site. Also these flow regime changes are likely to effect natural processes such as sediment transport, fish migration and shore erosion. Achieving a balance between achieving a high return on investment and ensuring minimal environmental impacts will be crucial to the success of any tidal farm or array project.

1.4 Aims and objectives

Following review of published literature to date, a number of gaps in the knowledge of tidal turbine rows have been identified. The scope of this research has been determined on the basis of this review and with the aim of filling these gaps. The overall aim of the research is to establish the influence on loading and downstream velocity field of the location and geometry of a row of tidal turbines located within both open and split tidal energy channels.

The specific objectives of the investigation attempting to achieve this aim are:

1. To develop and characterise a representative channel flow and split channel flow in experimental facilities to represent a tidal stream site.

2. To determine the influence of proximity to a lateral boundary (sidewall) on loading of a porous structure.

3. To determine the influence of proximity to a lateral boundary (sidewall) on the far field flow downstream of this porous structure.

4. To determine the influence of stream-wise proximity to a channel split on the loading of a porous fence.

5. To determine the influence of stream-wise proximity to a channel split on the volumetric flow-rate distribution through a split channel system.

Chapter 2

Literature review

2.1 Analytical models for tidal power extraction

As well as linear momentum theory models, some other models have been proposed for examining the power potential of tidal channels and their effect on the surrounding hydrodynamic environment. Rather than focusing on specific performance of devices as in the previously reviewed models, these studies are more concerned with understanding the nature and extent of the resource available. This has been carried out extensively for normal open channels. More recent studies have also begun to examine more complex split tidal channels, and clearly demonstrated their resource to be quite different in terms of analysing the power available for turbines and the effect of power extracting turbines once they are installed.

2.1.1 Analytical models of open channels.

A study on the hydrodynamic impact of tidal power extraction was detailed by Bryden et al. [2004]. The authors considered a simple tidal channel, of constant width, linking two infinite oceans, shown in figure 2.1. The hypothetical channel dimensions were length 4000m and flow driven by a head difference of 0.4m between inlet and outlet. The inlet head was 40m, thus this 0.4m figure represented a 1% drop across the channel. The authors then also assumed tidal power extraction at a distance of approximately 2000m from the inlet, and developed a model to examine the changes to flow channel properties which occurred as a result. The developed model was based on applying the momentum equation and conservation of mass to a fixed flow rate. The initial 0.4m reduction in water surface elevation was assumed to occur due to energy losses caused by the retarding drag force on the fluid due to shear stress between the bed and sides of the channel. The authors accounted for the process of energy extraction by deriving an additional shear stress term. This additional term was proportional to the magnitude of power extracted and was added to the shear stress due to friction between the water and the boundaries of the channel. The additional shear stress due to power extraction resulted in another sudden reduction in water surface elevation across the plane of extraction. This reduction in water surface elevation resulted in a smaller cross sectional area of flow in the channel downstream of the plane of extraction (Figure 2.3). Due to the continuity principle and conservation of mass, this led to an increase in the average

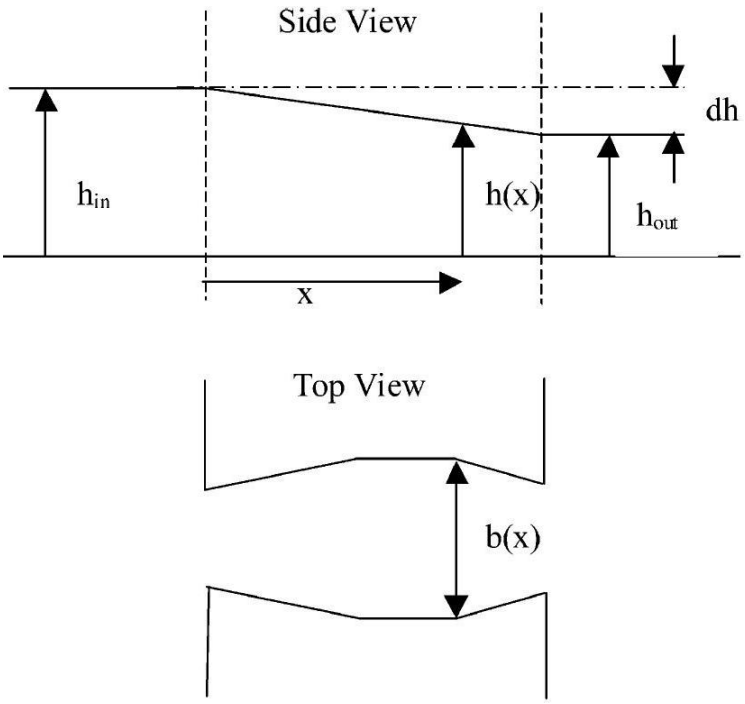

Figure 2.1: Simple tidal channel of constant width examined by Bryden et al. [2004].

flow velocity at any plane downstream of the plane of extraction. The authors assumed two scenarios, extraction of 10% and 20% of the kinetic energy in the channel. Extraction of 10% energy resulted in a 3% increase in average flow velocity downstream, while extraction of 20% led to a 6% increase.

This result is important in the context of the work of this thesis. One of the aims of this research is to examine how changing the position of an array in a tidal channel can constrain the flow in certain regions and cause increases in flow velocity compared to ambient conditions. However the model presented by Bryden et al. [2004] suggests that the process of power extraction itself will lead to increase in flow velocity due to the reduction in water surface elevation associated with extraction. A reduction in water surface elevation will result in a lower cross sectional area of flow downstream, and thus for a fixed volumetric flow rate the velocity must increase. Quantifying the reduction in water surface elevation which occurs during experimental analysis will give some indication of what proportion of the increase in velocity can be attributed to this reduction in water surface elevation. The theoretical explanation for this reduction in water surface elevation is explained in section 2.5.2, while the model of Bryden et al. is presented in section 2.5.7.

Another consequence of the reduction in flow depth is the possibility of altering the fundamental nature of the flow. Open channel flow can be categorised as being either subcritical or supercritical. Subcritical flows are generally deep and slow moving, while supercritical flow are generally fast shallow flows (Hamill [2011, p.248]). As water approaches conditions required for supercritical flow, it will exhibit unsteady water surface profiles, which hold practical difficulties for analysis. A demonstration of the importance of the crossing of this threshold between subcritical and supercritical flow in the context of tidal turbines is shown in Myers and Bahaj [2007]. It was demonstrated for a scaled down tidal turbine that a drop

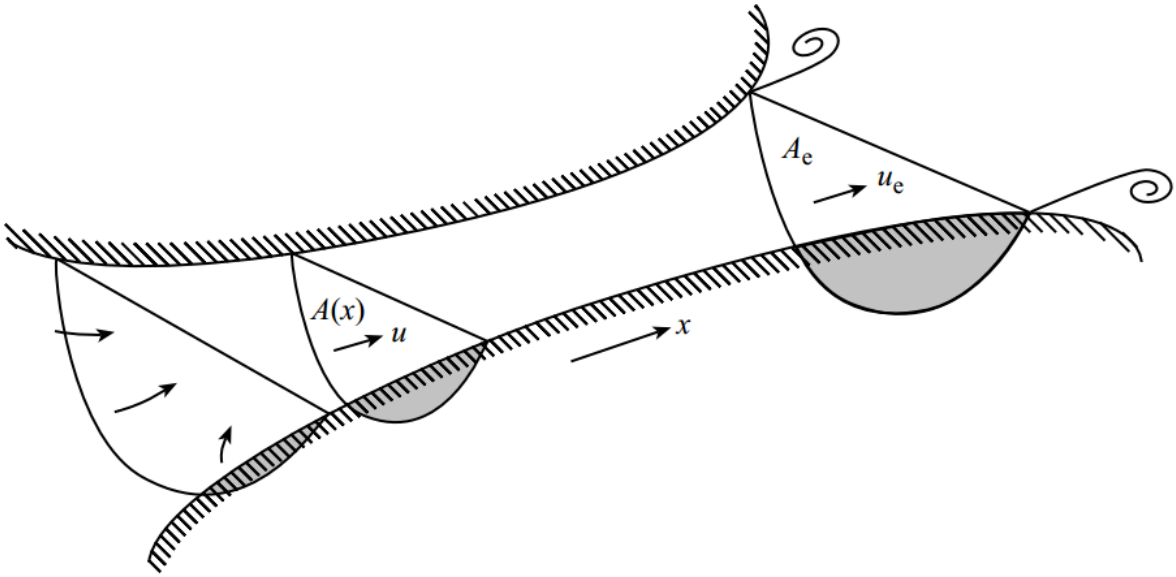

Figure 2.2: Hypothetical channel examined by Garrett and Cummins (2005)

in water surface elevation downstream of the rotor of about 25%. This led to a change to supercritical flow, which in turn led to a major change in the flow regime and a considerable loss in energy. Should the drop in head observed downstream of any actuator fences lead to similar results, the implications for experimental results could be significant. The open channel hydraulics theory referred to here is explained in more depth in section 2.5.6.

One of the main assumptions of the work of Bryden et al. was that kinetic energy flux was the most appropriate measure of maximum power in a channel. A study where authors disputed this and attempted to determine alternative expressions for maximum power potential under different conditions was Garrett and Cummins [2005]. One of the main reasons why the authors disputed the kinetic energy flux method was the assumption of constant cross sectional area in a channel, a condition unlikely to be acceptable in many real tidal channels. The authors also noted a "choking" phenomenon, where too many turbines would cause too much induced drag leading to lower overall power output compared to fewer turbines which do not "choke" the flow. The authors developed theoretical expressions for the maximum power potential, derived from an initial momentum equation, in hypothetical channels with different driving forces and varying channel cross sections. The channel which the authors consider was assumed to be a constricted channel between two water bodies, where currents through the channel did not affect the tides on either end of the channel. This is shown in figure 2.2. Another assumption made by the authors was that the tidal fence in the channel occupies the entire cross section, and hence frictional effects of turbines are independent of lateral position.

The authors initially presented the dynamical momentum equation for the channel, and assumed the channel is short compared to the tidal wavelength. This momentum equation was then given by:

$$c\frac{dQ}{dt} - g\zeta_o = -\int_0^L F dx - \frac{1}{2}U_e|U_e| \tag{2.1}$$

Where:

- c was the integral of area over the entire length of the channel given by $c = \int_0^L A^{-1} dx$.
- Q was the volumetric flow rate at any instant in time over the tidal cycle.
- ζ_0 was the change in water surface elevation between the inlet and outlet of the channel.
- U_e was the flow velocity at the exit of the channel.

The authors firstly addressed the highly simplified case of a channel with negligible natural background friction and no head losses due to flow separation at the exit to the channel. The power extracted by the turbines in this case was given by the integral of density, volumetric flow rate, velocity and the local frictional force associated with the presence of the turbines. Over the tidal cycle, the total power extracted by turbines was given by:

$$P = \overline{\rho Q \int_0^L F dx} \tag{2.2}$$

The assumption was then made that drag was linearly proportional to the current velocity. The power at any instant in the tidal cycle was then arrived at as:

$$P = \frac{\frac{1}{2}\rho\lambda g^2 a^2}{\lambda^2 + c^2\omega^2} \tag{2.3}$$

Where:

- λ is related to the number of turbines and their position along the channel.
- a is the tidal amplitude.
- ω is the tidal frequency.
- With the maximum occurring when $\lambda = c\omega$, and then the maximum average power is:

$$P_o = \frac{1}{4}\rho g^2 a^2 (c\omega)^{-1} = \frac{1}{4}\rho g a Q_o \tag{2.4}$$

The authors then moved on from this to examine the case where the drag is quadratic with the current velocity, as opposed to linearly. This was stated by the authors to be a more realistic representation of turbine drag. In this case, through non-dimensionalising parameters in equation 2.1 and assuming negligible background friction and exit separation effects, the authors arrived at the following expression for maximum power output of turbines, in the case of negligible background friction and exit separation effects:

$$P_o = \frac{1}{4}\rho\omega L_{eff} A_{min} U_{max}^2 \tag{2.5}$$

Compared to the maximum undisturbed kinetic energy, the ratio between these is:

$$\frac{P_o}{P_{flux}} = \frac{3\pi}{8}\frac{\omega L_{eff}}{u_{max}} \tag{2.6}$$

Where:

- A_{min} is the minimum channel cross sectional area over the entire channel length.
- U_{max} is the maximum flow velocity at the lowest cross sectional area plane of the channel.
- L_{eff} is an effective channel length given by the expression $c = \int A^{-1}dx = \frac{L_{eff}}{A_{min}}$.

The authors then attempted to account for background friction, by assuming it is quadratic with the current and represented by the expression $C_d\frac{U^2}{h}$, where C_d is the drag coefficient and h is water depth. The momentum equation then becomes:

$$c\frac{dQ}{dt} - g\zeta_o = -\int_0^L F_{turb}dx - \alpha Q|Q| \tag{2.7}$$

where:

$$\alpha = \int_0^L C_d\left(hA^2\right)^{-1}dx + \frac{1}{2}A_e^{-2} \tag{2.8}$$

The authors then began examining the limits of the equations derived. The power produced by turbines, using equation 2.7, was given by:

$$\rho Q\int_0^L F_{turb}dx = \rho Q\left(g\zeta_0 - \alpha Q|Q|\right) \tag{2.9}$$

The maximum of this power at any instant in time, found as Q was varied, was given by $0.38\rho g Q_1\zeta_0$. Averaged over the entire tidal cycle, the authors then give the following expression for maximum average power over the entire tidal cycle as:

$$P = 0.21\rho g a Q_{max} \tag{2.10}$$

Both of these studies were among the earliest to examine the theoretical limits of power extraction in tidal channels, and shed light on the nature of the tidal resource. However a number of assumptions and simplifications meant that their ability to quantify power in real tidal channels was limited. The most obvious simplification was the assumption of a tidal fence occupying the entire channel width. Due to constraints such as shipping and navigational, and the effects of turbines on environmental processes such as fish migration, there is a much higher probability of tidal fences which partially block a channel being installed in tidal sites. Studies which are reviewed later in section 2.2.2. These show the power potential estimates in these cases to be considerably different, and to also be dependent on flow conditions in other parts of the flow domain which can be directly attributed to the influence of turbines on that domain.

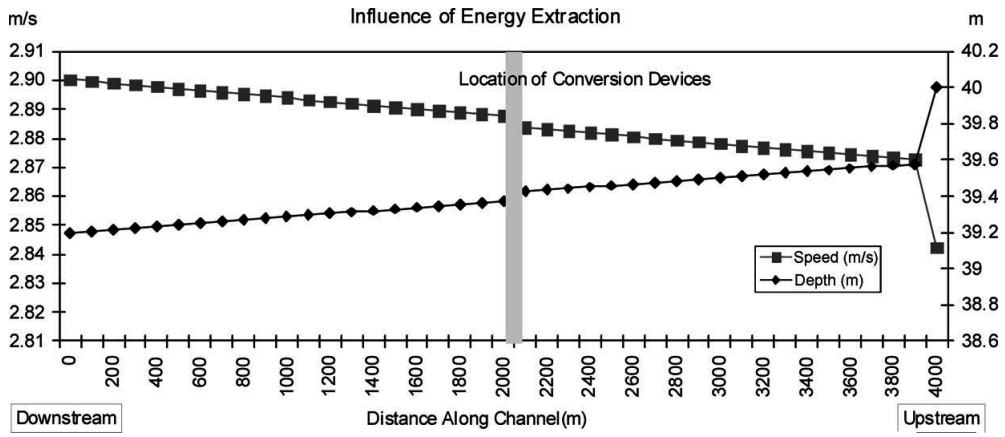

Figure 2.3: reduction in water surface elevation resulting from power extraction demonstrated by Bryden et al. (2004)

2.1.2 Analytical models of split tidal channels.

Relatively few theoretical models have been developed specifically for split tidal channels, where a single open channel branches into one or more sub channels de to the presence of impenetrable land masses. This is despite the fact that many sites worldwide where such topography is present show promising tidal energy potential. Examples of such sites include Hoy in the Pentland Firth, Scotland (Black and Veatch [2005]) and Puget Sound, USA (Polagye et al. [2009]). Despite these high potential resources, one drawback is that the topography of these sites makes them much more complex to analyse from both a resource assessment and environmental impact point of view.

One study which aimed to develop an analytical model for power potential in a split tidal channel was by Atwater and Lawrence [2010]. The authors examined the simple split tidal channel displayed in figure 2.4. The authors derived expressions for the power potential of the entire system and the power extracted by turbines as a function of head loss across the channel. It was shown that for the channel analysed, the extraction efficiency was a function of head loss coefficients at various points throughout the entire system. Another conclusion was that extraction efficiency was dependent on the imbalance in volumetric flow rate between the impeded channel and free channel. This imbalance was due to the diversion of flow from the impeded channel into the free channel due to the installation and operation of tidal turbines.

This diversion of flow is simply a consequence of the continuity principle. Blockage of the impeded channel means less flow can go through it, and so it must divert around through the unblocked channel to obey conservation of mass. For the geometry presented, the model could predict how much power could potentially be extracted and what imbalance in volumetric flow rate between both sub channels would achieve this. The authors therefore applied their model to Current Passage, Johnstone Strait, Canada, a split channel tidal site. Following application of the model, and assuming no losses due to turbine drag and wake mixing, the paper stated that the maximum extraction efficiency for this tidal site was 3.8%, leading to a maximum potential power output of 75MW. It should be noted however that this paper contains a calculation error. The actual value according to the model is 5.7%, leading to a

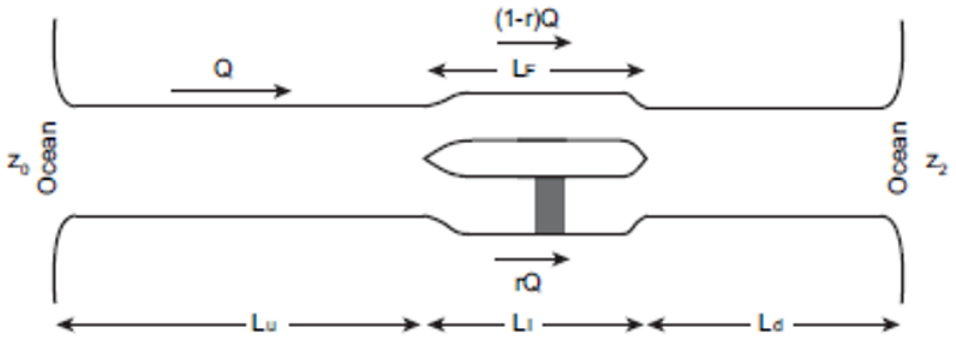

Figure 2.4: Split tidal channel examined by Atwater and Lawrence [2010].

potential power output of 112MW (J. Atwater, personal communication). The extraction efficiency was based on the maximum amount extractable theoretically from the following available power estimate.

$$P = \frac{1}{2}\rho U^3 A \tag{2.11}$$

The authors considered the theoretical maximum single channel power limit. They did this by assuming the flow being forced entirely through the impeded channel. The model suggested that this leads to a maximum efficiency for a single channel of 38.49%, that is that 38.49% of the power available estimate given in the above equation can be extracted. This result agrees with an analysis of open single channels by Garrett and Cummins [2005].

A more recent development of split tidal channel theory was carried out by Cummins [2013]. In this case, the author examined a similar split tidal channel configuration to Atwater and Lawrence, but with the addition of a closed basin at the end (Figure 2.5). The author examined the maximum power potential of the channel by introducing the analogy of an electrical circuit. As with the Atwater and Lawrence model, the analytical model in this work assumed a complete tidal fence blocking one of two sub channels, and the entire flow in the impeded channel was directed through this fence. The electrical circuit analogy worked as follows:

- Pressure in the flow channel was equivalent to voltage in the electrical circuit
- Volumetric flow rate in the flow channel was equivalent to magnitude of electric current in the electrical circuit.
- There was an impedance, with both a resistive and inductive component, associated with each section of the channel. This was given by the expression:

$$ZI = RE + i\omega L \tag{2.12}$$

Where RE represents the resistive component and $i\omega L$ represents the inductance. In the case of the impeded channel, the resistive component was equivalent to the natural bottom friction drag in the impeded channel. This was given by the expressions:

$$RE_1 = \rho\alpha_1 \tag{2.13}$$

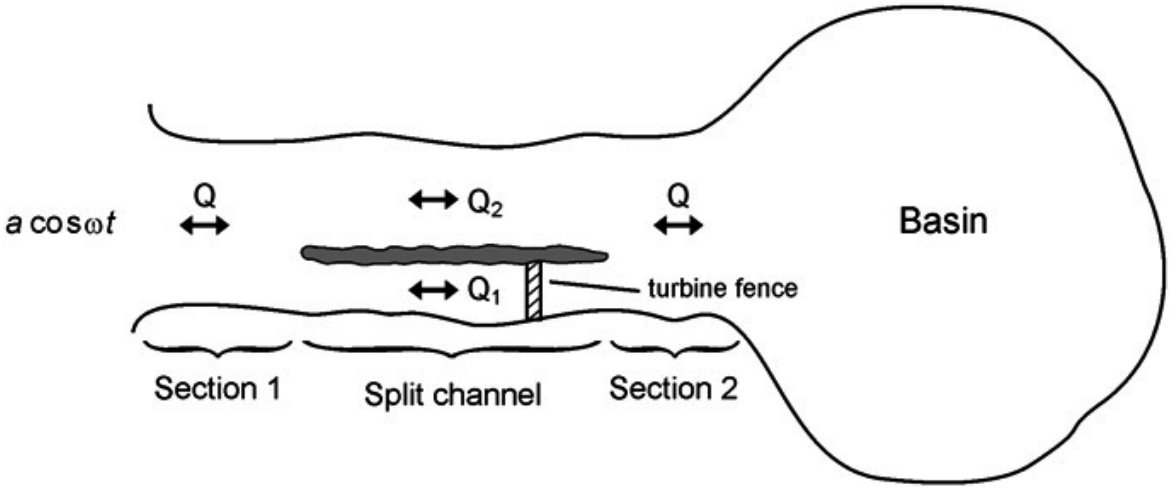

Figure 2.5: Split tidal channel configuration examined by Cummins [2013]

The load resistance R_L in the equivalent electric circuit was due to the drag of the turbine fence. This was given by the expression:

$$RE_L = \rho\alpha_t \tag{2.14}$$

Here α_1 and α_t are constants given by:

$$\alpha_{1'} = \int rd_1 A_1^{-1} dx \tag{2.15}$$

$$\alpha_{t'} = \int rd_t A_t^{-1} dx \tag{2.16}$$

Where rd_1 and rd_t are the background frictional drag of the sub channel and drag due to tidal turbines respectively.

The inductive component L_1 was associated with acceleration of flow in certain regions due to the presence of turbines. This was given by the expression:

$$\omega L_1 = \omega\rho c_1 \tag{2.17}$$

Where ω represents the angular frequency of the tidal flow and c_1 was a constant given by:

$$c_{1'} = \int A_1^{-1} dx \tag{2.18}$$

- There are also impedances associated with both the free channel and the other sections of the channel between the island and mouth of the channel and the island and basin.

The equivalent electrical circuit is displayed in figure 2.6. The top figure shows the channel in figure 2.5 displayed using the developed analogy. The bottom figure represents a simplification of the electrical circuit using Thevenin's theorem. This theorem is used to simplify complex electrical circuits with numerous resistances, voltages and impedances into a circuit with a

single equivalent value for each. This is so that quantities such as resistance or voltage at specific points in the circuit can be identified more easily (Dorf and Svoboda [1996, p. 186]). After applying Thevenin's theorem, the authors then applied the maximum power transfer theorem to determine the maximum power output of the equivalent electrical circuit. It can be demonstrated by mathematical expressions (Dorf and Svoboda (1996, pp. 199-220) that the maximum power transfer theorem shows that maximum power is transferred to the resistor RE_L at the bottom of figure 2.6 when its numerical value is equal to the impedance ZI_T. The application of this gave the following expression for the maximum extractable power of the split channel in terms of the electrical circuit analogy used as:

$$P_{max} = \frac{|ZI_T|\,|VI_T|^2}{2\,|ZI_T + |ZI_T||^2} \tag{2.19}$$

Where ZI_T and VI_T are the equivalent impedance and voltage respectively of the idealised circuit in figure 2.6. Using this as well as other expressions used in the developed electrical circuit analogy, it was possible to estimate the power potential of any given tidal channel. However the author acknowledged that estimates from this expression only represent an upper bound to power extractable, and does not account for mechanical and electrical losses or losses due to drag on turbines and support structures and wake mixing.

After development of this theory, the authors then applied it to a simple hypothetical split channel with the following geometrical parameters:

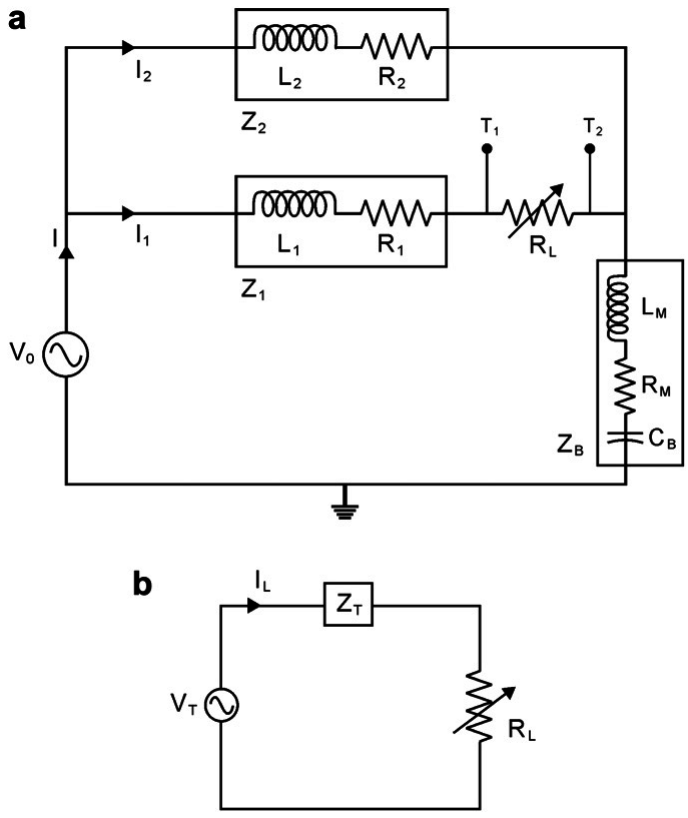

Figure 2.6: Equivalent electrical circuit as proposed by analogy developed by Cummins (2013).

- Both sub channels with a length of 5km
- Both sub channels with flow depth of 15m
- The impeded channel had a cross sectional area of 0.75 x $10^4 m^2$, while the free sub channel had a cross sectional area of 1.5 x $10^4 m^2$.
- Impedance of both sub channels was assumed negligible as both sub channels are sufficiently short.
- M2 tidal forcing at mouth of channel assumed to have amplitude of 1m.
- Flow velocity of the current was assumed to be 1m/s.
- The authors assumed varying basin areas between 0 and 5 x $10^9 m^2$.

The results of the application of the model to this simple channel are displayed in figures 2.7 and 2.8. Figure 2.7 shows the change in power available with basin area, while figure 2.8 shows the fractional change in volumetric flow rate in the impeded (S_1) and free (S_2) sub channels. These fractional changes are given by the author by the following expressions:

$$S_1 = \frac{|Z_T|}{|Z_T + |Z_T||} \tag{2.20}$$

$$S_2 = F_1 \frac{|Z_1 + |Z_T||}{|Z_1|} \tag{2.21}$$

The only geometrical parameter which was altered was the basin area. The solid line in figure 2.7 shows the maximum power available for each basin area along with the geometrical parameters listed above, while the dotted line shows the power output predicted by Dorf and Svoboda [1996] for the single impeded channel without the presence of the free channel. The results showed that for the particular geometry examined, the power for the split channel was lower than for the single case up to a basin area of just over 1 x $10^9 m^2$, after which it increased and achieved a maximum at a basin area of approximately 2 x $10^9 m^2$.

Despite many similarities, there are also some differences between the models presented by both sets of authors. The most obvious is the inclusion by Cummins of the basin at the mouth of the channel, which the author's model suggest greatly influences the available power.

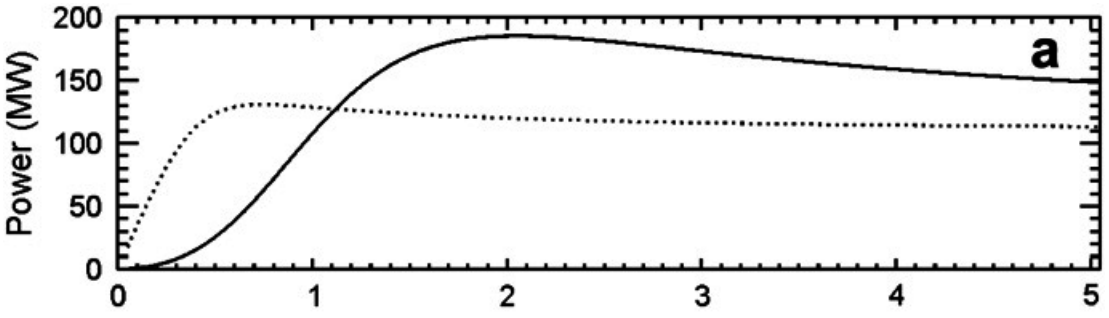

Figure 2.7: The variation of extractable power with basin area for simple channel analysed by Cummins (2013)

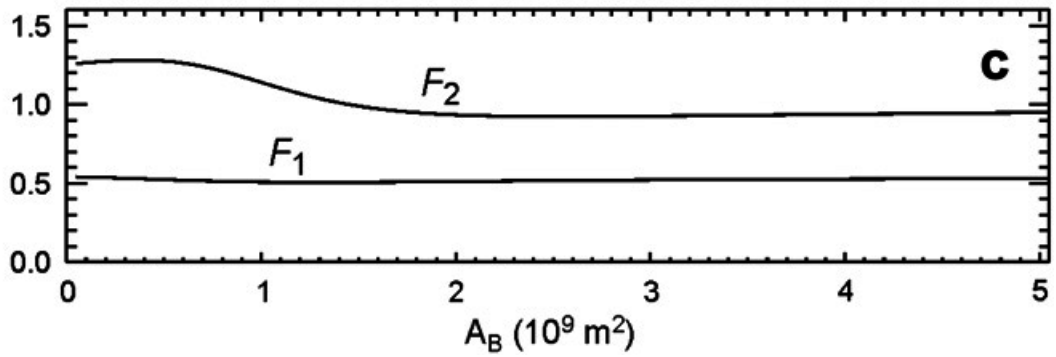

Figure 2.8: The variation of volumetric flow rate in impeded and free sub channels with basin area for simple channel analysed by Cummins (2013)

Another major difference in the Cummins model is the differing sizes and cross sectional areas of both the impeded and free channels. In contrast, the Atwater and Lawrence model only examined evenly split sub channels, and it is unclear how applicable their model would be to the hypothetical channel examined by Cummins. From a tidal developers perspective, arguably the greatest advantage of the Cummins model is that it can be modified to examine power potential resources in split channel with more than two sub channels. The author claims this can be done by replacing the impedance of the single free sub channel with an equivalent impedance of any number of free sub channels before application of Thevenin's theorem.

Considering the importance of imbalance in volumetric flow rate found by the authors, further investigation could identify whether or not there is an optimal positioning and blockage ratio of tidal turbines in split channels, and through experimental studies indicate how much of a consideration tidal turbine position and channel blockage will be for any tidal developers wishing to exploit the resources in areas such as Hoy or Puget Sound. As this would be an investigation of very fundamental aspects of flow behaviour, the judgement was made that experimental analysis would be an ideal starting point, and could potentially be followed by validation or more in depth research with numerical modelling at some stage in the future.

Some comment should be made on how these analytical models can be used alongside experimental results. The model of Atwater and Lawrence can be used in the experimentation for this analysis. The reasons for this is the simple layout of the channel they present, which can easily be replicated in a suitably wide flume with the use of an impenetrable obstruction to represent the island splitting the channel. But a crucial detail with this model is also that the authors assume two infinite oceans on either side. This means all the water travelling into the system from the inlet goes directly through and is not recirculated. Such a system can be replicated in a gravity driver water flume, such as that available for this work. In contrast, the analytical model of Cummins (2013) assumes a tidal channel connecting the open ocean to a basin located some distance downstream of the impenetrable land mass. Water would recirculate in this basin after it had passed through the sub channels of the split tidal channel, and hence its flow characteristics are considerably different to those of the split channel set-up examined by Atwater and Lawrence. Replicating the channel of Cummins (2013) would

require very specific experimental facilities, which unfortunately were not available for the work presented herein.

For that reason, experimental results have only been compared to calculations from the Atwater and Lawrence model. The analytical model, along with the calculations involved in applying it to the Johnstone Strait site, are presented in section 2.5.10. The experimental procedure for examining split tidal channels is outlined in section 3.5, while the results of this analysis are outlined and explained in section 6.2.

2.2 Linear momentum theory applied to tidal channels

2.2.1 Theoretical models of unconstrained channels

The development of wind turbines represented a new area of investigation in terms of how to apply fundamental principles of fluid mechanics to newly developed technology. The main concern with wind turbines was how to determine the maximum amount of energy they may be capable of extracting for given flow conditions such as undisturbed flow velocity, and turbine parameters such as rotor cross sectional area.

One of the most well known examples of the application of fluid mechanics to wind turbines is by Burton et al. [2001]. The authors considered a generic design of a wind turbine by introducing the concept of an actuator disc, an energy extracting device in a wind flow. The authors assumed the flow field shown in figure 2.9, and separated the flow surrounding the disc into upstream undisturbed flow, flow at the disc and wake flow in the region immediately downstream of the disc. To develop equations for the thrust and power on the wind turbine, the authors then applied the following steps:

- Applied the continuity equation to all three flow regions.
- Introduced the concept of an axial induction factor, which is a measure of the extent to which flow velocity has reduced between the upstream undisturbed flow and the flow at the front of the actuator disc.
- Apply the momentum equation across the disc to find an expression for the force on the disc as a function of flow velocity values and disc cross sectional area.
- Apply the Bernoulli's equation separately to both upstream and downstream of the disc to obtain an expression for the pressure difference across the disc as a function of wake and undisturbed flow velocity.
- The force on the disc is then subsequently found by simply multiplying this expression by the disc area.
- The power output of the disc is then found by multiplying force by the value of velocity at the disc.
- The authors then find non-dimensional power and thrust parameters. These can be expressed as functions of flow velocities and disc area, but can also be expressed solely in terms of axial induction factor.

- The maximum value for power coefficient was found by differentiating the expression for power coefficient in terms of axial induction factor, and equating it to zero. The maximum value was found to be 0.593. This was consistent with results from previous work by Lanchester and Betz, which found that a propeller was theoretically capable of extracting a maximum of 59.3% of the undisturbed kinetic energy of the flow which it is located within.

One of the most interesting outcomes of this work for those carrying out experimental analysis of tidal turbines is the relationship between thrust and power coefficient found by these authors. Thrust coefficient in terms of axial induction factor was found to be given by:

$$C_T = 4a\,(1-a) \tag{2.22}$$

While power coefficient was given by:

$$C_P = 4a\,(1-a)^2 \tag{2.23}$$

Thus the thrust and power coefficients are related by (1-a), where a is the axial induction factor. This demonstrates that despite the simplification of a turbine which an actuator disc represents, changes to forces acting on it can give an indication of the corresponding power output changes in a real tidal turbine installation. This opens the possibility of simplifying experiments greatly by removing the need to use large and costly rotating turbines. This is extremely useful when examining experimentally the fundamental behaviour of tidal turbines in a tidal channel, or examining how their power output may change with changes in flow conditions, inter-device spacing, or other variable parameters in a tidal turbine installation.

The similarity between wind and tidal energy technology has often been cited as one of the main advantages of tidal power. This has been claimed by many authors to be due to the understanding already gained by wind turbine studies. While this is true to some extent, the constrained nature of the tidal resource compared to the largely unconstrained nature of wind energy, as examined in the work by Burton et al. (2001), means some fundamental differences between them exist. The constrained nature of the tidal resource means that

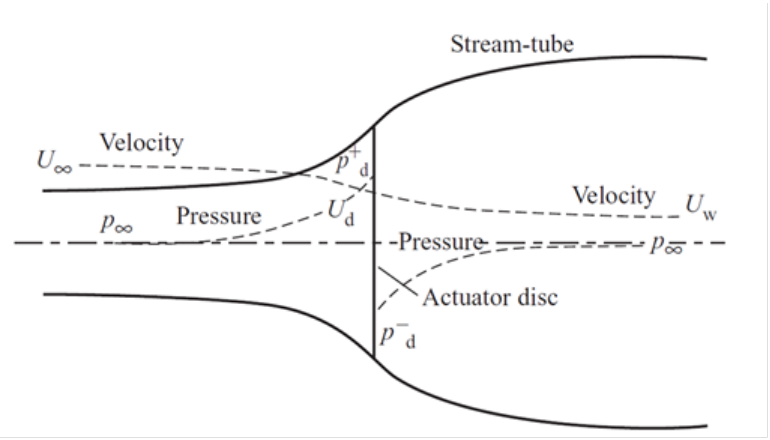

Figure 2.9: An actuator disc and Stream-tube from Burton et al. [2001]

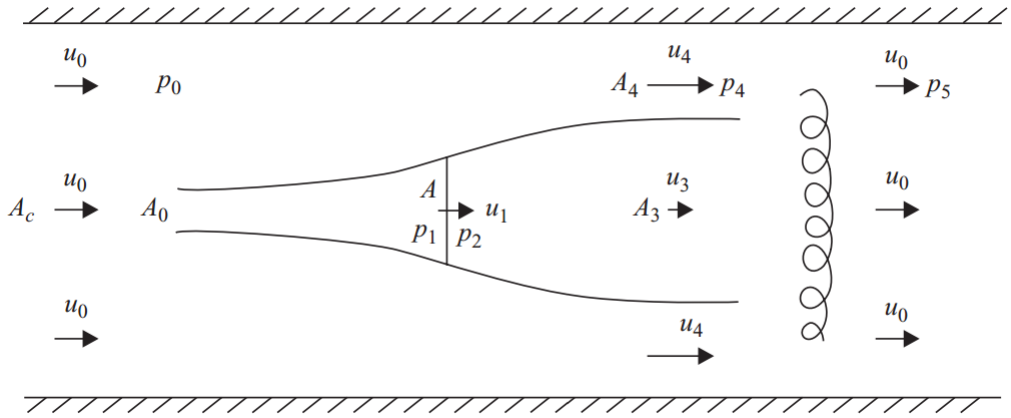

Figure 2.10: Flow regime surrounding tidal turbine examined by Garrett and Cummins [2007]

alterations to existing theory need to be made. The following section gives some examples of attempts to account for the constrained nature of tidal channels when examining the power potential of tidal turbines.

2.2.2 Theoretical models of constrained channels

The open channel tidal resource studies reviewed in section 2.1.1 assumed tidal fences spanning the entire width of their respective open channels. Furthermore, the linear momentum theory reviewed in the previous section assumed an infinitely wide flow domain with no blockage effects. In reality, there are many tidal sites where these assumptions would be invalid, and so the theory of these models does not account for blockage effects or the influence of partial blockage of tidal turbines in a bounded channel. Many studies have aimed to advance the knowledge gained by these aforementioned studies by accounting for blockage and the effects of turbines on the natural flow regime.

An examination of the maximum extractable power in a partially blocked channel was examined by Garrett and Cummins [2007]. The authors aim was to extend on previous work in Garrett and Cummins [2005] by considering channels with only a fraction of their cross sectional area occupied, as opposed to the entire cross section in the previous work. The authors examined the tidal turbine in a constrained channel as shown in figure 2.10, and separated the flow into two streamtubes. One streamtube was assumed to travel directly through the fence and expand into a wake downstream, and the other was the bypass flow surrounding the turbine. The authors then applied the following steps:

- Applied the continuity equation to both streamtubes to determine relationships between areas and flow velocities upstream and downstream of the turbine cross sectional plane.
- Applied the momentum equation to upstream and downstream sections of the turbine to determine an expression for the force on the turbine in terms of areas and flow velocities.
- Applied the Bernoulli equation to a streamline in the bypass flow region, and also to upstream and downstream of the turbine, to determine a second expression for the force

on the turbine in terms of areas and flow velocities.

- Equated these two expressions for force on the turbine to determine the following expression for disc velocity:

$$u_1 = \frac{u_3\left(u_4 + u_3\right)}{u_4 + 2u_3 - u_0} \tag{2.24}$$

Which when combined with the expression for force on the turbine, gives the following expression for power output of the turbine in terms of surrounding flow velocities:

$$P = \frac{1}{2}A\frac{u_3\left(u_4 + u_3\right)\left(u_4^2 - u_3^2\right)}{u_4 + 2u_3 - u_0} \tag{2.25}$$

As the cross sectional area of the channel tends towards infinity, and hence the turbines occupy an almost negligible cross sectional area, the term u_4 tends to u_0, and hence the power output simplifies to:

$$P = P_{LB} = \frac{1}{4}A\left(u_0 + u_3\right)\left(u_0^2 - u_3^2\right) = \frac{1}{2}\left(1 + r\right)\left(1 - r^2\right)x\frac{1}{2}Au_0^2 \tag{2.26}$$

It is found that the maximum power in an unconstrained channel is 0.59 times the undisturbed kinetic energy flux, a result consistent with the conclusions of Lanchester -Betz analysis.

- The authors then combine the expression for disc velocity in equation 2.24 with expressions previously determined by applying continuity to both streamtubes to determine the following expression for bypass velocity in terms of upstream flow velocity, wake velocity and turbine blockage ratio ϵ:

$$u_4 = \frac{u_0 - u_3 + \left[\epsilon u_0^2 - 2\epsilon u_0 u_3 + \left(1 - \epsilon + \epsilon^2\right)u_3^2\right]^{\frac{1}{2}}}{1 - \epsilon} \tag{2.27}$$

Further manipulation of mathematical expressions derived were then combined to determine the following expression for maximum power output of turbines in terms of blockage ratio and surrounding flow velocities:

$$P_{max} = \frac{16}{27}\left(1 - \epsilon\right)^{-2}x\frac{1}{2}Au_0^3 \tag{2.28}$$

Some of the main conclusions from this analysis are:

- The Lanchester - Betz limit, which was stated as the maximum theoretical power output of turbines in an unconstrained field, is increased by a factor of $\left(1 - \epsilon\right)^{-2}$ in a constrained flow field.

- When considering the maximum energy which could be extracted by a fence occupying the entire channel cross section, the fraction of this energy which could be exploited by a partial fence is dependent on the fence blockage ratio. This fraction is stated by the authors to be 2/3 for a small blockage ratio, or 1/3 for a larger blockage ratio (without giving any specific figures for where the threshold between these two fractions was). This clearly demonstrates the principle, as stated in many other studies, that adding

turbines increases the hydrodynamic drag on the channel, and effectively "chokes" the flow, and so actually reduces the amount of power available for turbines to extract.

In the context of the work presented herein, the most important and interesting conclusion is the dependence of power output of turbines on surrounding flow velocity values and blockage ratio. The expressions for disc velocity, turbine power and bypass velocity in expressions 2.24, 2.25 and 2.27 respectively, all of which were derived from fundamental fluid mechanics principles, clearly show the complex dependence of the performance of turbines on surrounding flow velocities. This in turn shows the importance of wake recovery downstream for performance of turbines and surrounding flow environment. The value for wake velocity (u_3 in the aforementioned theory) is completely dependent on wake expansion and recovery characteristics. Thus any changes to either of these phenomena will clearly have major implications.

While this blockage model explores optimal flow conditions for a given along channel flow, a blockage model developed on the basis of a head loss across a channel was developed by Vennell [2010]. The authors developed a model to examine the optimum internal configuration of a tidal farm for maximum power production. The developed model is a combination of the model of Garrett and Cummins (2005), which includes the bottom friction of a channel, with the model of Garrett and Cummins (2007), which neglects bottom friction. The authors consider the channel shown in figure 2.11, and the model is developed using the following steps:

- The authors begun with the 1D shallow water momentum equation for the channel by Garrett and Cummins (2005), and simplified the equation by non - dimensionalising velocity by the amplitude of velocity with no turbines or background friction, and non -dimensionalising time by the frequency of the driving tide causing the head loss across the channel,
- The authors then presented an expression for the non-dimensional power lost by the flow relative to the channel's maximum potential as a function of non-dimensionalised flow velocity, natural background friction in the channel and bottom friction introduced by the installation of turbines.

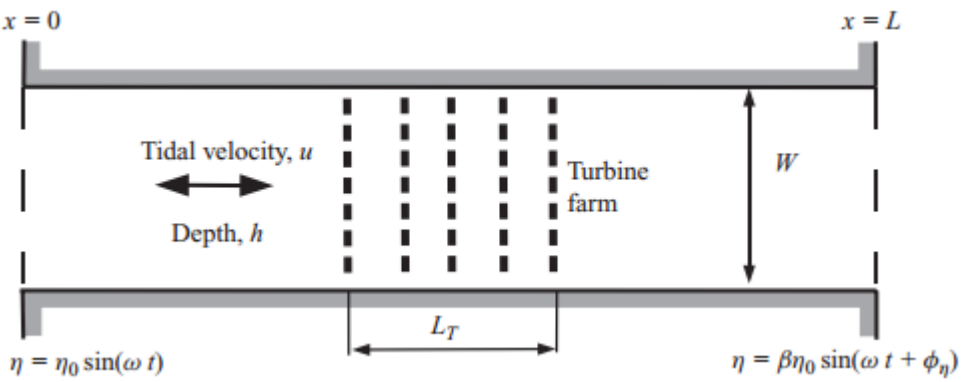

Figure 2.11: Channel with model by Vennell (2010).

- These equations were solved numerically to give flow velocity and turbine bottom friction values.
- The equations for power lost and power available as a function of turbine bottom friction and natural background friction, which the authors derived from simplifying the Garrett and Cummins (2005) model, were then combined with expressions the same powers as a function of turbine velocity and blockage ratio found from Garrett and Cummins (2007) model. This combination led to the results displayed in figure 2.12, which give the relationships between blockage ratio, wake velocity (shown as r_3 in the figure), drag coefficient associated with introduced turbines and peak power available.

These results show the complex relationship between many different parameters affecting the power output of turbines and the potential of the channel available for extraction. The authors follow on from these results by fixing a number of parameters, and looking at the effects of varying other parameters. The following scenarios were examined:

- Negligible bottom friction and a fixed number of turbine rows. The authors then displayed the resultant power available, power lost by the flow due to different fluid streams mixing, power available to turbines relative to maximum channel power, and reduction in velocity relative to an undisturbed channel, with different combinations of values for blockage ratio and r_3, the wake velocity downstream of turbines.
- A fixed blockage ratio of 0.25. The same aforementioned power values were then displayed for different combinations of number of rows of turbines and values for r_3, the wake velocity downstream of turbines.
- Fixed values for r_3. The fraction of a channels power available for production was then displayed for a combination of blockage ratios and number of turbine rows.

This work expanded on the knowledge gained by Garrett and Cummins (2007). One of the main advancements was the demonstration that power available for extraction did not reduce

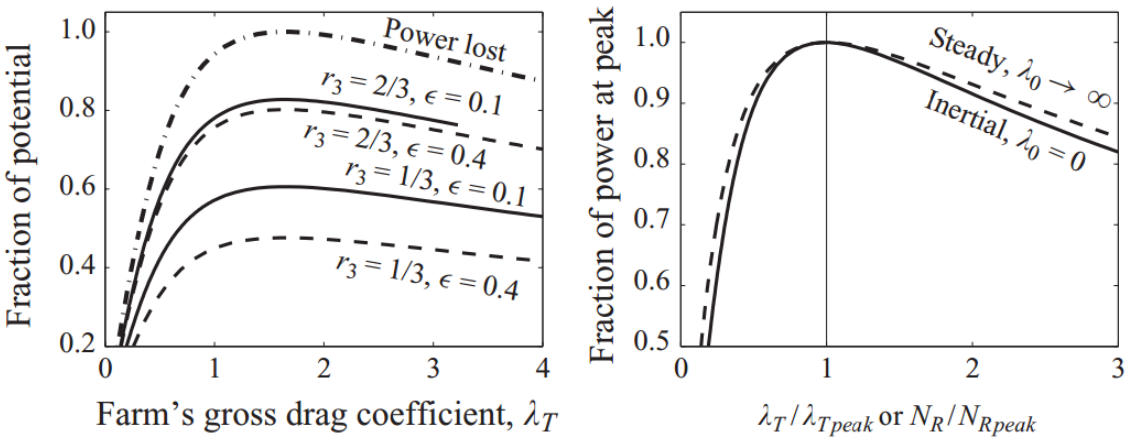

Figure 2.12: Results of combined expressions of two Garrett and Cummins models proposed by Vennell (2010).

as the blockage ratio increased. Garrett and Cummins (2007) suggested that the fraction of power available reduced from 2/3 for a small blockage ratio to 1/3 for a larger blockage ratio. Vennell (2010) appears to suggest that, if turbines are "tuned" to ensure appropriate wake velocity values, then the maximum power which can be extracted by turbines is dependent solely on the amount of turbines in a row. As such, the author suggests that as many optimally tuned turbines should be installed in a channel as permitted by navigational and environmental constraints. Furthermore, Garrett and Cummins stated that the theory they developed for power output on a turbine would be applicable to rows of several turbines, provided the downstream spacing between them was sufficient to allow a fully dissipated wake and return to freestream conditions for each row. However Vennell showed that, even for optimally "tuned" turbines, there is a diminishing return with addition of rows, and the amount of power per row reduces as the amount of rows increases.

An alternative extension to the theory of Garrett and Cummins (2007) was proposed by Nishino and Willden [2012]. The authors considered a simple arrangement of a tidal turbine in a channel very similar to that of Garrett and Cummins, as shown in figure 2.13. However they proposed a separation of flow scales, one being flow around an entire array of turbines and the other being flow locally around a single device within this array. For the array scale, the authors assumed the following:

- Flow entirely two-dimensional.
- The array was assumed to be a single power extracting fence.
- The array spanned the entire vertical direction of the channel, but only partially spanned the channel laterally across its cross section.
- The channel is sufficiently long to allow the wake of the array to dissipate entirely before the end of the channel.

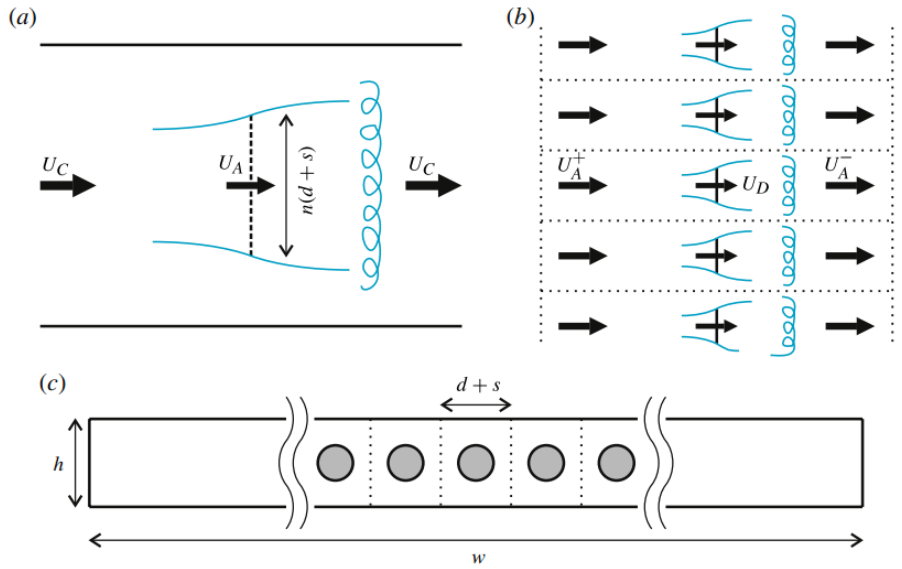

Figure 2.13: Array scale flow (a) and local scale flow (b) examined by Nishino and Willden (2012)

In developing the device scale, the authors made the following assumptions:

- The array consisted of an arbitrary number of devices, with device assumed to have its own local flow "passage". Within this local flow "passage", the device is assumed to be a certain diameter d, and the entire width of each individual flow passage is s+d.
- The inlet flow velocity to each individual device was assumed to be identical, and equal to the inlet flow velocity of the array assumed in the array scale model.
- The flow velocity in the wake of each individual device "passage" was assumed to be identical, and equal to the wake velocity of the array assumed in the array scale model.

The authors then developed three different sets of expressions for blockage ratio, axial induction factor, thrust coefficient and power coefficient. The three sets of expressions were one each for the array scale flow, the device scale flow, and also a global scale flow. Two crucial details in the development and use of the model were:

- For the device scale, blockage ratio was assumed to be the device diameter (d) divided by the cross sectional area of the local flow passage of the device (hx(s+d)). At the array scale, the blockage ratio was assumed to the summation of blockage ratio of all individual devices in the array divided by the channel cross sectional area.
- For the device scale, thrust was calculated using individual device thrust and device area. At the array scale, thrust coefficient was calculated using the thrust on an individual device multiplied by the number of devices, and the cross sectional area of the entire array. These two different expressions allowed a definite relationship between thrust coefficient at both scales to be determined.

The authors then apply conservation of mass, momentum and energy at the device scale, in a similar manner to Garrett and Cummins (2007), to determine an expression for thrust coefficient on each device as a function of wake velocity and blockage ratio (in this case blockage ratio is ratio of turbine cross sectional area to area of its individual "passage"). These fundamental principles were also applied at the array scale to determine thrust coefficient on the entire array as a function of its wake velocity and blockage ratio. Then using the relationship between thrust coefficient between both scales found previously, the authors were able to examine the effects of changes to local device scale and array scale blockage ratios on thrust and power coefficients. One particularly interesting result was where the authors considered the case of an infinitely wide channel, where only the local blockage ratio of devices within their own flow "passage" affects the maximum power available which can be extracted. In this case, as shown in figure 2.14, the proportion of the kinetic energy flux which can be extracted is 0.798, which is considerably higher than the Lanchester - Betz limit of 0.59 which was also suggested by Garrett and Cummins (2007).

The array scale blockage ratio represents the cross sectional area of the channel occupied by turbines, which is a parameter also examined by the two previously mentioned blockage models. However this model has advanced on both of these previous studies by examining local device blockage ratios, which in practical terms is a consequence of different inter device

spacing within a given sized array. This therefore opens the possibility that smaller blockage ratio arrays may actually extract more power than larger blockage ratio arrays, on condition they have an inter device spacing which achieves values of wake velocity which, as shown by the previous models, can a greater change in momentum across the plane of extraction, and hence a higher power force on turbines.

All of the above studies are two dimensional models, and so, as explicitly acknowledged by Vennell (2010), they are unlikely to be able to predict real values of thrust or bypass flow velocity of tidal turbines installed in real channels. The common assumption between all studies of uniform flow across the channel cross section is one which particularly limits its applicability to resource assessment in full scale tidal arrays. In reality, the flow regime in a channel will be highly dependent on boundary layer profiles off both channel sidewalls and the channel bed. Nonetheless, there is no question that they have shed greater light on the complex relationship that exists between blockage ratio, wake velocity, bypass flow velocity, thrust and power in rows of tidal turbines. Vennell (2010) and Nishino and Willden (2012) have also shown that, provided there is optimal tuning of turbines and inter-device spacing, the maximum amount of power which may be extracted may be considerably higher than the 59% of kinetic energy flux previously thought, Thus any changes to the layout and arrangement of a row of tidal turbines, and the consequent effects on flow parameters such as wake velocity, are likely to be of considerable interest to tidal developers.

One such possible change which has not been examined in any of the above studies is the specific position of a row of turbines with respect to flow boundaries. The most likely reason for this is that all of the models have assumed uniform flow across the channel cross section, both at the inflow to turbines, and also in the wake and bypass flow regions. In reality, the non-uniformity of these reasons, and viscous effects of flow off channel boundaries, means that it is possible that changing the distance between turbines and surrounding boundaries could cause changes in surrounding flow conditions. Given the dependency of performance of turbines on these flow conditions which has been demonstrated by these reviewed studies, an examination of changing wake and bypass flow effects associated with changing the position of turbines in a channel, and the possible reasons for any changes found, is certainly justified.

2.3 Site specific tidal models

As well as research on devices and generic analytical models, much research has also been carried out on specific tidal sites. There are many issues with specific sites which determine how effectively tidal turbines will operate in these, and also what effects the process of extraction will cause. Some factors of sites include:

- The flow velocity, and hence kinetic energy flux, at a site.
- The depth of flow at a site.
- The specific bathymetry at a site.
- The proximity of a site to population centres.

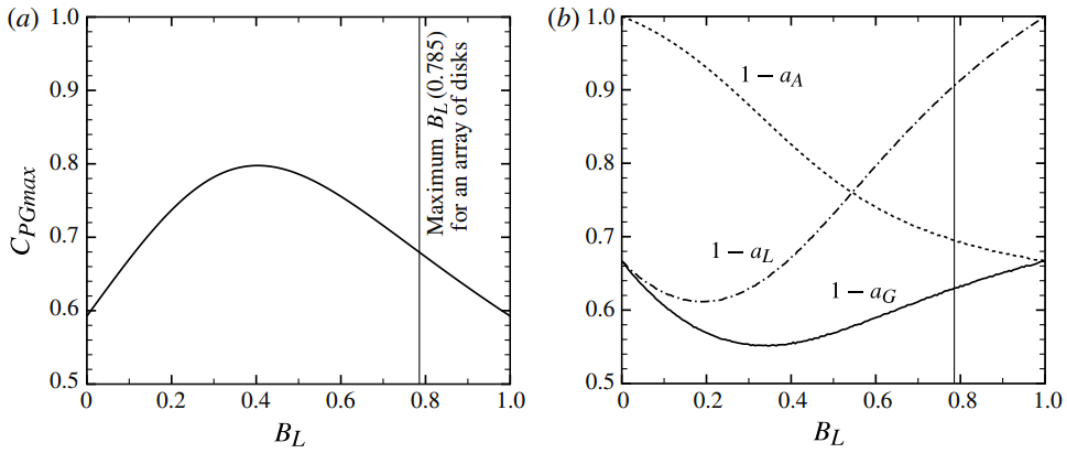

Figure 2.14: Changes in power coefficient with blockage ratio for infinitely wide channel by Nishino and Willden (2012)

All of these factors means that an extensive examination of any site must be undertaken before tidal turbines are installed. Numerical models are very useful in this respect, as demonstrated by the following analyses and their conclusions.

2.3.1 Site specific open channels

An attractive site for the installation of tidal turbines lies at Portland Bill, near Weymouth along the Southern coast of England. As well as having high velocity, the site is also located very close to population centres. This represents a major advantage for tidal developers. Deployment at this site would avoid the high cabling costs and losses associated with deployment in sites further offshore such as in the Pentland Firth.

The initial potential resources at the site were examined by Blunden and Bahaj [2006]. In this analysis, the TELEMAC 2D numerical model was used to examine the entire flow field of the site, with a view to examining where might be the most suitable exact point for tidal turbine installation. The TELEMAC model solves the vertically integrated equations of continuity and momentum within the flow domain to which it is applied. A mesh of the Portland Bill site was created, with the inputted Bathymetry of the site taken from data sheets compiled by the National Oceanography Centre, Southampton. The numerical model was initially assumed to have mean sea level in the entire flow domain. It was then applied with an expression for tidal elevation at any point in time as a function of parameters such as amplitude and angular speed. The initial values for these parameters were determined from linear interpolation of data from tidal gauges throughout the English channel. The TELEMAC model was validated in two ways:

- By comparing tidal elevations with those recorded by a tide gauge deployed at Weymouth, in the middle of the flow domain.

- By comparing flow velocity at specific points in the model from those shown for the same points on tidal diamonds on navigational charts.

It was shown that the 2D model predicted tidal elevations at Weymouth to within 9.6% Although the authors do not give any quantification of the agreement between model flow velocity values and those observed in the field, they do state that "The agreement of the maximum speeds is reasonable".

This work was then followed by an examination of the effects of energy extraction in Blunden and Bahaj [2007]. The overall aim of this analysis was to examine changes to flow velocity, tidal amplitude and phase of the main semi diurnal lunar tide (M2). M2 is a tide whose movement is driven by the gravitational pull of the moon on the earth, and it has a period of just over 12 hours (internet ref). The authors stated that inclusion in the model of full scale tidal turbines would have rendered the analysis too-computationally intensive, and identified a number of possible alternative methods for examining flow changes. The method chosen was one where additional shear stress was applied to certain nodes in the mesh of the numerical model representing the regions where tidal turbines were to be installed. This is very similar to the method used in the model developed by Bryden et al. (2004). This additional shear stress applied retarding forces to the flow, causing "sinks" in momentum equivalent to those which would occur with tidal rotors. This sink in momentum was then added to the vertically integrated momentum equation applied by the TELEMAC model, and the resulting flow effects would be demonstrated in model results.

Some of the main conclusion of this analysis included:

- Energy extraction caused a decrease in flow velocity in many regions, with a decrease of up to 50% in some areas.
- There were however increases in flow velocity of up to 15% in the region constrained between the headland and the array (See figure 2.15).
- Changes to tidal phase of the M2 tide occurred due to power extraction, with the largest reduction in phase compared to freestream being 50 degrees, or approximately 25%.

In the context of the research for this work, the results of energy extraction presented in figure 2.15 are extremely important. It is a clear indication that the process of energy extraction does cause an increase in flow velocity in certain regions of the flow domain. Also crucially, this is not the only site specific analysis to demonstrate this phenomenon.

An examination of a high potential site in the Pentland Firth in Scotland was carried out by Easton [2010]. The site in question is the Inner Sound of Stroma, a 10KM long by 3KM wide channel lying between the Scottish mainland and the Island of Stroma. The objective of this study was to firstly create and validate a numerical model of the present conditions in the Inner Sound, and then examine the changes to the flow regime in the region by simulating the presence of tidal turbines. The numerical model chosen in this study was the MIKE21 flexible mesh solver, which solves the Reynolds Averaged Navier Stokes (RANS) equations. These are again simply the representations of the continuity and momentum equations to a coastal domain. A mesh of the region was created and publicly available bathymetry data was interpolated onto the mesh. The natural flow conditions in the sound were simulated in MIKE21, and the results of the model were validated against flow measurements in the region taken by a research vessel using an acoustic Doppler current profiler (ADCP). As

with the analysis of Blunden and Bahaj (2007), the simulation of actual tidal rotors was carried out by increasing the bed shear stress, and including in it an additional shear stress in a specific region of the mesh calculated on the basis of the amount of power extraction being simulated. Two scenarios were examined, one with energy extraction of 900MW and another with extraction of 160MW. The results of this analysis are presented in figure 2.16. It shows that there is a large decrease in flow velocity in the region downstream of the plane of extraction. For extraction of 900MW there is a 50% decrease in current speed, and a decrease of approximately 10% with extraction of 160MW. But also demonstrated is a major increase in flow velocity in the regions between the turbine array and flow boundaries. The magnitude of these increases is in some areas almost as high as the decrease downstream of the turbines.

Another high potential tidal energy site is the Severn Estuary, a stretch of water beginning at Gloucester in England and separating Southern England from Southern Wales. This area has long been the subject of investigation for a barrage, although high costs and environmental impact have prevented its construction up to the time of writing. However Ahmadian et al. [2012] examined the potential for tidal turbine rows in this region. The authors used a 2 dimensional hydro-environmental model known as DIVAST to simulate an array of 2000 10m diameter tidal turbines in an area of the estuary of $7.2km^2$. The DIVAST model solved depth integrated Navier - Stokes and solute transport equations, and was able to examine changes in water levels, flow velocity distribution, suspended sediment levels and faecal bacteria levels for a number of values of power extraction. Bed elevation data was found from bathymetry

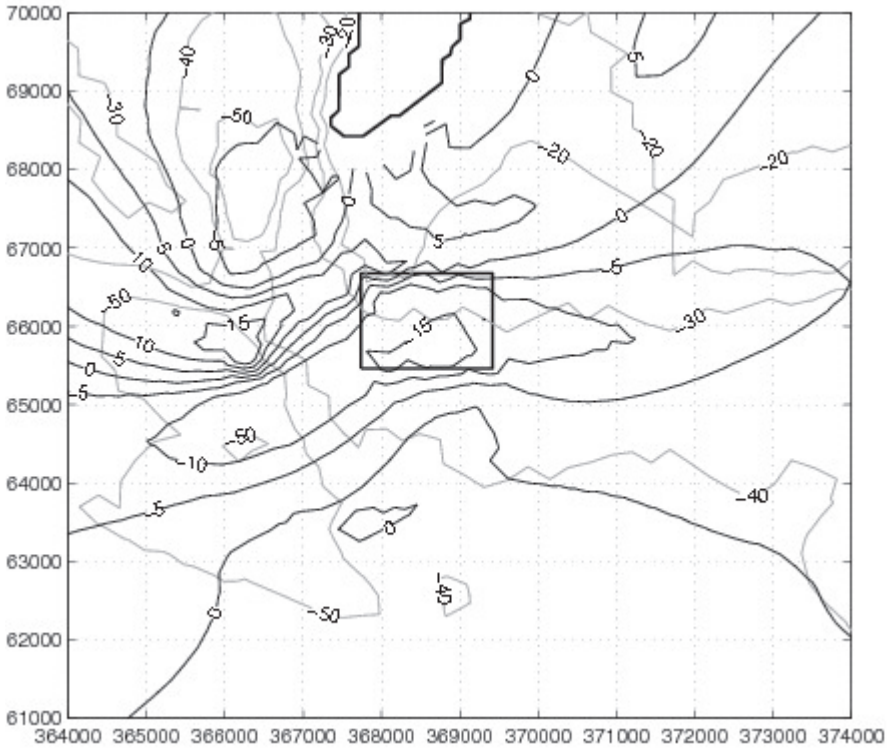

Figure 2.15: Percentage change in flow velocity due to energy extraction at Portland Bill from Blunden and Bahaj [2007]

data on admiralty charts, and publicly available volumetric flow rates from a number of rivers flowing into the Severn Estuary were also included in the model. The model was validated by examining field data of water elevations and flow velocity from sites in the estuary and comparing these with those predicted by the model. The model was shown to agree quite well with measured field data, as demonstrated by figures 2.17 and 2.18 which display the water elevations and current speeds predicted by the model at a location in the model flow domain known as Southerdown, one of two validation sites used in the study.

The inclusion of 10m diameter tidal turbines was then carried out by revising the momentum equation in the shallow water equations to include the axial force and drag forces acting on the turbines in the region where tidal turbines were assumed to be present. The specific area was chosen purely for model demonstration purposes, and the authors acknowledge that no specific criteria, such as flow velocity or proximity to grid connection, were considered. After simulation of turbines, some of the major conclusions included:

- Changes in water levels due to power extraction were quite small, with reductions of less than 10cm in areas where mean flow depth was 20m (a 0.5% change).
- Reductions in flow velocity of up to 25% in regions upstream and downstream of the array, but also increases in regions surrounding the sides of the array (figure 2.19).
- There were noticeable changes in suspended sediment and faecal bacteria levels in the region up to 15KM away from the tidal array, although no specific numbers are given.

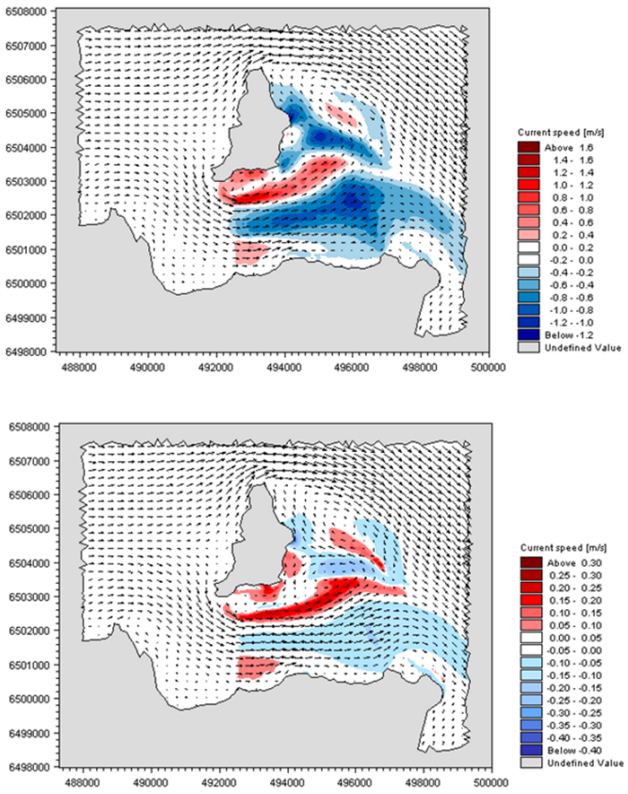

Figure 2.16: Effects of energy extraction of 900MW (top) and 160MW (bottom) predicted from MIKE21 model of Easton [2010]

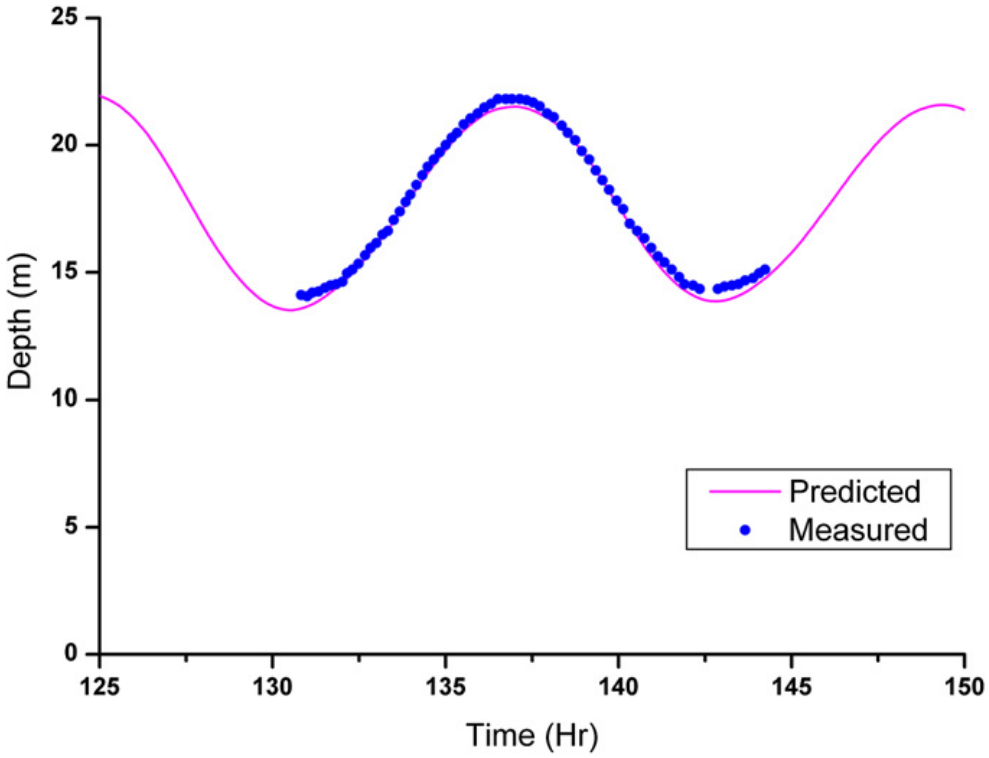

Figure 2.17: Comparison of predicted and measured water elevations at Southerdown site from analysis of Ahmadian et al. [2012].

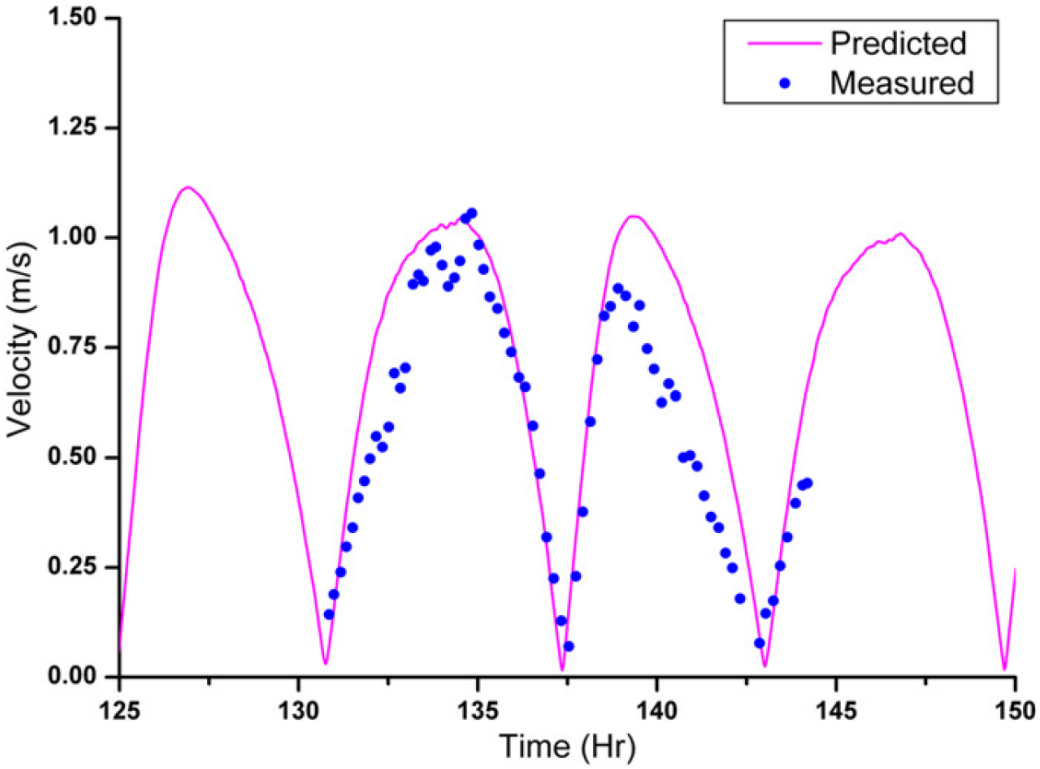

Figure 2.18: Comparison of predicted and measured current speeds at Southerdown site from analysis of Ahmadian et al. [2012].

The reduction in flow velocity downstream of turbines shown in these studies is a phenomenon which has received wide attention from the academic research community. Literature from Myers and Bahaj (2010) and Maganga et al. (2010) have demonstrated that this region of slow moving fluid, and understanding the processes which govern its recovery have been the subject of extensive research. However each of these reviewed studies show that, consistent with linear momentum theory applied in a constrained flow, a bypass flow with velocity greater than the ambient flow develops between an array and a flow boundary. Although there appears to be little examination of this particular region, its potential significance is discussed by Blunden and Bahaj (2007). They state that it may have implications for sediment transport, a process which is quite sensitive to flow velocity and fluctuations. This increase in flow may also be important in examining other natural processes such as cliff erosion and fish migration. Tidal developers are also likely to have great interest in what implications these flow current changes may have to the power output of a tidal array of fixed layout and rated power.

Easton (2010) has also shown this flow velocity increase to be dependent on the level of power extracted by tidal turbines. But despite the significance of the flow velocity increase acknowledged by Blunden and Bahaj (2007), two areas which may affect this increase which have not been examined are:

- How the increase in flow velocity in this constrained region is dependent on array size, and hence channel blockage ratio.
- How the increase in flow velocity is dependent on the proximity of the array to the flow boundary of the channel.

In addition to these, there are also other questions which still remain despite the advances

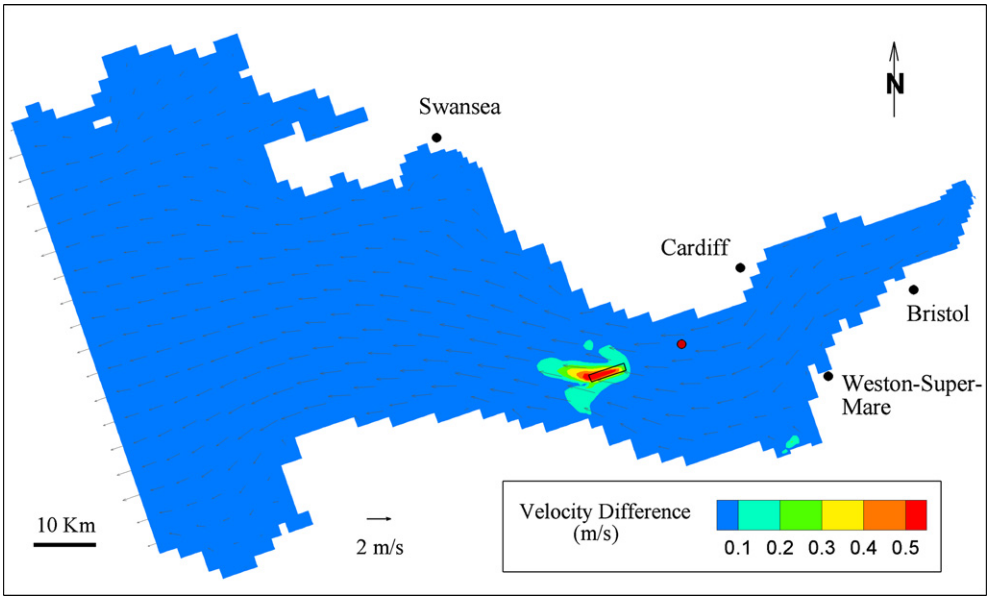

Figure 2.19: Changes in flow velocity in the Severn Estuary due to tidal turbines examined by Ahmadian et al. [2012]

made by these analyses, and which are likely to be of significant interest to tidal developers wishing to extract the resources of these or other sites.

- Whether there is a certain size or position of a row of turbines which results in excessive blockage of flow in the region between the turbines and a nearby flow boundary, and hence a reduction in flow velocity compared to ambient conditions in this region.

- How would changing the proximity of the array to flow boundaries affect its own performance in terms of power output.

- What if any changes to the wake region of the array would occur with changes in proximity to flow boundaries, and what implications might this have for further tidal turbines which may be installed further downstream.

2.3.2 Site specific split channels

The two analyses mentioned in the previous section demonstrated some of the changes to flow regimes which occur for tidal turbines. However these were in sites with relatively simple bathymetry, which consisted of an open channel bounded by either one or two land boundaries. Analysis of the effects of tidal turbines is likely to be more complex in areas where split tidal channels are present. This can mainly be due to diversion of flow between sub channels, as referred to in the analytical models of Atwater and Lawrence [2010] and Cummins [2013]. But the large amounts of energy available at certain split channel sites has meant analysis of some of these sites has still been attempted. Once again, numerical models have proved very useful in this respect.

An examination of a large area of Johnstone Strait, Canada was carried out by Sutherland et al. [2007]. Within Johnstone Strait lies Current Passage, the channel where Atwater and Lawrence applied their analytical model to determine the maximum extraction efficiency and hence extractable power. The specific area examined covers just over $19000km^2$, and is displayed in figure 2.20. The aim of the analysis was to use a numerical model to simulate tidal turbines in three regions of the domain and to examine the maximum power potential and the far field effects of tidal power extraction in each case. The three regions, specified in figure 2.20 were Northwest Johnstone Strait, Discovery Passage and Cordero channel. The numerical model used was TIDE2D, a 2D solver which solves the 2D shallow water equations in the simulated domain, similar to the TELEMAC model used by Blunden and Bahaj (2007). The mesh for the solver was created using acquired bathymetry and coastline data for the region and TRIGRID, a grid creator for the TIDE2D model. The authors used a similar method to Easton (2010) and Blunden and Bahaj (2007) for simulating the presence of tidal turbines, namely an increase in bed friction in certain regions of the numerical grid. The authors used the following expression to relate added bottom friction to power dissipated:

$$P_t = \frac{k_t}{k_o + k_t} P \tag{2.29}$$

Where P represented the natural power dissipation due to natural bed friction given by:

$$P = \int \int_A \rho C_d U^3 dA \tag{2.30}$$

Where C_d represented the quadratic bed drag coefficient and dA was an elemental area of the seabed. To examine the maximum power potential of any channel, the bed friction due to turbines k_t was continually increased and the volumetric flow rate in the channel recorded. The volumetric flow rate at each recording was then inserted into the following expression, developed by Garrett and Cummins [2005]:

$$\frac{P}{P_{max}} = \left(\frac{3^{\frac{3}{2}}}{2}\right)\left(\frac{Q}{Q_{max}}\right)\left[1 - \left(\frac{Q}{Q_{max}}\right)^2\right] \tag{2.31}$$

To validate the numerical model, the authors initially close off other channels and assume all flow is diverted directly through the Discovery Passage channel. They then compared the maximum power from the model to an analytical expression also developed in the same Garrett and Cummins reference, where for a single channel the maximum power potential is given by:

$$P_{max} = \gamma \rho g s Q \tag{2.32}$$

where γ is a coefficient between 0.2 and 0.24. The authors found that the model predicted power output in Discovery Channel, when all other channels are closed off, of 886MW, which agreed to within 10% of the figure of 826MW predicted by the application of equation 2.32. Subsequent to this, tidal turbines were also simulated in Discovery Passage without closing off other channels, and also in Cordero Channel and North-western Johnstone Strait. Some of the main conclusions of the analysis included:

- The maximum power potential of North-western Johnstone Strait according to the model was 1335MW, which agrees remarkably well with the 1320MW predicted from equation 2.32.
- The maximum power potential of Discovery Passage, in the natural case where flow is not directly entirely through it, was 401MW. This is considerably lower than the 886MW value predicted by the model in the case of flow diverted entirely through it.
- When the volumetric flow rate which achieved the 401MW value was inserted into equation 2.32, the equation predicted a power available of 573MW. Thus there is a discrepancy between theory and the model of approximately 30%.
- When the same analysis was carried out with turbines simulated in Cordero Channel, the model predicted a power of 277MW and equation 2.32 predicted a power output of 598MW. This meant a discrepancy of 54%.

The last three main conclusions have clearly shown conventional analytical theory developed for open channels to be inapplicable to split channels. They have also shown the diversion of flow between sub channels, and the resulting changes in volumetric flow rates in certain regions of the domain, to be significant drivers of power output. This analysis has then

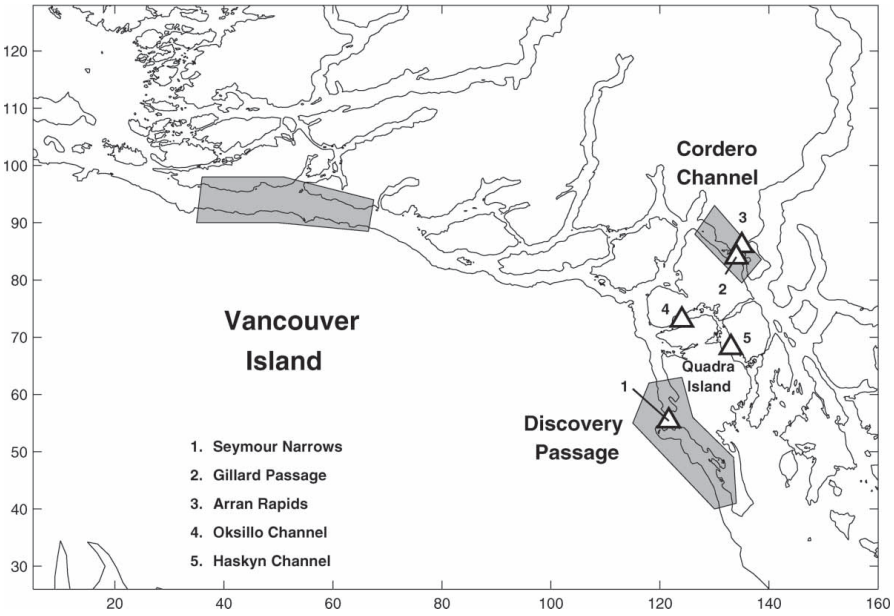

Figure 2.20: Area of Johnstone Strait and specific channels where tidal power extracted is simulated in analysis of Sutherland et al. (2007)

justified the development of analytical theory specifically for split tidal channels carried out by Atwater and Lawrence (2010). In the context of the work proposed for this PhD project, a very crucial assumption made by the authors was that tidal turbines occupied the entire cross section of the channel in which they were simulated. It is possible that if turbines only occupied part of the channel in each case, the diversion of flow and distribution of volumetric flow rate may have been very different. As demonstrated both by this analysis and by Atwater and Lawrence, this could have implications for the power which tidal developers could potentially exploit in these split channels.

Another site specific split channel was examined by Polagye et al. [2009]. The site examined by these authors was Puget Sound in Washington State, USA. For the purposes of this study, the authors idealised the entire site examined into a network of 37 channels of constant cross sectional area, as shown in figure 2.21. A modelling approach developed in Polagye et al. [2008] was used. This involved taking the shallow water equations and applying a finite difference approximation using what the authors describe as a "predictor-corrector MacCormack algorithm". This then placed the governing equations in a form which could be applied to estimate changes due to power extraction in a channel of fixed geometry. Tidal power extraction was accounted for by including in the equations a discontinuity in the following energy compatibility relation across the plane of extraction:

$$\frac{U_1^2}{2g}(1-k_1)+h_1=\frac{U_2^2}{2g}(1-k_2)+h_2 \tag{2.33}$$

Where k here is an energy extraction coefficient given by:

$$k=\eta\frac{A_t}{A_c} \tag{2.34}$$

Where $\frac{A_t}{A_c}$ is the blockage ratio of turbines across a channel and η is a turbine coefficient

of performance.

To create the model of the Puget Sound region, the authors used publicly available bathymetry data and interpolated it onto a 250m grid, and for each segment of the overall domain, mean depth, surface area and effective length. Segment depths were adjusted such that at rest, each segment had a water depth of mean sea level. To calibrate the initial model, the tidal amplitude and phase of six tidal constituents in the model were compared to observed values on the ground at 43 locations, as well as comparing the amplitude of the M2 tide and kinetic power density in major basins of Puget Sound. Once the model was calibrated, tidal power extraction was simulated in two areas of the domain, Admiralty Inlet and Tacoma Narrows.

Once again, this analysis makes the assumption, similar to much reviewed literature already discussed, that the blockage ratio of the tidal array in each case is fixed (1/3rd) and only one location in each is considered. They also assume the fence is distributed uniformly across the channel. As well the lunar semi diurnal (M2) tide, the authors also examined effects on the lunar diurnal (K1) tide. The K1 tide is one which results due to an imbalance in the two M2 tides daily, and has a period of just under 24 hours. (Internet Ref) The results of the analysis suggested that for the first case, where 400MW of power was extracted from the Admiralty inlet channel:

- The amplitude of the M2 tide was reduced by 10%, and reduced in the K1 tide by 5%
- The phase of the M2 tide lagged by 10 degrees and the K1 tide lagged by 2 degrees.
- The cumulative transport reduced by 10%.

For tidal extraction in Tacoma Narrows of 100MW:

- The amplitude of the M2 tide reduced by 6%, and reduced in the K1 tide by 2%
- The phase of the M2 tide lagged by 2 degrees and the K1 tide lagged by 0.5 degrees.
- The cumulative transport reduced by 4%.

This analysis has given some insight to tidal developers of what far field effects can be expected from tidal extraction in Puget Sound. But the analysis has only considered a blockage ratio of of a third of the vertical section of the channel, a uniform distribution of turbines across the channel cross section and has not considered any change to lateral or longitudinal position of the energy extracting devices.

Common gaps in the knowledge of the specific split tidal channels in both of these site specific analyses can be identified. Neither have examined the implications for the flow regime or power extraction, with regard to partially blocking a channel or changing the lateral position of a partial fence. The continuity principle, along with the theory of Atwater and Lawrence, strongly suggests that reducing or increasing the area of a channel blocked by turbines will affect volumetric flow rate in other regions. It is also unclear whether changing the longitudinal position of turbines with respect to the front or rear of impenetrable land masses would have in some way changed the distribution of the volumetric flow rate

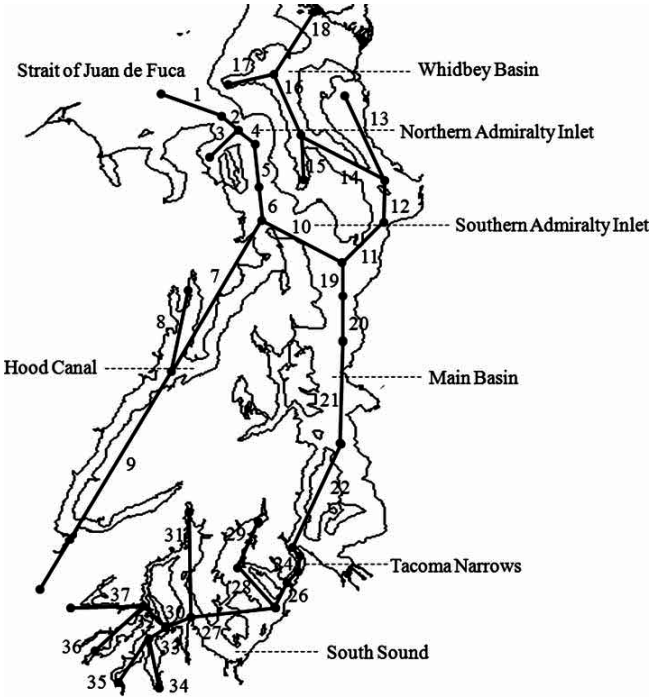

Figure 2.21: Idealisation of Puget Sound region into channels of constant cross section by Polagye et al. (2009)

throughout the system. It is certainly plausible that the specific point at which the retarding forces on the flow associated with extraction act may affect the distribution of volumetric flow rate throughout the system.

2.4 Wakes of tidal turbines

The extraction of power by tidal turbines causes a major decrease in the flow velocity in the region immediately downstream. This occurs due to the extraction of energy from the flow and the restriction of mass flow through the tidal turbines. This region of slow moving fluid gradually recovers to freestream conditions at some point due to turbulent mixing with freestream flow surrounding it re-energising this region. This section of fluid immediately downstream of tidal turbines is commonly referred to as the wake.

2.4.1 Wakes of individual tidal turbines

Experimental work to examine the development of the wake of a tidal turbine was outlined by Maganga et al. [2010]. The experimental analysis was carried out in a flume tank with a 0.7m tidal turbine rotor. According to the authors, this gave a blockage ratio of 5% of the flume tank area. Rotor performance was examined using three and six component load cells, while flow velocity was measured using a Laser Doppler Velocimeter (LDV). The authors examined how certain alterations to the flow conditions affected both the performance of the rotor and the development of the wake downstream. The specific flow alterations made were:

- Ambient turbulence intensity levels of 8% and 25%. Turbulence intensity was controlled

in the experiments via honeycomb straighteners at the inlet of the tank.

- A transverse left to right velocity gradient across the width of the channel of 8%.
- Each of the above conditions with the rotor axis placed at depths of 0.3, 1.57 and 2.04 turbine diameters from the free surface.

The parameter the authors used to quantify the effects of the wake and its recovery downstream was the velocity deficit, given by:

$$U_{deficit} = 1 - \frac{U_w}{U_\infty} \tag{2.35}$$

While the performance of the turbine rotor was examined using the non-dimensional measure of thrust coefficient, given by:

$$C_T = \frac{T}{\frac{1}{2}\rho U^3 A} \tag{2.36}$$

Some of the main conclusions the authors made from the results of their analysis included:

- The transverse velocity gradient of 8% did not affect the power output of the rotor, despite theoretical calculations suggesting the contrary.
- Higher ambient turbulence intensity resulted in greater fluctuations of thrust across the rotor over a given time period. The authors suggested that this would lead to greater fatigue loading on full scale turbines. This would inevitably affect their lifespan and the point at which failure may occur.
- The power available from the rotor in the 25% ambient turbulence intensity case was 15% lower than the case of 8% ambient turbulence.

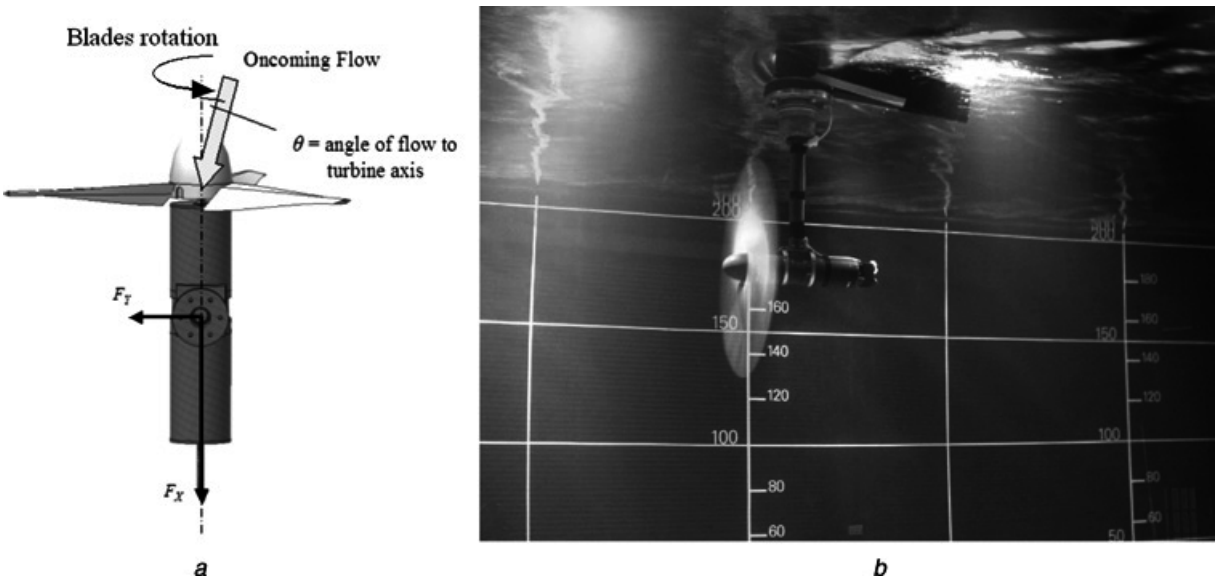

Figure 2.22: 0.7m diameter rotor examined by Maganga et al. [2010].

- Despite these issues associated with higher ambient turbulence, it did result in quicker recovery of the wake downstream of the rotor. In the case of 8% turbulence, 80% velocity recovery was achieved 9 turbine diameters downstream. However this same level of recovery was achieved at 3 diameters downstream in the case of 25% ambient turbulence.

- The authors found changing rotor depth did not effect the turbines measured power output.

A small scale analysis of the factors affecting tidal turbine wake development was also carried out by Myers and Bahaj [2010]. The authors presented the results of experimental analysis in a circulating water flume at the University of Southampton. In contrast to the aforementioned analysis, tidal turbines were represented by porous actuator discs. These were simply circular plates occupying one third of the depth of the flow in the water channel, which had holes drilled in to allow some flow directly through them. Some of the factors the authors used to justify the use of these porous media over scaled rotors were:

- Modelling of full scale rotors would have been impractical due to difficulties with accurate tip speed scaling and the swirl effects and large pressure gradients which would be introduced.

- The main differences between porous media and rotors would only be evident in the near wake region, which is up to 5 diameters downstream. Beyond this in the far wake region, studies with both wind and tidal energy had shown no major difference between rotors and porous media. One such example is given by a numerical modelling study by Masters et al. [2013]. Here the authors compared the results of flume testing with porous media against CFD models which used blade element momentum theory to incorporate blade profiles and the swirl effects associated with turbine blades. The results of this analysis showed good agreement, in the far wake region, between actuator discs in experiments carried out by Myers and Bahaj [2012] and tidal turbine rotors simulated in the blade element momentum model.

- Thrust coefficient was equally applicable to both rotors and porous media. It could therefore be used to apply the results of experiments to real life tidal turbine installations.

For their experimental analysis, the authors used Acoustic Doppler Velocimeters for measuring flow velocities at various points throughout the flume. These freestream flow rates were subsequently used to normalise against subsequent velocity measurements at the exact same points taken in the wake of actuator discs in experimentation. Thrust measurements to allow subsequent calculation of C_T were recorded by load cells. Initially velocity measurements were taken with the water flume empty to determine ambient flow conditions with no actuator disks present. The three main areas which the authors then investigated included:

- What if any changes occurred to the wake of the actuator disc as the thrust coefficient of the fence used was altered.

- What if any changes to the surrounding flow environment occurred as the depth of the flow at which the actuator disc was placed was altered.

- What if any changes occurred as the ambient turbulence intensity of the flow towards the bed of the flume was altered.

For the final part of the analysis, greater ambient turbulence and shear was induced by placing rough sediment along a section on the floor of the flume. Some of the main conclusions of this analysis included:

- Changes to the C_T values of the actuator discs did not result in any measurable change in velocity deficit beyond 7 diameters downstream of the actuator disc.

- When the actuator disk was placed deeper in the flow, there was slower wake recovery and the wake persisted further downstream (Figure 2.23). It was postulated that this occurred due to a reduced mass flow rate beneath the disc being available to re-energise the wake.

- The increased ambient turbulence caused by roughening of the bed of the flume did not reduce the persistence of the wake downstream in the bed region. This was in contrast to other works reviewed by the authors and the analysis of Maganga et al. [2010], which showed greater ambient turbulence leading to greater wake mixing and quicker wake recovery. The authors postulated that this was due to the fact that despite the higher turbulence intensity, the flow was still very slow moving in this region towards the bed of the flume.

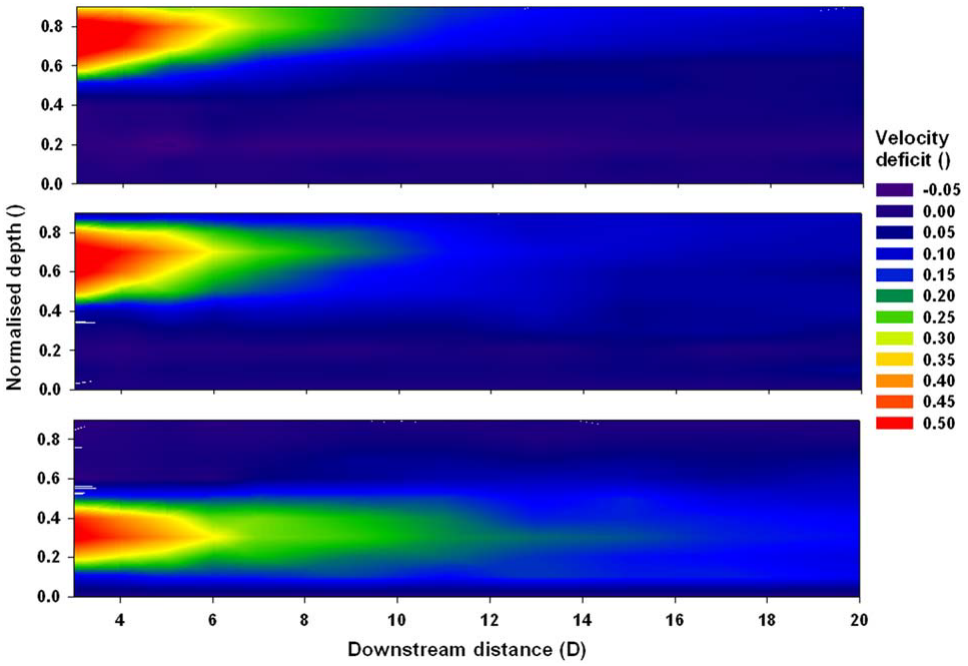

Figure 2.23: Changes to actuator disc wake with change in depth demonstrated by Myers and Bahaj [2010].

An interesting common area of investigation in both of these studies was the examination of changes in turbine performance with changes in flow depth. The results of Maganga et al. appear to suggest that turbine power output is not affected by depth, while Myers and Bahaj showed slower wake recovery with smaller proximity to the bed of the domain in which the rotor was placed. As well as for single rotors, the effects of proximity to surfaces will also be a crucial parameter in tidal turbine rows.

However an additional variable in tidal arrays which may affect their performance, and also downstream flow conditions, is the proximity between individual rotors within an array. This parameter was the subject of an investigation by Stallard et al. [2013]. The authors used scaled down tidal turbine rotors of 270mm diameters in a circulating water flume to examine how changing the lateral spacing between rotors in an array affected the level of mixing between the rotor wakes and the freestream. Flow measurements were taken using acoustic Doppler velocimeters in a 5m wide and 12m long water flume at the University of Manchester. Thrust measurements were also taken using strain gauges, however thrust results were the subject of a separate study and so were not reported. The wake of a single rotor was examined initially, and then compared to downstream conditions from the array configurations displayed in table 2.1. Some of the main conclusions from this study included:

- For a single individual rotor, the authors found that the velocity along the central lateral plane of the rotor was 80% lower than ambient conditions at 2 diameters downstream, 20% lower at 10 diameters downstream and 10% lower 20 diameters downstream.
- A lateral separation distance between rotors of 3 diameters resulted in the wake of each individual rotor being very similar to that of an individual rotor.
- Considerable changes were observed with lateral spacings of 2 diameters or less. The wakes of each individual rotor began to merge together, to eventually result in a single wake at approximately 4 diameters downstream of a row of rotors.
- Close lateral spacing did not appear to change centreline velocity recovery, but did result in higher maximum turbulence intensity. With close spacing, maximum turbulence intensity was 18%, as opposed to 15% in the case of an individual rotor.
- After wake merging, the width of the outermost rotor wake expanded from 1 diameter to 2 diameters at a longitudinal position of 10 diameters downstream of the rotors.
- With lateral spacings of 2 diameters or less, the outermost rotors displayed an asymmetrical wake profile, while the central rotor wake recovered quicker to freestream conditions.
- The authors also examined the effects of waves on wake recovery, and concluded that the velocity deficit immediately downstream of the rotor was lower than without waves. This is most likely due to greater turbulence intensity due to the action of waves on the surface.

Each of these studies made very novel contributions to knowledge of the wakes of tidal turbines and how they develop and dissipate. One of the most interesting in the context of

No. of rotors	First row	Row spacing	Second row
1	1	-	-
2	2 at 1.5D	-	-
2	2 at 2D	-	-
2	2 at 3D	-	-
3	3 at 1.5D	-	-
3	3 at 2D	-	-
3	3 at 3D	-	-
5	5 at 1.5D	-	-
6	3 at 1.5D	8D	3 at 1.5D
6	3 at 2D	8D	3 at 2D
7	3 at 1.5D	4D	4 at 1.5D
7	3 at 1.5D	8D	4 at 1.5D
8	5 at 1.5D	8D	5 at 1.5D

Table 2.1: Tidal array configurations examined by Stallard et al. (2013)

this particular project is the effect of turbulence intensity. Ambient turbulence intensity was demonstrated by Maganga et al. to be one of the critical parameters governing wake recovery. However Myers and Bahaj demonstrated that higher turbulence intensity was in itself not sufficient for quicker wake recovery. According to their postulation, higher turbulence intensity must be accompanied by sufficiently quick flow velocity and mass flow rate in regions between the tidal rotor and flow domain boundaries. Looking at wake turbulence intensity, Stallard et al. results suggested that spacing between individual rotors also had an influence on level of turbulence intensity within the rotor wake, which Maganga et al. demonstrated is an important parameter when examining fatigue loading of turbines further downstream.

All of these studies also give some conclusions of changes to both wake and turbine performance with proximity to certain boundaries. The results of Myers and Bahaj suggested positioning closer to the bed of a channel would lead to slower wake recovery, while Stallard et al. also showed that the proximity of tidal turbines to other turbines within an array had a considerable effect on downstream flow conditions, including the width of the wake. In a real tidal channel, these downstream flow conditions will have a considerable influence on environmental effects associated with operation of turbines, and well as the performance of other rows of turbines further downstream in a channel. Maganga et al. went further by examining the thrust on turbines, appearing to conclude no change in thrust and power output of turbines when positioned closer to the bed of a channel.

Despite the advances made by these studies, some aspects of tidal turbine wakes remain unclear.

- It is not clear whether the longer and more persistent wake which the work of Myers and Bahaj suggested would occur by placing turbines deeper in a channel (and hence closer to flow bed) would also hold for placement of turbines (or rows of turbines) closer to lateral channel flow boundaries.

- There is no analysis of where increases in flow velocity may occur in the regions around the turbine rotor. There is also no indication of how large these increases might be

depending on specific position of turbines. Any increase would have implications for the placement of tidal turbines or rows of turbines in other areas of the flow domain as part of a tidal array.

- It is unclear whether the changes in turbulence intensity within the wake itself demonstrated by Stallard et al. might also occur if turbines were positioned close to solid channel boundaries.

- There is no examination of whether the observed effects of these will also occur with higher blockage ratio turbines.

Much of the scope of the current work has been determined on the basis of these identified gaps. The reviewed studies have also helped to determine the methodology used. The use of porous media by Myers and Bahaj, and the justification given, has also been used in this study due to its modest resources. Discs were used to represent single turbines in this study. It is also possible to use several of these devices to replicate rows of tidal turbines, but doing so does present certain challenges. Using discs of a similar size to those used in these reviewed studies (100mm diameter) to replicate a row of turbines would require very wide experimental facilities, and would also involve a considerable amount of machining. It may be possible to use much smaller discs, however machining these would still present a strain on project resources. However as the next section will demonstrate, an alternative to actuator discs is available for specifically examining rows of tidal turbines.

2.4.2 Wakes of rows of tidal turbines

A rectangular shaped porous media, referred to henceforth as an actuator fence, presents an alternative to several actuator discs for modelling rows of turbines. Actuator fences have the same effect on fluid flow as actuator discs, namely a change in fluid momentum and dissipation of kinetic energy through small scale turbulence. Many small scale studies, such as Whelan et al. [2009] and Harrison et al. [2008], have used rectangular actuator fences to model rows of tidal turbines in experimentation.

The work of Whelan et al. [2009] was carried out to develop a theoretical blockage correction model. The authors discussed how many blade element momentum (BEM) theory and Navier Stokes models were successfully used to examine the performance and flow behaviour of wind turbines. However these all disregarded blockage effects, which needed to be accounted for in the case of tidal turbines due to the constrained nature of the tidal resource. The authors therefore developed a model which would correct the results of BEM codes, and thus give the enhanced performance results compared to unblocked flow.

Before developing their model, the authors made the following assumptions about the flow:

- Crossflow velocities were negligible.

- Flow was homogeneous in the transverse direction.

- The turbines were fully submerged.

- The flow was separated into a flow streamtube which travelled through the rotor, and also flow around the rotor (or bypass flow as the authors refer to it).

- The bypass flow was uniform.

The authors then applied fundamental theory, such as the continuity principle, Bernoulli's equations and the momentum equation to both the bypass flow and streamtube of fluid through turbines to determine a quartic equation. This quartic equation related Froude number and blockage ratio to coefficients relating wake and bypass flow velocity to freestream flow velocity. These coefficients could then in turn be used to predict both thrust and power coefficient for a given combination of Froude number, blockage ratio, wake and bypass flow velocity.

In order to validate the developed model, the authors carried out experimental tested using porous media in a circulating water flume. The authors tested both an actuator disc, similar to that used by studies mentioned in the previous, and also a porous strip made of the same material as the disc. The reasoning behind the testing of an individual disc was to examine if the model would predict enhanced performance of a single turbine in an array. However the strip was also tested, as the authors also wished to determine if their correction model would also apply to groups of turbines where spanwise homogeneity of the flow could be assumed. In the testing, the authors carried out force measurements on both the disc and strip, each with a blockage ratio of 0.33 working in flow conditions with Froude numbers between 0.1 and 0.3. The authors found that the disc and strip displayed similar thrust coefficients at higher Froude numbers, but thrust coefficients were dissimilar (approximately 1.1 for a disc and 1.3 for a strip) at the lowest tested Froude number. This discrepancy at low Froude number was claimed by the authors to be attributed to an absolute error in thrust readings giving a larger relative error at low Froude number. In terms of the accuracy of the free surface blockage model, the results (displayed in figure 2.24) appeared to show a discrepancy between predicted and measured thrust coefficient of about 10%. Further on in this work, the authors attempted to further examine their model by inserting it into a standard BEM code, and comparing the results of the BEM code in both a blocked and unblocked case with experimental results for a full rotor in both a water flume (blocked case with blockage ratio 0.64) and also in a wind tunnel (blockage ratio 0.05, assumed unblocked case). The results suggested that the blockage correction predicted the thrust and power coefficient of the rotor in the blocked case with "reasonable agreement" at low tip speed ratios. However this agreement broke down at higher tip speed ratios due to due reversed flow in the wake (or "brake state") and the inability to apply Bernoulli's theorem in this case.

The most important aspect of this work in the context of the research presented herein is the use of both a disc and porous strip in experimentation. The agreement in thrust values between these under the same Froude number and with the same blockage ratio gives support to the use of strips (herein referred to as actuator fences) to simulate the loss in energy in the flow associated with tidal turbine power extraction. Therefore where the flow effects of a large row of turbines are being examined, these actuator fences may represent a simpler alternative to several individual porous discs.

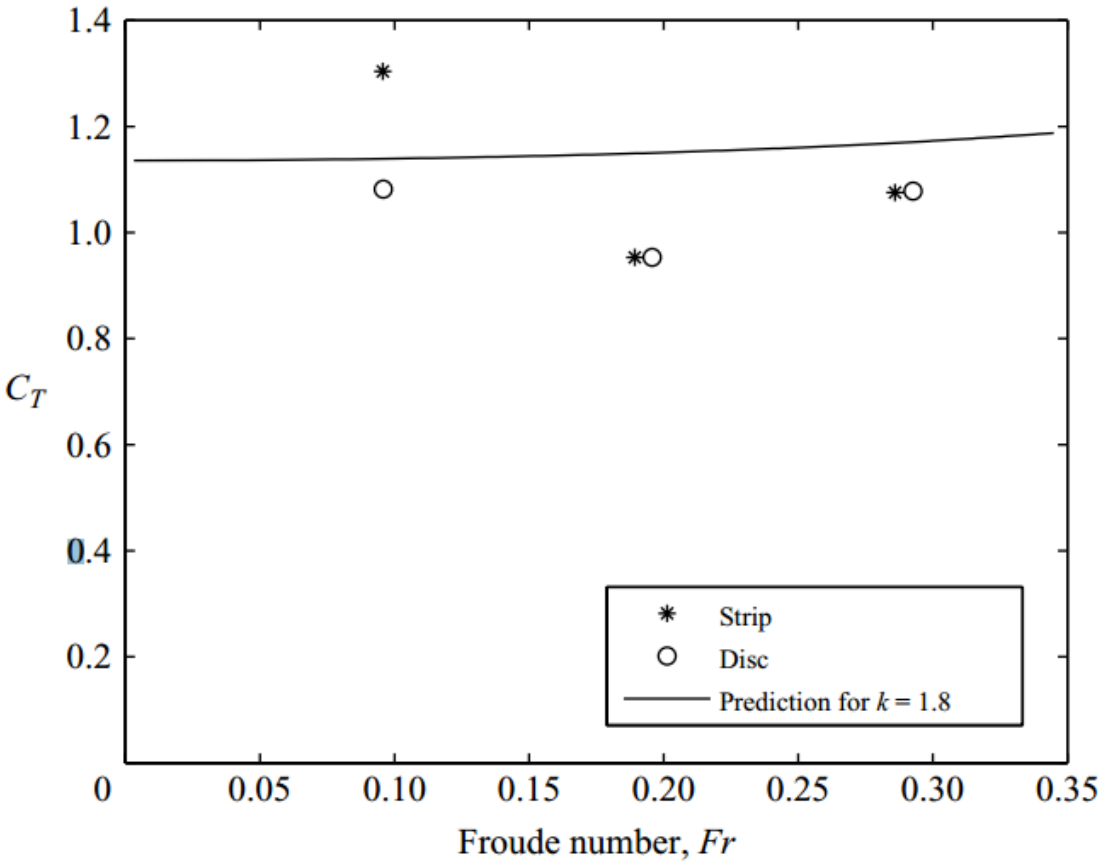

Figure 2.24: Thrust coefficient results of results by Whelan et al. (2009)

The use of actuator fences to simulate rows of tidal turbines is also presented in the work of Harrison et al. [2008]. The purpose of this study was to examine possible techniques which could be used to model tidal turbines computationally. The authors particularly focus on examining the validity of what is referred to as a "boundary layer model" for examining the wakes associated with tidal turbines. The authors discuss two computational methods for examining the performance of both wind and tidal turbines, namely a field model and boundary layer model. A field model is a numerical solving of the Navier Stokes equations across a set of finite volumes, which together form the entire geometry of the flow field being examined. The problem is simplified by time averaging the solution and also including turbulence models to estimate the turbulence structure of the flow. However in the case of wind turbines, the model makes no assumptions about the vertical velocity profile. In contrast, the "boundary layer model" makes a number of assumptions, such as:

- A logarithmic velocity profile in the case of wind turbines.
- The effect of turbines on the surrounding flow field is examined by assuming an initial ground roughness, which is then increased by the turbines depending on the number of turbines and amount of power they extract and generate.
- A tidal array can be assumed to have uniform roughness across its area.

However due to the more constrained nature of the environment in which tidal turbines

operate, applying the same boundary layer model to both wind and tidal turbines may not necessarily be valid. The purpose of the computational and experimental work carried out by Harrison et al. was to compare the performance of many rows of tidal turbines found from both methods, and then discuss the possible implications of the results for the use of boundary layer models in research on tidal turbines.

The experimental method involved using porous actuator fences in a circulating water flume to represent a row of tidal turbines. The authors initially discussed previous studies which used porous discs, and then discuss the fundamental differences between both. The main differences would be the vortices generated off the edges of both, and also the fact that porous fences would be unable to replicate the effects of turbine spacing and the flow between turbines in an array. However the differences in vortex structure would not lead to inaccuracies when examining the far wake of an array, as these vortices have been shown to be fully dissipated approximately 4 diameters downstream. With regard the turbine spacing issue, this difference would not lead to inaccuracies provided the row of tidal turbines being examined is closely packed and has close spacing between rotors relative to the overall size of the channel. In closely packed arrays, wakes of individual turbines would all merge together to give a single array wake.

In experiments, a total of four actuator fences, with porosity of 0.9, were placed downstream of each other in a circulating water flume. The longitudinal spacing between each fence was 7 fence diameters. The authors initially examined flow conditions downstream of a single fence, and then repeated this for the case of 2, 3 and 4 fences 7 diameters downstream of each other. Force measurements were taken on each fence, while flow measurements were also taken throughout the width and depth of the flow at several positions downstream of each fence using an Acoustic Doppler Velocimeter. The computational analysis involved the use of Ansys CFX modelling software. An exact replica of the experiments in the circulating water flume were simulated. The Menter shear stress transport turbulence model was used as the closure model for the Navier Stokes equations, while the actuator fences themselves were modelled as porous domains within the flow volume. These porous domains were applied with a momentum loss given by the following expression:

$$k = \frac{C_T}{\partial x_i} \tag{2.37}$$

where ∂xi is the thickness of the actuator fence and k is a momentum resistance coefficient applied to the CFX boundary conditions.

Some of the main conclusions from this research included:

- Recovery of velocity over a shorter distance downstream occurred in multiple fence scenarios compared to a single fence case. This was postulated to occur due to increased turbulence intensity downstream of each fence in multiple fence cases.

- Reasonable agreement was found between modelled and experimental velocity deficits, although there were some differences in velocity profiles in both the wake and freestream. This was postulated to be due to lower bed shear stress in the computational model.

- Although specification of the correct pressure drop in the CFX simulation to achieve the correct thrust coefficient was difficult, general trends in thrust coefficient values with fence number were similar between the model and experiments.

- The authors concluded that the reasonable agreement between experiments and the field model gave a preliminary validation of the use of distributed roughness, as assumed by a boundary layer model, in modelling tidal turbines.

The above studies have clearly demonstrated that porous fences can be used to examine the wakes of groups of tidal turbines. For this use to be valid, two conditions must be met. Firstly, as with porous discs, only the far wake of the array can be examined due to the inability of porous media to simulate the vortex shedding off tidal turbine rotor blades. Secondly, as actuator fences cannot simulate the flow between individual rotors in a row of turbines, they can only represent rows where there is relatively close spacing between rotors such that individual rotor wakes merge into a single array wake. Provided these conditions are met, any changes to the far wakes of rows of turbines due to changes in flow conditions, row size or positioning of rows can be accurately examined in experiments with actuator fences.

The main justification for the use of actuator fences as opposed to series of disks in this research is the elimination of the inter device spacing variable. Changing the lateral distance between tidal turbine rotors has been demonstrated in previous work (such as Stallard et al. [2013]) to have a bearing on wake structure downstream. However the scope of the work presented herein was to focus solely on fundamental wake structure changes associated with both blockage ratio and specific lateral position of a row of turbines with respect to flow boundaries. It was felt that introducing the third parameter of inter device spacing using porous disks would not have allowed a fully in depth examination of any of these parameters, and that the significance of inter device spacing meant that this research could not have given it the attention it deserves.

2.4.3 Further studies on influence of upstream conditions

One of the most interesting findings of Maganga et al. [2010] was the influence of changes in turbulence intensity on the wake region development and power output of tidal turbines. This was not the only study to examine the influence of inflow conditions upstream of turbines to the development of flow conditions downstream, and the possible resulting implications for tidal developers.

An extensive examination of turbulence parameters in a tidal channel was carried out by Blackmore et al. [2014]. This paper gave the results of CFD modelling, which, as opposed to the traditional RANS solvers, used a large eddy simulation (LES) solver known as OpenFoam. As well as examining the effects of varying inflow turbulence intensity to an actuator disc, the study went deeper than Maganga et al. and other previous studies by also examining the integral length scales of the inflow turbulence. The length scale are defined by the authors as the characteristic length of the largest kinetic energy carrying turbulent eddies before dissipation by viscous effects (this is discussed further in section 2.5.9). The use of an LES solver was justified as, unlike RANS solvers which make a number of assumptions and

estimations on turbulence, LES is able to capture the transient effects of turbulence. Hence LES was necessary to examine the time dependent effect of the largest energy carrying eddies. The authors examined an actuator disc in a flow domain such as to ensure low blockage of 1.5%, as shown in figure 2.25.

Two inlet conditions were examined, one being a constant uniform velocity of 0.3m/s. The second was a grid pattern on the inlet boundary, with the flow past the solid boundaries of the grid generating turbulence intensity and length scale values which vary with downstream position from the inlet to the channel. Two grid patterns were used to create small scale turbulence with length scales less than 1/3rd of the disc diameter, and body scale turbulence with length scales greater than $\frac{1}{2}$ the diameter of the disc. The disc itself was also modelled as a circular grid, as shown in figure 2.26, to generate turbulence in the wake region, and was applied with momentum sinks to simulate the removal of energy from the flow due to power extraction by a turbine. The authors varied the inflow turbulence intensity and length scales to the actuator disc by varying the longitudinal position of the actuator fence with respect to the inlet. The parameters whose results they investigated with changes in turbulence intensity and length scales were:

- The value and specific position downstream of the disc of the maximum velocity deficit.
- The magnitude of u'u' and u'w' velocity fluctuations, which are related to the Reynolds shear stresses, which in turn indicate momentum transfer between freestream and wake fluid streamlines.
- The position laterally across the domain of the wake edge. The edge of the wake was assumed to be the point where the wake flow velocity was equivalent to 95% of the flow freestream velocity.

The main findings of this research were:

- An increase in ambient turbulence intensity reduces the maximum velocity deficit at

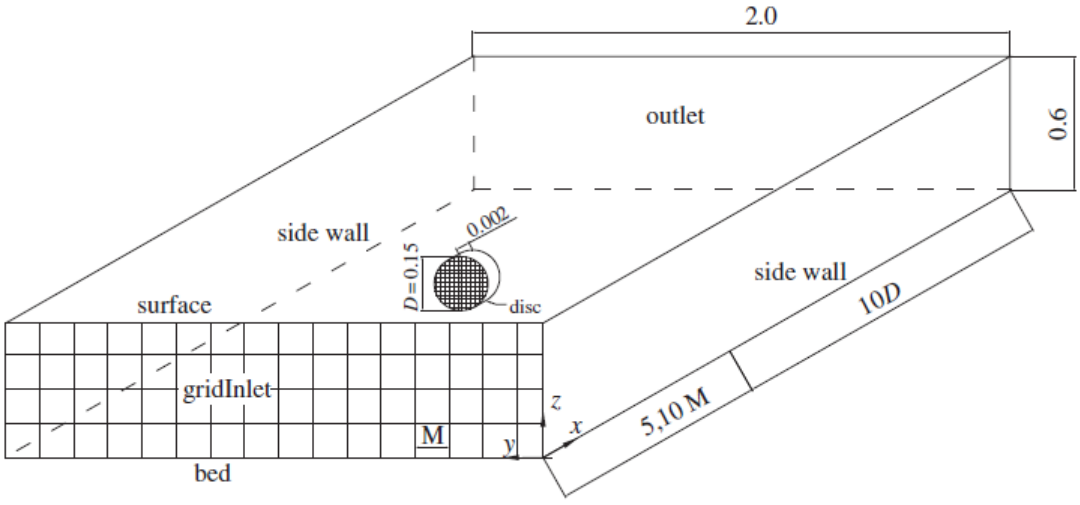

Figure 2.25: Flow domain examined by Blackmore et al. (2014)

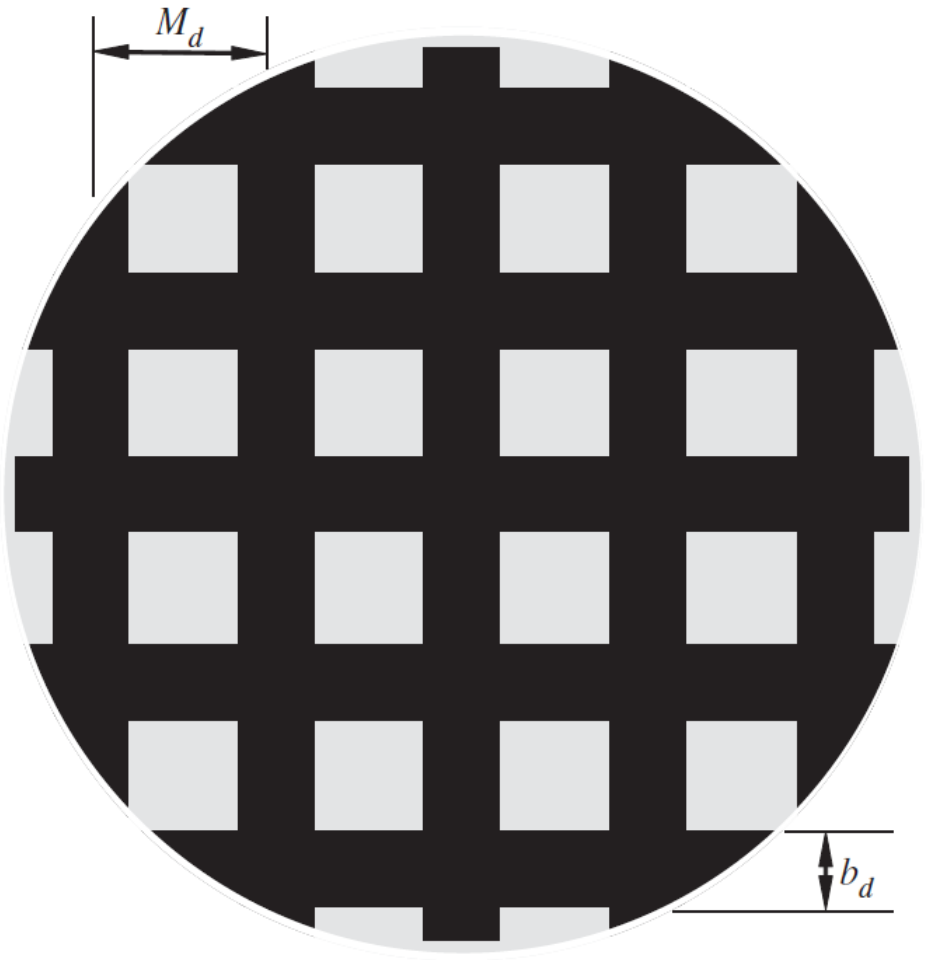

Figure 2.26: Actuator disc grid used for numerical modelling of Blackmore et al. (2014).

any given position downstream of the actuator disc. This is consistent with the analysis of Maganga et al. [2010].

- Increasing the integral length scale was found to increase the velocity deficit in the near wake, and resulted in quicker recovery of the wake to freestream conditions downstream of the actuator disc.
- Increasing the integral length scale was found to increase the width of the wake. However turbulence intensity changes were not found to have any influence on wake width.
- The authors compared their results to published experimental literature, and found good agreement with measured velocity and turbulence in the far wake region.

A study which inputted velocity and turbulence measurements from a tidal site into a CFD model of a tidal turbine was carried out by McNaughton et al. (2013). One of the main aims of this study was to examine and demonstrate the differences in turbine performance, loading and wake development between the flood and ebb tides of the tidal cycle. The site in question from which measured data was taken was at the European Marine Energy Centre (EMEC) in Scotland. The flow domain examined was a depth of 43m, claimed by the authors

to be representative of the mean depth at EMEC. The tidal turbine examined was a 1MW capacity turbine based on the design of tidal generation Ltd (TGL).

As with the study of Blackmore et al. (2014), the authors assumed a low blockage ratio, in this case 3.4%. The solver used was the open source code – saturne RANS solver, which was capable of generating a mesh which would resolve all the blades and geometry of the TGL device. The authors examined the following three velocity profiles, which are shown in figure 2.27:

- A uniform flow velocity of 1.8m/s.
- A flow velocity profile through the depth of the flow based on measurements at EMEC during the flood tide of the tidal cycle.
- A flow velocity profile through the depth of the flow based on measurements at EMEC during the ebb tide of the tidal cycle.
- For all of the above conditions, inlet turbulence intensity values to the turbine of 1% and 10% were examined.
- Unlike the work of Blackmore et al. (2014), the authors assume a fixed integral length scale of 0.7 times the hub height of the turbine.

Some of the parameters which the authors examined for changes in these variables were:

- Power and thrust coefficients of the turbine.
- Bending moments on a single blade of the turbine.
- Wake and turbulence intensity profiles at various positions downstream of the turbine.

Some of the main conclusions of the analysis were:

- In uniform flow conditions, an increase in turbulence intensity from 1% to 10% resulted in an increase in thrust coefficient form 0.845 to 0.862, and a decrease in power coefficient from 0.431 to 0.43.
- For uniform flow with 10% turbulence intensity, there was equal loading on a single turbine blade at either side of the support structure in a single 360 degree rotation. However in the 1% case, the blade experienced higher thrust and power coefficient after it had passed the support structure.
- Flapwise bending moments were examined about the chord of the blade, at both the root of the blade and midway along its span. Edgewise bending moments were also recorded perpendicular to the chord of the blade and at 35% of the chord length from the leading edge. It was found that an increase in turbulence intensity from 1% to 10% resulted in minimal change in flapwise bending moments, but an increase in edgewise bending moments. The values in question were not directly reported, but the results are shown in figure 2.28. This result demonstrates clearly, as was claimed by Maganga et al. [2010] that increasing turbulence intensity results in increased loading on turbine blades.

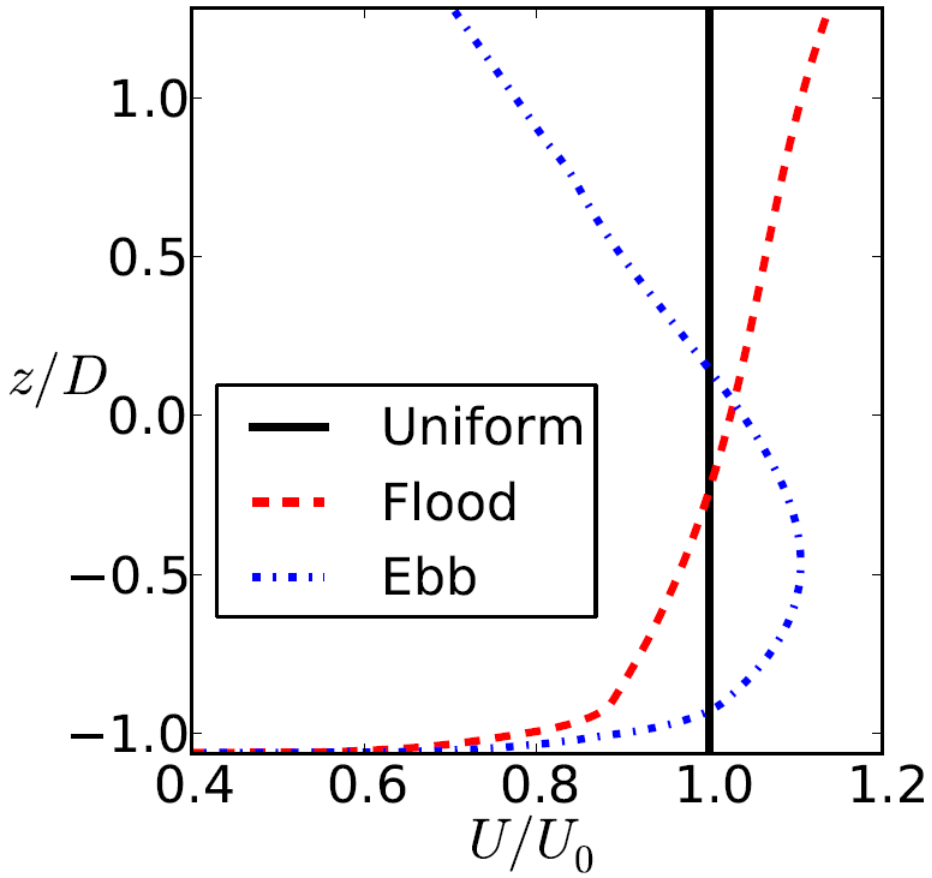

Figure 2.27: Uniform, ebb tide and flood tide profiles examined by McNaughton et al. (2013).

- In the wake region 4 to 6 diameters downstream of the turbine, the wake recovers to freestream flow conditions more rapidly with 10% turbulence intensity compared to 1% turbulence intensity.

These studies have clearly demonstrated the importance of examining natural flow conditions in a channel when determining the potential output of turbines, and also the optimum layout of a tidal farm. Another implication of the results of these authors analyses is that in any study which examines changes in geometric parameters of rows of turbines, or a turbines position with respect to channel boundaries, it must be ensured that the region of the flow domain where this examination takes place has reasonably steady and uniform flow conditions. Failure to ensure this could lead to erroneous conclusions being drawn on the effects of changing position or turbine row geometry, such as blockage ratio.

2.5 Theoretical analysis

2.5.1 Principle of continuity

The continuity equation is derived from the conservation of mass. It states that in any closed system where the flow can be assumed incompressible, the volumetric flow rate at any two points in the system remains constant. This is represented by the expression:

$$Q = U_1 A_1 = U_2 A_2 \tag{2.38}$$

This very fundamental relationship explains many of the flow effects observed in reviewed literature. Firstly, there is the increase in flow velocity around tidal turbine rows, as demonstrated by the results of analysis by Blunden and Bahaj (2007), Easton (2010) and Ahmadian et al. [2012]. To ensure continuity, the flow diverting around the sides of the array must be travelling at a much faster velocity than that in the wake region.The continuity principle also explains the volumetric flow rate imbalance in split tidal channels from the models of Atwater and Lawrence (2010) and Cummins (2013). There will be a certain volumetric flow rate in each channel when no obstructions are present. When an obstruction is placed in one of these sub channels (in this case a tidal turbine row), it blocks some of the volumetric flow rate through that channel. To maintain continuity, the blocked flow must be diverted elsewhere.

2.5.2 Bernoulli's equation

Bernoulli's equation follows from the conservation of energy. It states that in a closed system where the only forces acting are those due to gravity and pressure of the fluid, the sum of potential, kinetic and pressure energy is conserved. This is represented by the expression:

$$\frac{p_1}{\rho g} + h_1 + \frac{U_1^2}{2g} = \frac{p_2}{\rho g} + h_2 + \frac{U_2^2}{2g} \tag{2.39}$$

However the above expression assumes no energy losses in the flow between the two points in question. A more realistic expression for open channels would be:

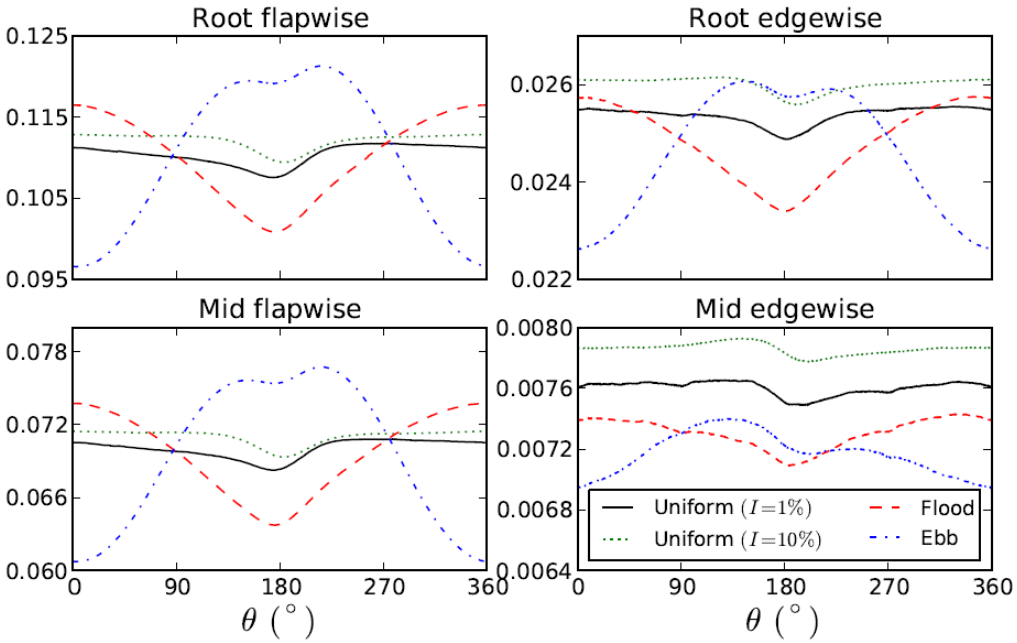

Figure 2.28: Bending moment results of McNaughton et al. (2013).

$$\frac{p_1}{\rho g} + h_1 + \frac{U_1^2}{2g} = \frac{p_2}{\rho g} + h_2 + \frac{U_2^2}{2g} + losses \tag{2.40}$$

In a free flowing open channel with no energy extracting objects present, these head losses would mostly be due to friction between the fluid and the sides of the channel. In the case of tidal energy turbines, additional head losses would occur due to the energy extracted by the turbine, along with any other losses such as:

- Friction across the rotor of the tidal turbine
- The drag on support structures of the turbine.
- Head losses due to friction between the boundaries of the channel and the flowing fluid.
- Turbulence in the downstream wake.

These losses due to power extraction and friction losses is the basis of the open channel model by Bryden et al. [2004]. This model specifies how to quantify the head losses which occur depending on the level of friction and energy extracted and dissipated, and is discussed in section 2.5.7.

How conservation of energy applies in the case of actuator discs is explained by Burton et al. [2001, pp.65 - 66]. As the flow upstream of the actuator fence reaches the fence surface, it is slowed down due to the fact that not all flow can pass directly through the fence. By equation 2.40, this results in an increase in static pressure and hence potential energy. Any flow which cannot travel directly through the porous fence spreads radially outwards from the front of the fence, and eventually reaches the fence edge. At this point it has relatively little kinetic energy due to viscous forces, and there is not enough static pressure to provide the kinetic energy necessary to allow it to continue flowing around the edge. The flow therefore separates outwards into the freestream. As it does so, it accelerates, causing a reduction in static pressure and pressure head according to equation 2.40. This explains the imbalance in pressure upstream and downstream of an actuator fence, which ultimately causes the force acting on the actuator fence.

2.5.3 Conservation of momentum

Momentum is a physical quantity of an object, which by definition is given by its mass multiplied by its velocity. Newton's second law states that the rate of change of momentum is equal to the magnitude of the force acting on this object. By applying this principle to an incompressible fluid streamline with no change in cross sectional area, the force acting between any two points 1 and 2 in the x direction is given by:

$$F_x = \dot{m}\,(U_{x2} - U_{x1}) \tag{2.41}$$

This is the theoretical expression which governs the forces exerted on actuator fences. It shows how the extent to which velocity of a flow is reduced, and the resulting flow velocity in the wake region, can have an effect on thrust experienced.

2.5.4 Actuator disc theory

Burton et al. [2001] gives a thorough discussion of how the continuity, Bernoulli and momentum equations are applied to the situation of an actuator disc in an unbounded flow. The application of the continuity equation to the actuator disc shown in figure 2.9 gives:

$$A_\infty U_\infty = A_d U_d = A_w U_w \tag{2.42}$$

Further application of the aforementioned fundamental principles of fluid mechanics give the following expression for the force acting on the actuator fence:

$$F_d = \frac{1}{2}\rho A_d \left(U_\infty^2 - U_w^2\right) \tag{2.43}$$

Where $U_\infty$is the undisturbed freestream flow velocity upstream of the disc, and U_w is the flow velocity at any fixed point downstream in the wake:

$$U_w = (1 - 2a)\, U_\infty \tag{2.44}$$

Where a is the axial induction factor, which is a measure of the extent to which flow has slowed between the undisturbed freestream region and the upstream face of the disc, and is given by:

$$U_d = (1 - a)\, U_\infty \tag{2.45}$$

The thrust coefficient, which is a non dimensional quantity used to compare the thrust force acting on actuator fences and discs with varying inflow velocities and areas, is given by:

$$C_T = \frac{T}{\frac{1}{2}\rho U^2 A_d} \tag{2.46}$$

It was also demonstrated by Burton et al. that this thrust coefficient can also be given by:

$$C_T = 4a\,(1 - a) \tag{2.47}$$

The power dissipated from the fluid by the actuator disc can be given by the force on the disc multiplied by the instantaneous velocity at the disc. Multiplying the force in equation 2.43 by the value for velocity at the disc in equation 2.45 gives the following expression for power extracted.

$$P = 2\rho A_d U_\infty^3 a\,(1 - a)^2 \tag{2.48}$$

The non-dimensional power coefficient, which is used to compare the power performance of turbines with different rotor areas operating under with different inflow conditions is given by:

$$C_P = \frac{P}{\frac{1}{2}\rho U^3 A} \tag{2.49}$$

While power coefficient in terms of axial induction factor is given by:

$$C_P = 4a\,(1-a)^2 \tag{2.50}$$

Comparing this with the expression for thrust coefficient in Eqn.2.47 shows that power coefficient is the product of thrust coefficient and $(1-a)$. This shows that measurement of thrust coefficient is very useful in giving an indication of power extracted. As power is not mechanically extracted, but dissipated from the flow by using porous media (see section 2.5.9) , this thrust coefficient can be used in experiments instead. It is acknowledged that actuator fences are of a much different shape to actuator discs. However the above theory is just as applicable to these actuator fences, and the impact on the surrounding flow environment and how these demonstrate the effects of tidal power extraction in a channel are no less relevant.

However an issue with the above theory identified by Burton et al. (2001) was it assumes an absolute maximum axial induction factor of 0.5, corresponding to a maximum C_T of 1. Beyond this 0.5 value, the theory suggests a reversal of flow. Therefore the above theory is no longer applicable and an empirical modification to theory is required.

An empirical modification suggested by Glauert [1926, cited by Burton et al. (2001)] firstly assumes an experimental value for C_T of C_{T1} at axial induction factor of 1. There is also the condition, stated by Burton et al. (2001) that the empirically modified line must be tangent to the parabola of conventional theory at the point on the parabola where the theory breaks down. This condition leads to the following equation of the empirically modified line:

$$C_T = C_{T1} - 4\left(\sqrt{C_{T1}} - 1\right)(1-a) \tag{2.51}$$

With this line equation, it is also possible to find the value of axial induction factor at which conventional theory is no longer applicable, and equation 2.51 must be used.

$$a_T = 1 - \frac{1}{2}\sqrt{C_{T1}} \tag{2.52}$$

From figure 2.29, it can be seen that the value for C_{T1} lies close to 2, and Burton et al. suggests that a value of 1.816 gives the best fit to the experimental data of Glauert. It can also be seen that for the highly loaded cases examined in experimentation by Glauert, the suggested empirical modification gives a reasonable estimate of thrust coefficient for high axial induction factors.

2.5.5 Other proposed blockage correction models

As well as the above correction to actuator disc theory results proposed, many other authors have developed theoretical models to correct for the phenomenon of blockage in tidal stream turbine environments. Such models have also been implemented by many others in experimental and numerical results.

The Lanchester - Betz limit is a well known result of some early work on examining the maximum amount of power available for either a wind or tidal turbine. It stated that for a turbine of given cross sectional area A, the maximum power extractable was 59% ($\frac{16}{27}$) of the upstream kinetic energy flux. However this assumes an infinite flow field, which, although it

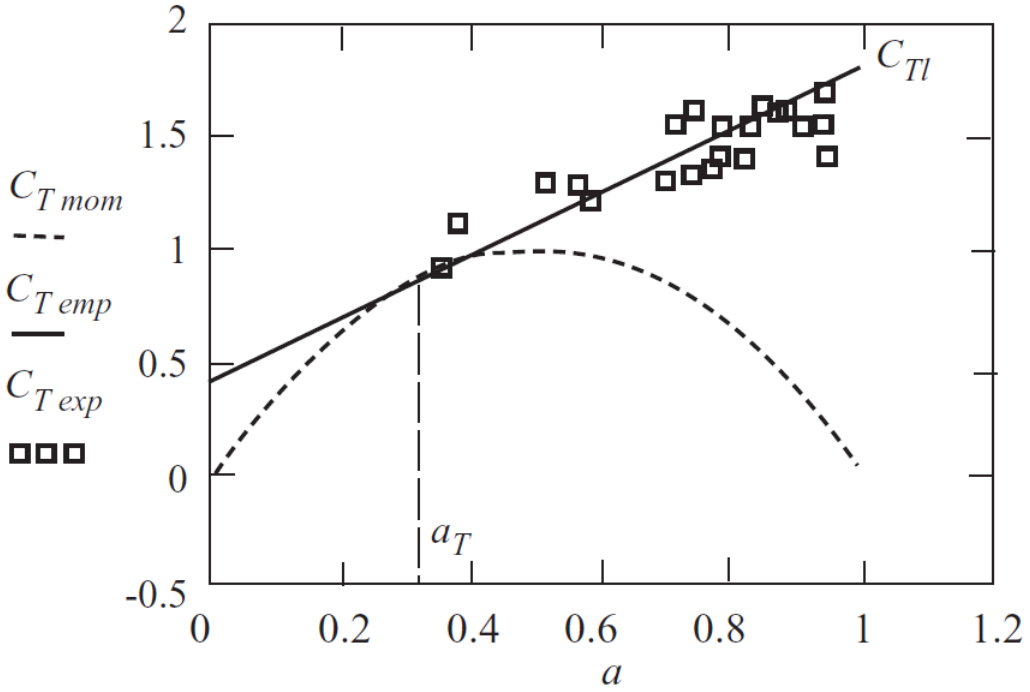

Figure 2.29: Results of experimental analysis and empirical modification suggested by Glauert (Burton et al. 2001, fig. 3.16).

may have some applicability to wind turbines due to the highly unconstrained nature of the resource, is unsuitable for the highly constrained environments tidal turbines operate in.

A blockage correction model developed by Garrett and Cummins [2007] proceeded to account for this constrained nature. The authors split the flow regime surrounding a tidal turbine into flow through the turbine and also bypass flow surrounding a tidal turbine occupying the entire cross section of its respective channel, as shown in figure 2.10. The authors applied the continuity, momentum, energy and Bernoulli's equation to each section of the flow and then used force equal to cross section area multiplied by pressure differential across the turbine to arrive at the following expression for power output of the turbine:

$$P = \frac{1}{2} A \frac{u_3 \left(u_4 + u_3\right) \left(u_4^2 - u_3^2\right)}{u_4 + 2u_3 - u_0} \tag{2.53}$$

As the cross sectional area of the channel tends towards infinity, and hence the turbines occupy an almost negligible cross sectional area, the term u_4 tends to u_0, and hence the power output simplifies to:

$$P = P_{LB} = \frac{1}{4} A \left(u_0 + u_3\right) \left(u_0^2 - u_3^2\right) = \frac{1}{2} \left(1 + r\right) \left(1 - r^2\right) x \frac{1}{2} A u_3^2 \tag{2.54}$$

Where P_{LB} is used as it refers to Lanchester - Betz power and r represents $\frac{u_3}{u_0}$. According to this expression, the maximum power is experienced at a value for r of $1/3$, giving a value of $16/27$ of the value of $\frac{1}{2}\rho U^3$, the upstream kinetic energy flux.

In order to determine the power output for a partially occupied channel, the authors deemed it necessary to determine the value for u_4 as a function of A, A_c, u_3 and u_0.

Using the continuity equation through both the streamtube travelling through the turbine

gave the following result:

$$A_0 u_0 = A u_1 = A_3 u_3 \tag{2.55}$$

While applying it to the entire channel gives:

$$(A_c - A_3)\, u_4 + A_3 u_3 = A_c u_o \tag{2.56}$$

Combining both of these equations gives the following expression:

$$u_3\,(u_4 - u_0) = \epsilon u_1\,(u_4 - u_3) \tag{2.57}$$

Where ϵ is given by $\frac{A}{A_c}$. u_1 was derived as a function of the aforementioned parameters by determining two separate expressions for the force acting on the turbines, one derived by applying Bernoulli's equation to a streamline in the streamtube outside that containing the turbine rotor, and another by applying the momentum equation upstream and downstream of the turbine. These two expressions are:

$$F = \frac{1}{2}\rho A_3\,(u_4 - u_3)\,(u_4 + 2u_3 - u_0) \tag{2.58}$$

$$F = \frac{1}{2}\rho A\left(u_4^2 - u_3^2\right) \tag{2.59}$$

For these two expressions to agree, it was found that:

$$u_1 = \frac{u_3\,(u_4 + u_3)}{u_4 + 2u_3 - u_0} \tag{2.60}$$

Inserting this expression for u_1 into equation 2.57 gives:

$$(1 - \epsilon)\, u_4^2 - 2\,(u_0 - u_3)\, u_4 + u_0^2 - 2u_0 u_3 + \epsilon u_3^2 = 0 \tag{2.61}$$

Numerical manipulation of this expression gives the following expression for u_4.

$$u_4 = \frac{u_0 - u_3 + \left[\epsilon u_0^2 - 2\epsilon u_0 u_3 + \left(1 - \epsilon + \epsilon^2\right) u_3^2\right]^{\frac{1}{2}}}{1 - \epsilon} \tag{2.62}$$

As opposed to the previously examined limit, where turbines are assumed to occupy a negligibly small cross sectional area, another limit which was examined was turbines occupying almost the entire cross section. For this particular condition, the following can be assumed:

$$u_4 = 2\,(1 - \epsilon)^{-1}\,(u_0 - u_3) \tag{2.63}$$

and:

$$u_1 = u_3 \tag{2.64}$$

This gives a power output of:

$$P = 2\left(1-\epsilon\right)^{-2} A u_3 \left(u_0 - u_3\right)^2 \tag{2.65}$$

The maximum value of this expression is found when $\frac{U_3}{U_0}$ is equal to 1/3, which interestingly the same as for the case of an almost unblocked or infinity wide channel. Thus according to this model, the maximum power for a channel partially blocked by tidal turbines is given by:

$$P_{max} = \frac{16}{27}\left(1-\epsilon\right)^{-2} x \frac{1}{2} A u_0^3 \tag{2.66}$$

Thus it is interesting to note that the Lanchester - Betz limit can actually be exceeded, with the most likely reason stated by the authors to be as a consequence of the greater increased pressure drop across turbines associated with the constrained environment. It is worth noting however that the above expression is a theoretical maximum only, and the actual amount of power is likely to be less due to factors such as:

- Energy dissipation due to wake mixing.
- Drag on support structures.

A limitation of this model identified by Vennell [2010] was that it considered a given through flow in a channel, and did not account for the effects of bottom friction of a channel. Thus, the authors developed a theoretical model which assumed a channel with tides driven by a head loss between both ends of the channel, and attempted to combine the model of Garrett and Cummins (2005), which accounted for bottom friction of a channel, with the model of Garrett and Cummins (2007), which did not account for this friction.

The authors assumed the channel in figure 2.11 with turbines installed, and began with the 1D shallow water momentum equation given by:

$$\rho A L \frac{\partial u}{\partial t} = -\rho g A \left(\triangle \iota\right) - \rho C_d B L |u| u - \rho C_{DT} A |u| u \tag{2.67}$$

where C_{DT} is the drag coefficient associated with turbines and C_D is the drag coefficient associated with the channel bottom friction. Also the term $\triangle \iota$ represents the difference in water elevation between the ends of the channel. The authors simplify the above equation by considering the inlet of the channel, and therefore $\triangle \iota$ goes to zero and the equation reduces to:

$$\frac{\partial u}{\partial t} = a sin\left(\omega t + \phi_g\right) - \left(\frac{C_d}{h} + \frac{C_T}{L}\right) |u| u \tag{2.68}$$

In the above expression, ω is the forcing frequency of the tide and ϕ_g is the phase of the water level difference between both ends of the channel relative to the phase at the inlet. The authors then non-dimensionalise time and the amplitude of velocity in the channel by dividing time by $\frac{1}{\omega}$ and velocity by $\frac{a}{\omega}$. Thus the equation becomes, as in Garrett and Cummins (2005):

$$\frac{\partial u'}{\partial t'} = sin\left(t' + \phi_g\right) - \left(\lambda_0 + \lambda_T\right) |u'| u' \tag{2.69}$$

Where λ_0 and λ_t are representations of the natural bottom friction and turbine induced friction respectively. The authors then give the following expression for the power potential of the channel which is lost due to the installation of turbines relative to the channels undisturbed power potential, over the entire tidal cycle:

$$\frac{\overline{P_{lost}}}{\overline{P_{max}}} = \frac{\lambda_T \overline{|u'(t', \lambda_0 + \lambda_T)|^3}}{\lambda_{TPeak} \overline{|u'(t', \lambda_0 + \lambda_{TPeak})|^3}} \tag{2.70}$$

In the above expression, λ_{TPeak} represents the turbine drag coefficient at the maximum power lost.

The authors then quote the following two expressions, for the power lost in a flow due to the presence of turbines and the power of the undisturbed channel respectively, which are derived from the model of Garrett and Cummins (2007):

$$P_{lost} = Fu = \rho M_R C_{TI} A u^3 \tag{2.71}$$

$$P_{available} = Fu = \rho M_R C_{TI} A u^3 r_1 \tag{2.72}$$

Where r_1 is the fraction of power lost to turbines. This power is lost mostly by energy being dissipated through mixing of bypass flow with wake flow downstream of turbines.

The authors then make the assumption that the tidal farm examined only takes up a short length of the channel's total length, and hence bottom friction is dominated by the actions of turbines. This allows them to combine the models of Garrett and Cummins (2005), which accounts for bottom friction, and Garrett and Cummins (2007) which neglects bottom friction. The combined model allowed the variation in power available and power lost to the flow for various combinations of parameters such as blockage ratio, wake velocity and number of rows of turbines to be examined. From the results subsequently presented by the authors, the complex interdependency of all these parameters on the power potential of a channel under certain conditions was quite evident.

One parameter which was beyond the scope of examination of these two studies was inter-device spacing. A blockage model which also accounted for this particular parameter was proposed by Nishino and Willden [2012]. The authors considered the tidal turbine arrangement shown in figure 2.13, and separated the flow into two scales. One scale was a local device level scale, while the other was an array scale which assumed the entire row of turbines as one solid power extracting fence.

At the array scale, the authors firstly defined an array blockage ratio, for n devices in the array, given by:

$$\epsilon_A = \frac{1 + \frac{s}{d}}{\frac{B}{nd}} \tag{2.73}$$

At the local device scale, blockage ratio is given by:

$$\epsilon_L = \frac{\frac{\pi d^2}{4}}{h(d+s)} \tag{2.74}$$

Where h(d+s) is the cross sectional area of the individual "passage" of flow assigned to each individual device.

The authors then defined a global blockage ratio, which is given by the sum of the cross sectional area of n devices divided by the channel cross sectional area:

$$\epsilon_G = \frac{n\frac{\pi d^2}{4}}{hB} \tag{2.75}$$

The authors then define an array, local and global scale value for axial induction factor:

$$a_L = 1 - \frac{U_D}{U_A} \tag{2.76}$$

$$a_A = 1 - \frac{U_A}{U_C} \tag{2.77}$$

$$a_G = 1 - \frac{U_D}{U_C} \tag{2.78}$$

A relationship between the three scales is then found by considering the thrust coefficient values for each scale. These are given by the following expressions:

$$C_{TL} = \frac{T_D}{\frac{1}{2}\rho U_A^2 \frac{\pi d^2}{4}} \tag{2.79}$$

$$C_{TA} = \frac{nT_D}{\frac{1}{2}\rho U_C^2 hn(d+s)} = (1-a_A)^2 B_L C_{TL} \tag{2.80}$$

$$C_{TG} = \frac{nT_D}{\frac{1}{2}\rho U_C^2 \frac{\pi d^2}{4}} = (1-a_A)^2 C_{TL} \tag{2.81}$$

Following on from this, local, array and global power coefficients are also defined as:

$$C_{PL} = \frac{T_D U_D}{\frac{1}{2}\rho U_A^3 \frac{\pi d^2}{4}} \tag{2.82}$$

$$C_{PA} = (1-a_A)^3 B_L C_{PL} \tag{2.83}$$

$$C_{PG} = (1-a_A)^3 C_{PL} \tag{2.84}$$

The authors then also developed alternative expressions for thrust coefficient at both local and array level by applying mass, momentum and energy conservation at both a local and array scale., in the exact same manner as Garrett and Cummins (2007). This yielded the following expressions for local and array thrust coefficient:

$$C_{TL} = (1-\vartheta_l)\left[\frac{(1+\vartheta_l) - 2B_L(1-a_L)}{(1-B_L(1-a_L)/\vartheta_l)^2}\right] \tag{2.85}$$

$$C_{TA} = (1-\vartheta_A)\left[\frac{(1+\vartheta_A) - 2B_A(1-a_A)}{(1-B_A(1-a_A)/\vartheta_A)^2}\right] \tag{2.86}$$

where ϑ represents the ratio of wake to upstream undisturbed flow velocity. Using these expressions, the authors then examined some of the relationship between blockage ratio, at both array and local device scale, wake velocity and thrust and power on turbines. The most crucial advancement in this work was the local device scale blockage ratio, which is a function of inter device spacing within a given sized array of turbines.

2.5.6 Specific energy and critical depth

In any analysis or installation of any devices in open channels, one of the most important first steps is determining whether the flow is subcritical or supercritical. Practically speaking, subcritical flow is a deep slow moving flow, while supercritical flow is a fast shallow flow.

One method of determining which category of flow is present in a channel is the Froude number of a flow. Similarly to Reynolds number or Mach number, this is a quantity used to allow accurate comparison of experimental results between different sized open channels. The Froude number is given by the expression:

$$Fr = \frac{Inertial - forces}{Gravitational - forces} = \frac{\rho h^2 U^2}{\rho h^3 g} = \frac{U}{\sqrt{gh}} \tag{2.87}$$

The flow is considered subcritical when the Froude number is less than 1, and supercritical when the Froude number is greater than 1. A Froude number of 1 represents what is known as critical or transitional flow.

One other method of determining the nature of flow, which is also useful for demonstrating one of the main differences between subcritical and supercritical flow, is to plot specific energy against flow depth. Specific energy is given by the expression:

$$E = h + \frac{\alpha Q^2}{2g\left(Bh\right)^2} \tag{2.88}$$

Where α represents an energy coefficient, which according to Hamill [2011, p.248] is usually assumed to be 1. (This energy coefficient is discussed further in appendix D). For a channel of fixed volumetric flow rate, it is useful to plot a graph of specific energy against flow depth. An example of such a graph can be seen in figure 2.30. Critical flow represents the flow of lowest possible specific energy, and is achieved at a flow depth known as the critical depth. This corresponds to a Froude number of 1. Above this critical depth represents slower moving deep flow, which corresponds to subcritical flow. Below this critical depth represents fast moving shallow flow, or supercritical flow. The critical depth for a rectangular channel can be calculated by the expression:

$$D_c = \left(\frac{Q^2}{gB^2}\right)^{\frac{1}{3}} \tag{2.89}$$

A difference between these flows in the context of tidal turbines shown by the graph is what happens to flow depth as energy is removed. In the subcritical region, removal of energy results in a decrease in flow depth, while in the supercritical region it causes an increase in flow depth. The behaviour in the subcritical region once again demonstrates the reduction in

water surface elevation from extraction of energy predicted by the analytical model of Bryden et al. (2004) and shows the necessity for examining reduction in water surface elevations in experimental analysis.

2.5.7 Analytical model of Bryden et al. (2004)

The model developed by Bryden et al. (2004) assumes a simple channel linking two open oceans. A fixed volume of water passes through a fixed plane in a time $\triangle t$. If the flow velocity is U and the area of the channel is A, the momentum of this fixed volume of water is given by:

$$AU^2\rho\triangle t \tag{2.90}$$

Force on this volume due to rate of change of momentum can be given by:

$$\frac{D\left(Momentum\right)}{Dt} = \frac{\partial}{\partial t}\left(AU^2\rho\right)\triangle t + U\frac{\partial}{\partial x}\left(AU^2\rho\right)\triangle t \tag{2.91}$$

Hydrostatic force due to changes in water elevation are given by:

$$F_h = -\rho g U\triangle t\frac{\partial h}{\partial x} \tag{2.92}$$

The drag force caused by friction between the moving water and the extremities of the channel can be given by:

$$F_d = -U\triangle t P_{er}\tau_\infty \tag{2.93}$$

In the above expression, τ_o represents the natural shear stress between the moving water and the extremities of the channel. The value of this can be estimated by the expression:

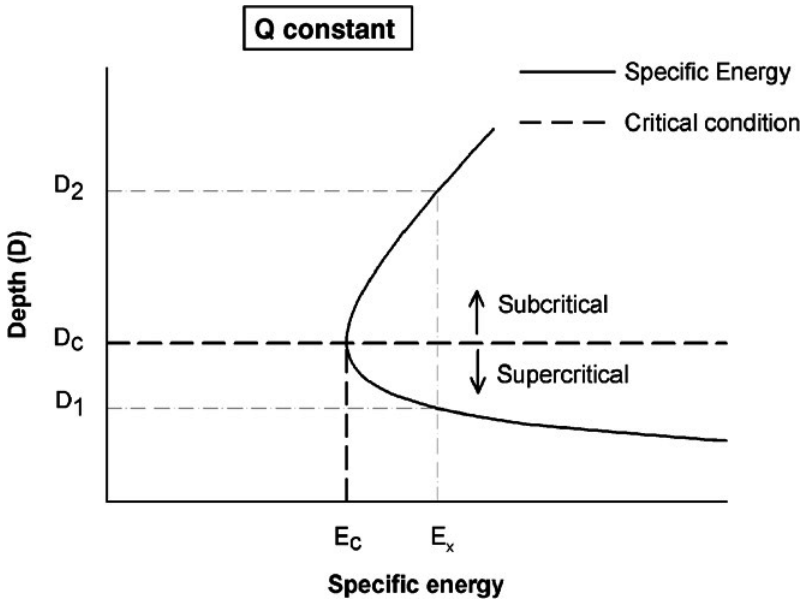

Figure 2.30: Example of plot of specific energy against flow depth displayed by Myers and Bahaj [2007]

$$\tau_o = \rho \frac{g}{C^2} U^2 \tag{2.94}$$

Where C is the Chezy friction coefficient given by:

$$C_Z = \frac{R^{\frac{1}{6}}}{n} \tag{2.95}$$

Where R is the hydraulic radius of the channel and n is the Manning's coefficient for the channel. The assumption is then made that the introduction of power extraction increases the effective shear stress of the channel. The additional shear stress due to power extraction is assumed to be proportional to the power extracted per unit volume of water P_x watts per cubic metre. The additional shear stress can be given mathematically as:

$$\tau_{add} = \frac{P_x R}{U} \tag{2.96}$$

The effective shear stress is then given by:

$$\tau_{eff} = \tau_{add} + \tau_\infty \tag{2.97}$$

Assuming steady flow and hence no time dependent terms, the full momentum equation for the simple channel presented can be given by:

$$U \frac{\partial}{\partial x} \left(A U^2 \rho \right) = -\rho g U A \frac{\partial h}{\partial x} - U P_{er} \tau_{eff} \tag{2.98}$$

Assuming the flow is incompressible means $\frac{\partial Q}{\partial x} = 0$. Using the expression $Q = UA$, equation 2.98 can be rewritten as:

$$-\frac{Q^3}{U^3} \frac{\partial A}{\partial x} \rho = -\rho g Q \frac{\partial h}{\partial x} - \left(\frac{Q}{A} \right) P_{er} \tau_{eff} \tag{2.99}$$

Which can also be written as:

$$\left(1 - \frac{Q^2}{h^3 B^2 g} \right) \frac{\partial h}{\partial x} = \frac{\partial B}{\partial x} \frac{Q^2}{g h^2 B^3} - \left(\frac{1}{\rho g B h} \right) P_{er} \tau_{eff} \tag{2.100}$$

To examine the possible reduction in water surface elevation across an actuator fence in the experimental work presented herein, this equation requires further manipulation. It is assumed that any changes to the width of the channel throughout its length is negligible, hence $\frac{\partial B}{\partial x} = 0$. Therefore the reduction in water surface elevation per unit length of power dissipation can be given by:

$$\frac{\partial h}{\partial x} = \frac{-\left(\frac{1}{\rho g B h} \right) P_{er} \tau_{eff}}{\left(1 - \frac{Q^2}{h^3 B^2 g} \right)} \tag{2.101}$$

Defining the additional shear stress in this model requires applying the power extracted. Quantifying this for actuator fences is more difficult than for tidal turbines due to the process of energy dissipation by turbulence.

A quantity which deserves special mention here is the Manning's n. This is a roughness coefficient which is used extensively in open channel flow, and also in the Bryden et al. model presented. It is predominantly an empirical quantity, with the choice by engineer's usually made on the basis of reference to engineering tables and engineering judgement. It is however also possible to estimate its value using measured velocity profile data, as this gives an indication of the roughness of a surface and the resultant turbulence driving the flow within the boundary layer of that surface.

2.5.8 Determination of Manning's n from experimental data

Using theory developed by a number of different authors, it is possible to estimate Manning's n, an important quantity in open channel flow analysis, using data from field measurements.

The first step is the determination of the Darcy friction factor. This is a non-dimensional coefficient used to estimate head losses in pipes and open channels due to the effects of friction between the flow and bounding surfaces. A commonly used equation for estimating this coefficient is the Colebrook - White equation, which is given by:

$$\frac{1}{\lambda} = -2log\left(\frac{k}{3.7D} + \frac{2.51}{Re\sqrt{\lambda}}\right) \tag{2.102}$$

Where:

- λ is the Darcy Friction factor
- D is the pipe diameter in the case of pipe flow, or flow depth in the case of an open channel (Myers and Bahaj [2008]).
- k is a roughness height, which is an estimate of the height of protrusions on a surface. A number of different values are given for different materials in many engineering tables, and also by Hamill (2001, p195).

Using this established value of Darcy friction factor, it is then possible to determine a modified version of the Reynolds number, known as the Reynolds roughness number (Re*), which is given by:

$$Re* = Re\left(\frac{k}{D}\right)\sqrt{\frac{\lambda}{8}} \tag{2.103}$$

This can then be used to determine a friction velocity U*, the velocity associated with the Reynolds roughness number, which is given by Shah and Sekulic [2003] as:

$$Re* = \frac{kU*}{\upsilon} \tag{2.104}$$

A number of equations have been put forward by many authors for estimating the velocity profile which extends off any roughened surface. The purpose of these laws is to allow an estimate of flow velocity at any given point away from a roughened surface. One such law, developed for sediment transport by Dyer [1986], and used for modelling of an experimental flume by Harrison et al. [2010], is the Dyer boundary law. This is given by:

$$U(y) = 2.5ln\left(\frac{yU*}{\nu}\right) + C \tag{2.105}$$

where y is the distance from the boundary in question, and C is a constant used to curve fit data to the equation.

Using the above steps, it is possible to examine a number of different values of k, the empirically derived roughness height, and after calculating friction velocity, compare the resulting Dyer boundary law profile to the measured profile.

The value for k which then gives the most accurate fit to measured data can be used in the following expression, originally proposed by Leopald and Wolman [1957], and cited by Limerinos [1970], to relate roughness height with Manning's n:

$$\frac{1}{\sqrt{f}} = \frac{0.0926}{\frac{n}{R^{\frac{1}{6}}}} \tag{2.106}$$

This method therefore gives a procedure whereby measurements can be used to predict issues in open channel flow where Manning's coefficient is used, such as total volumetric flow rate in a channel, friction head losses throughout the entire length of a channel and the effective Manning's n for a channel with boundaries composed of different materials.

2.5.9 The energy cascade

The process of energy dissipation in turbulence is known as the "energy cascade", and is discussed extensively by Pope [2000, pp.182 - 188]. The concept of an energy cascade was first introduced by Richardson [1922, cited by Pope (2000, p.183)]. Richardson considered a turbulent flow to be composed of a number of different sized eddies. These eddies are simply some particular turbulent motion. Richardson postulated that each eddy had a characteristic length, flow velocity, time-scale and Reynolds number given by:

$$length = l \tag{2.107}$$

$$velocity = u(l) \tag{2.108}$$

$$Timescale = \frac{l}{u(l)} \tag{2.109}$$

$$Re = \frac{u(l)\,l}{\nu} \tag{2.110}$$

Richardson further postulated that within each eddy lay a number of smaller eddies. For the largest sized eddies, their particular local Reynolds number is quite high compared to the overall flow Reynolds number, and so the effects of viscosity are initially negligible. However Richardson postulated that large eddies eventually broke up due to their instability, and transferred their energy to smaller eddies. These smaller eddies then break up and transfer the energy to smaller eddies. This cycle, or "energy cascade" continues, and energy is continually

transferred between smaller and smaller eddies. This continues until the Reynolds number of the smallest eddy becomes small enough for the eddy motion to become stable. At these small eddy Reynolds numbers, the overall Reynolds number of the flow is considerably higher, and so the effects of viscosity are no longer negligible. The kinetic energy of the smallest eddy is therefore dissipated by molecular viscous forces.

With an actuator fence, these energy dissipating eddies will be the vortices generated due to the velocity gradient (and hence viscous forces) between fluid particles at the solid edge of a hole of the fence and those travelling through the hole. There will also be eddies generated off the solid sides of the actuator fence, due to the velocity gradient between the edge and the fluid freestream.

2.5.10 Analytical model of Atwater and Lawrence (2010).

The literature reviewed in section 2.3.2 demonstrates the complexity of split tidal channels and how they respond to tidal power extraction. Research in Sutherland et al. [2007] has shown how dramatically conventional channel theory can be erroneous in assessing both power available and far field effects. An attempt to develop theory for split tidal channels was carried out by Atwater and Lawrence [2010].

Their model assumes a channel split into two sub channels of equal width and depth by an impenetrable landmass, as shown in figure 2.4. The assumptions are made that head loss is proportional to square of velocity, and that a fence of tidal turbines is operating in one sub channel. The head loss across the entire channel, can be given firstly by examining the impeded channel:

$$\triangle h_{tide} = h_o - h_2 = \left(q_{en} + q_u + r^2(q_I + q_t) + q_D + q_{ex}\right) Q^2 \tag{2.111}$$

It can equally be expressed by examining the unimpeded sub channel:

$$\triangle h_{tide} = h_o - h_2 = \left(q_{en} + q_u + (1 - r^2)q_f + q_D + q_{ex}\right) Q^2 \tag{2.112}$$

In the above terms, q represents the head loss coefficient. The head loss coefficient q for any region of the split channel is given by:

$$q = \frac{fL}{2RgA^2} \tag{2.113}$$

Where L is the longitudinal length of the section, f is a bottom roughness coefficient and R is the hydraulic radius of that section. The subscripts are explained as follows:

- t represents the turbine
- I represents the impeded channel
- f represents the free channel
- u represents upstream
- D represents downstream

- en represents the entrance to the channel
- ex represents the channel exit
- r represents the fraction of the volumetric flow rate Q passing through the impeded channel.

Equating equations 2.111 and 2.112 gives the following expression for the fraction of overall volumetric flow rate through the impeded channel:

$$r = \frac{1}{1 + \sqrt{\alpha + \beta}} \tag{2.114}$$

Where:

$$\alpha = \frac{q_T}{q_f} \tag{2.115}$$

$$\beta = \frac{q_I}{q_f} \tag{2.116}$$

The power extracted by the turbines is considered to be a function of both the reduction in water surface elevation across the turbines and the fraction of the overall volumetric flow rate passing through the impeded channel.

$$P_{extracted} = \rho g(rQ)\triangle h_t \tag{2.117}$$

Similarly the amount of power available in the channel is considered a function of the volumetric flow rate through and reduction in water surface elevation across the impeded channel naturally with no energy extraction.

$$P_{available} = \rho g Q_o \triangle h_{tide} \tag{2.118}$$

Combining equations 2.117 and 2.118 and using other expressions developed gives the following expression for extraction efficiency:

$$\eta = \frac{P_{extracted}}{P_{available}} = \frac{\alpha\left(1 + \sqrt{\alpha + \beta}\right)^{-3}}{\gamma + \left(1 + \sqrt{\beta}\right)^{-2}\beta}\left(\frac{Q}{Q_o}\right)^{-3} \tag{2.119}$$

The term $\left(\frac{Q}{Q_o}\right)$is close to unity and so left as a separate term:

$$\frac{Q}{Q_o} = \sqrt{\frac{\gamma + \left(1 + \sqrt{\beta}\right)^{-2}\beta}{\gamma + \left(1 + \sqrt{\alpha + \beta}\right)^{-2}(\alpha + \beta)}} \tag{2.120}$$

Where γ is given by:

$$\gamma = \frac{q_{en} + q_u + q_d + q_{ex}}{q_f} \tag{2.121}$$

The authors then applied this model to a split tidal channel known as Current Passage, in Johnstone Strait, Vancouver Island, Canada. Entry of the values for hydraulic parameters

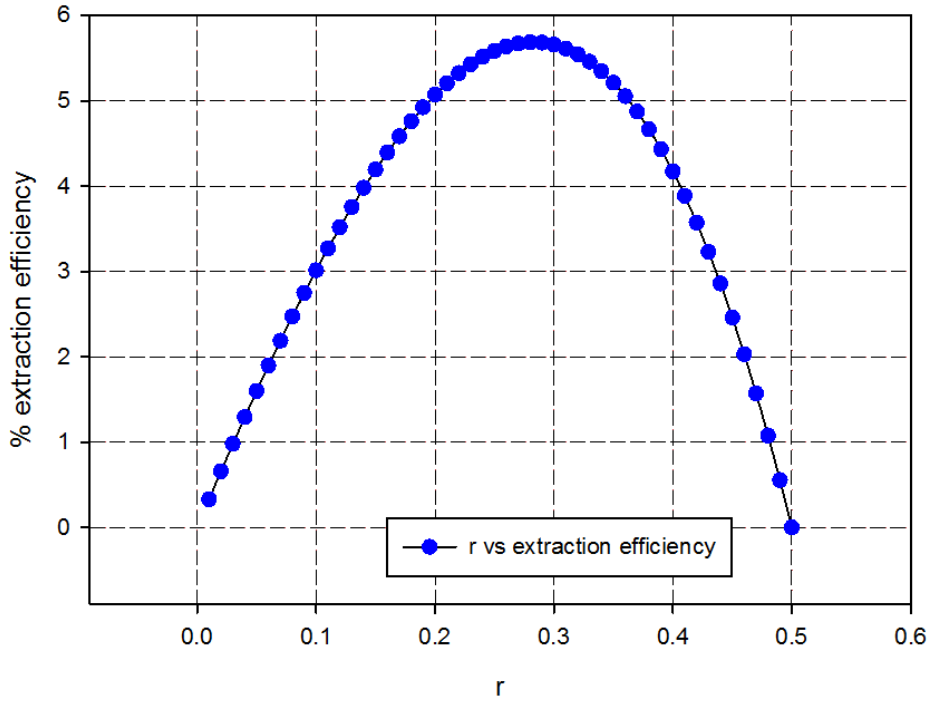

Figure 2.31: r (fraction of volumetric flow rate through impeded channel) vs extraction efficiency for Current Passage, Johnstone Strait, Canada.

into equation 2.121 gave a value for γ of 1.5 and β of 1. The maximum possible extraction efficiency for Johnstone Strait was then found by inserting these values for β and γ into equation 2.119, and assuming a number of values for α. It was found that for Current Passage, the maximum extraction efficiency of turbines was 5.7%, achieved at a value for α of 6.31. The value for r, the fraction of overall volumetric flow rate through the impeded channel which achieves this maximum efficiency, can be determined from inserting this value for α and the value for β into equation 2.114. Figure 2.31 gives the variation in extraction efficiency with r, and shows the ideal value for r to be 0.27. In practical terms, all of this analysis means that the maximum extraction efficiency for Current Passage of 5.7% is achieved when 27% of the overall volumetric flow rate is directed into the impeded channel and the remaining 73% is directed through the free channel.

Equation 2.119 shows how the overall efficiency of power extraction is affected by changes in volumetric flow rate due to operation of tidal turbines. Where experimental analysis could add to the knowledge already gained is by examining what if any changes to the imbalance in volumetric flow rate occur when the position of the tidal array with respect to flow boundaries is altered. It is also worth examining how volumetric flow rate is altered with the level of blockage of the impeded channel. It may be the case that there is an optimal position and blockage to give the maximum power potential. The results of this analysis are likely to be of great interest to tidal developers wishing to exploit the tidal resource in split tidal channels.

2.5.11 Turbulence intensity

Consider the X, Y and Z directions, which have average flow velocity of $\overline{U}$, $\overline{V}$ and $\overline{W}$ respectively over a given time period. At any instant in this time period, the velocities u, v and w will be equal to the mean value plus the fluctuation from the mean at this instant. If the fluctuations from the mean are u', v' and w', the instantaneous velocities can be given by:

$$U = \overline{U} + u' \tag{2.122}$$

$$V = \overline{V} + v' \tag{2.123}$$

$$W = \overline{W} + w' \tag{2.124}$$

The turbulence intensity is given by the root mean squared of the average velocity fluctuations over a given time period divided by the root mean squared of the average flow velocities over this same time period.

$$TI = \frac{\sqrt{\overline{(u'^2)} + \overline{(v'^2)} + \overline{(w'^2)}}}{\sqrt{(\overline{U})^2 + (\overline{V})^2 + (\overline{W})^2}} \tag{2.125}$$

This represents turbulence intensity for the 3D flow. An important detail to remember is that the terms on the numerator represent the average of the square of the velocity fluctuations at each instant over the time period. This is not the square of the average velocity fluctuation, as averaging the velocity fluctuation by itself over the time period will simply lead to a value of zero, as all the fluctuations will cancel out. The particular term in equation 2.125 is for the 3D flow, but can be broken down into constituent parts in all directions:

$$TI_x = \frac{\sqrt{\overline{(u'^2)}}}{\overline{U}} \tag{2.126}$$

$$TI_y = \frac{\sqrt{\overline{(v'^2)}}}{\overline{V}} \tag{2.127}$$

$$TI_z = \frac{\sqrt{\overline{(w'^2)}}}{\overline{W}} \tag{2.128}$$

The importance of ambient turbulence intensity in the context of tidal turbine wake recovery has already been demonstrated by reviewed literature by Myers and Bahaj [2010] and Maganga et al. [2010]. There is however in both of these studies a lack of examination of induced turbulence intensities in a flow due to the development of the wake of tidal turbines. This is despite the fact that it would most likely have an impact on the performance of further turbines downstream. Maganga et al. [2010] has stated how greater turbulence intensity would lead to greater fluctuations in the thrust experienced by a tidal turbine over a given time period. The greater fatigue loading associated with this could affect a tidal turbines

lifespan or the level of regular maintenance required on it.

2.5.12 Viscous shear stresses

A good explanation of viscosity and viscous shear stresses is given by Massey and Ward-Smith [2006, p.23]. Consider the two fluid layers in figure 2.32. The slower moving layer on the bottom will travel with a flow velocity u, while the faster layer on top travels with a velocity $u+\partial u$. The distance between both in the Y direction is ∂y. The faster moving layer on top will attempt to drag the slower moving fluid layer along with, and exerts a force on the slower layer. Newton's third law dictates that the slower layer must exert an equal and opposite force on the faster layer, attempting to slow down the faster moving layer. There is a shearing stress associated with these forces which is proportional to the difference in their flow velocity divided by the distance between them. Numerically this can be displayed as:

$$\psi \propto \frac{\partial U}{\partial Y} \tag{2.129}$$

The exact value for shear stress in this case is dependent on the value of a constant known as dynamic viscosity for the fluid in question. If the dynamic viscosity of the fluid is μ, the magnitude of this viscous shear stress between these two fluid layers is given by:

$$\psi = \mu \frac{\partial U}{\partial Y} \tag{2.130}$$

The dynamic viscosity of a fluid has the units of kg/ms. It is a constant for each fluid at a particular temperature. The most common area where viscous stresses are present is in the boundary layer of flows. Any fluid flow which is in contact with a solid boundary will have a development of flow from the boundary to freestream flow. Examples of such boundaries for this work include the bed and sidewalls of the flume, and elements of the actuator fences.

2.5.13 Reynolds shear stresses

In turbulent flows, there will be differences between the velocity of fluid layers in all directions. This imbalance in velocity will mean momentum will be transferring between these layers. By Newton's second and third laws, this momentum transfer and change in momentum of any particular fluid layer must be accompanied by equal and opposite forces acting on the fluid layers. These forces will in turn cause shear stresses to act on the fluid layers. These are known as Reynolds shear stresses.

An explanation of Reynolds stresses is given by Massey and Ward-Smith [2006, pp. 341-

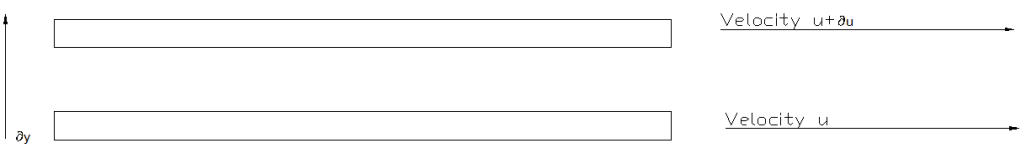

Figure 2.32: Fluid layers of different flow velocity and viscous forces shown by Massey and Ward-Smith [2006, p.23]

343]. Consider a surface parallel to the y direction and separating two fluid layers, as in figure 2.33. The mean flow velocity in the x direction over any given period of $\overline{U}$. However during this time the velocity will fluctuate to some extent from this mean value. Assume the fluctuation from the mean velocity at any instant in time can be given by u'. Therefore the instantaneous velocity u at any instant in time will be given by the mean value over the selected time period plus the fluctuation at that instant in time.

$$U = \overline{U} + u' \tag{2.131}$$

Similar relationships hold in the y and z directions.

$$V = \overline{V} + v' \tag{2.132}$$

$$W = \overline{W} + w' \tag{2.133}$$

The expression for average transfer of momentum between the two fluid layers in the XZ plane over the time period is given by:

$$\rho\overline{u'v'}dA \tag{2.134}$$

This expression represents the rate of change of momentum between the two fluid layers. By Newton's second law that is also the force acting to cause this transfer of momentum. The shear stresses associated with this can be given by force divided by area. Therefore the magnitude of Reynolds shear stress due to momentum transfer between fluid layers in a turbulent flow on the xz plane can be given by:

$$\varphi_{xy} = -\rho\overline{u'v'} \tag{2.135}$$

The negative sign is introduced due to a sign convention mentioned by Massey and Ward-Smith [2006, pp.23-24]. The positive sense of a force or stress is assumed to be the same as

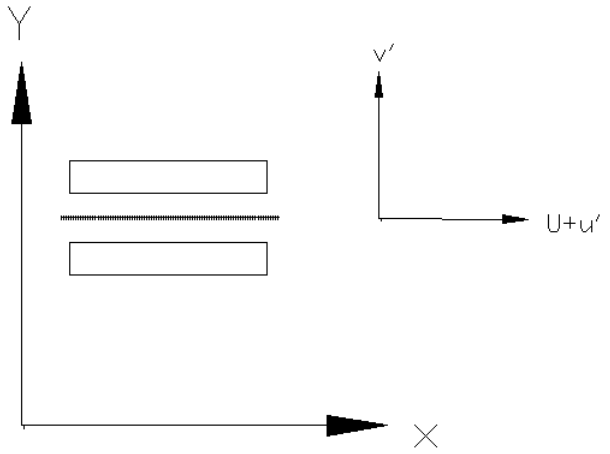

Figure 2.33: Fluid layers parallel to each other in X direction shown by Massey and Ward-Smith [2006, p.342]

that of flow velocity. This means for the viscous forces shown in figure 2.32, a positive stress means the upper layer is moving faster, and so this positive stress is that which results due to an accelerating force attempting to speed up the slower moving lower layer. However in the fluid layers displayed in figure 2.33, the lower layer would be moving faster for a positive value of u' and a negative value of v'. Therefore a negative force, and hence negative Reynolds shear stress, is required to speed up the slower moving layer in this case.

Similar expressions hold for the yz and xy planes.

$$\varphi_{yz} = -\rho\overline{v'w'} \tag{2.136}$$

$$\varphi_{xz} = -\rho\overline{u'w'} \tag{2.137}$$

The momentum transfer between fluid streamlines which results in these Reynolds shear stresses is responsible for wake mixing in tidal turbines. The fluid streamlines in the slow moving wake region directly downstream of a tidal turbine row interact with fast moving fluid streamlines in the freestream flow. The momentum transfer between these streamlines causes re-energisation of the wake region until it eventually recovers to freestream conditions at some point downstream of the tidal array. Examining the magnitude and pattern of Reynolds shear stresses directly downstream of an array can therefore give an indication of the level of wake mixing which is taking place. It can also be used to examine where exactly this mixing between and freestream fluid is occurring, as well as any changes to wake mixing effects which result due to decrease in the proximity of arrays to flow boundaries.

2.6 Literature review summary

The reviewed literature has displayed just some of the research which has been carried out on the subject of tidal energy. Authors have developed theoretical models, carried out scaled down experimental tests and also site specific studies in order to examine the effects of power extraction on tidal flow regimes. Some general conclusions which can be made from the reviewed literature include:

- The process of power extraction can potentially have a major effect on the flow regime, both immediately downstream of tidal turbines and in the surrounding far field environment.
- The flow effects due to power extraction in a channel can be dependent on site specific factors, such as ambient turbulence intensity levels in the flow, turbulence length scales, channel topography and roughness of channel boundaries.
- The extraction of power in one particular channel can have implications for the flow regime in other unoccupied channels within a specific flow domain.

Throughout the reviewed literature however, it is clear that there were two specific factors associated with tidal turbines whose effects were beyond the scope of each study. These were:

- The specific lateral or longitudinal position of a row of turbines with respect to channel boundaries.

- The dependence of any effects associated with changing lateral or longitudinal position on the blockage ratio of a row of turbines.

The fact that these two factors were beyond the scope of these studies means many questions about the effects of tidal power extraction still remain unanswered. If the analytical models of Atwater and Lawrence [2010] and Cummins [2013] are examined first, these models make clear that the distribution of volumetric flow rate within split tidal channels has an effect on the power which it is physically possible to extract. But the above mentioned factors cannot be accounted for with the developed theory. Both of these studies have assumed in their respective impeded channels a tidal fence spanning the entire width of the channel with all flow being directed through tidal turbines. Cummins (2013) acknowledges this will only lead to calculation of a theoretical upper bound of power available, but it is questionable as to how useful this might be to tidal developers wishing to exploit resources in any given split channel. There are also a number of questions on the nature of the flow in split channels which these models cannot answer. These include:

- Whether the position of tidal turbines with respect to the island splitting the channel affects the distribution of volumetric flow rate between the channels, and hence the maximum extractable power.

- How the distribution of volumetric flow rate, and hence extractable power, changes as the fraction of the impeded channel blocked by turbines changes.

- Whether the optimised imbalance in volumetric flow rate is physically possible with a single row of turbines, or if several rows would be required.

From the site specific split channel analyses by Polagye et al. [2009] and Sutherland et al. [2007], it is clear these factors are also not accounted for when examining the flow effects associated with power extraction. Therefore a tidal developer is completely unaware of whether or not specific array position or channel blockage are factors which need to be examined and accounted for when designing their specific tidal farm to the specifications required of their tidal project.

The issue of partial blockage was examined, for open channels, in studies by Garrett and Cummins [2007], Vennell [2010] and Nishino and Willden [2012]. These studies showed that when the assumption of a fence spanning the entire width of a channel is removed, the estimates of the power potential of turbines in a channel are considerably different. They also demonstrated that variables associated specifically with partial fences, such as bypass flow velocities, blockage ratio, and inter device spacing, can have a major influence on the maximum extractable power. They therefore advanced on previous work by Garrett and Cummins (2005) and Bryden et al. (2004) by showing that the power potential of tidal energy sites can not be determined exclusively by examining natural flow conditions. However as with the studies previously mentioned, the issue of the specific position with respect to

channel boundaries was not explored. It is also clear that the theory developed by the authors would not, in its current state, be able to examine this variable. This is mainly due to a number of simplifications made by the authors, such as uniform flow velocities in wake and bypass regions and inviscid flow downstream of a row of tidal turbines.

The scaled down wake analyses of Myers and Bahaj (2010) and Maganga et al. (2010) have shed some light on the possible effects of positioning tidal turbines closer to flow boundaries. In both cases, the effect of positioning tidal turbines closer to the bed of their respective channel was examined, with some interesting conclusions. Myers and Bahaj (2010) found deeper immersion led to slower wake recovery, with the postulation for the cause of this being that less mass flow in the region below the turbine meaning less re-energisation and turbulent wake mixing in the wake region. Maganga et al. examined the implications of deeper immersion for the power output of a given turbine. The results of this analysis found no change in power output with deeper immersion. Stallard et al. examined positioning tidal turbines closer to other turbines within an array. The results of this analysis showed that with close enough lateral spacing, the resulting downstream conditions were very different to those of either a single turbine rotor, or a row of rotors with sufficiently large lateral spacing such as to avoid merging of wakes or local increases in flow velocity in the region between rotors. But it was beyond the scope of these analyses to examine if similar effects, or otherwise, would occur to the flow conditions downstream if tidal turbine rows were positioned closer to the lateral boundaries of channels.

An experimental or numerical investigation could potentially fill this gap in the knowledge. However the results of studies by Blackmore et al. [2014] and McNaughton et al. [2013] have shown the importance of examining natural flow conditions when examining the changes associated with parameters such as specific position. Their studies showed clearly that natural flow turbulence conditions such as turbulence intensity are themselves very influential in determining the structure of the wake of any given turbine or row of turbines. Both studies showed increases in turbulence intensity to lead to quicker wake recovery downstream. The implications of this for experimental analysis is that the natural conditions of the experimental flow domain must be extensively examined to determine where steady and uniform conditions exist. This will ensure that any conclusions made on changes to wake conditions, or thrust on tidal turbines, which are attributed to changes in the specific position with respect to flow boundaries are not simply a result of changes to the inflow conditions in the specific experimental facility being used.

The site specific analyses of Blunden and Bahaj (2007), Easton (2010) and Ahmadian et al. [2012] have shown one particular effect of power extraction which is likely to be of major interest to tidal developers. This is the increase in flow velocity compared to ambient flow conditions which results due to the operation of tidal turbines. This occurs due the constraining of flow between a boundary and an array and the requirement of the flow to obey the continuity principle. The most obvious reason why this will interest tidal developers is the increase in potential power that will result. There are also some of the ecological effects referred to by Blunden and Bahaj (2007) such as the impact on cliff erosion and sediment transport. These two phenomena are likely to be a major part of any environmental impact

assessment for any tidal power project. But as yet it is unclear to what extent proximity to the channel boundary and array size determine the increase in flow velocity observed in this region. It is also unclear whether this increase in any way affects the performance of the array. Finally, it is unclear whether or not there is a certain proximity or array size at which the flow is blocked such that this increase no longer occurs. Should this scenario occur, the improvement in performance of turbines installed in this region would no longer occur, and the ecological impacts could potentially no longer be an issue.

It is the absence of any analysis of the implications of tidal array position and blockage ratio that has determined the hypothesis to be tested herein. It will be examined what if any changes to performance of a tidal array and corresponding flow effects within the flow domain can be attributed to changes in these parameters. Some specific factors to be examined include:

- Changes to the wake downstream of a tidal array, in terms of parameters such as wake recovery to freestream conditions, Reynolds shear stresses and wake turbulence intensity.
- Changes to the magnitude of increase in flow velocity compared to ambient conditions.
- Changes to the distribution of volumetric flow rate between sub channels in a split tidal channel flow domain, and the implications for extractable power available in the domain.

An experimental investigation will be conducted to examine these factors. It is expected that this will add to the knowledge of tidal turbines gained from the analyses of reviewed literature and allow tidal developers to make more informed decisions when deciding the design and specifications of their specific tidal power projects.

In terms of how to examine the flow effects of rows of turbines experimentally, literature has given a clear insight into what valid methods are available for projects with limited resources. Myers et al. and Stallard et al. have demonstrated that porous discs can be used to experimentally examine the flow conditions in the far wake downstream of individual tidal turbines. While groups of these discs could also replicate groups of turbines, Harrison et al. (2008) and Whelan et al. (2009) have shown porous fences to be equally valid under certain conditions. The methods used in reviewed research has been carefully considered, along with the time and resources available for this research, to determine the methods of research which will presented later in this thesis.

Chapter 3

Experimental method

3.1 Circulating water flume in Chilworth hydraulics laboratory

All experimental investigation carried out in this study took place in the indoor circulating water flume of the Chilworth hydraulics laboratory, shown in figure 3.1. The flume is a conventional gravity fed flume, which has a length of 21m and width of 1.37m. As the water flow in this type of channel is gravity fed, it differs from some other water channels, in that inflow conditions are unaffected by the presence of obstructions in the working section. Water is contained in sumps beneath the open channel working section, and three pumps draw the water into three pipes. These pipes run from the sumps of towards the inlet of the channel, and consist of valves which can be opened and closed to control the amount of water entering

Figure 3.1: Indoor circulating water flume of Chilworth laboratory

the channel. After passing through the valves, the water falls vertically into a sump at the upstream end of the working section, whereupon it flows down the channel under the force of gravity. Upon reaching the end of the open channel, the water spills over a weir gate, which can be adjusted to control the depth of the flow in the channel. The water spills back into the sumps beneath the open channel to be recirculated again. The valve and weir gate settings used in these experiments were such as to ensure a freestream flow velocity of between 0.3m/s and 0.33m/s and a flow depth of approximately 0.3m was used. This gives a Froude number of 0.19, which is in the low Froude number range usually associated with tidal sites, for reasons already discussed in section 2.5.6.

Between full scale (prototype) system and scaled down (model) experimental models, similarity of Froude number is required to ensure the ratio of inertial to gravitational forces are equal in both. In the case of open channel flow, this condition is absolutely essential due to the fact that flow is driven by gravitational forces. Also ideally, we would have Reynolds number parity between model and prototype, which is the ratio of inertial to viscous forces. However this is not physically possible with the same model as both Froude and Reynolds numbers are dependent upon the characteristic length of a system and they do not scale equally; Froude number scales with $\sqrt{l}$, Reynolds with l^{-1}. Disparity between Froude and Reynolds scaling is accepted providing that the Froude number disparity does not result in an un-representative flow and that resulting Reynolds number of the small scale experimental setup is in the same turbulence classification as the full scale system. For experiments conducted as part of this work the Reynolds number was of the order of 90000, which is classified as turbulent.

When examining experimental results from this flume, one consideration which was made was the possible head losses between the inlet and outlet due to friction. Open channel hydraulics theory provides for estimating this head loss via the following expression given by:

$$S_f = \frac{U^2 n^2}{R^{\frac{4}{3}}} \tag{3.1}$$

Where n is a Manning's roughness coefficient specific to every material, R is the hydraulic radius of the channel (given by the wetted perimeter divided by cross sectional area) and S_f is the friction slope. To estimate the total head loss $\triangle h$ over a channel of length L and flow depth h can then be estimated using the expression:

$$\triangle h = S_f L h \tag{3.2}$$

In estimating this head loss for the Chilworth flume:

- the hydraulic radius was 0.2086m.
- the flow depth was approximately 0.3m.
- the Manning's coefficient chosen was 0.0155. This was a compound Manning's n for the Chilworth flume. This needed to be calculated due to the different materials within the wetted perimeter of the channel. This is discussed in more detail in section 3.7.5.
- the value for flow velocity was chosen as 0.3m/s. While it is acknowledged that this will

vary throughout the flume due to flow development, it was decided this value would give a good rough estimate of friction slope and possible head losses.

Inserting these values into equation 3.1 gave a friction slope of 0.0002. When inserted into equation 3.2, this gave a rough estimate for head loss due to friction along the entire channel of approximately 1.3mm, representing a reduction of 0.43%. The actual length of channel used for experimental analysis was much less than this, at most 3m. If a constant gradient is assumed from inlet to outlet, this means a reduction in water surface elevation of 0.18mm, or 0.06% of the depth.

A graphical description of the experimental flow domain, including the actuator fence in the flume, is shown in figure 3.2. The flow depth was kept constant at a depth of 0.3m. In normal open channel experiments, the longitudinal position of the actuator fence with respect to the inlet of the flow was kept constant at 12m, for reasons explained later in section 3.2.

3.2 Actuator fence and thrust measurements

An example of the actuator fences used in experimentation is shown in figure 3.3. As already discussed in section 2.4, these can represent rows of closely spaced tidal turbine rotors. The actuator fence was simply a rectangular plate of either PVC or perspex material which had holes drilled into it. Static disks require holes to appear semi-porous to the incoming flow in the same way that a set of rotating blades is. The effect of increasing the ratio of open to closed area (porosity) is to reduce the axial thrust acting on the disk (and hence coefficient of thrust) in the same way that reducing the blade tip speed on a mechanical turbine leads to

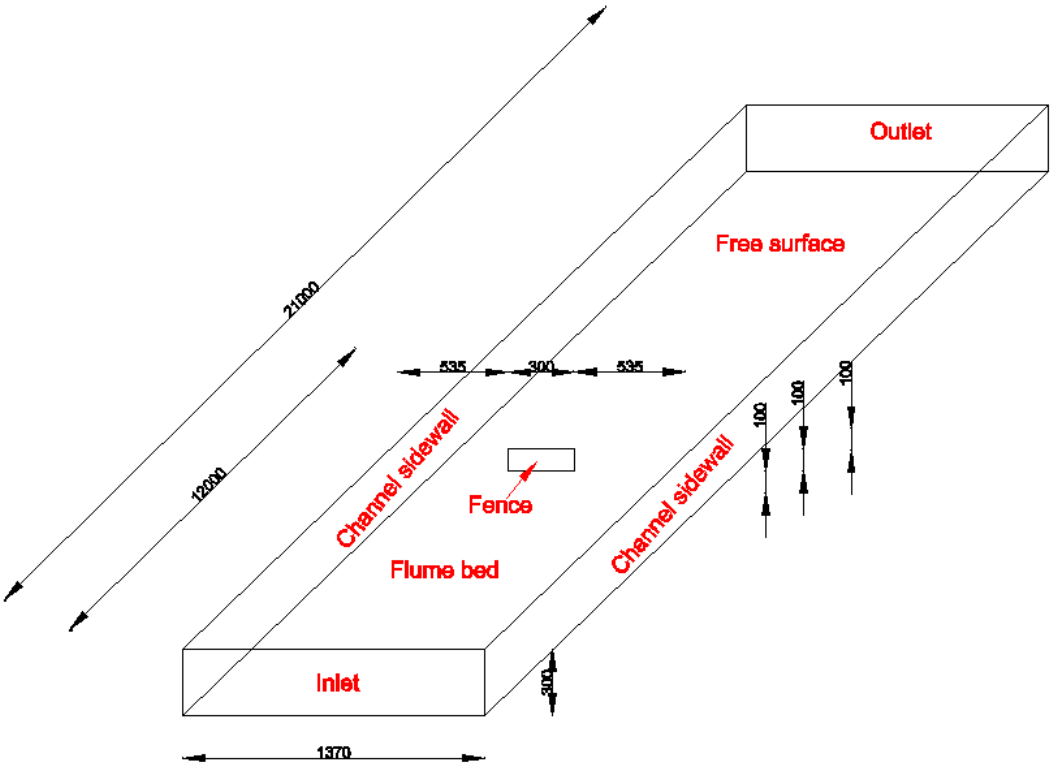

Figure 3.2: Graphical description of experimental setup in Chilworth flume

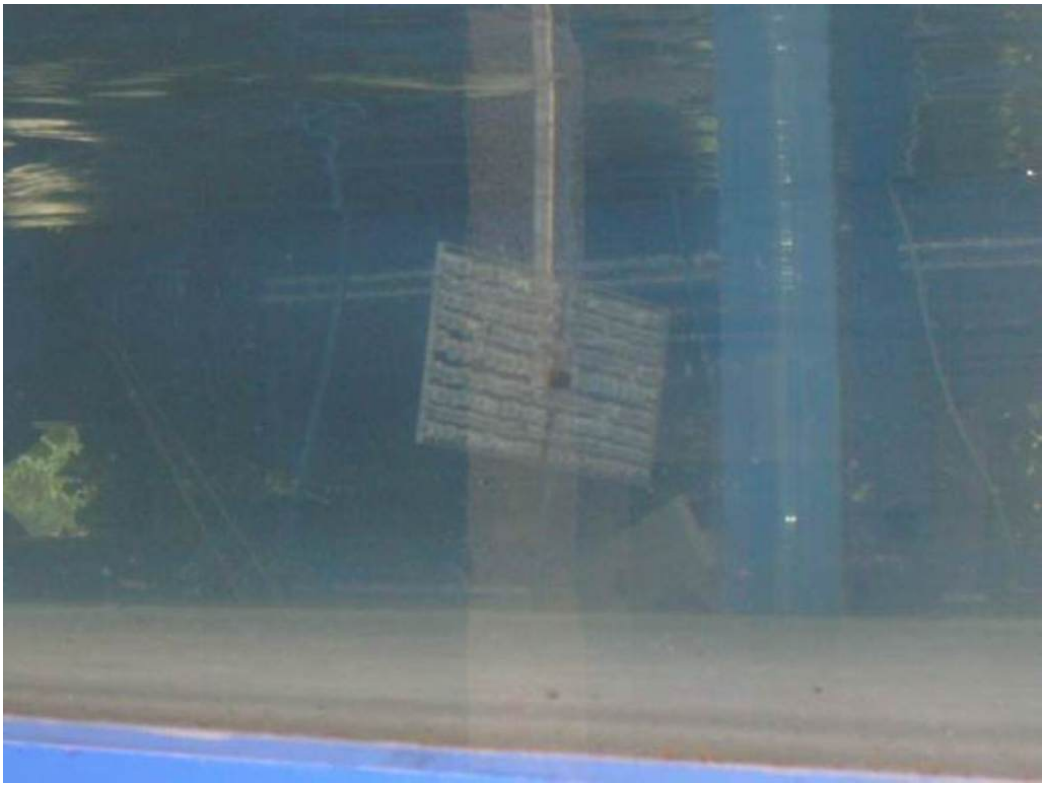

Figure 3.3: Actuator fence submerged in Chilworth flume

a reduction in thrust. Thus the porosity of a static fence can be tuned to be representative of a particular operating point of a mechanical turbine. At present there are no operating rows of tidal turbines to provide full-scale values of thrust coefficient but the aim of this work was to qualitatively investigate the effect of changing thrust force upon the diversion of flow around a row of turbines. Thus the porosity was approximated to that used with previous studies of single static disks. The hole pattern was designed such that the static fences could be reduced in width whilst retaining the same porosity or ratio of open to closed area.

To ensure thrust was distributed as evenly as possible, it was desirable that the hole pattern throughout the length and depth of the fence was approximately uniform. Also for the case where the fence was reduced in width in order to analyze changes due to different blockage ratios, a uniform hole pattern ensured that the open to total area ratio remained constant. In experiments involving different width fences, each fence was 100mm height and width between 300mm and 600mm. This represented blockage ratios of between 0.072 and 0.146 with the channel flowing full width and at 0.3m depth. The pattern of each 50mm increment of the fence is displayed in figure 3.4. The pattern is symmetrical through both the width and depth of the fence to ensure even thrust distribution, and was also observed to maintain its rigidity during testing and allow a fully developed actuator fence wake to form.

The height of the fence used was held constant at 0.1m, which from now on will be referred to as a fence diameter. As the fence represents closely spaced tidal turbines in a row, this is the same as an actuator disc diameter. For simplicity and to give some indication of the applicability of results to real turbine applications, many of the results outlined in chapter 5 will use actuator fence diameters as their unit of distance.

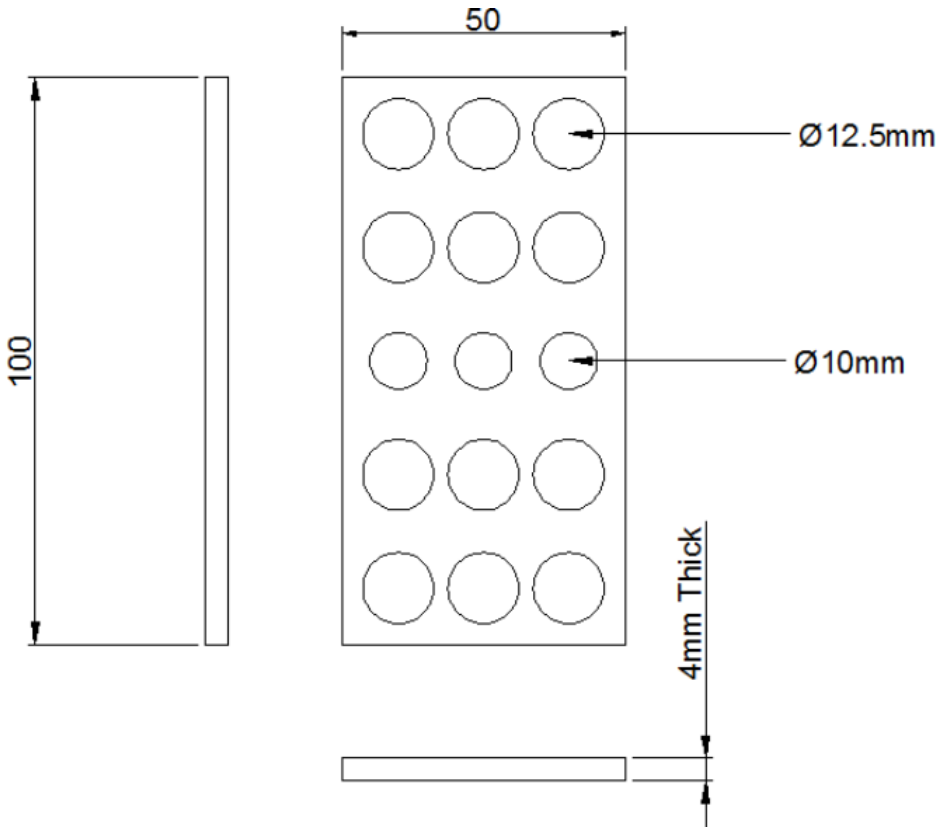

Figure 3.4: Hole pattern of each 50mm width for large actuator fences

3.2.1 Measurement of thrust force acting upon the actuator fences

Thrust and thrust coefficient are the main parameters by which the changes in performance of tidal turbines can be quantified with actuator fences. Therefore it was necessary to analyze how the thrust on the actuator fence changed with varying fence size and position. In these experiments, an S beam load cell was positioned at the top of a specially designed rig designed to mechanically amplify the relatively small forces exerted on the actuator fences. Also attached to this rig was a metal stem, onto which the actuator fence was in turn attached at the bottom and submerged in the water circulating through the flume (Figure 3.3). The mechanical force exerted by the water on the fence was mechanically amplified through the length ratio of fence to pivot and pivot to load cell. 1024 voltage readings were recorded over a period of one minute. The output voltage was recorded using a volt metre data acquisition system. An example of the calibration curve for one of the load cells is shown in figure 3.7.

Due to force variation over time, which can simply be attributed to the turbulence of the flow, it was decided the most appropriate method of gaining accurate force measurements was to acquire several one minute samples. A minimum of 5 such readings were taken, but more were taken if required to ensure that after each reading, another further reading did not change the cumulative average thrust by more than 1%. After thrust forces were calculated by applying output voltage to the calibration curve, thrust coefficient was calculated using equation 2.46.

A fully dimensioned engineering drawing of the load cell rig used for thrust measurements

is given in appendix A.

3.2.2 Estimating power dissipated by actuator fences

After determining the thrust and C_T results, it would be very useful to examine the amount of power which each actuator fence dissipates into unusable heat. There are however a number of difficulties associated with this, which make it very difficult to get an accurate and trustworthy estimate. The first possible method would be to use the actuator disc theory in section 2.5.4 to estimate the axial induction factor a, and from there calculate the power coefficient C_P and the power removed. However as the flow in question is highly constrained

(compared to a situation such as a single actuator disc) and the C_T is above the theoretical maximum of 1. In this case conventional actuator disc theory is no longer valid, as it assumes an infinite or unconstrained flow field. Even using the empirical modification in section 2.5.4 can only give a very rough estimate. When the values for C_T were applied to this theory, it predicted negative values for axial induction factor. From the theory of section 2.5.4, this implies an increase in velocity of the flow as it approaches the surface of the fence, which is obviously not the case as the flow velocity must reach zero at some point on the solid surface of the actuator fence.

Another possible method would be to multiply the thrust on the actuator fence by the velocity used to calculate C_T. But this method is also somewhat unreliable, a good example of which is provided by examining the largest 0.146 blockage ratio (600mm wide) fence. Using

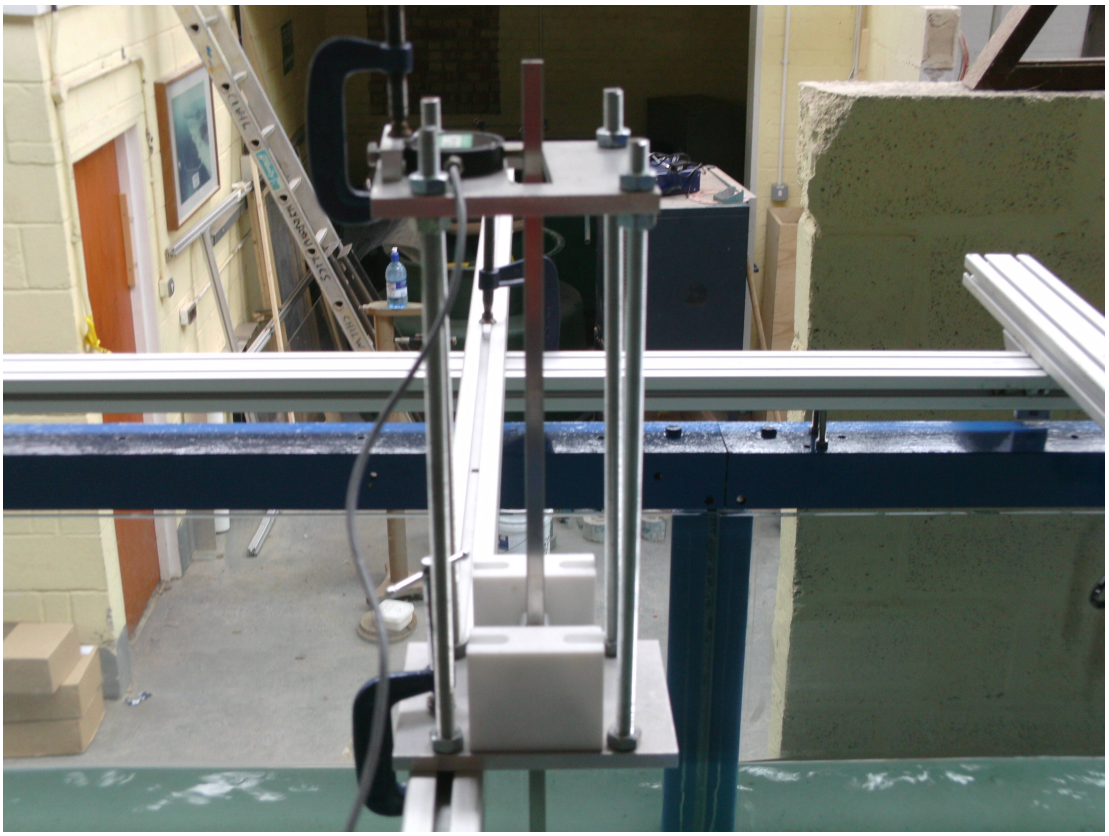

Figure 3.5: Load cell rig and Load cell

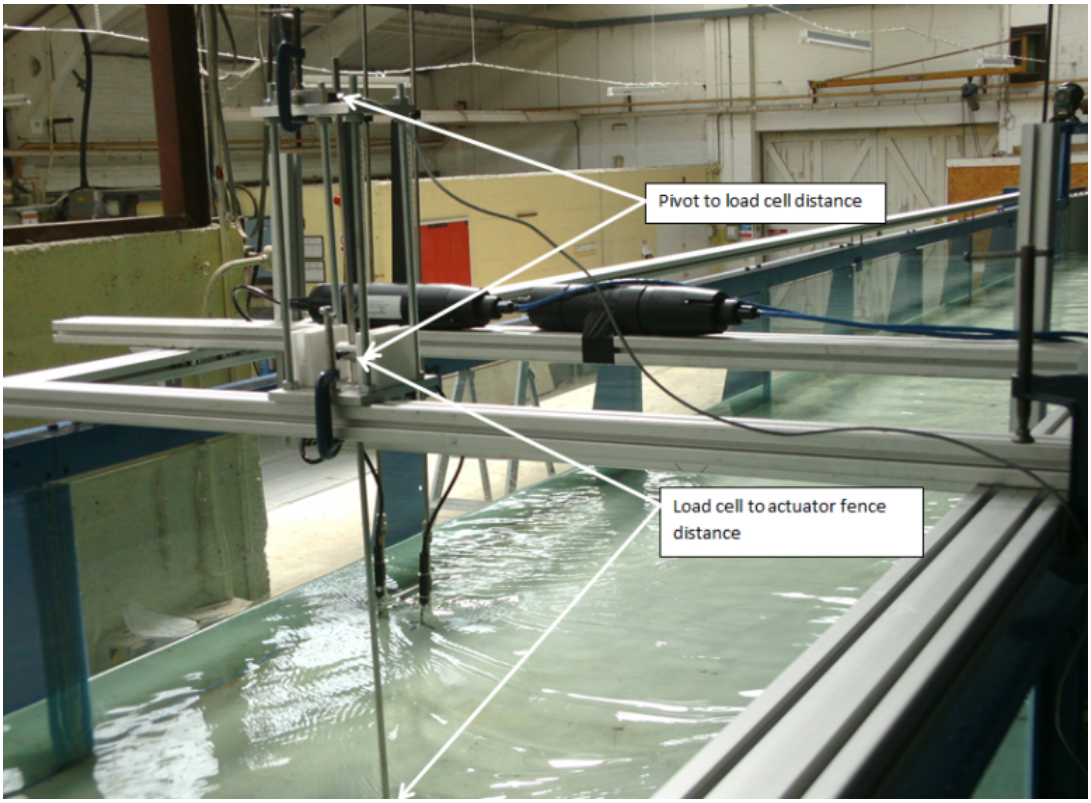

Figure 3.6: Distances required for thrust amplification correction

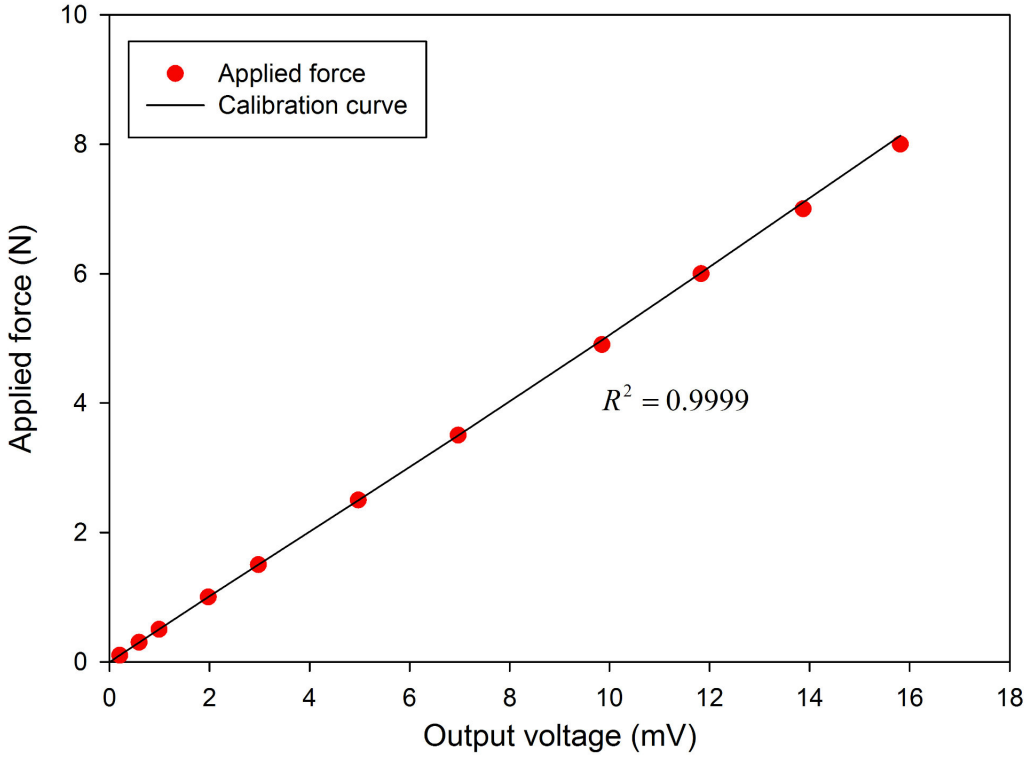

Figure 3.7: Example of calibration curve used for load cells

the value for average flow velocity across the flume cross section of 0.326m/s (determined in section 4), and inserting into equation 2.48 gives a power in the chilworth flume of 7.1 watts. The incident power on the largest actuator fence would therefore be 14.6% of this figure, or 1.03 watts. It is worth examining the corrected theoretical maximum limit available using equation 2.66 proposed by Garrett and Cummins (2007). The cross sectional area of the flume is $0.411m^2$(1.37m wide by 0.3m deep flow), while the area of the fence is 0.06m^{2} (0.6m wide by 0.1m deep). This gives a value for $1 - \epsilon$ in equation 2.66 of 0.854. When inserted into the expression, along with the aforementioned value for velocity of 0.326m/s, a theoretical value of 81.3% of incident power, or 0.886 watts is found. Multiplying each thrust reading for these fences by flow velocity used to calculate their respective thrust coefficient gives values between 0.99 and 1.16 watts, both of which are considerably higher than this theoretical limit. The argument could be made that a constrained flow may mean more flow is being entrained through the fence than either of the aforementioned authors theory may predict. But it is still not possible to consider the use of thrust multiplied by flow velocity as an entirely reliable method of estimating power dissipation by the actuator fences.

This means therefore that thrust and C_T, and the general trends which they follow, are the only reliable methods by which changes to turbine array performance can be examined in highly constrained flows involving porous media.

3.3 Acoustic Doppler Velocimeter (ADV)

The experimental analysis required quantification of the flow properties (velocity and higher order effects) at several points throughout both an empty and an occupied flume. There were a number of possible devices which could have been used for such measurements. However it was imperative in this instance that the device used did not intrude on or artificially alter flow velocities in any way. A non-intrusive flow measurement device known as an Acoustic Doppler Velocimeter (ADV) was used for these experiments. The ADV measures flow velocity in three directions at high frequency by utilizing a physical phenomenon known as the Doppler effect. This is defined by Rosen and Quinn-Gothard [2009, p.154] as the change in the observed frequency of a wave due to the motion of the wave source or observer.

3.3.1 Basic operation

The ADV consists of an end probe, with a 6mm diameter central stem and four receiver arms. (Figure 3.8). Sound pulses are emitted from the central stem of the ADV down into the water. The volume of water in which velocity is recorded is a cylindrical volume, the centre of which is 50mm from the end of the probe. These sound pulses are reflected by suspended sediment particles in the water, and the return signal is then detected by the 4 receiver arms. Due to the motion of the water and Doppler shifting effects, the apparent frequency of the returned sound pulse is different from the frequency of the sound pulse originally emitted. It is by measuring this apparent change in frequency that the ADV can calculate the flow velocity of the water in all directions. The original sound pulse frequency can be adjusted from 10 to 200 Hz. A frequency of 50 Hz was used in these experiments. This

relatively low frequency is recommended by Myers (n.d.), as higher frequencies can result in electrical noise falsely recording turbulent energy which is not actually present in the flow. Furthermore, an in depth analysis of the accuracy of the ADV by Voulgaris and Trowbridge [1998] (which is discussed in more detail in section 3.3.8). found that a frequency of as low as 25Hz gave values for mean velocity to within 1% of those measured by a laser Doppler velocimeter, and values for Reynolds stresses to within 1% of those calculated using a "ground truthing" theoretical method derived from fundamental theory of acoustics. Both of these findings from the respective authors meant that the judgement was made that 50Hz would be a sufficient sampling frequency for all experiments.

To ensure a balance between accuracy and experimental time, a 3 minute sample was chosen. A frequency of 50Hz and time of 180 seconds meant that for each spatial location, 9000 readings were recorded. A more in-depth discussion of the 3 minute sampling time and justification for its use is given later in section 3.3.6. For recordings at extremely close proximity (approximately 0.5 actuator fence diameters) to channel sidewalls, a normal vertical probe was unable to record due to the extension of its receiver arms outwards. For these recordings, a side looking ADV probe with its four receiver arms tilted 90 degrees to the vertical was attached to the ADV.

3.3.2 Accuracy of the ADV

The accuracy of measurements from the ADV is dependent on the concentration of suspended sediment in the fluid in which it is operating. It has only become more commonly used in approximately the last twenty years, but many studies have shown it to display similar experimental results to other devices such as Laser Doppler Velocimeters (LDV). As an example, a study by Voulgaris and Trowbridge [1998] showed that an ADV can measure flow velocity and Reynolds stress values to within 1% of the corresponding values for an LDV.

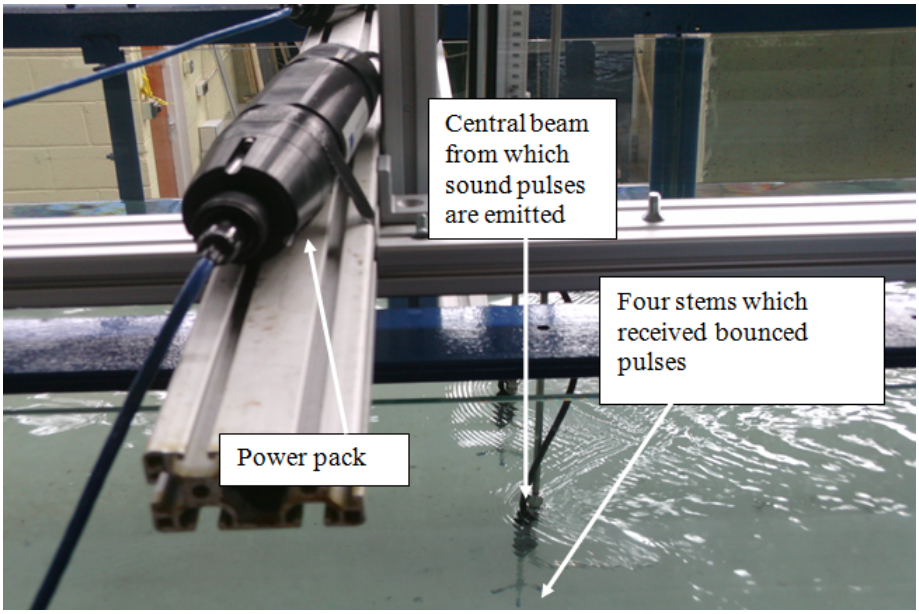

Figure 3.8: Description of ADV and its constituent parts

Two ways in which the user can analyze how accurately the ADV is performing is through the correlation and signal to noise ratios (SNR). Both of these are outputted, along with flow velocity values, by the specialized ADV software.

The correlation coefficient (R^2) is a widely used statistical analysis parameter. Its application to the ADV is discussed by Myers et al. [2008]. Here it is a measure of data quality calculated during Doppler velocity calculations. The correlation coefficient is defined by the following expression:

$$R^2 = e^{-2\pi^2\phi_r^2} \tag{3.3}$$

Where ϕ_r is the dimensionless spectral width, given by the product of the received signal width and time interval. Therefore though not being a physical quantity, it can still give an intuitive indication of how well the ADV is performing and whether there is a sufficient amount of suspended sediment. Nortek, the manufacturer of the Vectrino ADV used in these experiments, recommend correlation values remain above 70%.

Separately, the signal to noise ratio is the ratio of the strength of the ADV signal to the strength of signals of ambient noise, such as the pumps of the flume, electrical noise or vibrations induced near the bed of the flume by the movement of equipment during testing. If particularly strong in comparison to the ADV signal, noise can potentially interfere significantly with ADV readings. Nortek recommend a minimum SNR of 15 should be observed. As well as its non-intrusive nature, one other reason why the ADV was suitable to this investigation is that the Chilworth flume is located in a hard water area. This means that the flume already had a large concentration of suspended sediment in it. This meant that correlations and SNR were consistently above the recommended limits of 70% and 15 respectively.

One other issue which needed to be considered when using the ADV was reflection errors. These reflection errors are identified by Myers and Bahaj [2010] as occurring when a sound pulse which is returning to the four receiver arms of the ADV probe intercepts a subsequently emitted sound pulse within the measured sample volume. This leads to a large amount of energy artificially induced in the sample volume, with the result being that the ADV erroneously records data which suggests there is greater turbulence within the sample volume than is physically present. This phenomenon can give particularly erroneous results when examining higher order effects such as Reynolds stresses and turbulence intensity. As predicted in the aforementioned reference, such interception was observed when the conventional ADV probe was sampling at a height of 90mm above the bed of the Chilworth flume. It was also evident when the side looking probe was positioned between 70mm and 85mm from the flume sidewall. While filtering was one option for dealing with these reflection errors, it was judged that a more reliable method of avoiding reflection errors was to simply move the ADV a few millimetres until visual observation of live data with the Vectrino software showed no more reflection.

3.3.3 Configuration of the ADV

To account for the number of varying flow conditions under which the Vectrino ADV can operate in, there are certain configurations of the sound pulse it emits which can be altered. It is possible for the user to change this configuration to ensure as accurate a result as possible, and to ensure consistently high SNR and correlation. Three particular characteristics of the sound pulse which can be configured are:

(a): The transmit length. This represents the length of the sound pulse emitted from the ADV at the specified user acquisition frequency (Poindexter et al. [2011]), in this case 50Hz. With the Vectrino ADV five possible settings are available, 0.3mm, 0.6mm, 1.2mm, 1.8mm and 2.4mm.

(b): The sampling volume. This is the actual height of the volume of water within which flow velocities are measured by sound pulses bouncing off suspended sediment. In theory the transmit length and sampling volume are independent of each other. However for the Vectrino, each transmit length has 5 different options for sampling volume, with the Vectrino defaulting to the optimised sampling volume for each transmit length (Ramsay Lind, Nortek UK, personal communication). This is optimised in terms of what is likely to achieve the best possible correlation and SNR.

The sampling volume was chosen as 3.1mm. This represented approximately 1% of the depth, and was chosen as it was considered to give the best possible compromise between reducing velocity shear across the sample volume and maximising SNR and correlation values. The default optimised transmit length for this sample volume, 2.4mm, was also selected.

(c): The velocity range. This setting can be changed depending on the expected flow velocity to be measured. Physically, an adjustment of this setting changes the phase lag between consecutively emitted sound pulses (Rusello et al. [2006]), and so effectively change the wavelength of the sound pulses used to measure flow velocity. Rusello et al. (2006) details the benefits and possible problems associated with large or small velocity ranges. Having too small a velocity range can lead to too large a phase lag, which in turn can lead to poor correlation and possibly a greater chance of reflection errors (where sound pulses just emitted from the ADV can interfere with those returning to it after reflecting off suspended sediment). Too large a velocity range leads to small phase lags which may be more susceptible to the influence of background noise, reducing the SNR below the recommended values. Selecting the lowest possible velocity range for any particular flow is recommended by Rusello et al. For the flow in the Chilworth flume, a nominal velocity of 30cm/s was selected, which actually allowed a max U velocity of 94cm/s (Myers n.d.).

3.3.4 Long term variability of flow characteristics

Examination of possible variability in flow velocity was an essential step in quantifying experimental error. The flow velocity at any given point in the flow was likely to vary to some extent between measurements. There were a number of possible reasons for this, such as:

- Changes in the concentration of suspended sediment over time.
- The propagation of wake effects off small foreign objects.

- The propagation of wake effects off the panels on the floor of the flume.
- Heating of components in the pumps of the flume after a long period of operation.
- Small variations in pump speed or control valve position.

Quantifying and being aware of this variation is critical for assessing experimental results. This is particularly true where there is an examination of quantities such as thrust and shear stresses. This is because they are calculated from products or squares of velocity, and so will consequently be more susceptible to these errors.

Examination of long term repeatability simply involved measuring the flow velocity at certain points with the ADV, and then retaking these readings a long period of time later. The points examined were all at centre depth of the flow, and included points lying within the boundary layers coming from the sidewall of the flume. This area was possibly more prone to such variation due to the large pressure gradients present. In this case, flow velocity were recorded at a number of points laterally along the flume at a distance of 12m downstream of the inlet. The period of time allowed to elapse between readings was 6 hours, during which time the flume was constantly in operation.

The results of this analysis are given in table 3.1. They show a very steady flow in the Chilworth flume, the greatest deviation was 1.74%. This is consistent with the results of Myers and Bahaj (2010) which also showed flow velocity measurements in the Chilworth flume to be repeatable within 2%.

3.3.5 Filtering of ADV data using velocity correlation filter

Several methods have been put forward for removing seemingly corrupted data from groups of ADV data. Reasons why this corrupted data might be present in samples in this work

Distance from sidewall (mm)	Reading 1 (m/s)	Reading 2 (m/s)	% difference
20	0.2303	0.2263	1.74
40	0.2484	0.2462	0.89
60	0.255	0.257	-0.78
120	0.2638	0.266	-0.83
200	0.2675	0.27	-0.93
250	0.276	0.273	1.09
300	0.28	0.281	-0.36
340	0.28	0.282	-0.71
350	0.283	0.285	-0.71
360	0.283	0.284	-0.35
420	0.2867	0.288	-0.45
450	0.2869	0.284	1.01
490	0.2864	0.288	-0.56
550	0.2896	0.292	-0.83
600	0.2945	0.291	1.19
650	0.2908	0.294	-1.1
750	0.29	0.295	-1.72

Table 3.1: Results of examination of natural variation of flow velocity in Chilworth flume

include:

- The presence of debris in the water flowing through the channel.
- Background noise such as the noise of the flume pumps or electrical noise.
- Some small reflection errors due to interception of ADV sound pulses by other sound pulses returning to the ADV receiver arms.
- Entrained air in the water.
- Variation in concentrations of suspended sediment.
- Errors in instrument processing.

A good overview of four different methods was presented in Cea et al. [2007]. Upon review of all four methods, it was decided that a velocity correlation filter as described by the authors was the most appropriate for this work. The main reason for choice of this method is that it was the only of the four methods where the decision of whether or not to remove a reading was based on its relationship to the entire sample. There are also no user defined filtering parameters, which removes the need for making any possibly erroneous assumptions. This is in contrast to other methods, where criteria is on the basis of the relationship between consecutive readings and user defined parameters are required. This is unsuitable for flow domains where large regions of flow exist which have very different average flow velocity to other large regions of the flow domain. The wake of an actuator fence is a good example of such a flow.

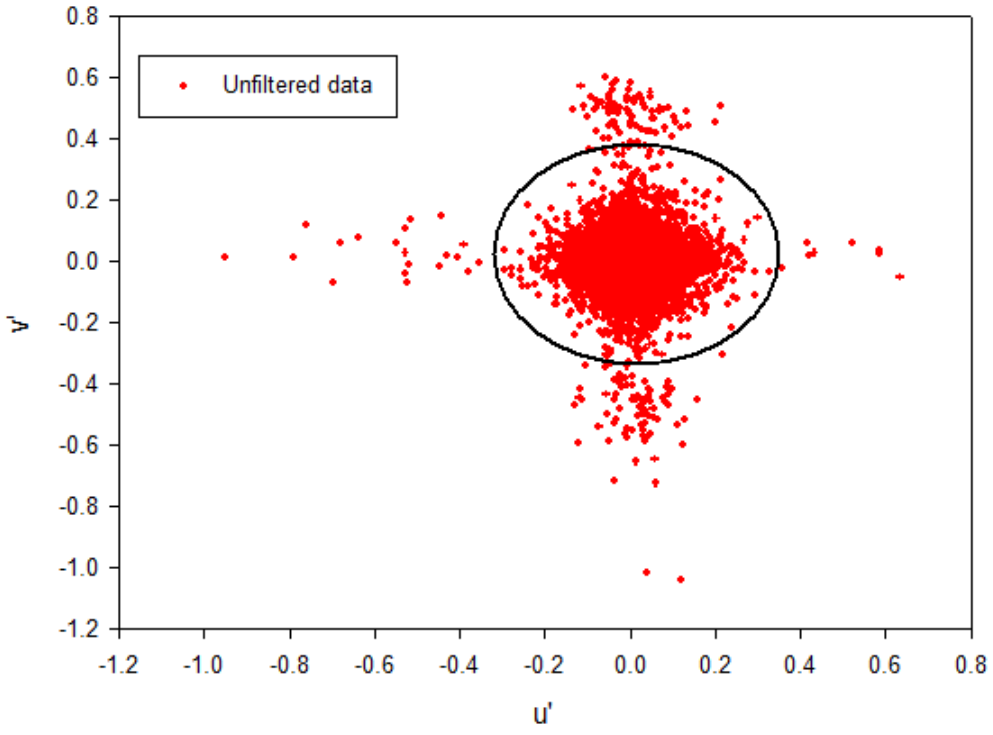

Figure 3.9: Demonstration of velocity correlation filter proposed by Cea et al. [2007]

The velocity correlation filter starts by calculating a mean value for all three components of velocity, U, V and W in the X, Y and Z directions respectively. Subsequently, the deviation of each reading from these mean values, u', v' and w' are calculated, and plotted against each other on axes as in figure 3.9. The origin of this plot represents mean sample velocity for both quantities. It can be seen from figure 3.9 that the majority of the data clusters together towards the origin. The velocity correlation filter acts by using statistical quantities to define the extents and angular rotation of an ellipse. A data point whose deviation from the mean is such that it lies outside this ellipse is considered erroneous and removed from the data set. Physical quantities of the flow are then recomputed using only the data lying within this ellipse. After corrupted data are removed from the sample, no replacement data is added and the value for all parameters, such as mean velocity and turbulence intensity, is recalculated using the remaining data points in the sample.

Linear regression analysis of the data is carried out to determine the dimensions of the ellipsoid. Considering only the plot of u' (deviation from sample mean in the X direction) and v' (deviation from sample mean in the Y direction), and assuming a linear fit between u' and v':

$$v' = mu' + b \tag{3.4}$$

The values for m and b in the above expression are given by:

$$m = \frac{N\sum u_i' v_i' - \sum u_i' \sum v_i'}{N\sum u_i'^2 - \left(\sum u_i'\right)^2} \tag{3.5}$$

$$b\sum u_i' = \sum u_i' v_i' - m\sum u_i'^2 \tag{3.6}$$

Assuming the mean of the deviations from the mean velocity is zero, the values for the coefficients b and m in the above expressions can be described by:

$$b = 0 \tag{3.7}$$

$$m = tan\Theta = \frac{\sum u_i' v_i'}{\sum u_i'^2} = \frac{\overline{u_i' v_i'}}{\overline{u_i'^2}} \tag{3.8}$$

In the above expressions, θ represents the angle of rotation of the principle u' and v' axes. The extents of the ellipse X_o and Y_o along the u' and v' axes respectively are given by the following expressions:

$$X^2 = \frac{(\lambda\sigma_u cos\Theta)^2 - (\lambda\sigma_v sin\Theta)^2}{cos^2\Theta - sin^2\Theta} \tag{3.9}$$

$$Y^2 = \frac{(\lambda\sigma_v cos\Theta)^2 - (\lambda\sigma_u sin\Theta)^2}{cos^2\Theta - sin^2\Theta} \tag{3.10}$$

Similar calculations for the above results are carried out for values in the v'w' plane and u'w' plane. This filter was applied by writing a code in the Matlab programming language.

The ADV sample sets were inputted, and Matlab outputted all relevant quantities from each measurement point after application of the above filter. The code also included provisions for calculating average flow velocities, turbulence intensities and Reynolds shear stresses.

3.3.6 Examination of short term variability in Chilworth flume

The sampling time for ADV measurements is an important consideration in ensuring experimental accuracy. While the Chilworth flume is considered a steady state flow, it was important to examine how much of an effect the length of sampling time had on the overall results, and whether or not there were any unsteady flow phenomenon which a 3 minute sampling period may not account for.

Figure 3.10 shows a 15 minute sample before and after the velocity correlation filter described in section 3.3.5 is applied. The total dimensions of the flume sumps are approximately 26m long, 1.2m wide and 1m high, giving an approximate volume of water contained in the sumps of $31.2m^3$. As will be explained later in section 5.2, the volumetric flow rate through the channel of the flume for much of the work presented herein was estimated to be $0.134m^3/s$. This means that over the 900 seconds of the 15 minute sample, approximately

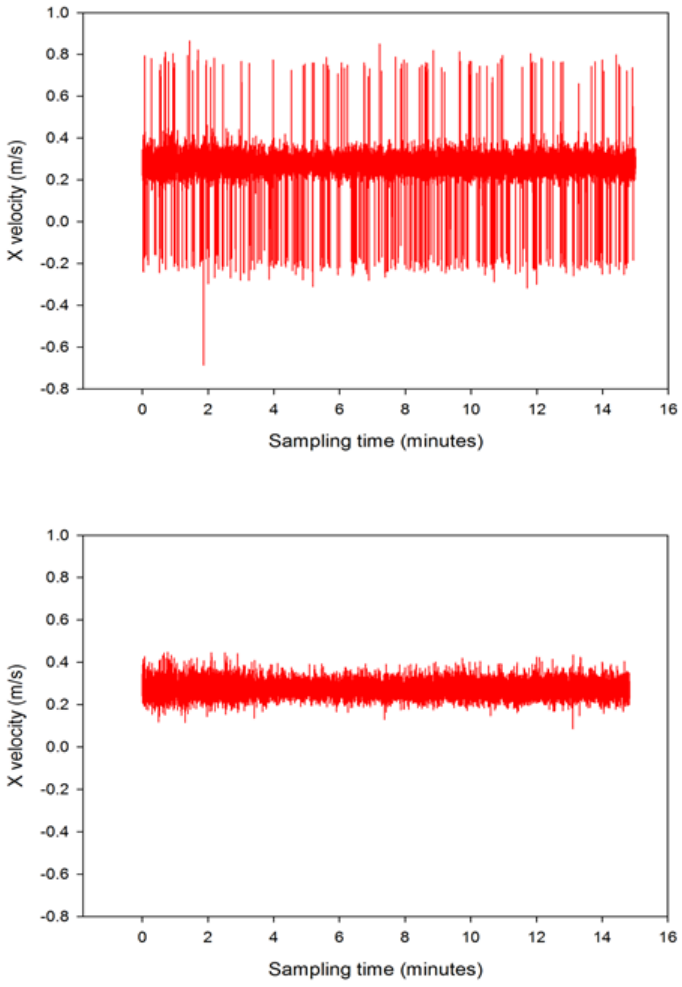

Figure 3.10: ADV data for 15 minute sample before filtering (top) and after filtering (bottom)

$120m^3$ of fluid has passed through any cross section of the channel. This means all the fluid contained in the sumps has traveled through the channel at least 3 times.In this particular case, the filter removed 490 points, or 1.1% of the total number of readings. These results suggest that after filtering, there are no immediately obvious unsteady flow phenomenon which occur over any length of time during the 15 minute sampling period.

To ensure an appropriate balance between experiment accuracy and duration, it was important to examine the necessary sampling period of the ADV. The accumulated mean of the 45000 readings was calculated, and compared to the accumulated mean after a number of other time increments. The results of this analysis can be seen in figure 3.11 and table 3.2. Once again, they clearly demonstrate the absence of any unsteady flow phenomenon over the 15 minute sampling period. On the basis of these results, it was decided that a sampling time of 3 minutes gave an acceptable balance between accurate results and experimental time.

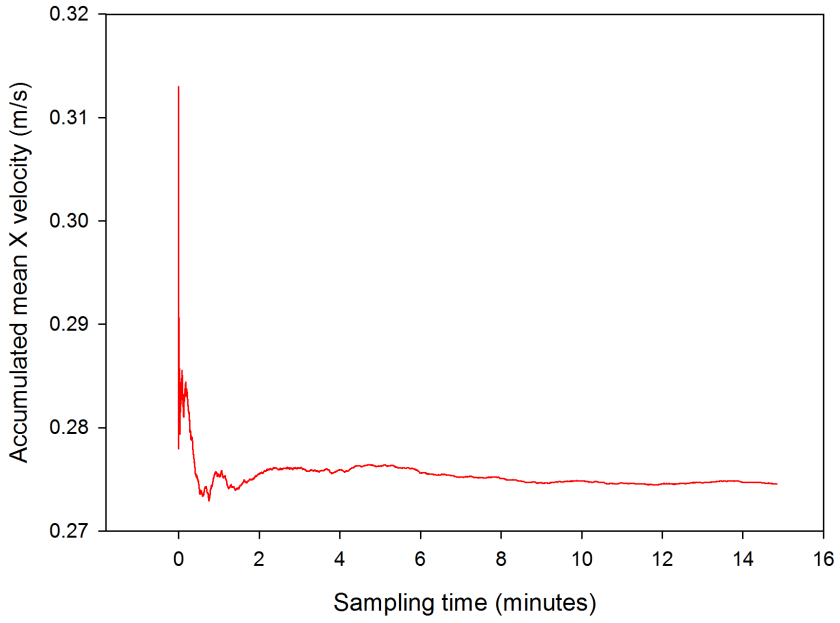

Figure 3.11: ADV data for 15 minute sample before filtering (top) and after filtering (bottom)

Time increment	Average flow velocity (m/s)	% difference from 15 min sample average
0-30 seconds	0.2803	1.81
0-1 minutes	0.2773	0.72
0-3 minutes	0.276	0.25
0-6 minutes	0.276	0.26
0-9 minutes	0.2757	0.15
0-12 minutes	0.2755	0.05
0-15 minutes	0.2753	0

Table 3.2: Changes in accumulated mean velocity over selected time periods of ADV sampling

3.3.7 Examination of interference between adjacent ADV Probes

One possible source of error associated with using two ADVs was identified. It was considered possible that closely positioning ADVs to each other may have led to artificial local flow

acceleration in the region between them. This in turn could have led to erroneous flow velocity readings. To examine this, flow velocity measurements were taken across the central depth of the flume for a number of scenarios. The first scenario was a single ADV by itself, and subsequent scenarios examined the use of two ADVs with various lateral spacings between them. The results for natural flow conditions in the flume is displayed in figure 3.12, while figure 3.13 shows these scenarios tested in the wake of an actuator fence, 5 diameters downstream of the fence itself. The results suggest that any difference in flow velocity measurements between the case of a single ADV or two ADVs are simply due to natural variation in the flow already discussed in section 3.3.4. It appears safe to conclude that, provided there is a lateral spacing of two actuator fence diameters between them, between them, introducing multiple ADVs to reduce experimental time does not affect the experimental results. Given this conclusion, and the specific points throughout the flume which needed to be examined for subsequent experiments, a lateral spacing between ADVs of two diameters was considered appropriate, and used in all experimental results displayed in chapter 5.

3.3.8 Accuracy of higher order flow parameters

An examination of the accuracy of the ADV device, which includes its ability to record Reynolds stresses and turbulence intensity, was carried out by Voulgaris and Trowbridge [1998]. These authors described how much previous work in examining ADV accuracy consisted of comparisons to measurements from other devices such as LDVs. However an obvious weak-

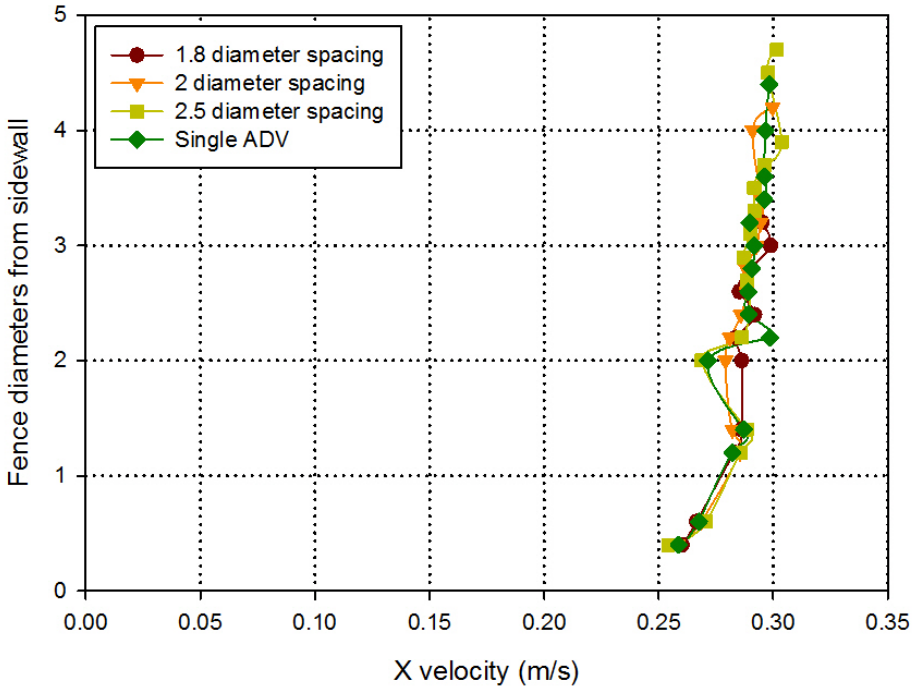

Figure 3.12: Lateral velocity profiles at centre depth with different lateral distances between ADV probes

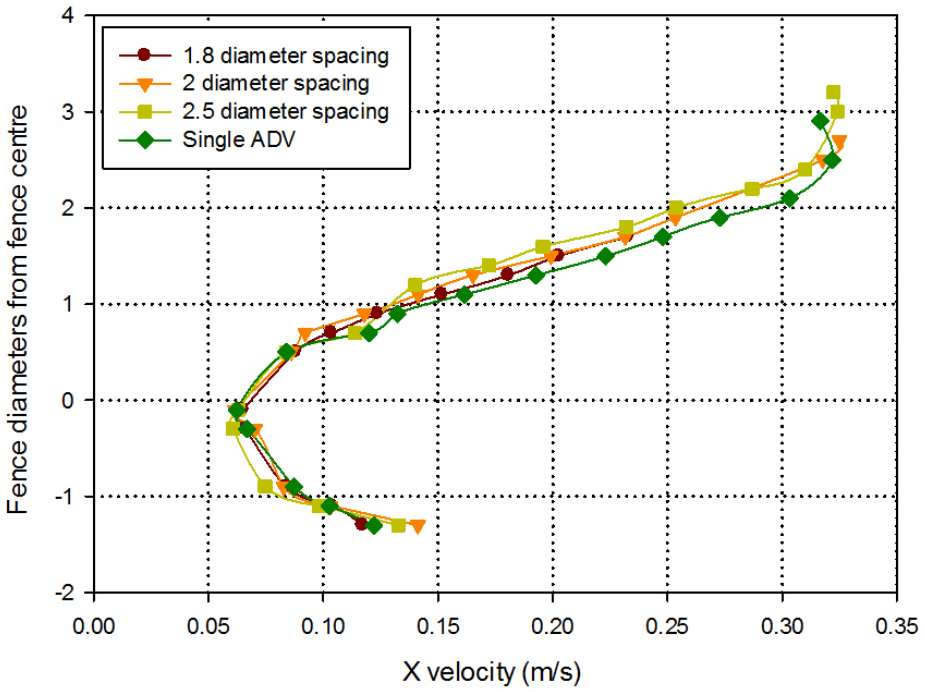

Figure 3.13: Wake velocity profiles 5 diameters downstream of actuator fence at centre depth with different lateral distances between ADV probes

ness with this approach is that no instrument is entirely error free. Therefore in this work, the authors carry out a series of experiments with flow measurements taken using both an ADV and LDV. The authors then apply a "ground truthing" technique of flow characteristics to obtain a true value for the following flow statistical parameters:

- The square of the average of velocity fluctuations in the downstream direction (u'^2)
- The square of the average of velocity fluctuations in the downstream direction (w'^2)
- The Reynolds shear stress associated with these two velocity fluctuations (u'w').

The value of the above parameters recorded by each device is considered to consist of a true value plus an error associated with noise in the instrument. The ground truthing method used by these authors involves estimating the noise associated with these two devices. In the case of the ADV, this involves the use of fundamental theory associated with acoustics, while with the LDV, fundamental theory associated with lasers is used.

In the context of this research, the most important conclusions from this work were:

- ADV readings led to values for Reynolds shear stress which were within 1% of estimated true values. Further support was given to the accuracy of these measurements by their close correlation with Reynolds shear stress profiles predicted by existing analytical models for open channel flow.
- Good agreement between measured and true turbulence intensity values was observed in the vertical direction. However high noise was recorded in the downstream direction,

with the result that turbulence intensity values recorded by the ADV were higher than predicted true values. A postulation for this was the size of the sampling volume used, along with the inability of the ADV sensor to resolve eddies smaller than 1.5cm in the horizontal. This however is an unavoidable feature of the ADV geometry.

The final issue with horizontal turbulence intensities identified by Voulgaris and Trowbridge [1998] was not considered detrimental enough to rule out the examination of turbulence intensity in the analysis presented herein. Rather than finding exact turbulence intensity values, this work is more concerned with general trends in the values of parameters as the geometry and positioning of rows of turbines are altered. As the anomaly of horizontal turbulence intensities is common to all measurements, it was still felt values measured and calculated could give qualitative indications of how turbulence intensity might change depending on specific position and blockage ratio. Also, the fact that the ADV recorded accurate values of Reynolds stresses while sampling at as low as 25Hz gave further confidence to the accuracy of Reynolds stresses found while sampling at 50Hz in the experimentation presented herein.

3.4 Combining experimental error

So far the error for both thrust and flow velocity have both been quantified. The error for thrust has been kept to within 1% by ensuring enough thrust measurements are taken such that the cumulative average thrust on the actuator fence does not change by more than 1% with more subsequent readings. The error associated with mean flow velocity measurements has been examined in section 3.3.4. and shown to be less than 2%. While these two error estimates were considered acceptably small in themselves, it was important to examine what overall error they would lead to when applied to quantities whose calculation required multiple values of these quantities. In this particular study, there are two of these such quantities. They are the thrust coefficient and the velocity normalised against ambient conditions when examining flow constraining due to change in actuator fence position.

Theory on combining experimental error is outlined by Squires [2001, p.29]. If a quantity Z

is given by $Z = A + B$ or $Z = A - B$, and the errors associated with A and B are $\triangle A$ and $\triangle B$ respectively, then the error $\triangle Z$ associated with Z is given by the expression:

$$\triangle Z = \sqrt{(\triangle A)^2 + (\triangle B)^2} \tag{3.11}$$

Similarly, if Z is given by either $Z = AB$ or $Z = A/B$, the error $\triangle Z$ associated with Z is given by:

$$\frac{\triangle Z}{Z} = \sqrt{\left(\frac{\triangle A}{A}\right)^2 + \left(\frac{\triangle B}{B}\right)^2} \tag{3.12}$$

For the normalised increase in flow velocity, given by the constrained divided by the ambient flow velocity, it is necessary to use equation 3.12, with the two quantities being the ambient and constrained velocity. In this case the error of both of these will be 1.74% of their

respective values. For thrust coefficient, it is necessary to use equation 3.12 twice. Firstly to examine the error associated with the U^2 quantity in the denominator of equation 2.46, and then combining this error with the 1% error for thrust, also used in equation 2.46. These errors are included as error bars in graphs presented for the respective quantities in chapter 5.

3.5 Configuration of Chilworth flume for split channel experiments

In analyzing split tidal channels, it was necessary to put in place some artificial obstruction to represent any natural impenetrable landmass which splits one channel into two or more sub channels. The set-up used is shown in figure 3.14. Two thin perspex sheets of length 2m and thickness 15mm were used to represent this impenetrable split mechanism.

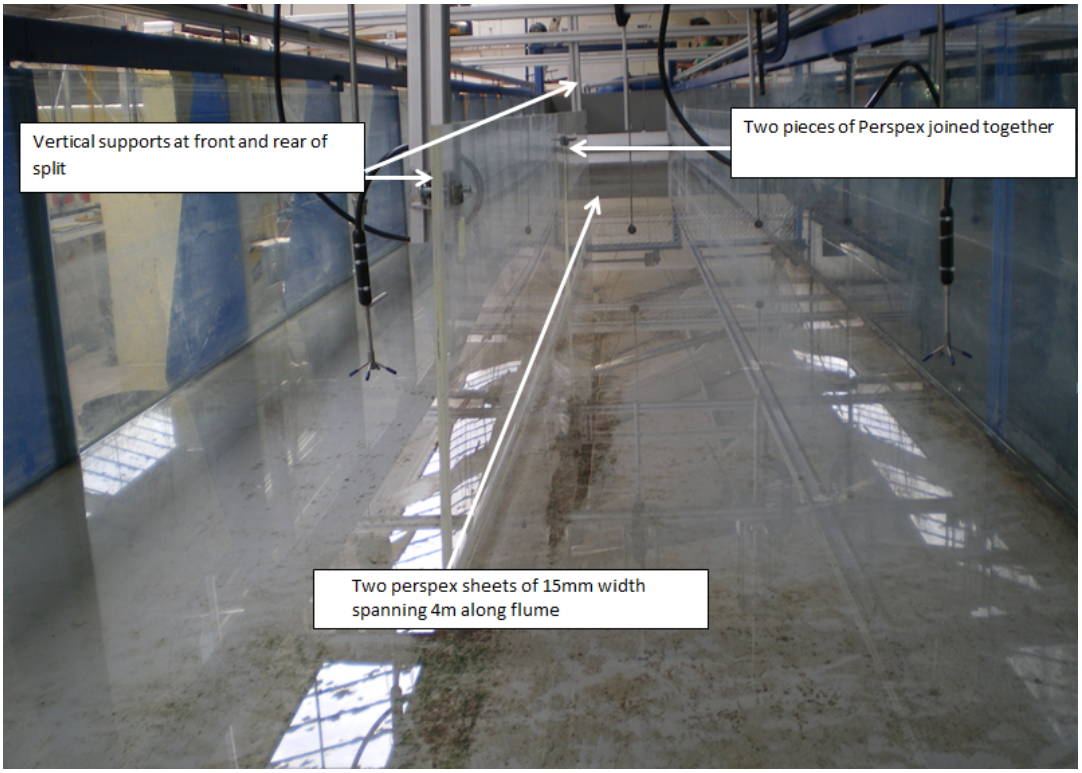

Figure 3.14: Two Perspex sheets held in flume to make 4m long split

3.6 Measurement of reduction in water surface elevation across actuator fences

The importance of changes in water surface elevation associated with the extraction of power from tidal turbines in the context of analyzing flow effects downstream has already been outlined in section 2.1.1. The model of Bryden et al. (2004) has shown a reduction in water surface elevation across a plane of energy extraction. This leads to a reduction in cross

sectional area of the flow, which must be accompanied by an increase in the average flow velocity across any plane downstream due to the continuity principle.

The head difference across an actuator fence was examined in the Chilworth flume using measuring cylinders. (Figure 3.15). These cylinders were both placed outside the channel itself, and were positioned such as to ensure that the bottom of each cylinder lay at the same elevation above ground level. Rubber tubes were attached to nozzles at the bottom of these cylinders. These tubes ran over the side of the flume and were taped to the bed of the flume. To ensure only static head was measured, plastic elbows were placed at the end of the rubber tubes, and these protruded up into the flow to ensure they were perpendicular to the oncoming flow. One rubber tube was placed 150mm upstream of a fence and one was placed 150mm downstream. The lack of an insertion point in the flume also meant that water needed to be syphoned out over the sides of the channel. This syphon was initiated using a water pump, and natural conditions allowed the syphon to operate when the entire rubber tubes were filled with water. An explanation of the physics behind the syphoning action used here can be seen in appendix C.

In order to quantify any change in static head across the experimental domain, measurements were taken for a case of a fence in-situ and with it removed from the flow. This particular analysis was carried out for a 600mm fence in both an open and split channel. In the open channel, this represented a blockage ratio of 0.146, while in the split channel the blockage ratio was 0.295. The presentation of the results of this analysis, along with theoretical calculations from the model of 2.1.1 are presented in section 4.

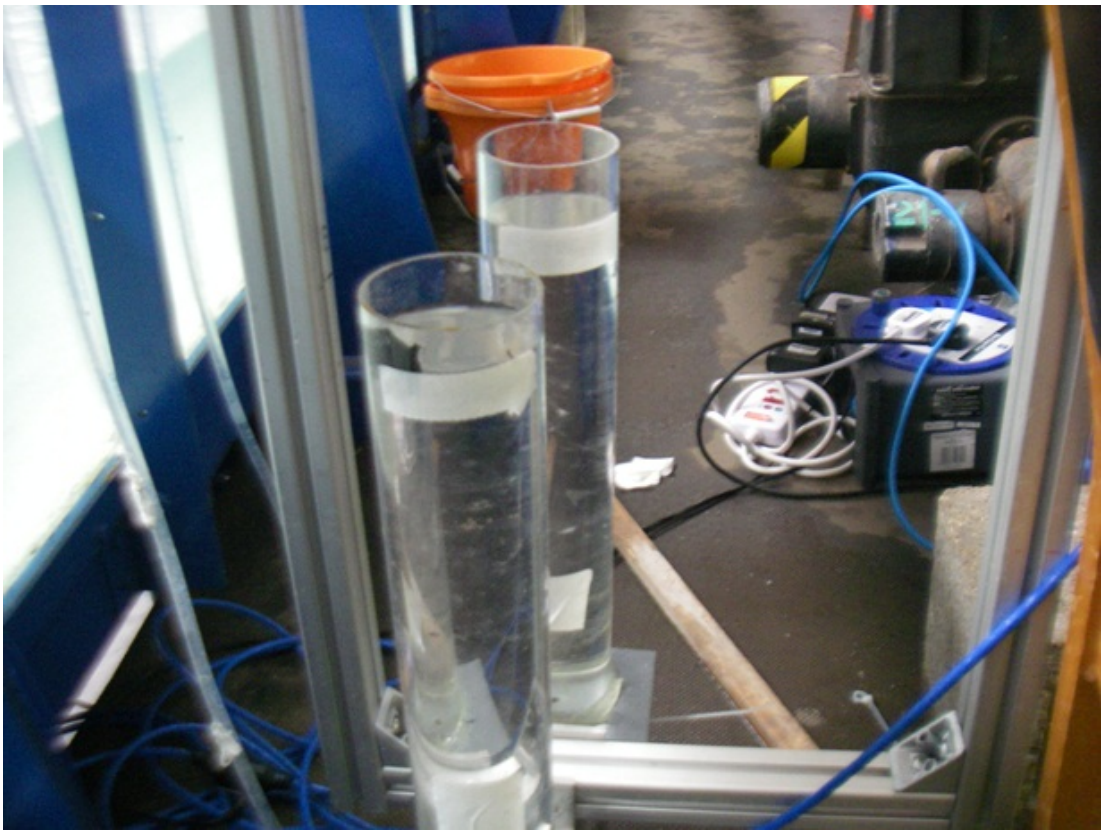

Figure 3.15: Measurement cylinders

3.7 Natural flow conditions in Chilworth flume

3.7.1 Conditions from inlet to outlet of flume

Before any experimentation with actuator fences, it was necessary to examine the natural flow conditions in the Chilworth flume. This was to ensure flow changes due to change in actuator fence position and blockage were not as a result of any major changes in ambient conditions throughout the experimental domain.

The first flow condition to be examined was the development of the flow from the inlet to the outlet of the flume. Measurements were taken at the following points, which are illustrated in figure 3.16:

- Downstream of the inlet of the flume at distances of 3m and in 3m increments up to 18m.
- For each downstream position, measurements were taken laterally across the flume at distances of 0.27, 0.54m, 0.84m and 1.1m from the flume sidewall. These represented 19%, 39%, 61% and 80% of the 1.37m channel width respectively.
- For each downstream and lateral position, measurements were made at depths of 0.03m, and in 0.03m increments up to 0.24m. 0.24m was the maximum depth which could be measured due to the overall flow depth of approximately 0.3m and 0.05m height above which the ADV probe needed to be placed to record velocity at a specific point.

The results of this analysis for the 0.84m lateral plane is displayed in figures 3.17 and 3.18. It can be seen from the contour plot in figure 3.17 the development of the boundary layer from the concrete floor. Due to friction between the flow streamlines and the flume bed, there is an infinitesimally small region where the flow velocity is zero. This is known as the no slip condition. The effects of retarding viscous forces are transmitted to fluid streamlines away from the boundary surface and attempt to slow them down. More of the fluid becomes affected by retarding forces and viscous shear as the flow moves downstream of the flow inlet, and hence the slower moving boundary layer gradually grows in thickness. As the flow moves further downstream, viscous shear forces eventually begin to weaken, and the boundary layer thickness eventually settles to a constant value. Both figures show development of the flow

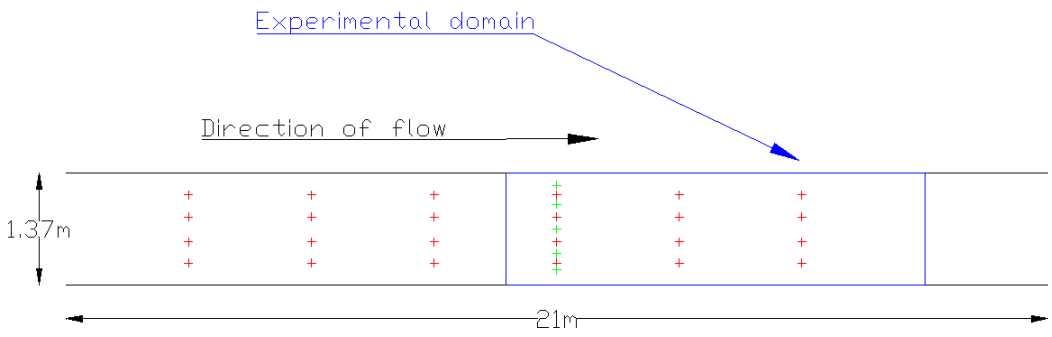

Figure 3.16: Plan view of positions downstream of inlet for ADV measurements of ambient flow conditions

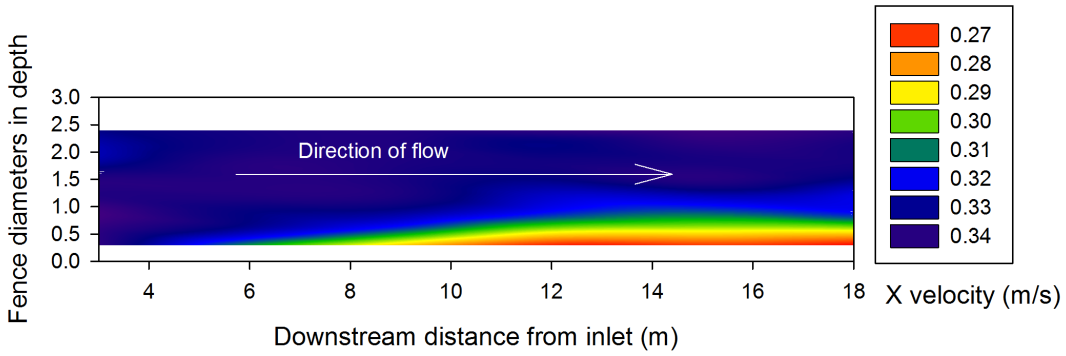

Figure 3.17: Flow velocity development at 0.84m lateral plane of Chilworth flume

is continual up to 12m from the inlet. However this point appears to be where the viscous forces have finally weakened such that there is no longer a continual disturbance of fluid layers through the depth, and hence the flow is fully developed.

The second parameter to be examined was ambient turbulence intensity. This has a strong bearing upon fluid mixing downstream of a tidal turbine or model simulator, as discussed in previously in sections 2.4 and 2.5.11. For experimental work, the turbulence intensity should ideally be steady in terms of longitudinal and lateral position, so that the rate of ambient mixing is steady.

Figure 3.19 shows the contour plot of ambient turbulence intensity in the X direction (inlet to outlet of channel) at the same 0.84m lateral position. Figure 3.20 gives a scatter plot of the development of turbulence intensity from the inlet to the outlet. Once again the results for the other lateral positions were almost identical and so have been omitted. The most immediately evident result is the large turbulence intensities throughout the depth towards the inlet of the flume. This is attributed to the nature of water delivery at the flume

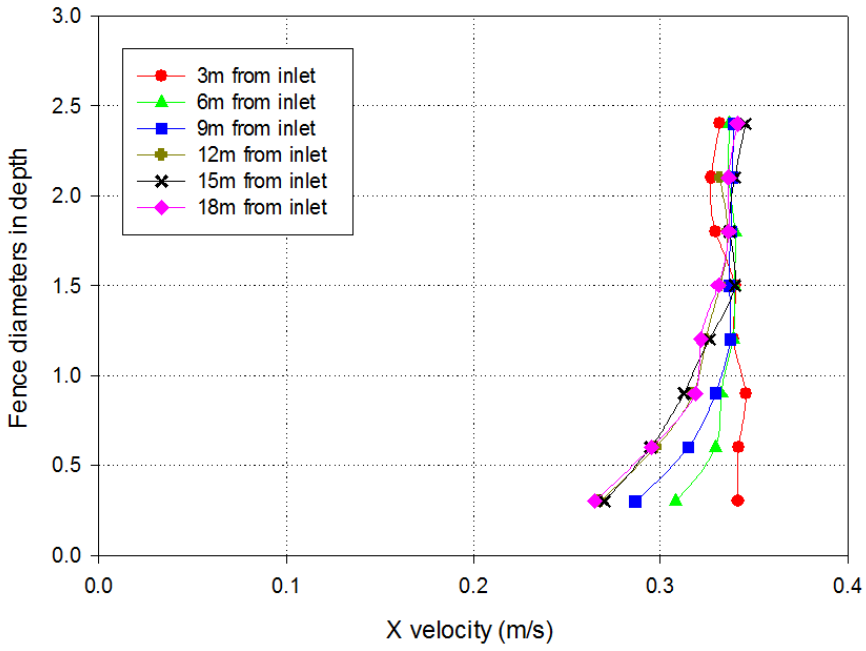

Figure 3.18: Velocity profiles at 0.84m lateral plane in Chilworth flume

inlet, whereby water rises into the channel from the sumps, leading to high velocity gradients and a high degree of rotation. It can be seen however that from approximately

6m onwards, the turbulence effects of water suddenly entering the channel have dissipated, as the bulk flow is downstream and fluid stream tubes become aligned in the longitudinal direction. Beyond this point, the turbulence intensity profile appears to be driven entirely by viscous forces and energy and momentum transfer between fluid layers in the boundary layer. Towards the outlet of the working section, some more instability in the flow is evident.

The slightly greater turbulence intensities in this region are most likely due to backwater effects associated with the weir gate controlling the flow depth towards the outlet (Section 3.5). But in the region between 12m and 15m, the central 1/3rd of the depth of the flow only

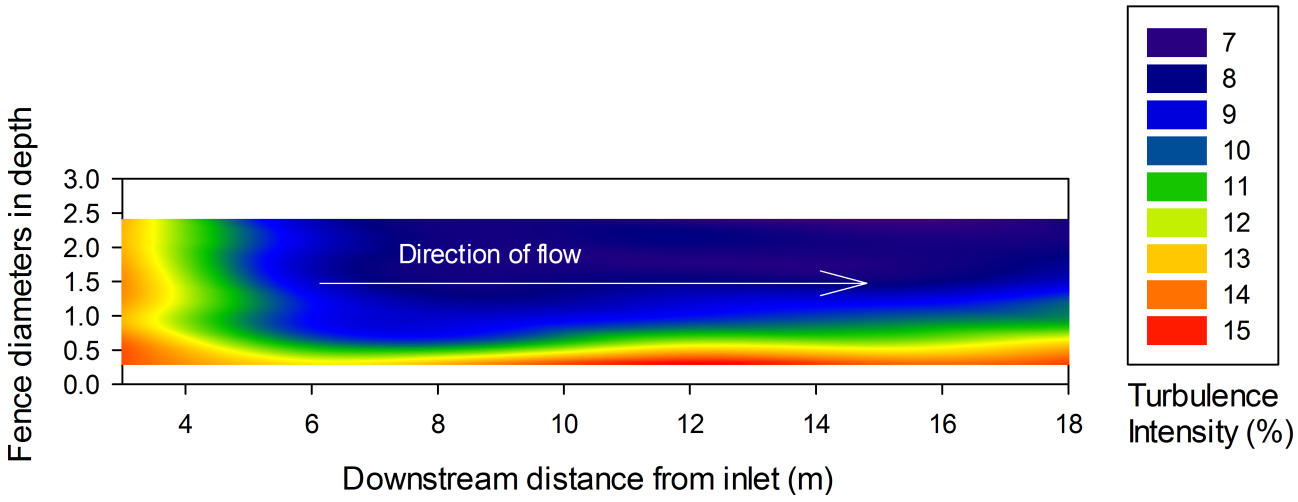

Figure 3.19: Ambient turbulence intensity development in X direction at 0.84m lateral plane of Chilworth flume

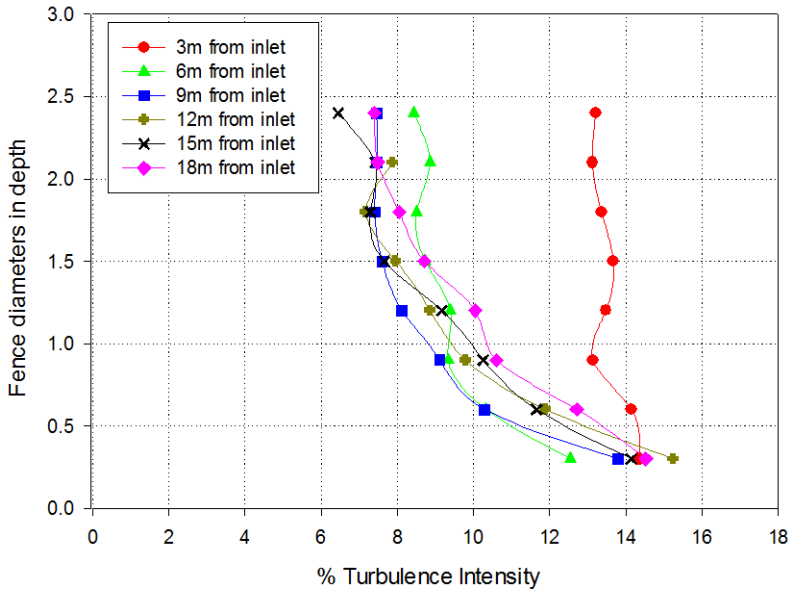

Figure 3.20: Ambient turbulence intensity profiles at 0.84m lateral plane in Chilworth flume

has a fluctuation between 8% and 10%. Therefore the flow in this region can reasonably be considered sufficiently steady.

3.7.2 Conditions at 12m downstream from inlet

The results of the analysis in the previous section suggested 12m downstream of the inlet was an appropriate location to initiate an experimental domain due to its steady flow characteristics. Figure 3.21 gives the points throughout the 12m cross section at which ambient flow conditions were quantified.The variation in velocity across the cross section is displayed in figure 3.22, while a similar plot for turbulence intensity can be seen in figure 3.23. These figures once again show the boundary layer occurring in the bottom 1 actuator fence diameter, or 1/3rd of the depth. There is some variation through the centre 1/3rd of the depth. But again it is restricted to a variation of about 2%, similarly to the examination of the longitudinal turbulence intensity.

All of these results have verified that the flow is quite steady in the domain between 12m and 15m which has been chosen for analysis.

3.7.3 Characterisation of sidewall boundary layer

Examination of the boundary layer off the channel sidewalls was important, as some work herein involved investigating the effect of proximity of tidal turbine rows to lateral boundaries. Measurements were taken very close to the channel wall at the centre depth of the flow.

Figure 3.24 gives a plot of the boundary layer off the channel sidewall. Once again error bars have been omitted for reasons already explained in section 3.7.1. It can be seen that sheared flow extends approximately 1 diameter from the flume wall. This plot clearly demonstrates that there will already be viscous shear stresses and forces acting in this region before any actuator fences are placed in the flume. But with flow diverging around the sides of actuator fences, it is clear that the velocity gradients, and hence shear stresses, will be greatly increased with the addition of an actuator fence. The possible consequences for these increases in viscous shear stresses are discussed in section 5.1.

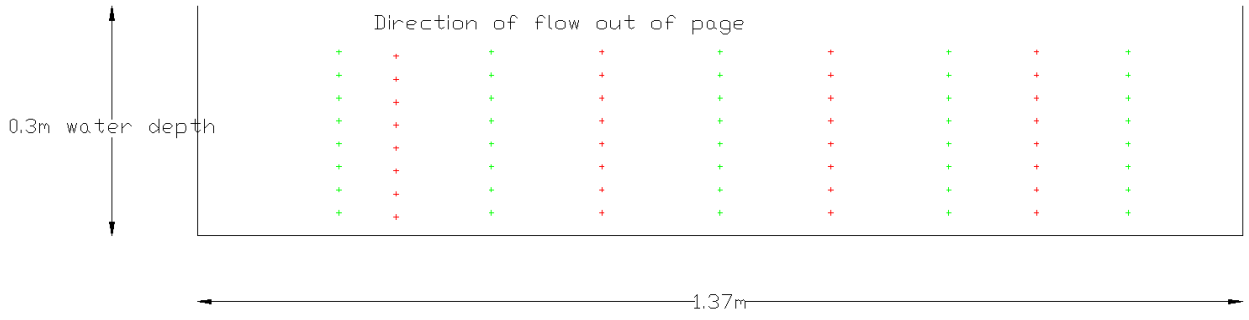

Figure 3.21: Positions of ADV for examination of flow conditions at 12m cross section of Chilworth flume

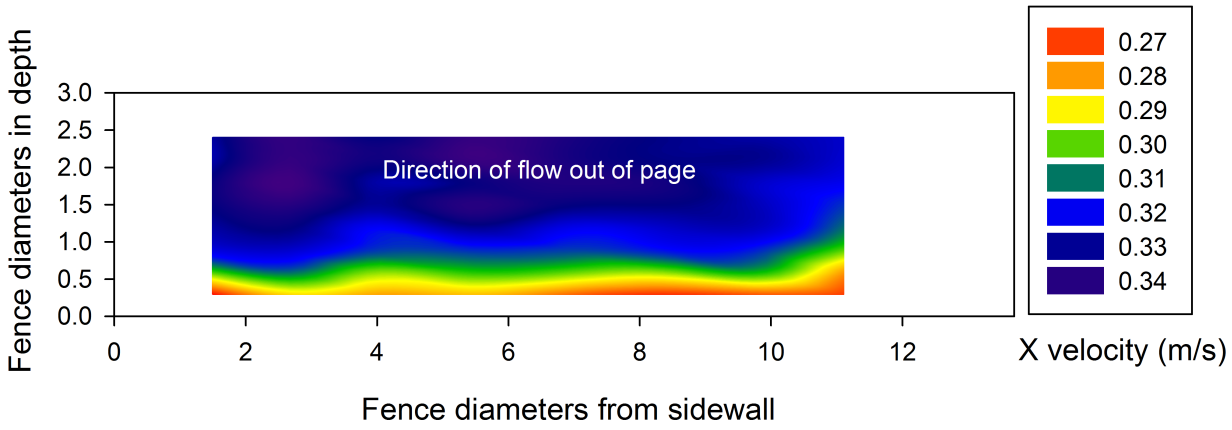

Figure 3.22: Flow velocity at 12m cross section of Chilworth flume

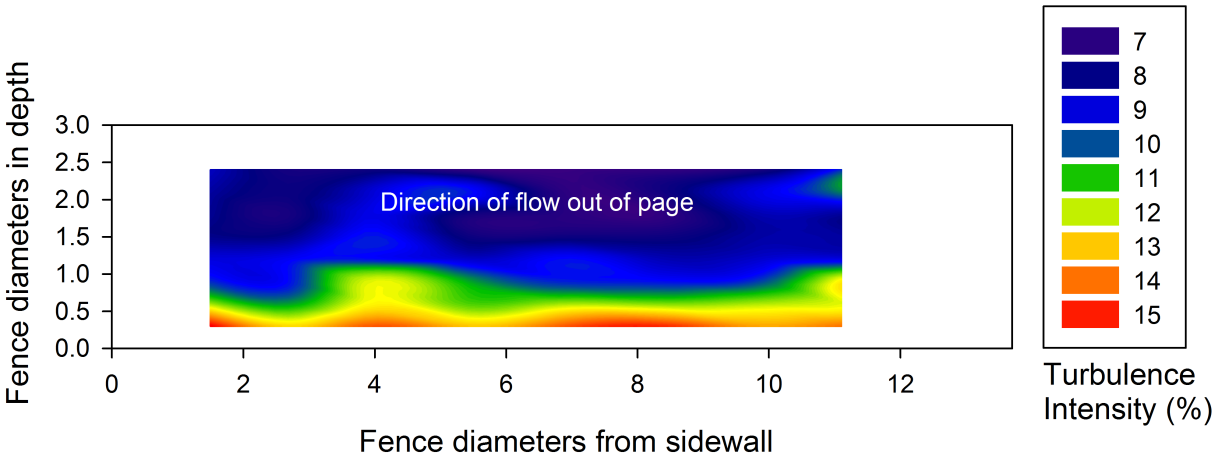

Figure 3.23: Ambient turbulence intensity at 12m cross section of Chilworth flume

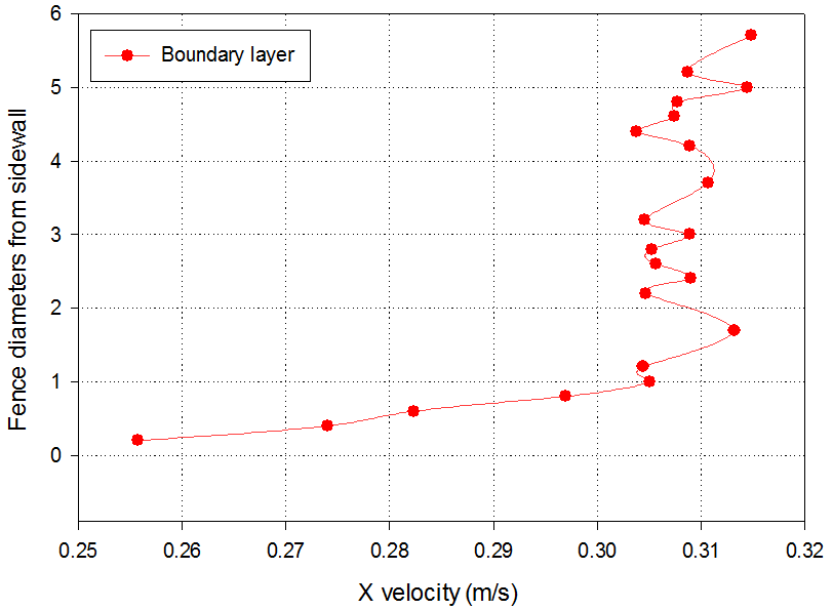

Figure 3.24: Boundary layer off sidewall of Chilworth flume at centre depth of flow

3.7.4 Estimation of Manning's n for both bed and sidewall of channel using measured data

Using the measured data presented in figures 3.18 and 3.24, it was possible to use the method outlined in section 2.5.8 to determine an estimate for the Manning's n of both the channel sidewall and the channel bed. These in turn were required to determine an entire channel compound Manning's n, the calculation of which is necessary in open channels with more than one material lining the wetted perimeter. The resulting compound Manning's n was required later for the following purposes:

- The use of the Bryden et al. model presented in section 2.1.1 to estimate the potential head drop across an actuator fence in the Chilworth flume.
- Estimating the entire natural head loss across the 21m length of the flume, as discussed in section 3.1.

Beginning with the flume bed, the k value inserted into the Colebrook-White equation to determine the Darcy friction factor. Also required were other flume variables, such as flow depth, average flow velocity, Reynolds number and hydraulic radius. The values of the input variables are displayed in table 3.3. The value for k was chosen with reference to Hamill (2001, p.195), and a value of 0.15mm, corresponding to precast concrete pipes, was chosen. Output variables are displayed in table 3.6, while the resulting velocity profile using the Dyer boundary law, and its fit with experimental results are shown in figure 3.25. The results show that, for an estimated roughness height of 0.15mm, the resulting boundary layer law fits quite well with the measured data throughout most of the depth of the flow. The only area where agreement breaks down is towards the free surface. This is most likely simply due to the fact that the influence of the roughness of the flume bed in driving the flow has weakened approaching the free surface. Nonetheless, the resulting Manning's n of 0.0174 would appear to be an acceptably accurate estimate. It is also worth noting that it is very close to the 0.012 to 0.017 range for concrete lined channels quoted by Hamill (2001, p233).

The results of the application of the same process to the glass sidewall of the flume is shown in tables 3.4 and 3.5, with the curve fit in figure 3.26. In this case, there is very poor agreement between the predicted theoretical profile and the measured data. There is also a large difference between the calculated Manning's n and the range of 0.009 - 0.01 stated by Hamill (2001, p233) for glass lined channels. The most likely reason for this is that the flow velocity measurements made off the sidewall, and displayed in figure 3.24 are not driven

Input parameter	Inputted value
Flow depth	0.3m
Flow velocity	0.326m/s
Reynolds number	109177
Assumed k value	0.15mm
Hydraulic radius	0.2086m

Table 3.3: Values inputted to equations in section 2.5.8 for determining Manning's n of concrete floor

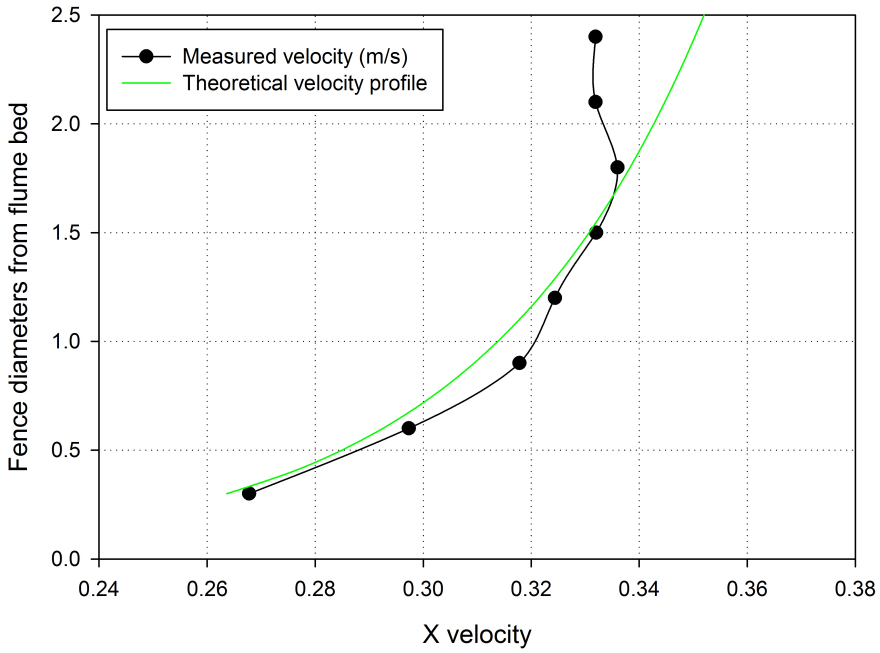

Figure 3.25: Fit between Dyer boundary law profile and measured Chilworth flume bed velocity profile

exclusively by the roughness of the channel sidewall. As these were taken at mid depth of 0.15m from the bed of the flume, it is postulated that the values of flow velocities off the channel sidewall at this depth are also influenced by the roughness of the flume bed, as well as that of the glass sidewalls. The reason why a similar interference from the glass sidewalls was not observed when examining flume bed velocity profiles was that these measurements were taken at 0.84m and 0.53m from both sidewalls, too far away for the turbulence generated by the protrusions from the glass sidewalls to affect the flow regime.

On this basis, while the proposed method of calculating Manning's n can be considered accurate in determining a value for the concrete channel, the influence of the bed of the flume on the measurements taken from the sidewall means the theory is not likely to give an accurate estimate for Manning's n for the glass sidewalls of the Chilworth flume. There also does not appear to be any method by which the theory can incorporate two different values for k from different materials. For this reason, the judgement was made that the calculation of compound Manning's n would use the calculated value for the flume bed, but that reference to engineering textbook was required for the value used for the glass sidewalls of the channel.

3.7.5 Compound Manning's n

Some different methods for estimating compound Manning's roughness have been postulated. A good discussion is given by Hamill [2011, pp. 242-247]. How applicable each method is depends on each specific case. The first equation cited by Hamill is recommended for British rivers, and is derived on the basis of N sections of a river channel having individual volumetric

Input parameter	Inputted value
Flow depth	0.3m
Flow velocity	0.326m/s
Reynolds number	109177
Assumed k value	0.03mm
Hydraulic radius	0.2086m

Table 3.4: Values inputted to equations in section 2.5.8 for determining Manning's n of flume glass sidewall

Output parameter	Value
Darcy friction factor	0.0177
Reynolds roughness number	0.051
Friction velocity	0.015m/s
Manning's n	0.016

Table 3.5: Values outputted from equations in section 2.5.8 for determining Manning's n of concrete floor

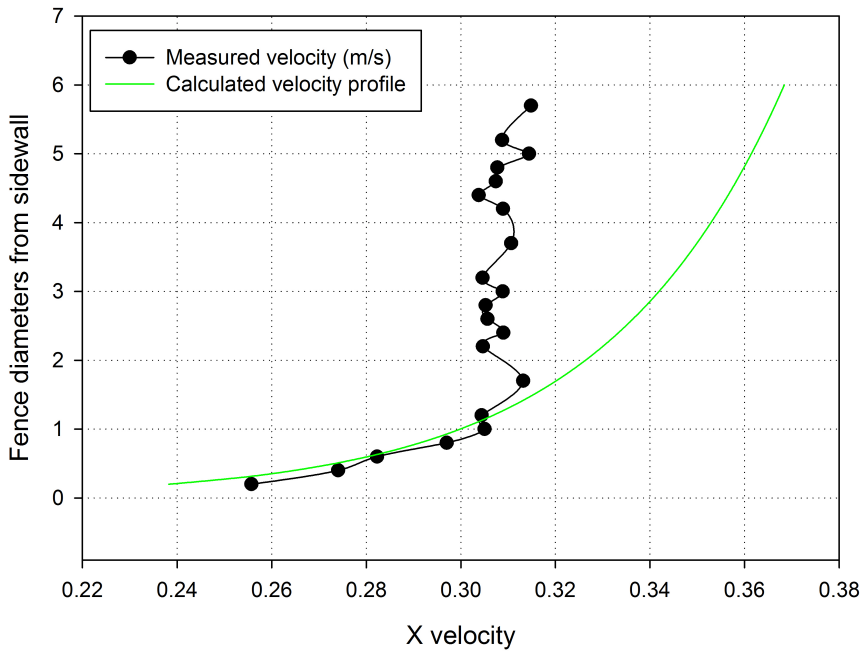

Figure 3.26: Fit between Dyer boundary law profile and measured Chilworth flume bed velocity profile

flow rates which comprise the total for the entire channel.

$$n_{av} = \left[\frac{PR^{\frac{5}{3}}}{\sum_{i=1}^{N} \frac{P_i R_i^{\frac{5}{3}}}{n_i}} \right] \tag{3.13}$$

This is however inappropriate for the Chilworth channel as it does not have multiple sections with individual volumetric flow rates.

The second method outlined by Hamill is derived on the basis that the average flow velocity in each section equals average velocity in the entire channel cross section.

$$n_{av} = \left[\frac{\sum_{i=1}^{n} P_i n_i^{\frac{3}{2}}}{P}\right]^{\frac{2}{3}} \tag{3.14}$$

Again this was considered unsuitable for the Chilworth channel as there are not multiple sections of volumetric flow rate and hence flow velocity.

The third method was considered the most appropriate for this particular case. It is derived on the basis that the total force resisting motion of fluid is the sum of the force resisting motion in each section. For the Chilworth channel, this will mean the total force being the resistance of the channel sidewalls and the channel floor. The following expression was therefore used to calculate the compound Manning's n for the channel:

$$n_{av} = \left[\frac{\sum_{i=1}^{n} P_i n_i^{2}}{P}\right]^{\frac{1}{2}} \tag{3.15}$$

Figure 3.27 shows how this applies to the Chilworth channel. The three separate sections are the two glass sidewalls and the smooth concrete floor. Assuming a flow depth of 0.3m, for both glass sidewalls:

- P = 0.3m
- n = 0.01 (Manning's coefficient for glass channels from Hamill (2011, p233))

For the smooth concrete floor:

- P = 1.37m (width of channel)
- n = 0.0174 (Manning's coefficient for smooth concrete channel calculated in section 3.7.4).

Inserting all of these values, and the total wetted perimeter of 1.97m into the above expression, gives a compound Manning's roughness for the Chilworth channel of 0.0152 for the full open channel. This value was used in the reduction in water surface elevation calculations using the model of Bryden et. al. (2004) and also estimating the friction slope of the channel in section 3.1.

It was also necessary to apply this same analysis to each of the individual sub channels in the split mechanism. This was to examine whether any changes to compound Manning's n

Output parameter	Value
Darcy friction factor	0.021
Reynolds roughness number	2.8
Friction velocity	0.017m/s
Manning's n	0.0174

Table 3.6: Values outputted from equations in section 2.5.8 for determining Manning's n of concrete floor

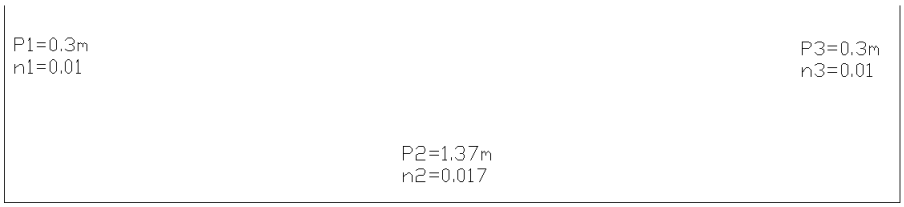

Figure 3.27: Application of Compound Manning's n values to Chilworth flume

in these sub channels compared to the open section were such as to allow a constant bottom roughness coefficient throughout the flow domain to be a reasonable assumption to make. In this case, the P and n values for the glass wall are the same. However the P value for the smooth concrete floor is now 0.6775m, which is half the width of the flume minus half of the 15mm perspex width. Also for the perspex wall of the split:

- P = 0.3m (depth of flow)
- n = 0.009 (Manning's coefficient for perspex lined channel from Hamill (2011, p233))

This gives a compound Manning's n for the sub channels in the split mechanism of 0.0155. This value was used in estimating the head loss across the entire flume length, as previously mentioned in section 3.1, and in estimating the head drop across the actuator fence, presented later in section 4.2.

Chapter 4

Examination of reduction in water surface elevations across actuator fences

4.1 Objectives of examination of water surface elevation reductions

The significance of changes in water surface elevation caused by power extracting tidal turbines was clearly demonstrated by the analytical model of Bryden et al. [2004]. Power extraction was demonstrated to cause a reduction in surface elevation downstream of turbines, resulting in a corresponding increase in the average cross sectional flow velocity. It was felt an examination of any possible occurrence of reduction in head during experimentation needed to be examined and noted. This was mainly due to the flow constraining analysis, which involved examining changes in localised flow velocity near channel boundaries as actuator fences were positioned closer to them. It was deemed necessary to examine what changes in flow velocity could be attributed to changes in water surface elevation, thus ensuring that no erroneous conclusions were drawn from the flow constraining analysis.

Two steps were carried out to examine possible changes in water surface elevation in the Chilworth flume:

- The reduction expected for the largest actuator fence was calculated using the theory of Bryden et al. (2004). A number of assumptions and estimations were required, each of which are clearly documented and explained, were necessary for this calculation.

- Water surface elevation changes between upstream and downstream were measured experimentally, using a combination of stilling cylinders, tubes and a water pump. The physical phenomenon of syphonic action was also used for this measurement. This procedure was outlined in detail in section 3.6 .

4.2 Calculation of water surface elevation changes

For the analytical model of Bryden et al. (2004), the power used to calculate the additional bottom shear stress in equation 2.96 was found by calculating the total power in the flume using the expression:

$$P = TU \tag{4.1}$$

For each fence, the value for thrust was that measured using load cells when the fence was positioned in the centre of the channel. To determine the value for U in the above expression, and also to determine an estimate for volumetric flow rate in the channel, the following method of interpolation was used:

1. Flow velocity was quantified throughout the depth and width of the channel at 12m downstream of the inlet. These readings were considered to have been taken in the centre of an element of the cross sectional area of the channel. The sum of these element areas made up the total cross sectional area. This is explained graphically in figure 4.1.

2. Each element area was multiplied by its respective velocity reading to give the volumetric flow rate through that elemental area.

3. The volumetric flow rates of each elemental area were summed together to give an approximate total volumetric flow rate through the entire cross section of the flume.

4. The results of this estimation gave an approximate volumetric flow rate of $0.134\frac{m^3}{s}$, which when divided by the flow cross sectional area of $0.411m^2$ (1.37m flume width multiplied by 0.3m flow depth) gave an average flow velocity of 0.326m/s.

Using this method, the inferred power values used in this analysis were 0.546, 0.739, 1.07 and 1.225 watts for blockage ratios of 0.072, 0.097, 0.122 and 0.146 respectively.

Some questions could be raised about the use of this method. Estimating power dissipation by porous media accurately is extremely difficult, for reasons already outlined in section 3.2.2. This section demonstrated that the use of force multiplied by velocity to estimate power dissipation resulted in figures which were considerably higher than the upper theoretical limits proposed byLanchester [1915] and Betz [1920]. However as subsequent results will demonstrate, theory suggests even these highly overestimated values for power dissipation will lead to immeasurably small reductions in surface elevation.

Any surface elevation change which occurs is most likely to be most evident in the very near wake downstream of the actuator fence. However to give some indication of what reduction might be present, a 0.3m section of the domain was chosen as the x value used for equation 2.101. It was across this same 0.3m distance that reduction in water surface elevation measurements were taken. The calculation was initially carried out for the largest actuator fence size, which had a width of 600mm and a blockage ratio of 0.146. Table 4.1 gives the theoretical reduction across 0.3m of power dissipation and the percentage change in flow depth this would result in for each size actuator fence, assuming an initial depth

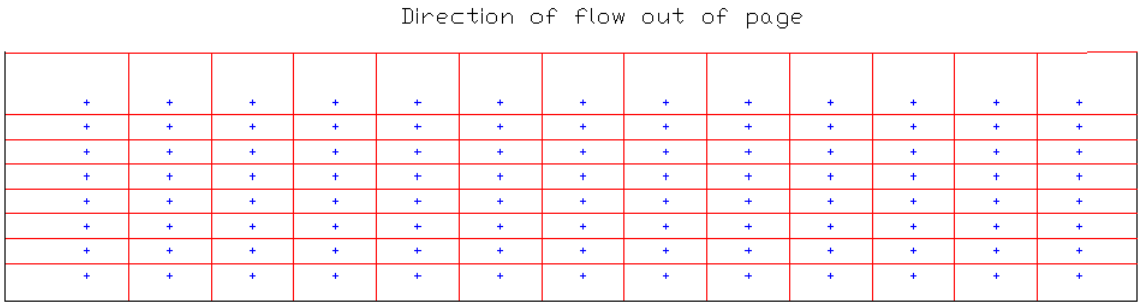

Figure 4.1: Flume cross section divided into element areas (red) to estimate overall volumetric flow rate using ambient flow measurements (blue)

of 0.3m. Table 4.2 gives the values for the open channel parameters required as applied to the Chilworth channel. It is again worth noting that the Manning's n value was 0.0155, as derived from the analysis presented in sections 3.7.4 and 3.7.5.

It is clear that the reduction in water surface elevation predicted is very small. The implications for changes in Froude number due to reduction in water surface elevation are also almost negligible. This is evident by examining the graph of specific energy (explained in section 2.5.6) vs depth for the Chilworth flume, shown in figure 4.2. This graph was developed using equation 2.88, and assuming the volumetric flow rate of $0.134\frac{m^3}{s}$. The energy coefficient in equation 2.88 was assumed to be 1. A more in depth discussion of this energy coefficient, and a justification for the use of 1, is discussed in Appendix D.

The graph shows for the Chilworth flume that the critical depth, where the transition between subcritical and supercritical flow occurs, is approximately 0.1m. The initial flow depth of 0.3m gives a Froude number for the flow of 0.19. This means a reduction in water surface elevation of 0.2m, or 66% of the initial 0.3m flow depth, would be required to achieve critical conditions. To achieve a Froude number of 0.5 (where unstable undular waves may begin to occur) would require flow depth of 0.16m, or a reduction in water surface elevation of almost 50%.

4.3 Measurement of water surface elevation changes

The change in water surface elevation measurement procedure outlined in section 3.6 was carried out to verify the results of the analytical model. A tube attached to one cylinder was placed 0.15m upstream of the largest fence, while the other was placed 0.15m downstream. The flow allowed to settle for a period of 30 minutes to allow water to enter the cylinders

Blockage	Width (mm)	$\frac{\partial h}{\partial x}$	Change in flow depth (mm)	% change
0.072	300	0.0004	0.12	0.04
0.097	400	0.0005	0.15	0.05
0.134	550	0.00056	0.168	0.056
0.146	600	0.0006	0.18	0.06

Table 4.1: Calculations for reduction in water surface elevations across actuator fences in Chilworth flume using model of Bryden et al. (2004)

on the outside of the flume. It was expected that any appreciable reduction in water surface elevation which existed would be evident in this region. After the water had filled both cylinders, a spirit level was once again used to verify that the bottom of both cylinders lay in exactly the same vertical plane. The water levels were then measured in both cylinders, and it was found that the corresponding depth change was 0mm. Again this was for a 600mm wide fence with a blockage ratio of 0.146, the largest being analysed.

The overall conclusion from this analysis is that reduction in water surface elevation across the actuator fence is an almost negligible contributor to the downstream velocity in this particular analysis.

Parameter	Value
Volumetric flow rate from interpolation (Q) $(\frac{m^3}{s})$	0.134
Width of channel (b) (m)	1.37
Assumed depth of flow (h) (m)	0.3
Cross sectional area (A) (m^2)	0.411
Wetted perimeter (P_{er}) (m)	1.97
Hydraulic radius (R) (m)	0.2086
Calculated value for Manning's n $\left(\frac{s}{m^{\frac{1}{3}}}\right)$	0.0152
Chezy friction coefficient $\left(\frac{m^{\frac{1}{2}}}{s}\right)$	45.302

Table 4.2: Values for constants from Chilworth channel used in theory of Bryden et. al (2004)

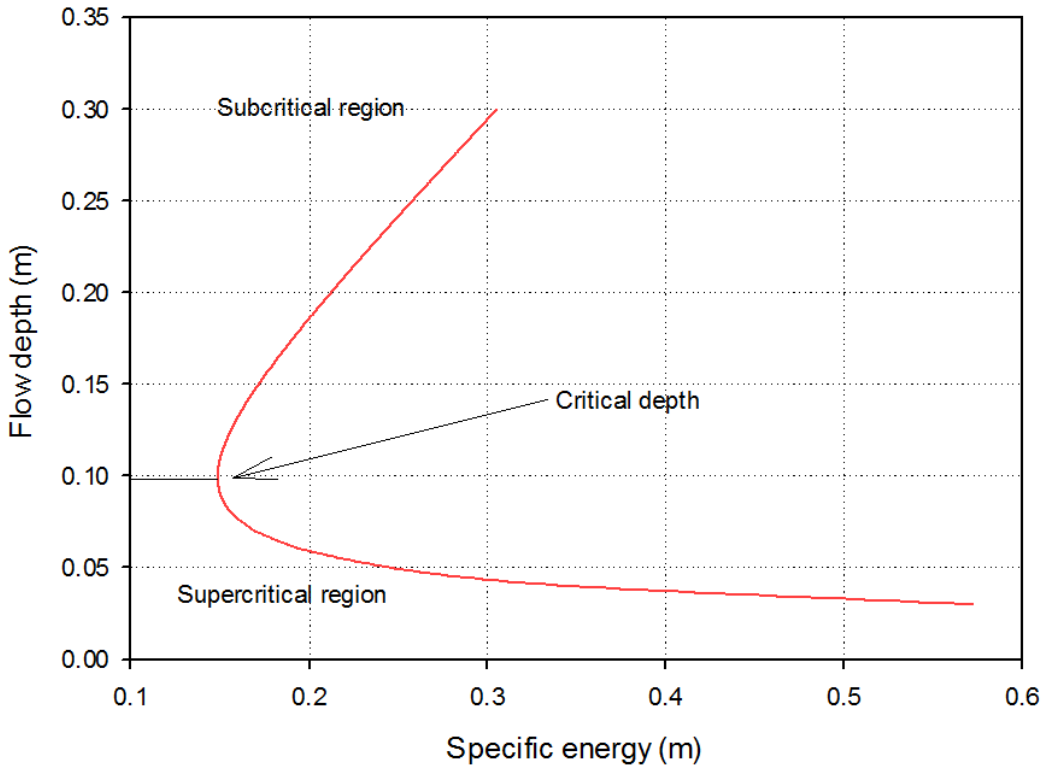

Figure 4.2: Plot of specific energy vs depth for Chilworth flume assuming volumetric flow rate of $0.134m^3/s$

Chapter 5

Results of analysis of tidal turbine rows in open channels

5.1 Effect of varying proximity of rows of turbines to lateral boundaries on local flow velocities

The purpose of this work was to examine in greater detail any changes in velocity that might occur when a tidal array is located close to a vertical wall. This phenomenon was observed from the results of site specific tidal array studies in literature reviewed in section 2.3.1. A graphical illustration of the geometric properties of the experiment is displayed in figure 5.1. Actuator fences of varying porosity were initially placed in the very centre of the flume, and subsequently moved incrementally towards the sidewall of the channel. For each fence position, the velocity was recorded at two fixed points, which lay 0.5 and 0.3 actuator fence diameters from the side and at a lateral plane 3 diameters downstream of the fence.

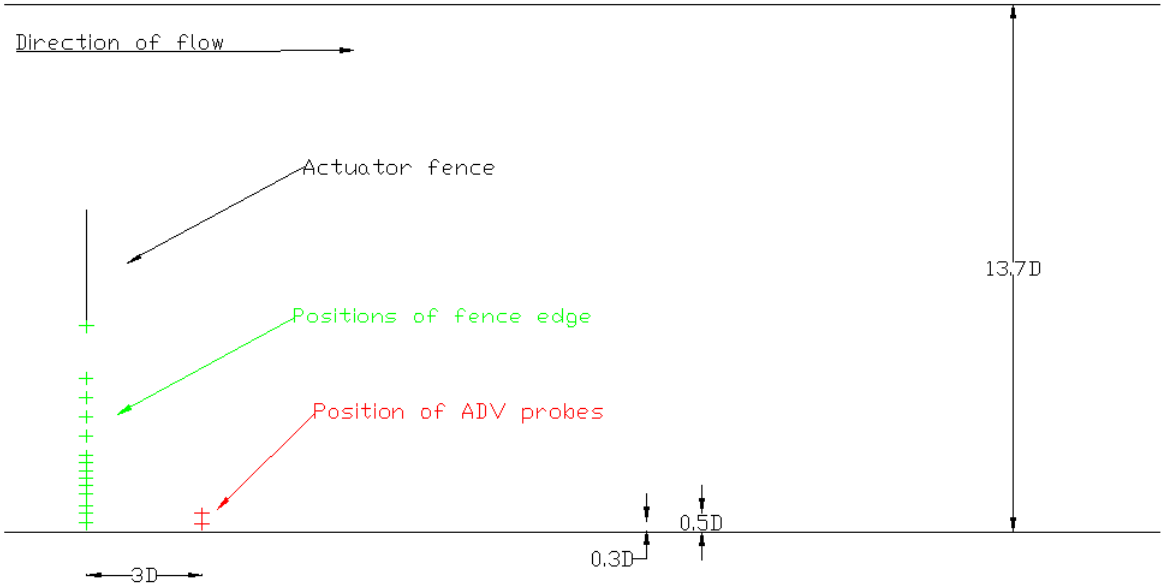

Figure 5.1: Points of actuator fence edge and ADV for flow constraining analysis

Porosity	Peak normalised velocity
0.34	1.208
0.38	1.194
0.4	1.169

Table 5.1: Peak increases in flow velocity compared to ambient for each porosity of actuator fence

The initial analysis was carried out to using actuator fences of differing porosity, but a constant width of 300mm and blockage ratio of 0.072. In the context of tidal turbines, this represents rows of tidal turbines with different density of turbines and hence power output. The results of this analysis are displayed in figures 5.2 and 5.3. These give the constrained flow velocities normalised against the ambient value, while the peak increases for each porosity fence is displayed in table 5.1. Figure 5.2 includes the error bars for the normalised velocity using the theory outlined in section 3.4. It can be seen that the errors calculated using the relevant theory are negligible, and so they have been omitted from subsequent figures.

The variation in flow velocity show an approximately linear relationship between distance from the channel sidewall and increase in velocity. This is a simple consequence of the continuity principle, where the reducing area causes an increase in flow velocity to maintain the localised mass flow rate. However some flow constraining becomes evident between 4 and 1 diameters, followed by a sudden reduction which occurs at approximately between 1 and 0.8 diameters from the sidewall. This same pattern can be seen for all 3 porosities, and also at both measurement points.

The results suggest that at around the 1 diameter proximity, the localised mass flow rate through the gap between the fence edge and sidewall is reduced. This is consistent with the wall velocity profile shown in figure 3.24, which shows the onset of gradually decreasing flow velocity compared to further away from the channel wall due to the presence of a boundary layer. Literature discussed in chapter 2 demonstrated that the expansion of the wake of an actuator fence and diversion of flow around its sides begins upstream of the fence itself. At the wall the velocity will be zero due to the no slip condition, while away from the wall outside the boundary layer, there will be fast moving flow around the sides of the fence. According to Bernoulli's equation, this must mean an area of high static pressure towards the wall and an area of low static pressure outside the boundary layer. This imbalance in static pressure will lead to resultant forces acting along the axis between the slow moving and fast moving fluid. This is the same reason for the thrust experienced on the actuator fence. A high static pressure exists upstream due to a reduction in flow velocity, while a low static pressure exists downstream due to the high velocity flow around the sides. These forces due to velocity gradient off the wall of the channel are the viscous shear forces outlined in section 2.5.12.

As the distance between the wall and the fence is reduced, there is an increase in velocity gradient and hence viscous shear forces. If these forces are not sufficiently high to retard the motion of the fluid streamlines around the sides of the fence, the streamlines will simply continue to obey continuity and the velocity will increase in this region. This appears to be what happens between 10 and 1 diameters from the sidewall. It is postulated that at some proximity, the velocity gradient between the wall and fence edge causes these retarding

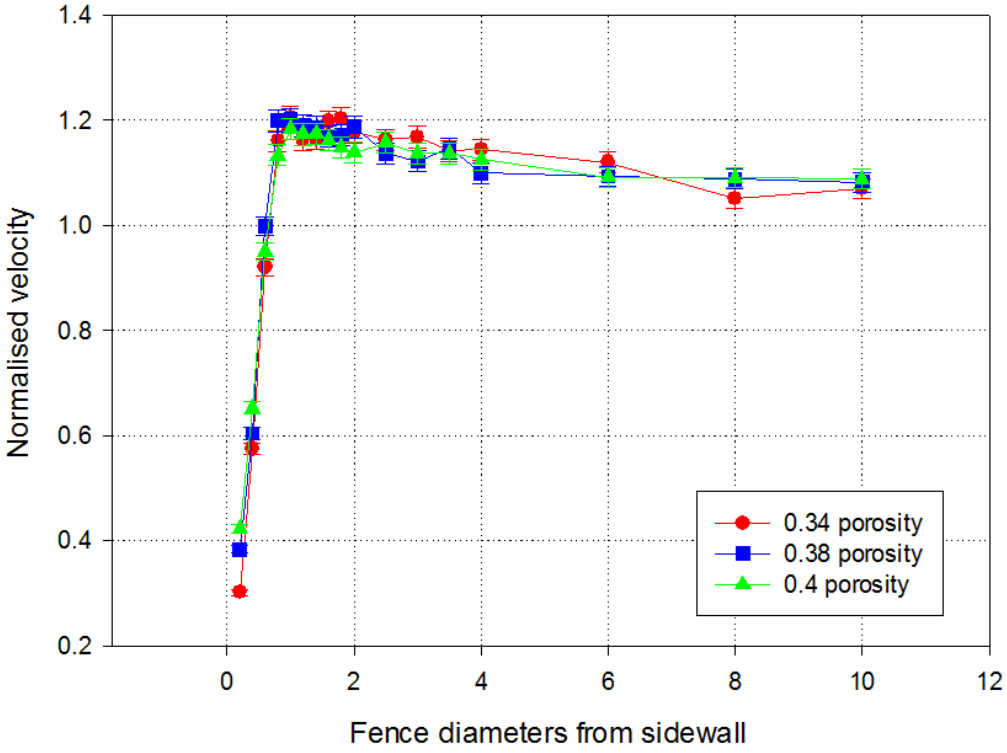

Figure 5.2: Increases in flow velocity compared to ambient conditions at 0.3 diameters from sidewall with fences of varying porosity

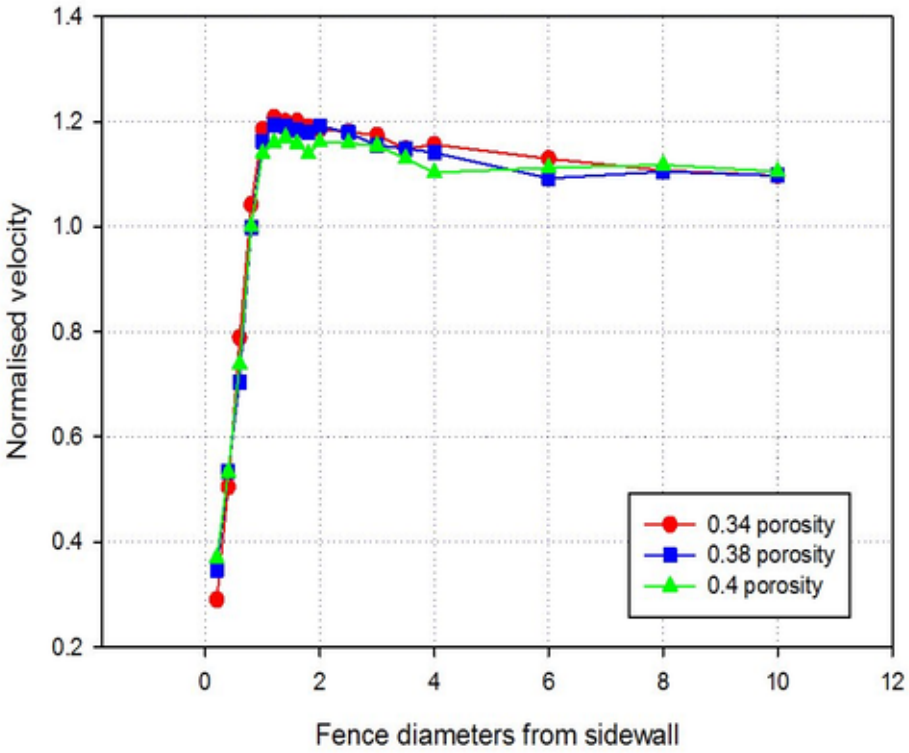

Figure 5.3: Increases in flow velocity compared to ambient conditions at 0.5 diameters from sidewall with fences of varying porosity

forces to become so high that they no longer allow these streamlines to flow around the sides. The high viscous stresses and retarding forces acting on the fluid streamlines cause them to be diverted away from the gap. While the overall mass flow rate throughout the entire channel is maintained, the localised mass flow rate through this gap between the array and channel wall is reduced. This explains the sudden reduction in flow velocity experienced at 1 diameter proximity. The fluid streamlines must be redirected either directly through the actuator fence or above or below the actuator fence.

The next step was to examine the same effects with different blockage ratios. For this particular analysis, the fence porosity was kept constant at 0.34. The analysis was as presented in figure 5.1, but was carried out with different width of actuator fences representing different blockage ratios. The width of actuator fences used varied from 300mm to 600mm, representing blockage ratios between 0.072 and 0.146. Also, due to the almost identical results displayed by the two examined points in the initial fence porosity analysis, the blockage analysis only examined the ADV position of 0.5 diameters from the sidewall. The results of this analysis are displayed in figure 5.4 and table 5.2.

The first observation is the variation in flow velocity at any point with blockage ratio. It can be observed that larger blockage ratios result in larger increases in flow velocity compared to ambient conditions. Once again the continuity principle can explain this effect. A larger blockage ratio means a greater area of flow in the channel is effected by the turbines, and hence the amount of fluid streamlines which are directed around the sides of the actuator fence is greater. This means that a higher blockage ratio leads to a greater increase in mass flow rate in the gap between the array edge and the sidewall of the channel. Many of the other observations from this analysis are broadly similar to those from the initial analysis with varying porosity and constant fence size. There is an approximate linear relationship between flow velocity and proximity up to about 4 diameters from the sidewall, followed again by some constraining between 4 and 1 diameters and a considerable reduction at approximately 1 diameters. These results once again gives further support to the postulation that the localised mass flow rate through this gap reduces due to higher viscous forces opposing the motion of fluid streamlines through this gap.

A brief comparative analysis was conducted with experiments on the opposite side of the channel to those presented in this section. This purpose of this analysis was to ensure that the observations made in the initial analysis already presented were not a consequence of any special flow conditions at this side of the Chilworth flume. This analysis was carried out exclusively for a 0.38 porosity fence with a 0.072 blockage ratio. As with the previous flow constraining results presented, the flow velocity was measured at a point 50mm from the channel sidewall with no actuator fences present. A fence was then placed in the flume, with the fence edge at varying distances laterally across from the channel wall and 3 diameters upstream of the flow measurement point. For each fence position, the flow velocity was recorded at the exact same position as when recorded with no fences present. Each flow velocity measurement for each position was then normalised against the value recorded with no fence present. The results of this analysis, displayed in figure 5.5, show once again a sudden reduction at a proximity of 0.8 diameters, thereby giving confidence to the observed

effects and postulations put forward to explain them.

It is worth noting that in real tidal channels, as well as being dependent on proximity of a row of turbines to channel boundaries, the strength of viscous forces acting will also be dependent on the Reynolds number of the flow. If the experiments which have been carried out here were to be performed at a lower Reynolds number, viscous forces would have had a greater influence on flow development, both off the sidewalls and bed of the channel. In this case, the expectation would be that the diversion of flow away from the gap between turbines and the channel wall would have occurred at proximities larger than the 1 diameter case found here. Conversely, higher Reynolds number would have meant less influence of viscous forces on flow development, which could possibly result in closer proximities being reached by a row of turbines at a closer proximity than the 1 diameter figure found from this research. This, along with a difference in localised flow velocity across both sides of the flume, may explain the slightly different trends which are observed in figure 5.5. In the Chilworth flume, as with other similar experimental facilities such as that used by Stallard et al. [2013], it has been observed that the flow velocity is slightly faster on one lateral side. Two pipes are used to deliver water to the header tank at the inlet of the flume, which overspills into the concrete channel. The most likely explanation for this imbalance between both sides of the channel is that the flume pumps deliver slightly more water to one of these two pipes. The resulting imbalance in velocity on either side will in turn lead to higher local Reynolds numbers, and hence different viscous force effects on either side.

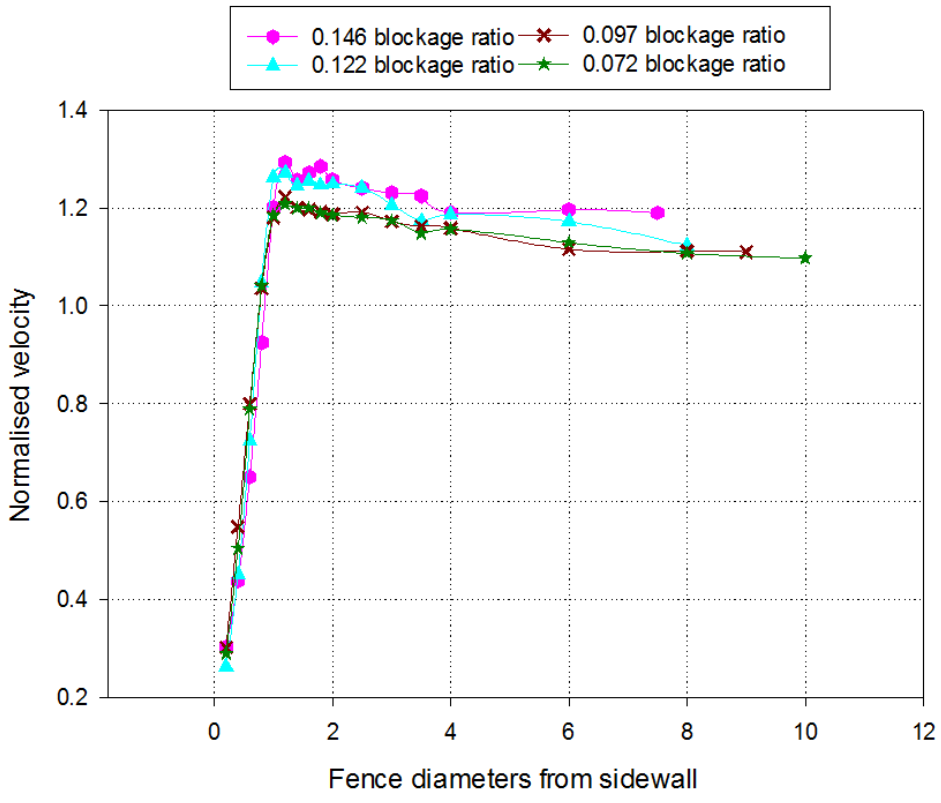

Figure 5.4: Increases in flow velocity compared to ambient conditions at 0.5 diameters from sidewall with fences of varying blockage ratio

Fence width (mm)	Blockage ratio	Peak normalised velocity
600	0.146	1.293
500	0.122	1.271
400	0.097	1.222
300	0.072	1.208

Table 5.2: Peak increases in flow velocity compared to ambient for each blockage ratio of actuator fence

As well as examining changes to flow velocity values close to shore, changes to power output of a tidal turbine row are also of considerable interest. Any changes to power performance of tidal turbines will have considerable implications. If it were found that the power output of an array were higher closer to shore, the potential gains may offset some of the potential negative effects of flow constraining previously outlined. One potential answer to the last question has already been suggested by the analysis of Myers and Bahaj [2010]. In this analysis the authors concluded that placing a tidal turbine very near the bed of a channel led to much slower recovery of the wake region to freestream conditions downstream. A postulation given for this was that the restriction of mass flow beneath the turbine due to the relatively low proximity to the bed resulted in a slow moving region beneath the turbine. This in turn led to less re-energisation of the wake. The results of this analysis suggest that should a similar effect occur with changes to lateral proximity to channel sides in rectangular channels, somewhere around 1 diameter represents the "tipping point" at which localised mass flow rate is reduced. For many tidal channels which are not rectangular, the location of this point will vary depending on the exact bathymetry of the site. Given the major changes in downstream flow associated with reaching this point, its approximate location could be a factor worth investigating during any resource assessment of any tidal site.

The results of an examination of changes to the wake region with lateral proximity are presented in section 5.3, while an examination of changes to tidal array performance is presented in the next section.

5.2 Changes to thrust and thrust coefficient with changes in lateral position

The thrust on the actuator fence was measured using the methods explained in section 3.2.1, while the non-dimensional thrust coefficient was calculated using the theory outlined in section 2.5.4. In order to determine the velocity value to be used in the equation for C_T, the following procedure was used:

1. For each fence position with different proximities which the actuator fence occupied, flow velocity measurements were taken across the centre depth of the flow depth. These were taken at several points across the lateral plane at which the fence was positioned in each case.

2. Each of these velocity values in m/s were summed, and then divided by the number of measurement points.

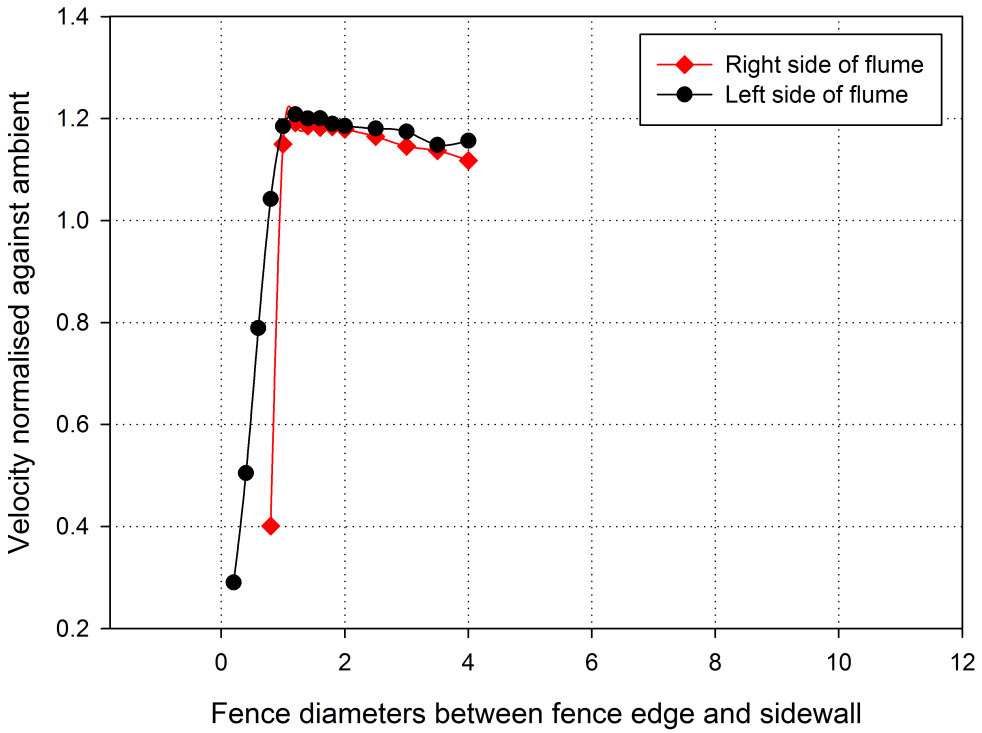

Figure 5.5: Results of constrained flow analysis on both sides of flume with porosity 0.38 and blockage ratio 0.072

3. This gave an average value across the lateral plane at which the fence was present. This value was then subsequently used in in calculations to determine the thrust coefficient at each point.

Also calculated and included in results was the error in C_T readings, calculated using the errors for thrust and flow velocity and combining them in theory outlined in section 3.4. As with the flow constraining analysis, the measurement of thrust coefficient was initially calculated for three actuator fences of varying porosity and a constant fence width of 300mm and blockage ratio of 0.072. The values of thrust can be seen in figure 5.6, while non-dimensional thrust coefficient can be seen in figure 5.7. It is worth noting that when the error associated with thrust, as demonstrated previously in section 3.2.1, was approximately 1.6%.

An assumption inherent in this approximation for C_T uncertainty is that there is no change in the centroid of pressure. When the thrust exerted on the entire surface of a body in contact with fluid is resolved into one single resultant force, the centroid is the point on the surface through which this resultant force acts. However the exact position of this point is dependent on pressure variations on the surface, which in turn is dependent on velocity variations over the surface submerged in a moving fluid. This means that there will be variations in the exact position of the centroid of pressure over time, meaning the variation and uncertainty of thrust readings, and hence C_T calculations, is also likely to change. While the uncertainty associated with changes in centroid of pressure is difficult to quantify, some

indication of its impact can be seen from the velocity, and hence pressure variations across the plane of which the actuator fence was present. Looking again at figure 3.22, it can be seen that, in the middle third depth of flow in the Chilworth flume, velocity variation across the cross section is approximately 0.02m/s, or approximately 6% of the average freestream flow velocity. The judgement was made that this was sufficiently small such that there would not be changes in centroid of pressure which would make the 1.6% estimation of thrust variation invalid or inaccurate.

It is first worth commenting on the variation of thrust coefficient with fence proximity. Results appear to suggest that, for any given fixed actuator fence porosity, no immediately obvious pattern of increasing or decreasing thrust coefficient with change in proximity to channel sidewall exists. Also worth noting is the errors associated with thrust coefficient, which are considerable compared to the almost negligible errors found from the flow velocity and thrust measurements. The error can be seen clearly, and so again supports the comment of no obvious pattern between fence proximity to channel boundary and thrust coefficient. When examining the actual thrust values in figure 5.6 however, it can be seen that the actual force experienced on the actuator fence is larger when it is towards the centre of the flume. This is postulated to be due to the larger flow velocity away from the wall of the channel, and the square relationship between thrust and velocity. It is also evident that thrust appears to decrease once again as the farther wall of the channel is approached. However in all cases, when non-dimensionalising to C_T, it can be seen this increase in thrust is counterbalanced

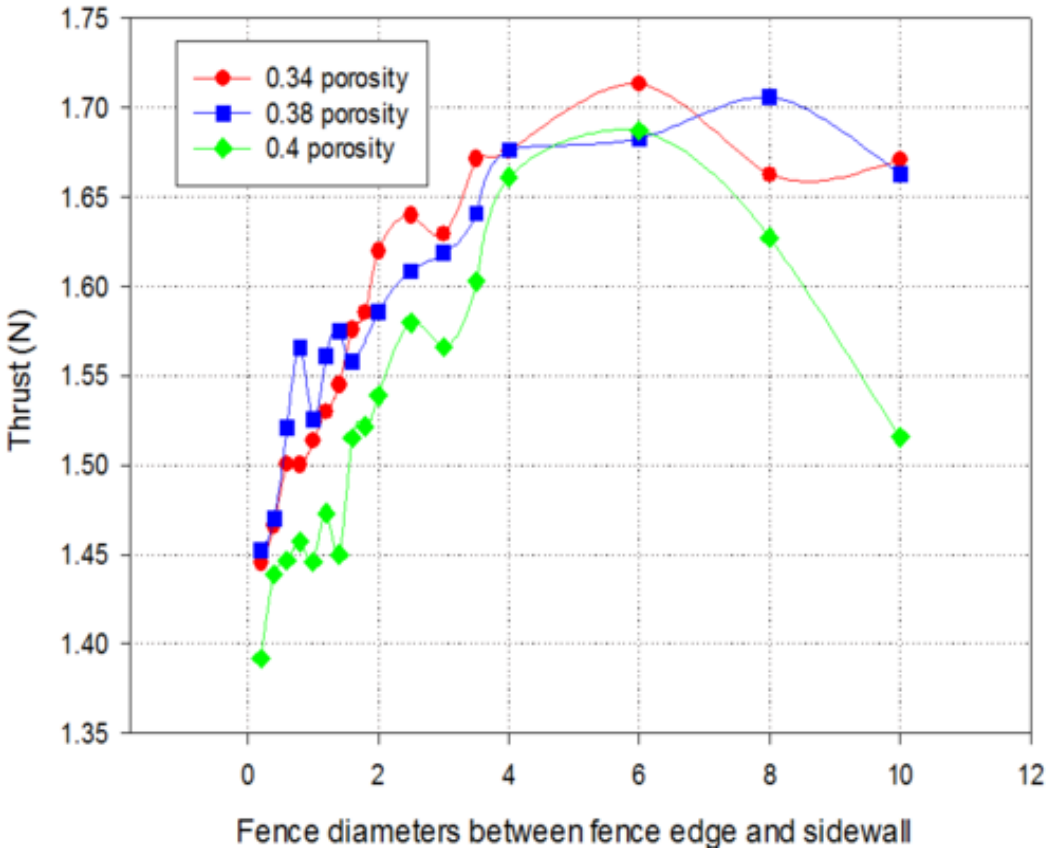

Figure 5.6: Variation in thrust with actuator fence position with varying fence porosity

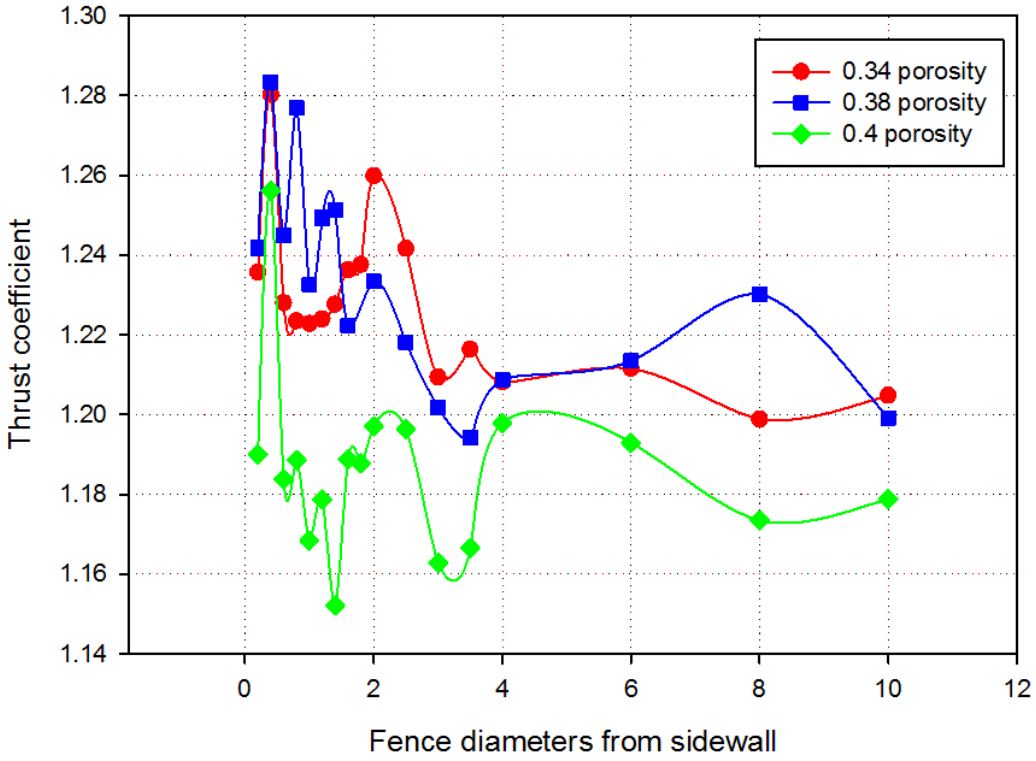

Figure 5.7: Variation in thrust coefficient with actuator fence position with varying fence porosity

by increase in flow velocity.

These results give an indication of how the flow behaves when mass flow rate is restricted between the channel wall and row of turbines in very close proximity cases. In the previous section, it was postulated that high viscous shear stresses resulted in fluid streamlines being diverted away from the gap between the wall and row of turbines. Were it the case that these shear stresses caused fluid streamlines to be diverted directly through the fence, one would expect this to result in higher thrust and thrust coefficient readings closer to the channel wall. However these results do not show such an effect, which therefore suggests that fluid streamlines must be diverted either above or below the actuator fence.

This is a result which has potentially significant implications for tidal developers. It suggests that constraining flow does not necessarily force more of the flow directly through a turbine array, resulting in higher thrust. Also considering the theory developed by the blockage models reviewed in section 2.2.2, it suggests the positioning of turbines closer to channel boundaries is causing changes in wake velocities. The force on an actuator disc as a function of bypass and wake velocity, among other fixed parameters, was given by Garrett and Cummins (2007) as:

$$F = \frac{1}{2}\rho A_3 \left(u_4 - u_3\right)\left(u_4 + 2u_3 - u_0\right) \tag{5.1}$$

This equation suggests that if the turbine area, upstream flow velocity and wake velocity remain constant, an increase in bypass velocity (as was found in the constraining flow analysis) should result in an increase in force on the turbine. The lack of such an observation therefore suggests that wake velocity of a row of turbines may be altered by the positioning of the row closer to channel boundaries. Further results examining where fluid streamlines are diverted when mass flow rate is restricted close to the channel wall is presented in section 5.5.

What the results also suggest is that thrust measurements appear to be more unsteady and unpredictable towards the sidewall of the flume. Looking again at figure 5.7 there appears to be larger increases and decreases in C_T between consecutive points in the region up to about 3 diameters from the sidewall. It was also observed during laboratory testing that more measurements were required to be taken in this region than in the middle of the Chilworth to achieve an accumulated mean value which would not change by more than 1% with further measurements. An example of how this can be demonstrated is by examining thrust readings, collected by two load cells, for the 0.122 blockage ratio (500mm wide) fence at proximity of 1.2 and 4 diameters from the sidewall. The positions of both stems attached to their relevant load cells on this large fence are shown in figure 5.8. The results of this are shown in tables 5.3 and 5.4. Load cell 1 is located is attached on the side of the actuator fence closest to the channel wall, while load cell two is attached further away towards on the middle of the channel. It can be seen that at 1.2 diameters, there is a much greater percentage difference in consecutive thrust readings when the actuator fence is 1.2 diameters from the channel wall compared to 4 diameters from the wall.

It is postulated that this greater unpredictability of thrust in this region is due to the boundary layer profile off the sidewall of the flume, as shown in figure 3.24. In explaining this, it is useful to consider the actuator fence as a series of elemental areas of arbitrary width. When the entire fence is placed in the centre of the channel, the inflow velocity to each individual strip will be broadly similar. However closer to the channel sidewall, each elemental strip will see differing inflow conditions due to the boundary layer. This would therefore lead to an imbalance in thrust between both ends of the actuator fence.

One might expect that any increase in flow velocity due to constraining fluid would be more apparent for decreasing values of fence porosity. From figures 5.6 and 5.7, it is possible to observe a weak trend, but values are quite similar and could not strongly support the postulation of increased thrust coefficient with lower porosity. Therefore, C_T measurements were taken with a solid plate of same size and thickness, effectively representing a zero porosity actuator fence. The results of this analysis superimposed on the results already presented can be seen in figure 5.10, and clearly demonstrate the phenomenon of higher forces on lower porosity fences. However for each of the porosities, and the solid plate, the lack of any definite relationship between proximity to flow boundaries and C_T is still evident.

The results for changing blockage ratio give more support to the results and postulations for changing fence porosity. In the results shown in figures 5.9 and 5.11, there again appears to be higher thrust readings away from channel walls for any given actuator fence blockage ratio, with a maximum in each case towards the centre of the channel. There also does not appear to be any immediate pattern between increasing or decreasing thrust coefficient with

change in proximity to channel walls. As with the 0.072 blockage ratio fences used in the porosity analysis, each of the fences representing different blockage ratios were moved right across the width of the channel as close as possible to both channel sidewalls.

Load cell 1 (N)	% change to previous point	Load cell 2 (N)	% change to previous point
1.22		1.61	
1.3	6.8	1.66	2.55
1.26	3	1.64	1
1.34	6.3	1.66	1.55
1.32	1.62	1.66	0.14
1.24	6.13	1.6	3.86
1.34	7.7	1.67	4.74

Table 5.3: Thrust readings taken to achieve less than 1% change in cumulative thrust coefficient with 0.122 blockage ratio fence 1.2 diameters from sidewall

Load cell 1 (N)	% change to previous point	Load cell 2 (N)	% change to previous point
1.2		3.02	
1.19	0.76	2.98	1.17
1.2	0.38	2.96	0.97
1.2	0.88	2.99	1.31
1.22	1	3.02	0.91

Table 5.4: Thrust readings taken to achieve less than 1% change in cumulative thrust coefficient with 0.122 blockage ratio fence 4 diameters from sidewall

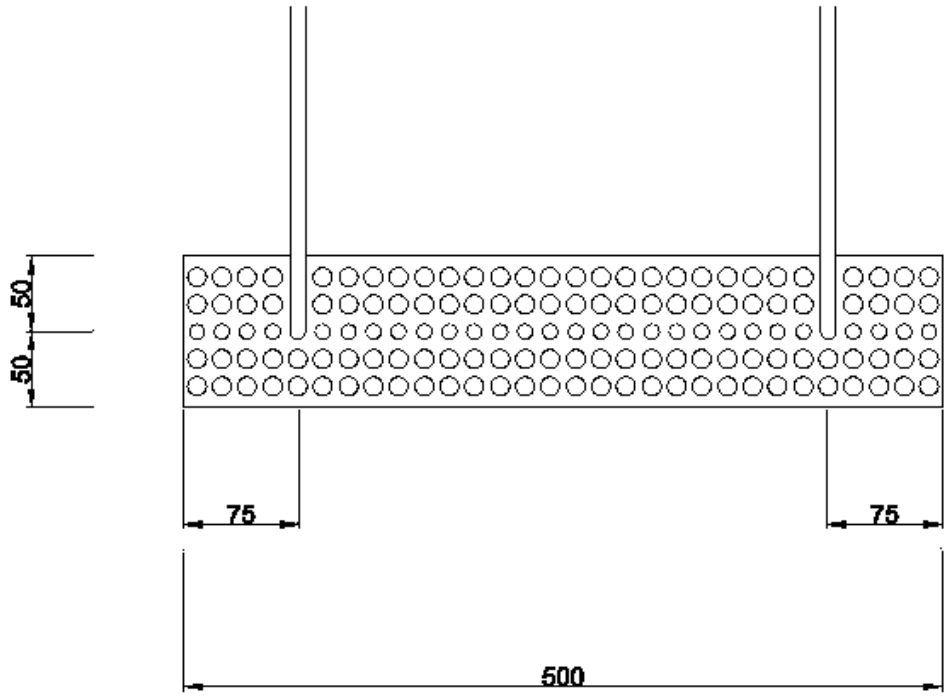

Figure 5.8: Positions of load cell stems on 0.122 blockage ratio fence

This results of this analysis support the hypothesis that fluid streamlines diverted by viscous forces, as postulated in the previous section, are not diverted directly through the fence. If this was the case, an increase in thrust closer to channel boundaries would be expected, however no such increase was found. This therefore suggests that the aforementioned streamlines are diverted either above or below the fence. An examination of the possible implications of this diversion for wake effects downstream of a row of tidal turbines is presented in the next section.

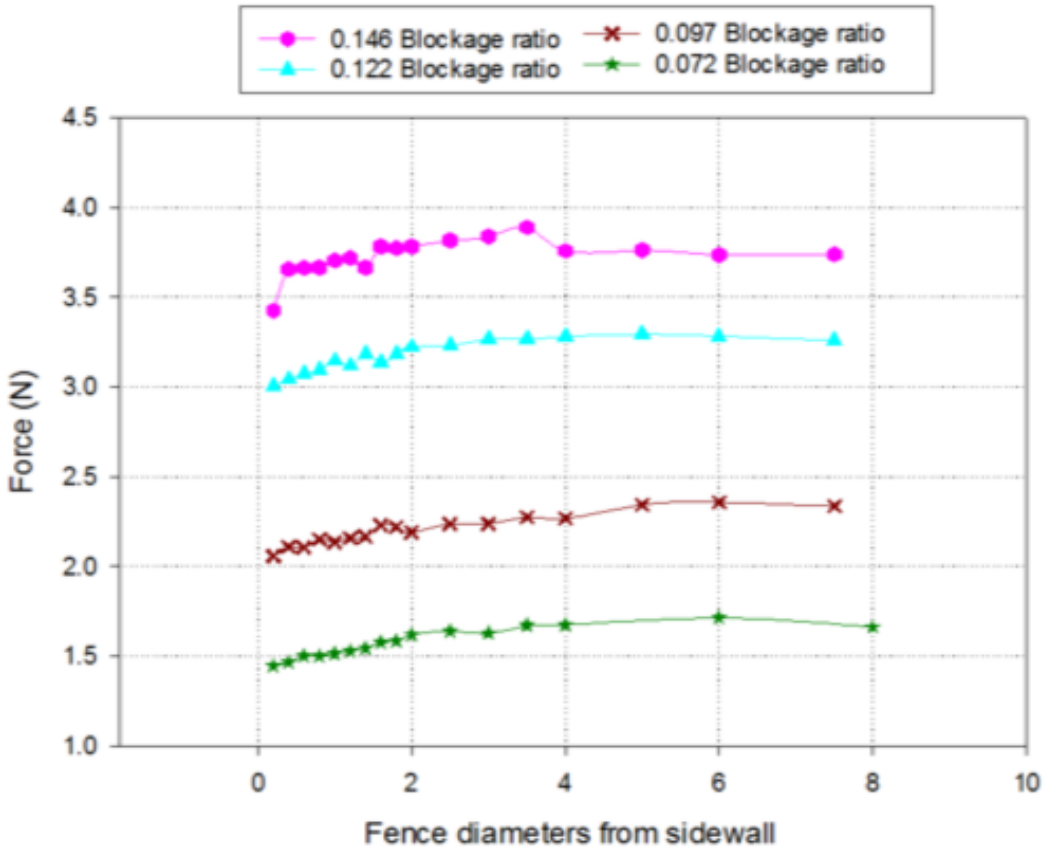

Figure 5.9: Variation in thrust with actuator fence position with varying blockage ratio and constant porosity of 0.34

5.3 Quantification of actuator fence wake for varying lateral position in a channel

5.3.1 Wake properties for 0.072 blockage ratio (300mm wide) actuator fence

The previous sections have shown some effects of mass flow rate restriction due to high viscous forces when a tidal array is positioned close to channel boundaries. Such fundamental changes to flow conditions would strongly suggest that wake recovery to ambient conditions may also be affected by these viscous forces. Given the importance of interaction between freestream and wake fluid streamlines for wake recovery, a restriction of freestream flow at

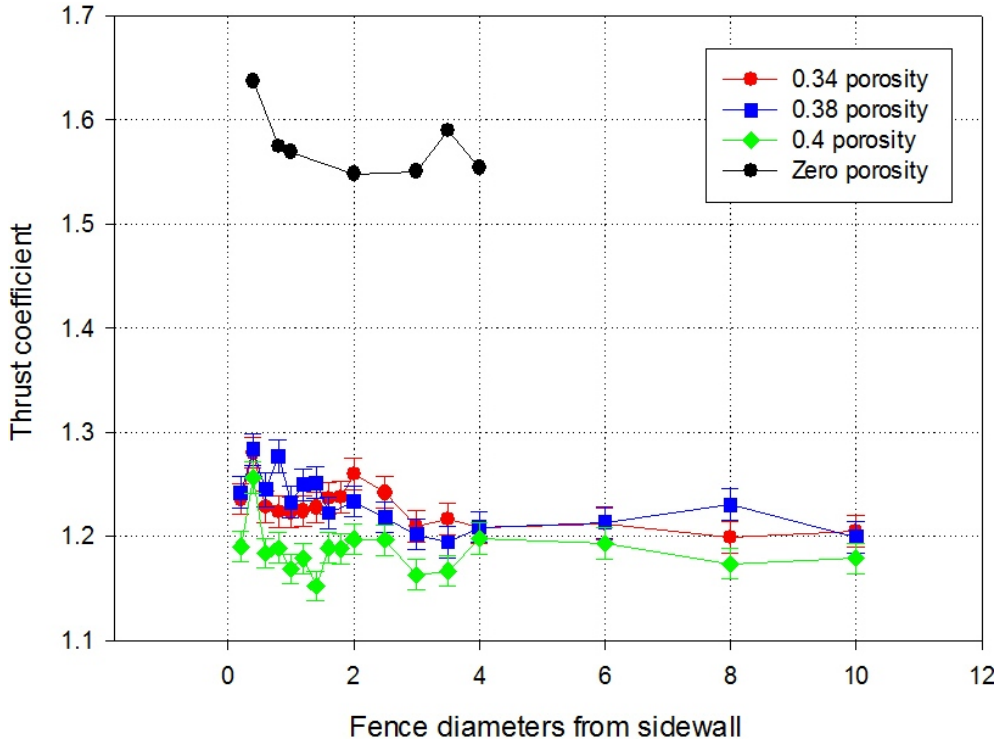

Figure 5.10: Variation in thrust coefficient with actuator fence position with varying fence porosity with inclusion of solid plate

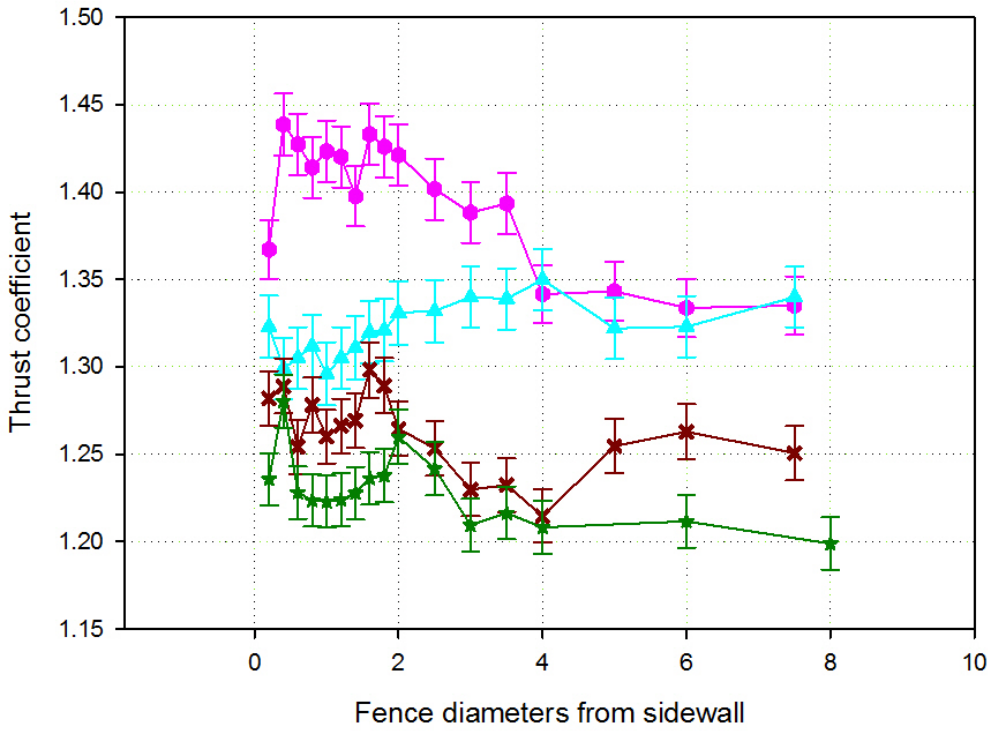

Figure 5.11: Variation in thrust coefficient with actuator fence position with varying blockage ratio

either end of the wake could potentially change the conditions downstream of a tidal array quite considerably.

The next step was to examine the implications for changing proximity to channel boundaries on the wake of the tidal turbine row. This was initially carried out with a 300mm wide fence, representing a blockage ratio of 0.072, and with a porosity of 0.34. The fence was placed with its edge at 4 different proximity to the channel sidewall. Firstly, the wake of the fence was examined with the fence touching the wall of the channel. This was done as it represented the most extreme case of close proximity of the tidal array to channel boundaries. The other positions examined were distances between the fence edge and sidewall of 1 diameter, 3.35 diameters and 5.35 diameters. The final proximity represented the fence directly in the centre of the channel.

These positions are illustrated graphically in figure 5.12. For each of these fence positions, flow velocity measurements were taken with the ADV at several lateral points and at 8 depths across the flume cross section, which are given in table 5.5.These were taken for both cases of an empty flume and with the fence in place.

As previously mentioned, it is widely accepted that actuator fences are only sufficient for examining the far wakes of tidal energy turbines. However the exact transition point between the near and far wake of tidal turbines is not universally accepted, and is in itself the subject of considerable research. One definition given by Myers and Bahaj [2013] is that the far wake begins where a sheared layer of flow at the boundary between slowed flow and ambient flow around the sides of the turbine rotor reaches the wake centreline. With some early studies on wind turbines, such as Connel and George [1981] and Sforza et al. [1981], the near wake was judged to be the region immediately downstream of the turbine rotor where high pressure and shear gradients, and large swirl effects, were present due to vortices off the rotating rotor blades. These swirl effects were seen to be dissipated at approximately 4 to 5 diameters downstream of the rotor. On the basis of this and other previous studies, the velocity measurements were taken 5 diameters downstream, and it was considered safe to conclude that this lay in the far wake of the actuator fence.

Distance from channel sidewall (mm)	Vertical distances from bed of flume (mm)
535mm (centre)	
450, 500, 550, 600, 650, 700,	30, 60, 90, 120,
750, 800, 850, 900, 950, 1000	150, 180, 210, 240.
335mm	
250, 300, 350, 400, 450, 500,	30, 60, 90, 120,
550, 600, 650, 700, 750, 800	150, 180, 210, 240.
100mm	
50, 100, 150, 200, 250, 300,	30, 60, 90, 120,
350, 400, 450, 500, 550, 600	150, 180, 210, 240.
0mm (against wall)	
50, 100, 150, 200, 250, 300,	30, 60, 90, 120,
350, 400, 450, 500, 550, 600	150, 180, 210, 240.

Table 5.5: List of velocity measurement points for each actuator fence position examined in 0.072 blockage ratio wake analysis

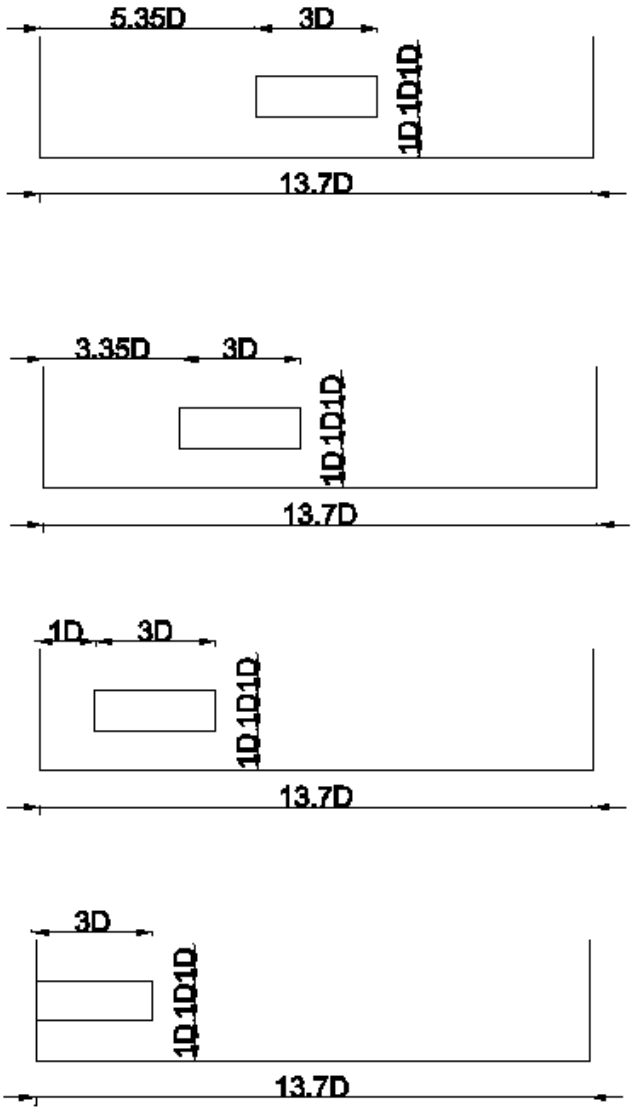

Figure 5.12: Illustration of actuator fence positions for wake analysis of 0.072 blockage ratio

The results of this analysis are displayed in figures 5.13 to 5.18, both as contour plots and line plots. The white rectangles in figures 5.13 to 5.15 indicate the positions of the actuator fence 5 diameters upstream. The purpose of these contour plots was to show the general trends in flow behaviour as the actuator fence position with respect to the channel sidewall was altered. The y axis on the line plots is the normalised distance from the end of the fence at which each measurement point was taken for the respective distance from the channel wall on that data set. The use of this relative distance from fence end on the Y axis allows all data sets to be overlaid on each other, therefore allowing an easy comparison between the actuator fence wakes for each fence position.

In all cases apart from the fence touching the channel wall, wake shapes and peak values for the examined parameters appear broadly similar. The u'v' Reynolds shear stress plots in figure 5.14 suggests that there is a similar amount of wake re-energisation in these cases, with the velocity deficit and turbulence intensity plots in figures 5.16 and 5.18 supporting

this by showing only marginal differences in other wake parameters. However when the fence touches the channel wall, some considerable changes to the wake are observed, which give some indication of the effects of mass flow rate restriction on wake properties. Wake mixing is in this case confined to the around the side of the fence towards the centre of the channel and also above and below the fence. In terms of peak values, this leads to considerably lower Reynolds stresses and turbulence intensity. Also looking at the velocity deficit scatter plot, it can be seen that there are increases in the peak value when the fence is closer to the channel wall, although these increases in value are quite marginal. It can also be seen that this change in areas of wake mixing changes considerably the shape of the wake. The case of the actuator fence touching the channel wall has a wake which occupies less of the overall depth of the flow, but has greater lateral width. The reduced height is due to greater re-energisation and quicker return to freestream conditions above and below the height of the fence, and simultaneously a slower recovery to freestream conditions around the sides results in a wider wake.

The contour plots for lateral Reynolds stress in figure 5.14 also show one interesting result, which it is argued gives more support to an observation given in the thrust coefficient analysis in section 5.2. The results of this analysis suggested that when the flow was constrained by positioning an array closer to a channel wall, there was no increase in thrust or thrust coefficient. The contour plot for the 1 diameter proximity appear to show that the lateral Reynolds shear stresses from depths of 0 to 1 diameter from the channel bed are much higher in the region close to the channel wall. This is a clear indication of momentum transfer occurring between fast moving fluid streamlines under the fence and slow moving streamlines in the wake. This result, combined with no increase in thrust close to the channel wall, give very strong indications that when mass flow rate is restricted in the region between an array and channel wall due to high viscous forces, fluid streamlines are diverted either above or below the fence. Interestingly, more support for this postulation of diversion of streamlines is given by examining shear stresses in the yz and xz directions (v'w' and u'w'). The contour plots for these shear stresses can be seen in figure 5.19 and 5.20. As with the lateral shear stresses displayed in figure 5.14, it can be seen that values are constant for all proximity apart from when the fence is touching the channel wall. However at the wall, the values are considerably higher, demonstrating greater momentum transfer between fluid streamlines in the wake and those above and below the actuator fence. But crucially, the higher velocity deficits closer to the channel wall would suggest that these streamlines cannot contribute to wake re-energisation to the same extent as fluid streamlines around the side of the fence. A possible reason for this is the slower moving boundary layer off the channel bed. It is possible that interaction between fluid streamlines diverted under the fence and streamlines in the boundary layer does not entrain the same volume of fluid into the wake, due to the smaller local mass flow rate in the boundary layer region.

As the results show some changes in wake properties with change in distance to the side-wall, it was decided many more proximities should be examined in more detail. Experiments were repeated for proximity in increments of 0.2 diameters up to 1.2 diameters from the side-wall. It was also repeated for the fence in the centre of the flume. Due to the high number of

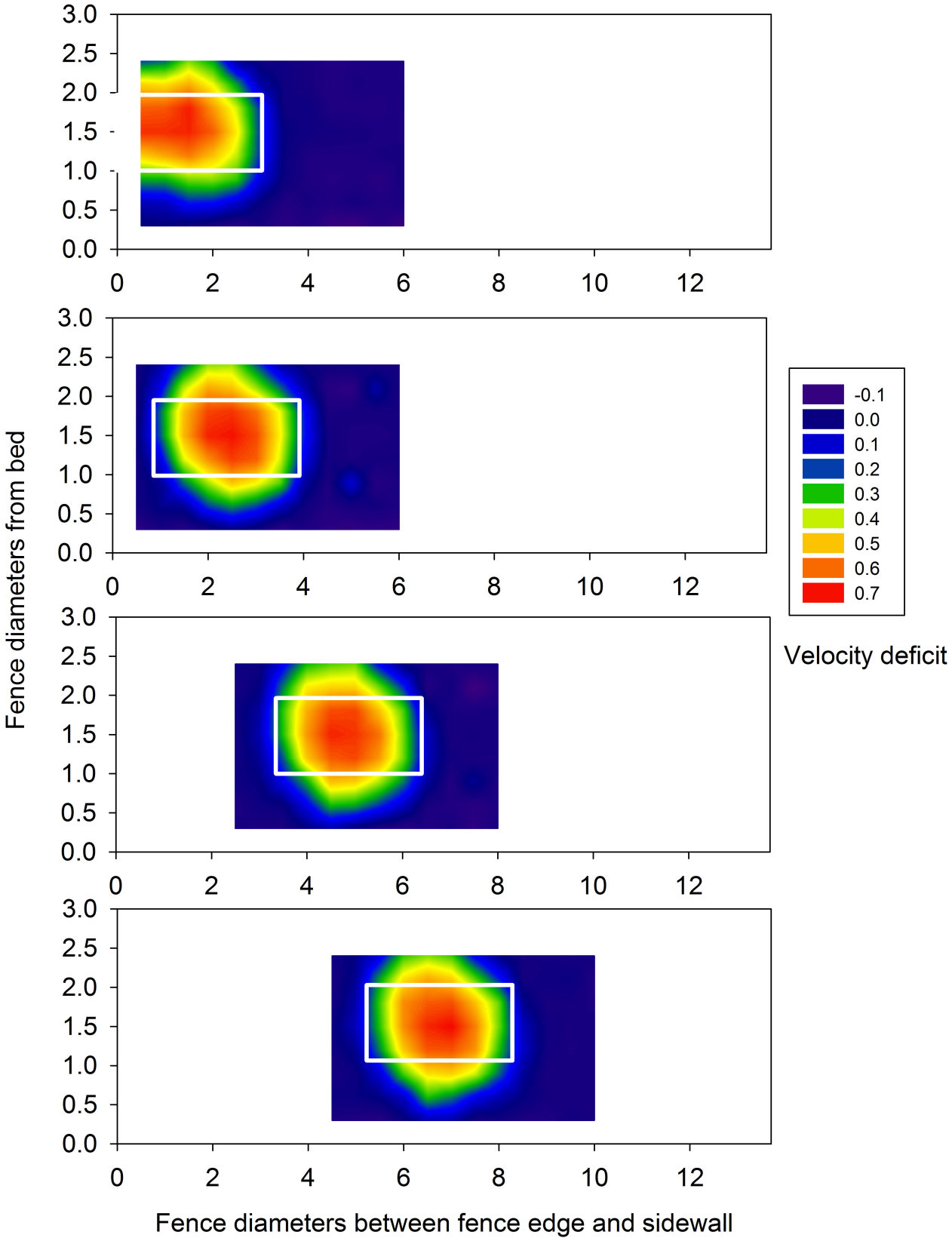

Figure 5.13: Contour plots of velocity deficit 5 diameters downstream of 0.072 blockage ratio actuator fence

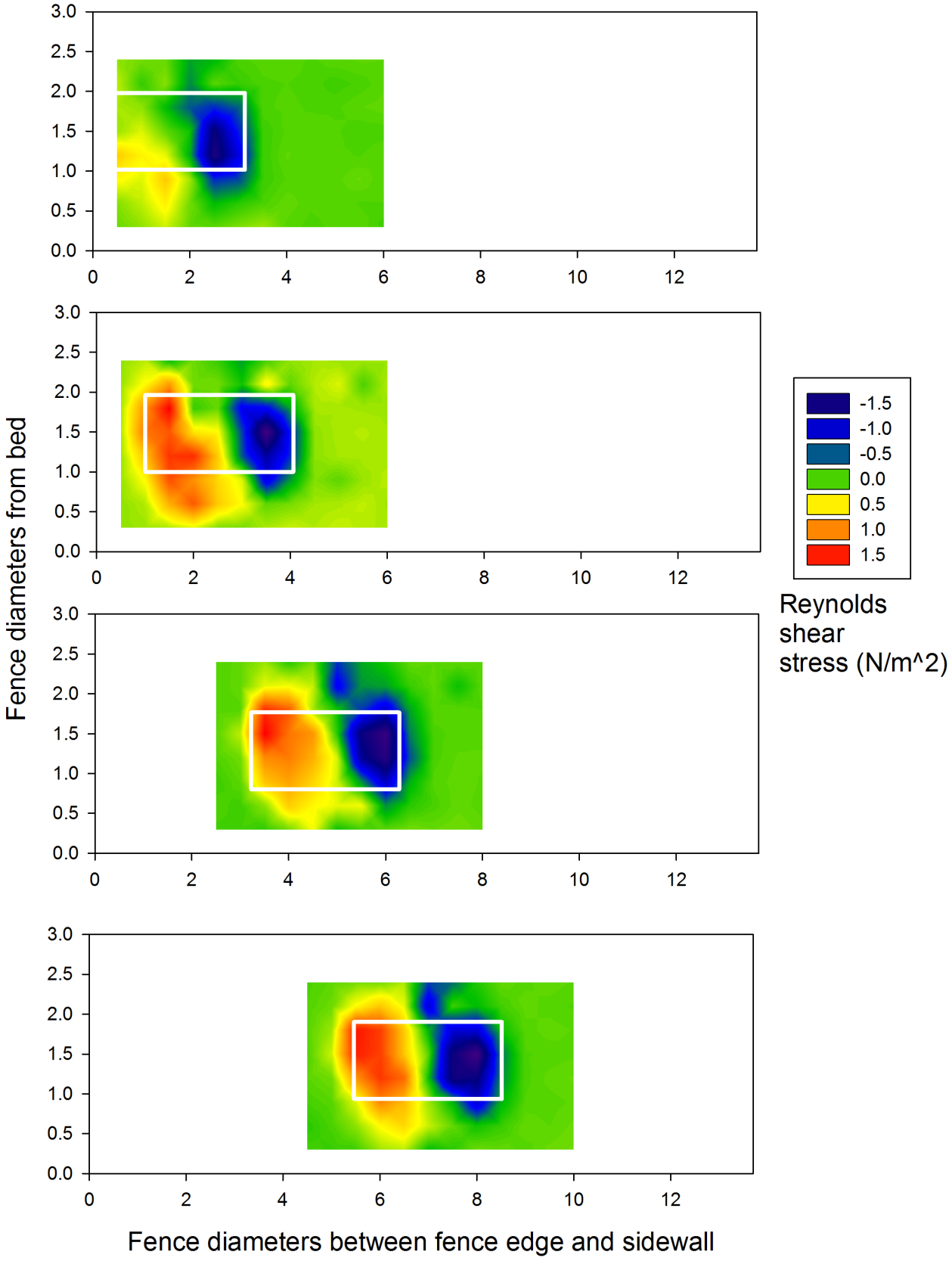

Figure 5.14: Contour plots of lateral Reynolds shear stress 5 diameters downstream of 0.072 blockage ratio actuator fence

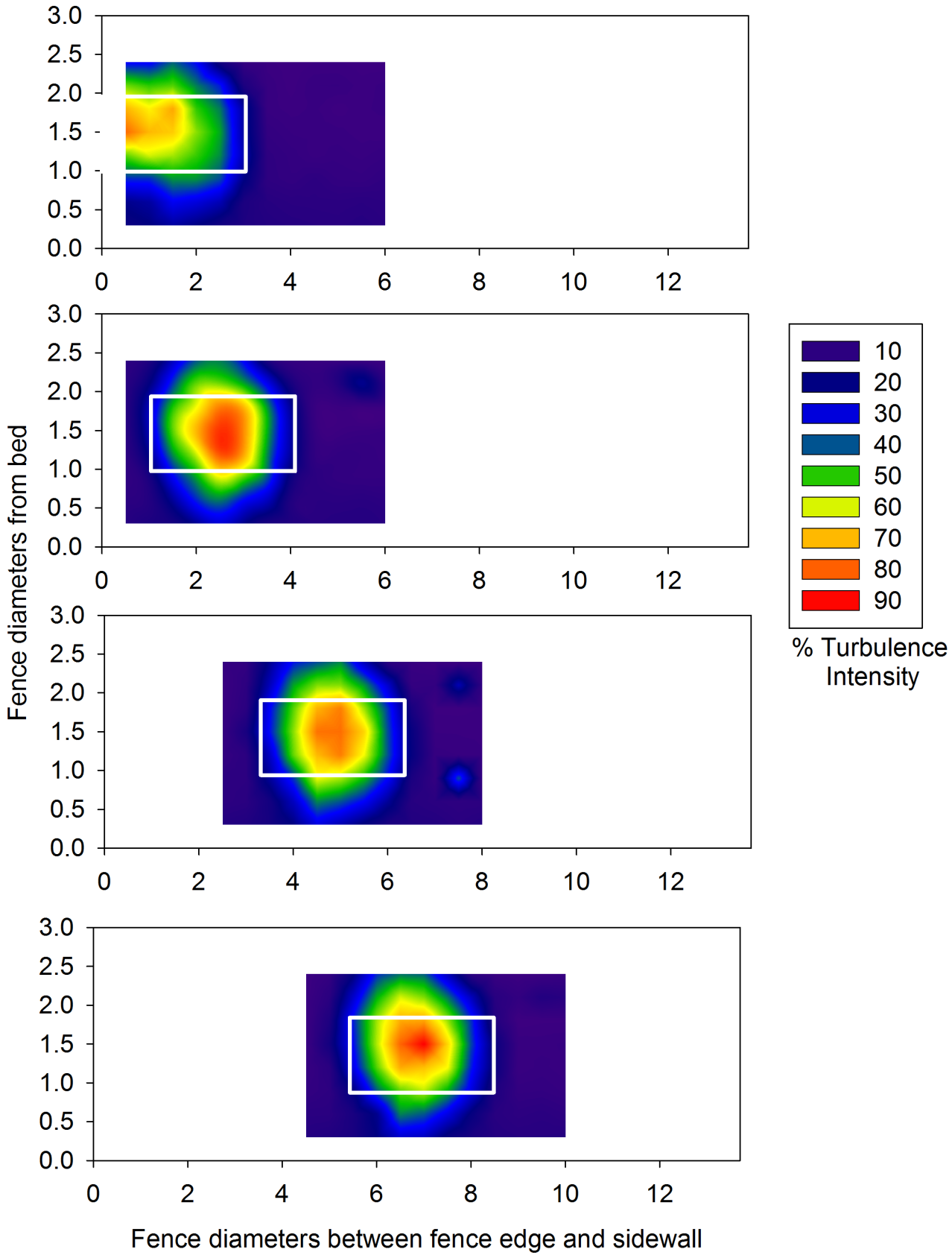

Figure 5.15: Contour plots of % Turbulence Intensity 5 diameters downstream of 0.072 blockage ratio actuator fence

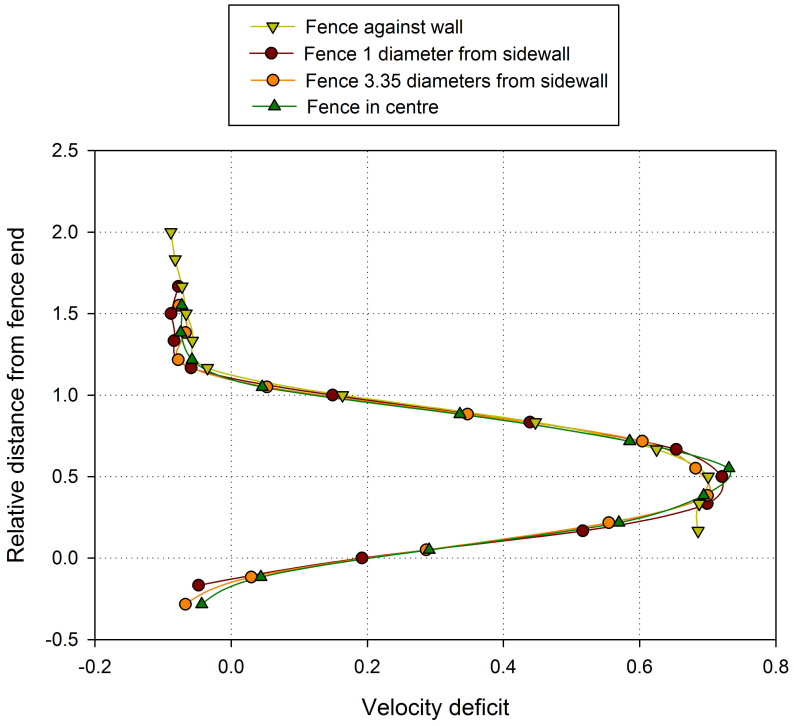

Figure 5.16: Scatter plot of velocity deficit 5 diameters downstream of 0.072 blockage ratio actuator fence

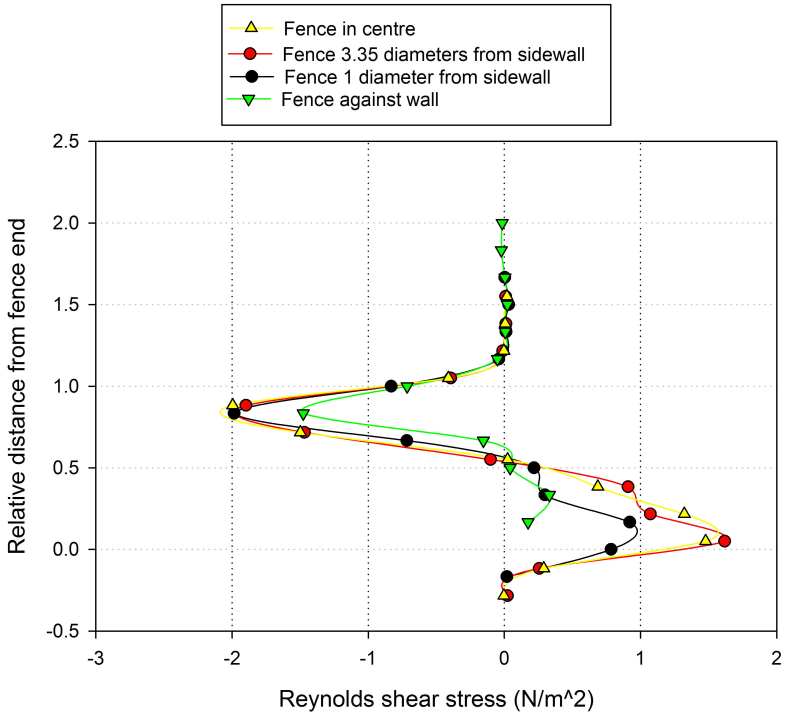

Figure 5.17: Scatter plot of lateral Reynolds shear stress 5 diameters downstream of 0.072 blockage ratio actuator fence

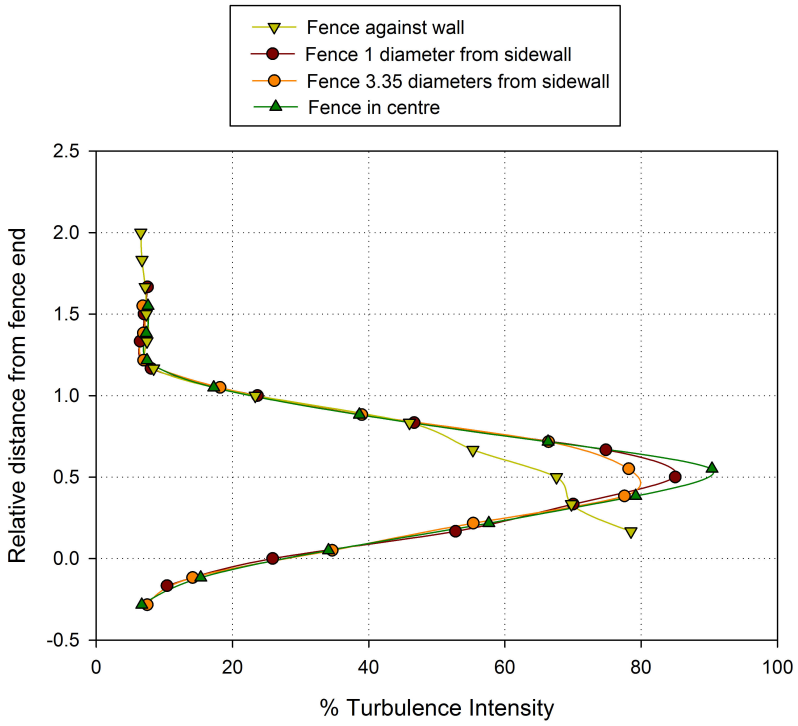

Figure 5.18: Scatter plot of % Turbulence Intensity 5 diameters downstream of 0.072 blockage ratio actuator fence

fence positions, detailed centre depth measurements were taken. The results of this analysis can be seen in figures 5.21 to 5.23.

In the case of all three parameters, there does not appear to be any considerable change or definite trend in peak values towards the very centre of the wake. The values for each of the parameters around the side of the fence closer to the centre of the channel are also identical for each proximity between the array and channel wall. However where very clear trends appear to be evident is at the side of the fence closest to the channel wall. Here it appears that positioning the array progressively closer to the channel walls leads to the following effects around the edge of the array:

- Increasing velocity deficit at the array edge closest to the channel wall.
- Decreasing lateral Reynolds shear stresses at the array edge closest to the channel wall.
- Increasing turbulence intensity around the array edge closest to the channel wall.

It is postulated that these changes to wake properties are a direct consequence of the restriction of mass flow rate in the region between the edge of the fence and the channel wall already discussed in section 5.1. Here it was postulated that positioning the actuator fence closer to the channel wall led to a gradually increasing velocity gradient between the wall and fence edge. This in turn led to higher viscous shear stresses and viscous forces, which would attempt to divert fluid streamlines away from this region and hence reduce the mass

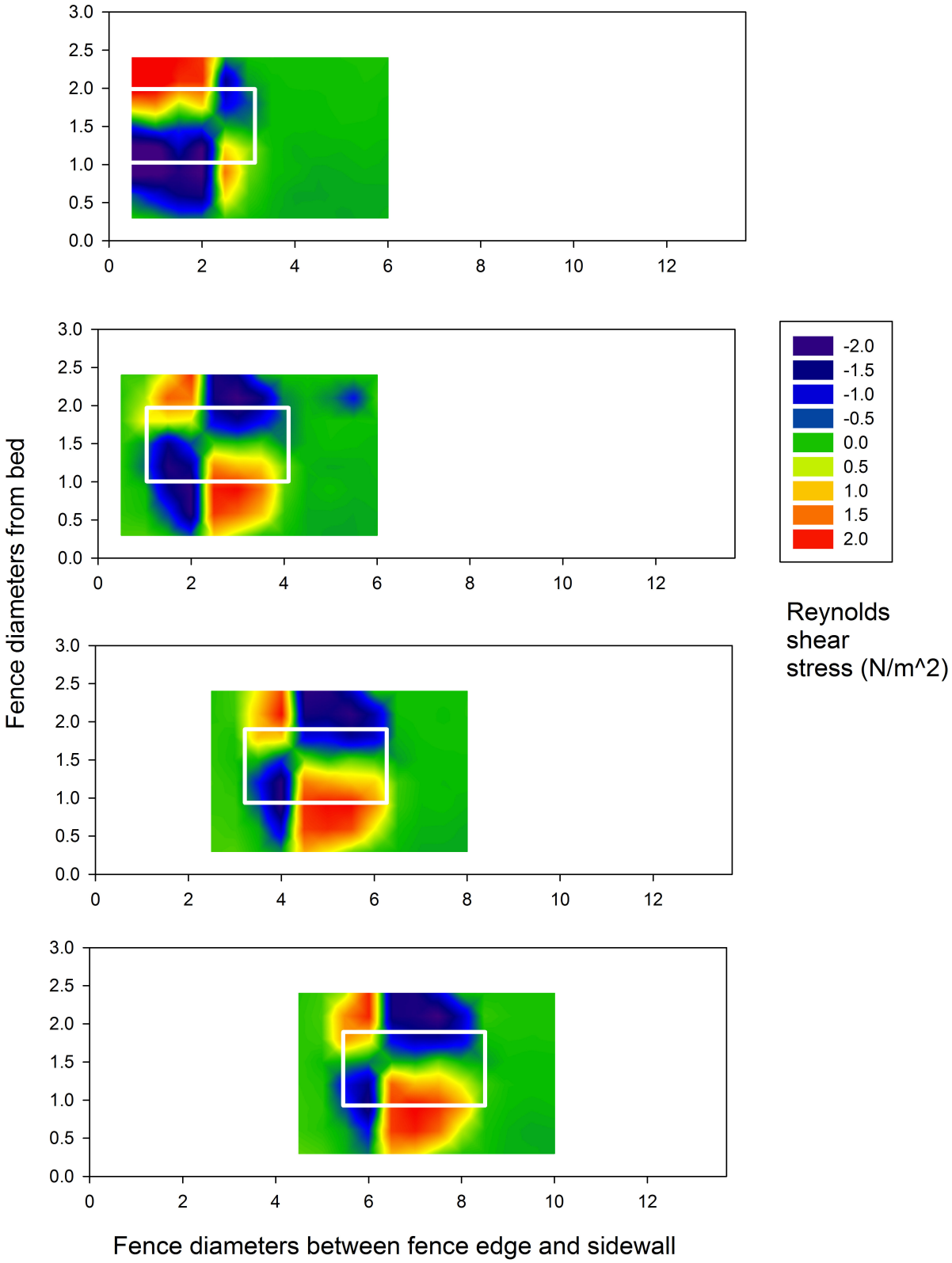

Figure 5.19: Contour plots of Reynolds shear stresses in the v'w' plane 5 diameters downstream of 0.072 blockage ratio actuator fence

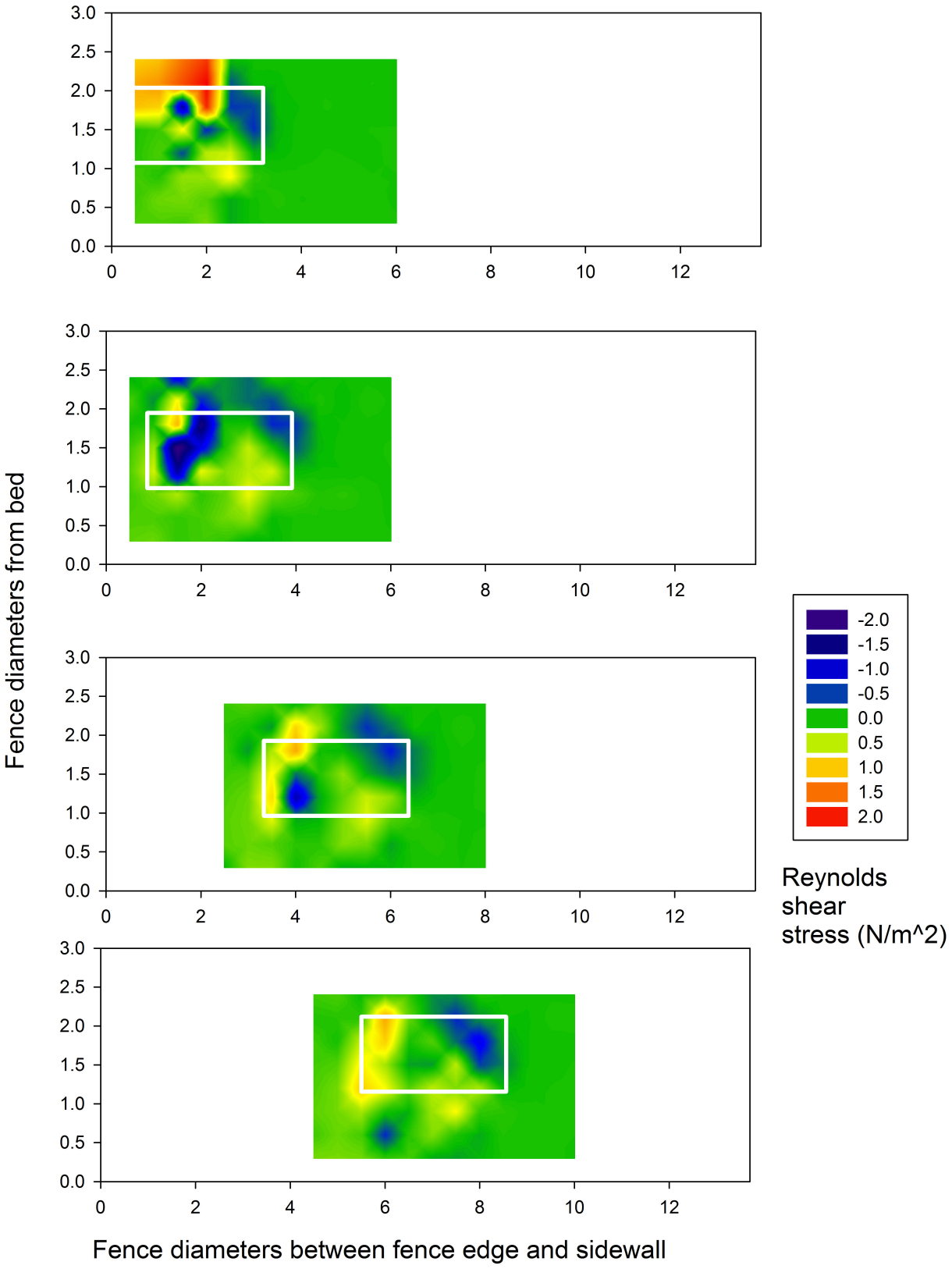

Figure 5.20: Contour plots of Reynolds shear stresses in the u'w' plane 5 diameters downstream of 0.072 blockage ratio actuator fence

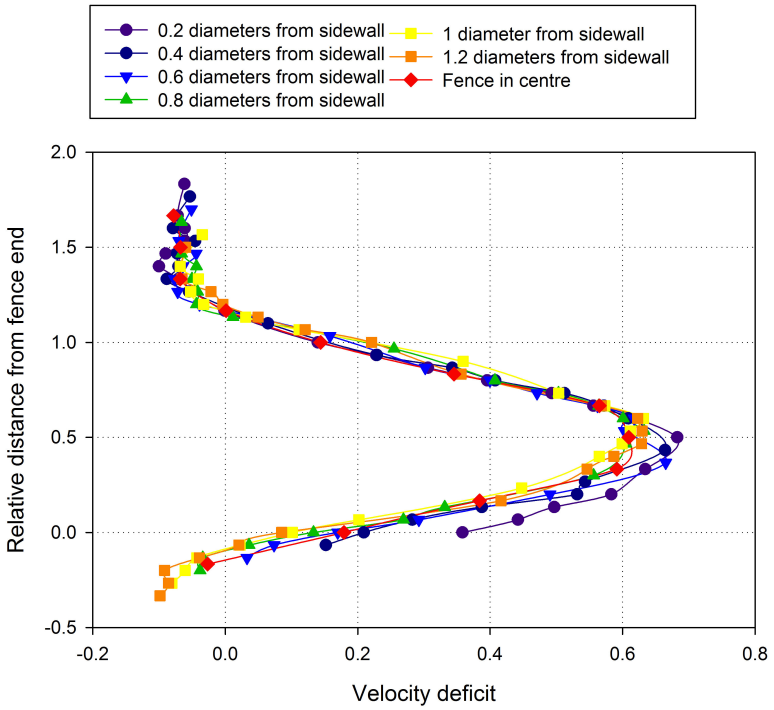

Figure 5.21: Scatter plot of velocity deficit 5 diameters downstream of 0.072 blockage ratio actuator fence very close to channel sidewall

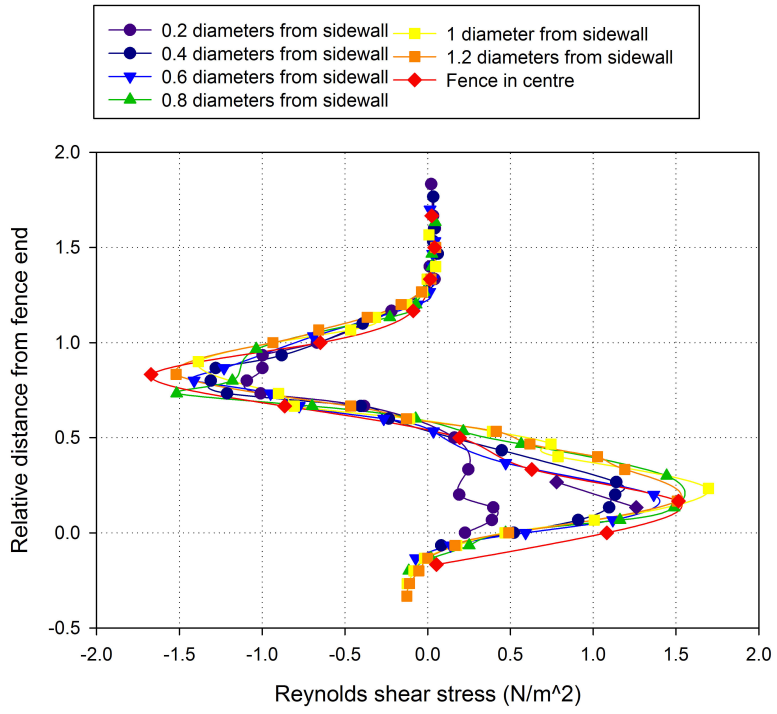

Figure 5.22: Scatter plot of lateral Reynolds shear stress 5 diameters downstream of 0.072 blockage ratio actuator fence at proximity very close to channel sidewall

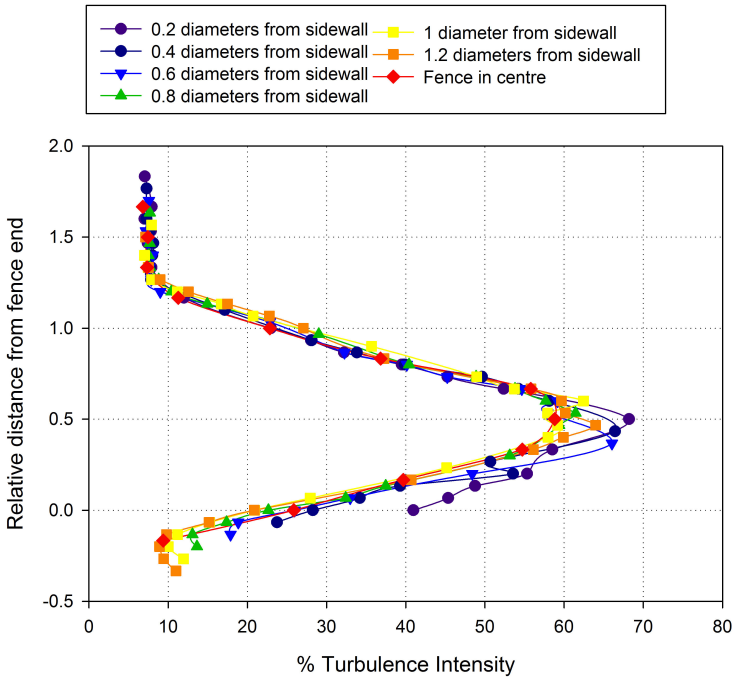

Figure 5.23: Scatter plot of % Turbulence Intensity 5 diameters downstream of 0.072 blockage ratio actuator fence at proximity very close to channel sidewall

flow rate through it. A reduction in mass flow rate between the fence edge and sidewall will lead to a reduced flow rate around the sides of the fence which can transfer their momentum to slow moving flow in the wake, and this is clearly evident from the lower value for lateral Reynolds shear stresses around the side of the array with closer proximity to the channel boundary. However these lower lateral stresses are accompanied by higher vertical stresses, and so do not explain by themselves why there is a higher velocity deficit and turbulence intensity closer to the channel wall. It is postulated that this is due to the fact that the higher vertical shear stresses are interacting with the boundary layer off the bed of the flume. This boundary layer is a region which has a smaller local mass flow rate than the region between the top of the fence and free surface, and also normally around the sides. Therefore there is less wake mixing and momentum exchange between the wake region flow and flow below the actuator fence, compared to similar mixing between the wake and other flow regions. This higher velocity deficit would also explain higher turbulence intensity close to the channel wall. As already mentioned, slower flow velocity will mean any given absolute deviation from a mean value at any instant in a given time period will be a greater relative deviation, hence leading to a higher turbulence intensity value.

To examine further the postulation given for changes to wake properties, two other scenarios were examined. So far the wake results 5 diameters downstream for an actuator fence with a blockage ratio of 0.072 have been presented. The following extra scenarios were also examined.

- The wake results 5 diameters downstream of a 0.072 blockage ratio fence when the

fence was moved to the opposite wall of the Chilworth flume. With respect to the flow direction from the inlet to the outlet of the flume channel, this is the left hand side of the flume. As with the constraining analysis on this opposite side presented in section 5.1, this was to ensure that the slightly faster flow on one side of the flume did not result in different observed effects of changing fence proximity to the channel wall.

- The wake results 9 diameters downstream of a 0.072 blockage ratio fence.

The examination of wake properties on the left hand side of the flume was carried out for a single proximity of 0.6 diameters between the edge of the fence and the edge of the opposite sidewall. It was felt this would be sufficient to examine whether the same changes to wake properties would be observed irrespective of changes in the localised flow conditions. A comparison of these results was also made to wake properties both in the centre of the flume and at the same proximity on the right hand side of the flume (with respect to flow direction from inlet to outlet), where most wake proximity experiments were carried out. The results of this analysis are displayed in figures 5.24 to 5.26. They show that the left hand side of the flume also gives higher velocity deficit, lower Reynolds shear stresses at the side of the fence closest to the channel wall, and higher maximum turbulence intensity compared to the centre of the flume. This verification of results gave greater confidence in the postulations put forward to explain these effects, demonstrating that the observed experimental results were not a consequence of special ow conditions close to either channel wall in the Chilworth flume.

The results 9 diameters downstream can be seen in figures 5.27 to 5.29. The results are broadly similar to the 5 diameter case. Once again, lower Reynolds shear stresses are observed around the side of the fence closer to channel wall with closer proximity to the wall. This in turn also leads to higher velocity deficit and turbulence intensity at these sides again. However as with the 5 diameter analysis, the centre of the wake, and the side of the array towards the centre of the channel, appear unaffected by changes in fence proximity to flow boundaries.

Clearly, the smaller localised flow rate around the side of the fence towards the channel wall has a considerable effect on wake development. As fluid re-energisation of the wake causes it to contract, and the edges of the wake on either side will draw ever closer until freestream conditions are achieved. It is postulated that the extent to which the edge of the wake closest to channel wall draws closer to the wake edge on the opposite side is dependent on the amount of freestream flow near the wall available for mixing and re-energisation. When the fence is very close to the channel wall, the amount of flow available in this region for mixing will be a minimum. However the localised flow rate available here will increase as the fence is moved further away from the channel wall. This postulation would fully explain why at the edge of the fence closest to the wall, both velocity deficit and turbulence intensity decrease, and Reynolds stresses increase, as the fence is moved towards the centre of the channel. The reason why the opposite side of the wake, as well as the centre of the wake, are not similarly affected, is most likely due to the much greater distance to the opposite channel sidewall, and hence the large amount of undisturbed freestream flow available for wake mixing on the opposite side of the wake.

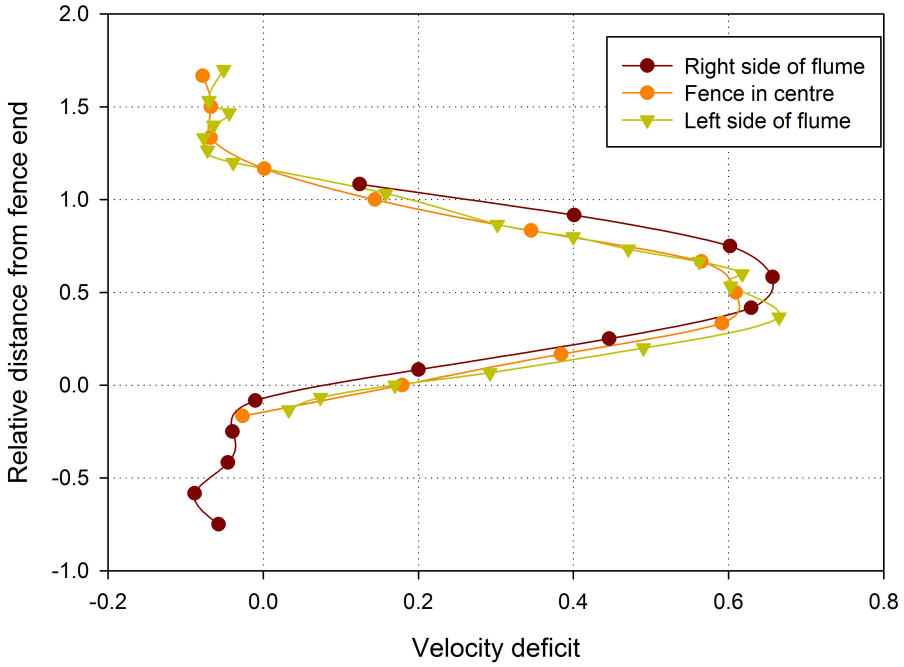

Figure 5.24: Scatter plot of velocity deficit 5 diameters downstream of 0.072 blockage ratio actuator fence very close to channel sidewall on opposite side of flume

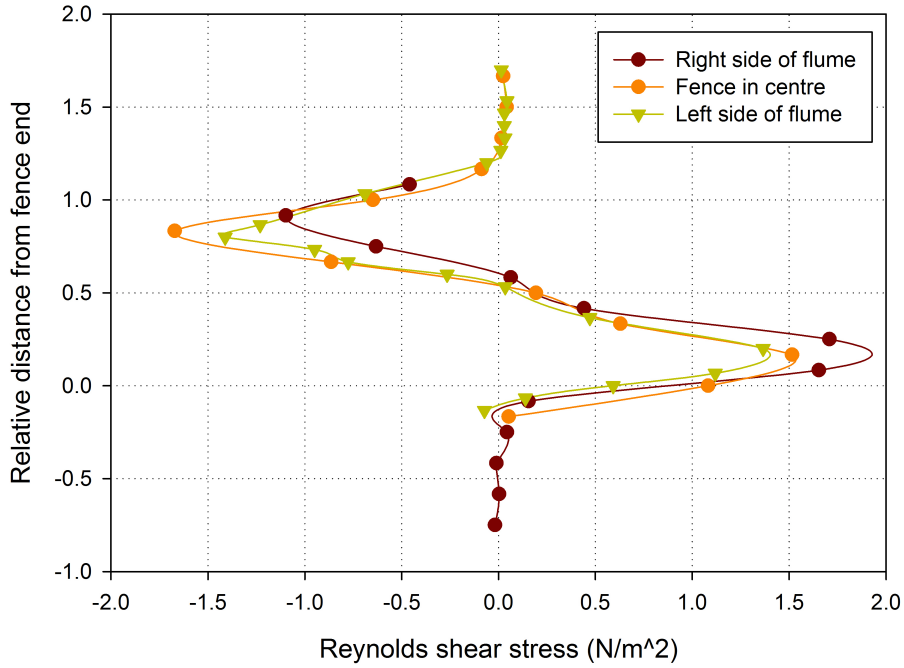

Figure 5.25: Scatter plot of lateral Reynolds shear stress 9 diameters downstream of 0.072 blockage ratio actuator fence at proximity very close to channel sidewall on opposite side of flume

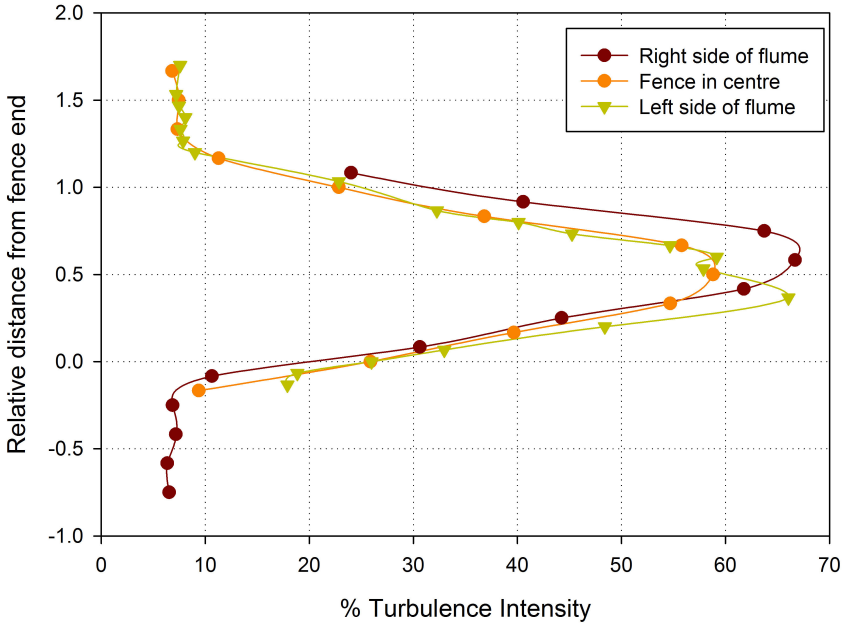

Figure 5.26: Scatter plot of % Turbulence Intensity 9 diameters downstream of 0.072 blockage ratio actuator fence at proximity very close to channel sidewall on opposite side of flume

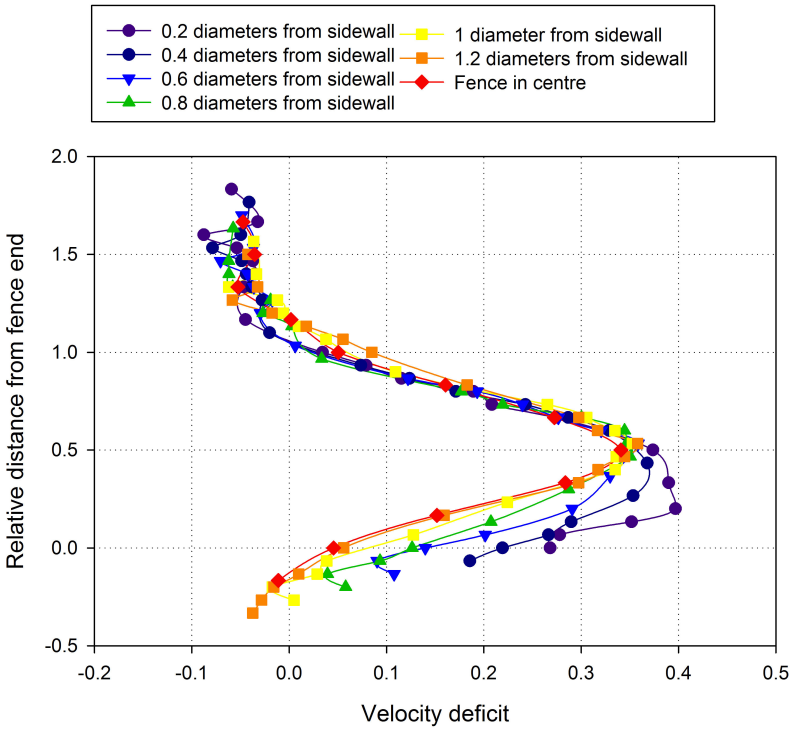

Figure 5.27: Scatter plot of velocity deficit 9 diameters downstream of 0.072 blockage ratio actuator fence very close to channel sidewall

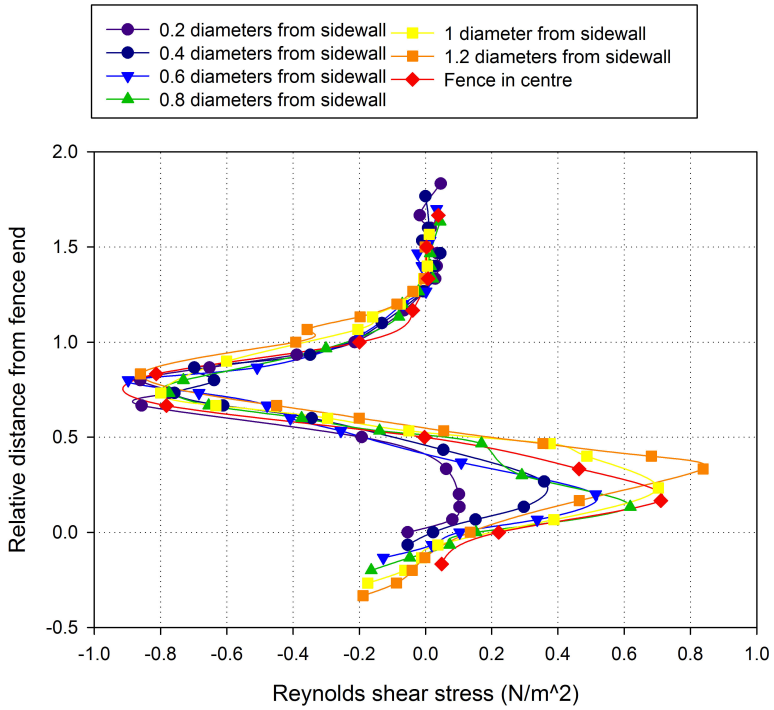

Figure 5.28: Scatter plot of lateral Reynolds shear stress 9 diameters downstream of 0.072 blockage ratio actuator fence at proximity very close to channel sidewall

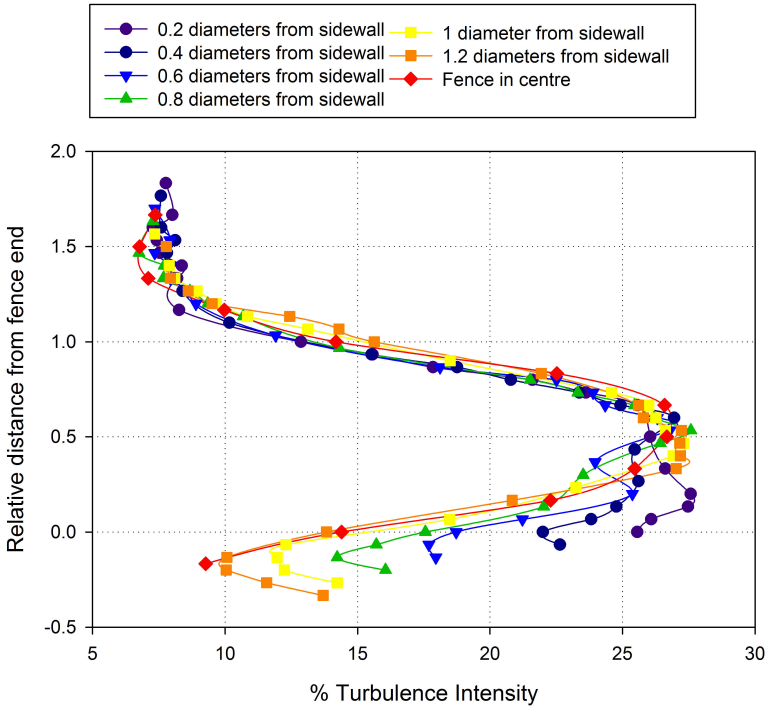

Figure 5.29: Scatter plot of % Turbulence Intensity 9 diameters downstream of 0.072 blockage ratio actuator fence at proximity very close to channel sidewall

5.3.2 Wake changes for 0.146 blockage ratio (600mm wide) actuator fence

In the previous section, examination of velocity deficit, u'v' Reynolds shear stresses and turbulence intensity 9 diameters downstream and the opposite side of the channel were two methods of verifying wake changes due to postulated mass flow rate restriction. A third method also considered was to examine the wake at centre depth 5 diameters downstream of a 0.146 blockage ratio fence.

The results of this analysis can be seen in figure 5.30 to 5.32. An immediate similarity between these results and those presented for the case of 0.072 blockage ratio in the previous section is the results of the examined parameters around the side of the fence closest to the channel wall. At this side, the highest values for velocity deficit and turbulence intensity, as well as the lowest values for lateral Reynolds shear stresses, occur when the fence is positioned closest to the channel wall. As already explained in the previous section, this shows evidence of mass flow rate restriction due to high viscous forces.

There do however appear to be some very fundamental differences between the wakes also. The shape of the wake of the 0.146 blockage ratio fence is also quite different to that of the 0.072 fence discussed in the previous section. The peak values for velocity deficit and turbulence intensity no longer occur in the centre of the wake, but instead around the side closest to the channel wall. These results suggest that the centre of the wake is in some way being re-energised by freestream flow being entrained into the wake from some region other than around the sides of the fence. This postulation is strongly supported by the scatter plot in figure 5.31, and also the contour plot in figure 5.33. In these, it can be seen that, as

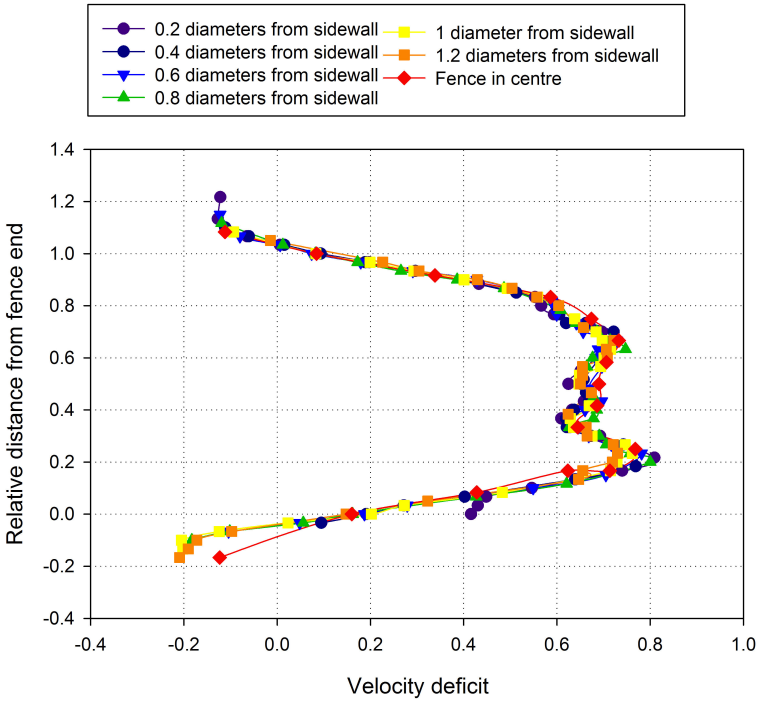

Figure 5.30: Scatter plot of velocity deficit 5 diameters downstream of 0.146 blockage ratio actuator fence very close to channel sidewall

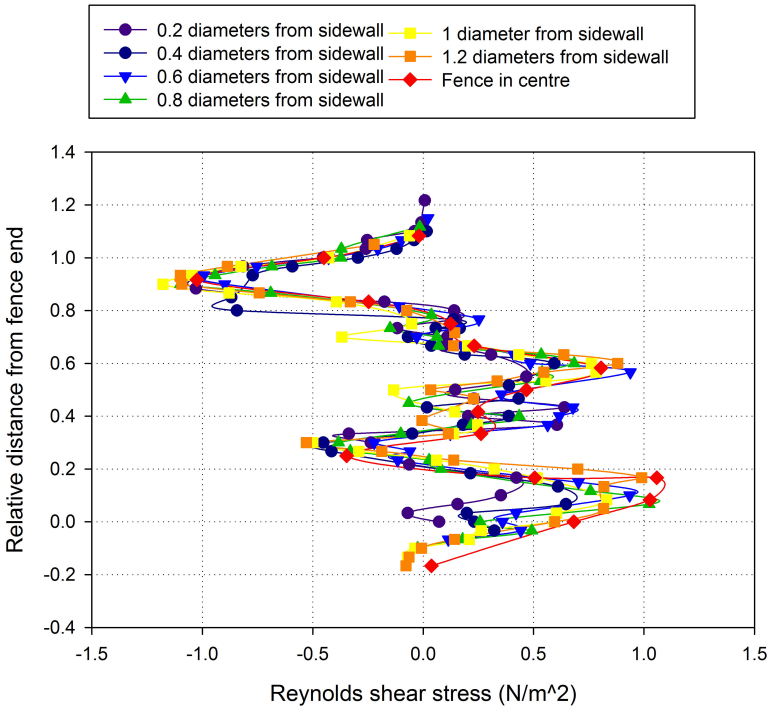

Figure 5.31: Scatter plot of lateral Reynolds shear stress 5 diameters downstream of 0.146 blockage ratio actuator fence at proximity very close to channel sidewall

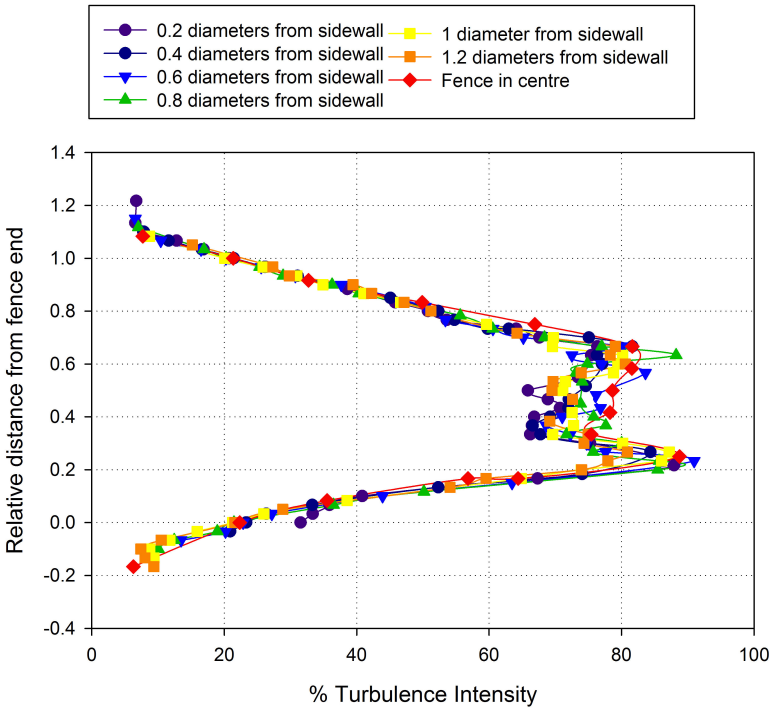

Figure 5.32: Scatter plot of % Turbulence Intensity 5 diameters downstream of 0.146 blockage ratio actuator fence at proximity very close to channel sidewall

opposed to the lower blockage ratio cases, the highest lateral Reynolds stresses are no longer confined to directly around the sides of the fence.

It is postulated that the difference in wake mixing behaviour between the larger and smaller blockage ratio fences is due to different behaviour of fluid streamlines approaching the fences. When fluid streamlines approach a porous fence, the majority will travel around the fence while the remainder will travel through it. All streamlines will ultimately want to take the path of minimal obstruction to flow. For fluid streamlines approaching closer to the edges, they will experience less obstruction to flow by accelerating around the sides than travelling either through the fence or around the top of the fence. However for fluid streamlines approaching closer to the fence centre, the distance which they would have to travel to be directed around the sides is larger. For some of these streamlines, less obstruction to flow is offered by either flowing directly through the fence, or above and below it if the fence is submerged in relatively deep flow. Therefore the larger distance required by fluid streamlines towards the centre of a fence to travel around the sides is the reason for the different wake structures compared to a narrower fence.

Another difference in the analysis of larger blockage ratios is the asymmetry of certain wake profiles. Results show that at very close proximity to the channel wall (0.2 to 0.6 diameters), the velocity deficit and turbulence intensity appears to be larger towards the side of the fence closer to the channel wall. Further away from the channel wall, at proximity of about 1 diameter and towards the centre, the highest values for velocity deficit and turbulence intensity appear almost equal on both sides, while closer to the channel wall they are higher on the near side. This is another observation which the action of viscous forces might explain. It is these forces that will divert fluid streamlines away from the region between the side of the array and the wall of the channel, and some results already presented have demonstrated that some streamlines are diverted above the fence. The direction in which they will be acting depends on fluid pressure values, and will be in the direction from high pressure to low pressure, due to Bernoulli's principle. The exact strength and magnitude of these forces will be dependent on the localised flow conditions and the local Reynolds number, with the strength of viscous forces being proportional to the magnitude of local Reynolds number. Applying those same fundamental principles to this analysis, the viscous forces due to the velocity gradients will be diverting fluid streamlines away from the wall. Due to the no-slip condition, zero velocity at the wall will mean a high pressure region, while non-zero velocity away from the wall will mean lower pressure. It is therefore postulated that fluid streamlines diverted above the fence are diverted in the direction of the centre of the channel, and this may be why the wake velocity is larger (and hence velocity deficit is lower) on the side of the fence closer to the centre of the channel in certain instances. This then raises the question of why this same wake asymmetry is only evident for certain proximity, and does not appear at all for the smaller blockage ratio fences. To give a possible explanation for this, it is worth again noting that viscous shear stresses are proportional to velocity gradient. Large blockage ratio fences very close to the channel wall will cause the highest velocity gradients than smaller fences due to the greater increase in velocity in this region, as already demonstrated by results in section 5.1. It is postulated that for smaller blockage ratios, the increase in velocity

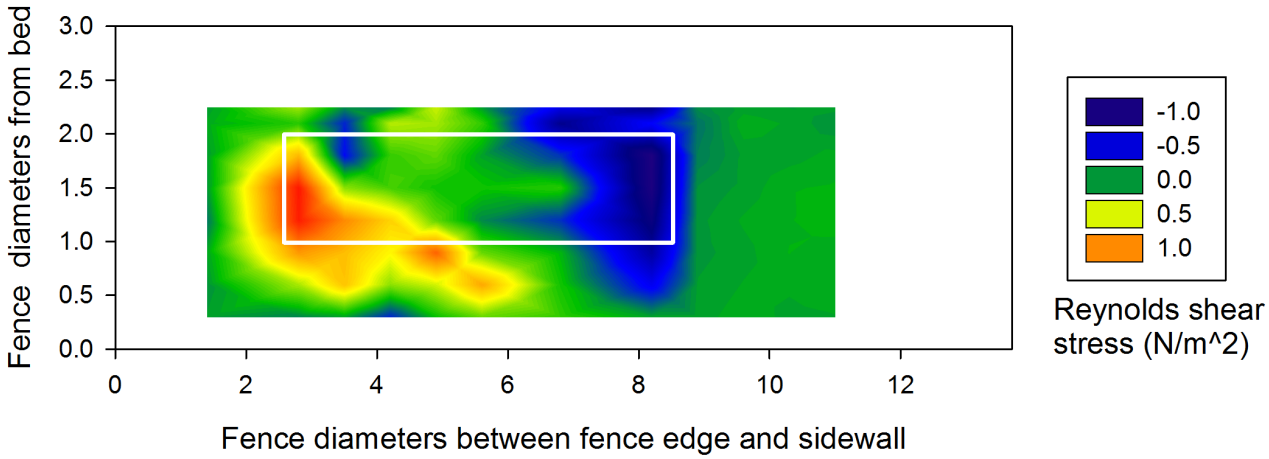

Figure 5.33: Contour plots of lateral Reynolds shear stress 5 diameters downstream of 0.146 blockage ratio actuator fence

is not sufficient for viscous forces to be strong enough to cause this extreme diversion of fluid streamlines towards the centre of the channel. Similarly, it is postulated that for the larger blockage ratio fences, proximity outside of about 0.8 diameters do not ensure a large enough velocity gradient to cause this same phenomenon.

Given the considerable differences between the wake structure of smaller and larger actuator fences, a direct comparison between the wake properties was considered appropriate. The results for this comparison are presented in figures 5.34 to 5.39. All three wake parameters have been examined for both blockage ratio fences at two positions, in the centre of the flume and with the fence edge 0.6 fence diameters from the channel wall. In the case of both fence positions, the following results are observed:

- Maximum velocity deficit values are larger for the higher blockage ratio fence.
- The magnitude of maximum lateral Reynolds shear stress is lower for the larger blockage ratio fence, but there are more areas where wake mixing with the freestream flow is occurring.
- Turbulence intensity in the wake is larger for the 0.146 blockage ratio fence.

Results in the previous section demonstrated the reasons for the different shapes of the lateral Reynolds shear stress plots in figures 5.34 and 5.35. With the larger blockage ratio fence, less momentum transfer occurs around the sides of the fence, and more above and below the fence. These differences in wake mixing can be demonstrated graphically by the illustration in figure 5.40. In the case of the 0.072 blockage ratio fence (which is 3 diameters wide), fluid streamlines diverted around the sides of the actuator fence have a relatively large volume of fluid which they can entrain into the wake, as there is more than 5 diameters width between the edge of the fence and the channel walls.

Figures 5.36 and 5.37 show that the smaller magnitude of lateral Reynolds stresses have in fact led to a slower wake 5 diameters downstream of the larger actuator fence. This is despite the larger value for vertical Reynolds shear stresses, and is again postulated to be

due to the smaller mass flow in the boundary layer, and hence the smaller volume of fluid entrained into the wake vertical shear stresses compared to lateral shear stresses.

A further reason postulated for the larger peak velocity deficits is the higher thrust coefficient on the larger actuator fence. Looking again at the thrust coefficient results given in figure 5.11, the higher thrust per unit area and flow velocity on the higher blockage ratio fences also indicates a great rate of the change of momentum of the water travelling through the fence. As the upstream conditions to both sized actuator fences are the same, this means the fluid immediately downstream of the larger blockage ratio fence will have lower momentum and hence a lower velocity. This water therefore requires more momentum to return to freestream conditions upstream, which does not occur due to the blockage phenomenon already described.

Finally, figures 5.38 and 5.39 show quite different values for the turbulence intensity in the wake of both fences. In both cases, the 0.146 blockage ratio fence wake has considerably higher values for turbulence intensity. It is postulated that these higher turbulence intensity values are a direct consequence of the slower wake associated with the larger blockage ratio. As already discussed in section 5.3.1, any absolute deviation from the mean flow velocity at any instant in a given fixed time period will represent a greater percentage deviation from the mean, and hence higher turbulence intensity, in a slower wake.

The results in this section have shed more light on some of the differences between the wakes of different sized fences. The conclusions can be summarised as follows:

- Larger blockage ratio wakes have smaller values for Reynolds shear stresses. This means that at least around the sides of the fence, less fluid is entrained into the wake than in the case of a smaller blockage ratio.

- The additional wake mixing above and below the actuator fence in larger blockage ratios does not compensate for the lower magnitude of wake mixing around the sides. Therefore at any given point downstream of the fence, the wake is slower. This will also mean a longer distance downstream required for the wake to recover to freestream conditions.

- Larger blockage ratio fences have higher values for turbulence intensity at any given point downstream. This is postulated to be a direct consequence of the slower wake.

The results presented have demonstrated that viscous effects and increases in viscous forces associated with closer proximity to channel walls can have a considerable influence on the structure of a wake downstream of a row of turbines. Also by examining two sides of the same experimental domain with slightly different localised flow conditions, it has also been demonstrated that the same changes can be expected irrespective of flow conditions, although the magnitude of these changes will obviously be different. It has also been demonstrated that proximity to channel boundaries is not the only influential parameter in these changes. The differences in fundamental flow behaviour associated with increased viscous forces have been shown to have varying effects on the magnitude of velocity deficit, Reynolds stresses or turbulence intensity, with these varying effects also being dependent on the specific position

downstream in the wake being examined and the blockage ratio of the row of turbines in question.

5.3.3 Comparison of measured wake and bypass flow velocities with theoretical estimates

Much of the scope of the results presented was on the basis of literature reviewed in section 2.2.2. The studies presented aimed to develop theory which explained the physical processes at work in partially blocked bounded open channels, thus advancing on previous work which assumed an infinitely wide flow field and fully blocked channels. They also showed clearly the

dependence of the power output of turbines on parameters such as blockage ratio, wake and bypass flow velocities (which were in turn demonstrated by literature reviewed in section 2.4.3 to be dependent on upstream turbulence conditions) and inter device spacing. However a number of assumption and simplifications were made by these authors, which may limit their applicability in full scale 3D tidal sites. However the data presented in these experiments does offer an opportunity to determine to what extent these simplifications may render these models inaccurate.

Of the three blockage models reviewed, Garrett and Cummins (2007) is one which allows direct calculation of flow velocities in certain regions of the flow, specifically the bypass flow region surrounding the actuator fence. The equation these authors gave for the bypass flow U_4 as a function of upstream flow velocity U_0, wake velocity U_3 and blockage ratio ϵ was

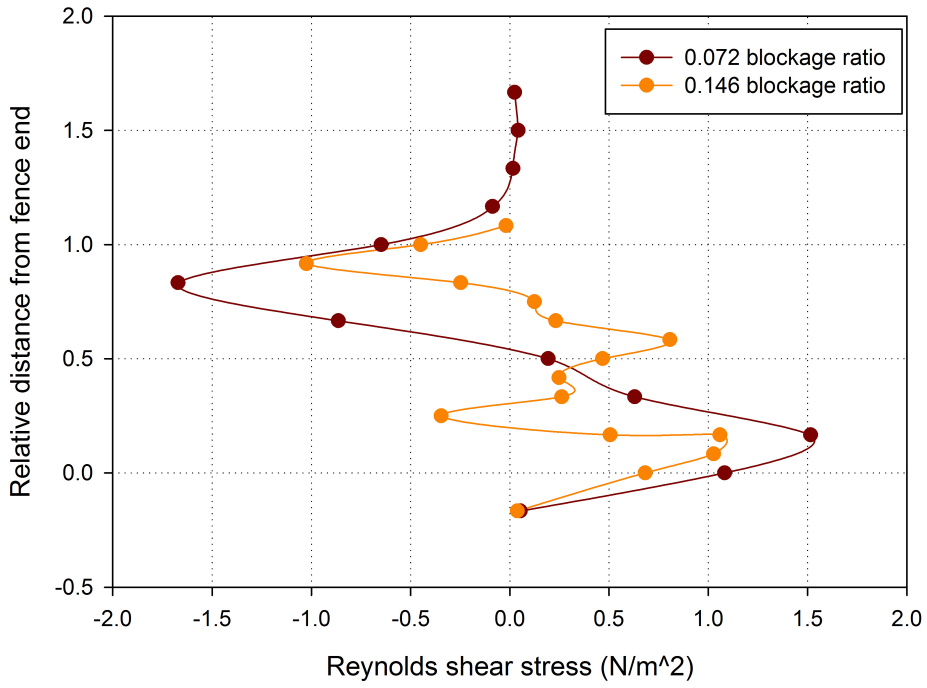

Figure 5.34: Comparison of Reynolds shear stress 5 diameters downstream of 0.072 and 0.146 blockage ratio fences positioned in centre of flume

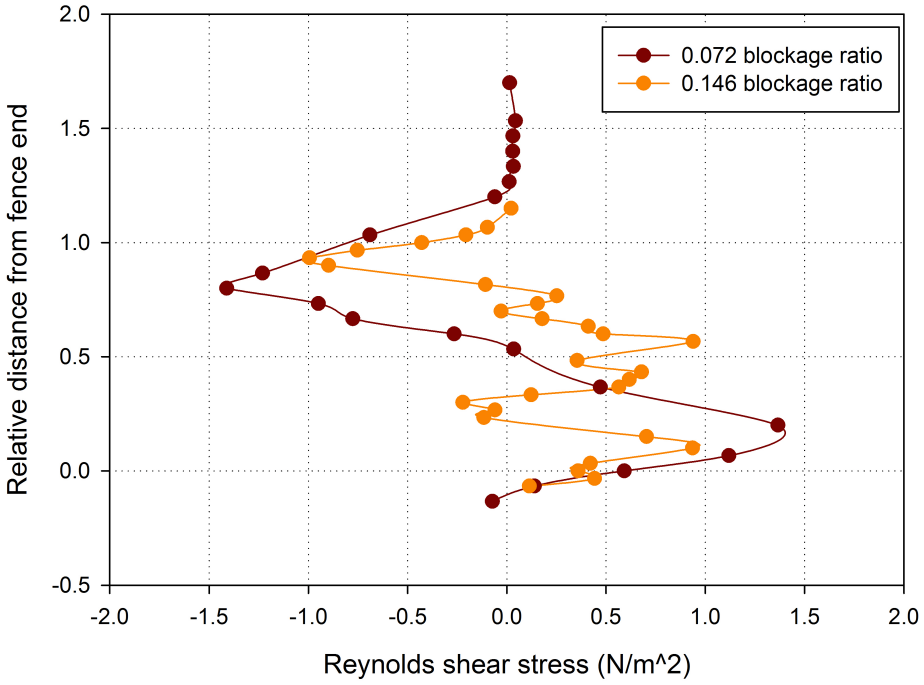

Figure 5.35: Comparison of Reynolds shear stress 5 diameters downstream of 0.072 and 0.146 blockage ratio fences positioned 0.6 diameters from sidewall of flume

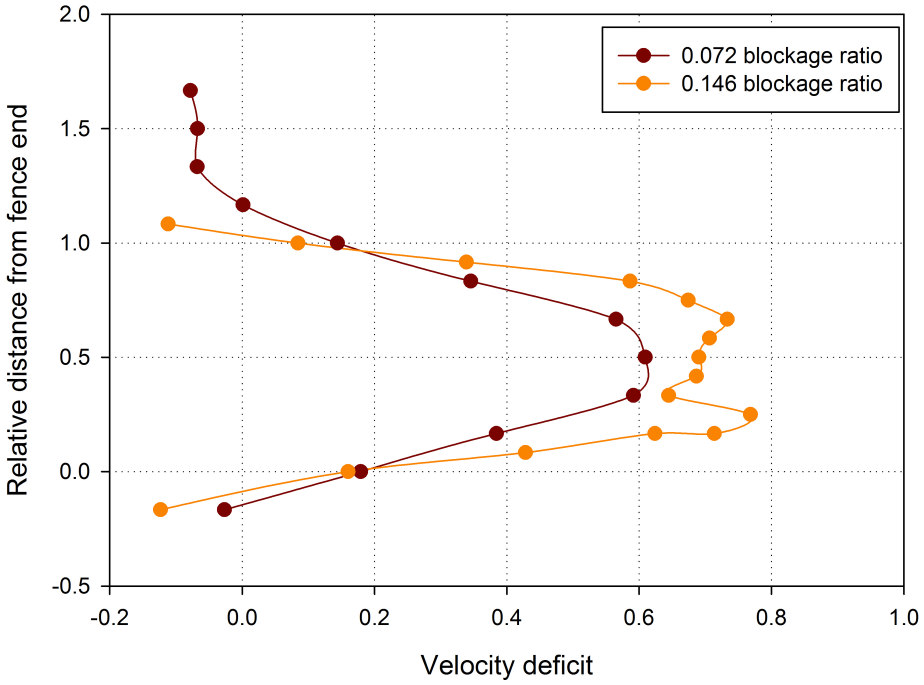

Figure 5.36: Comparison of velocity deficit 5 diameters downstream of 0.072 and 0.146 blockage ratio fences positioned in centre of flume

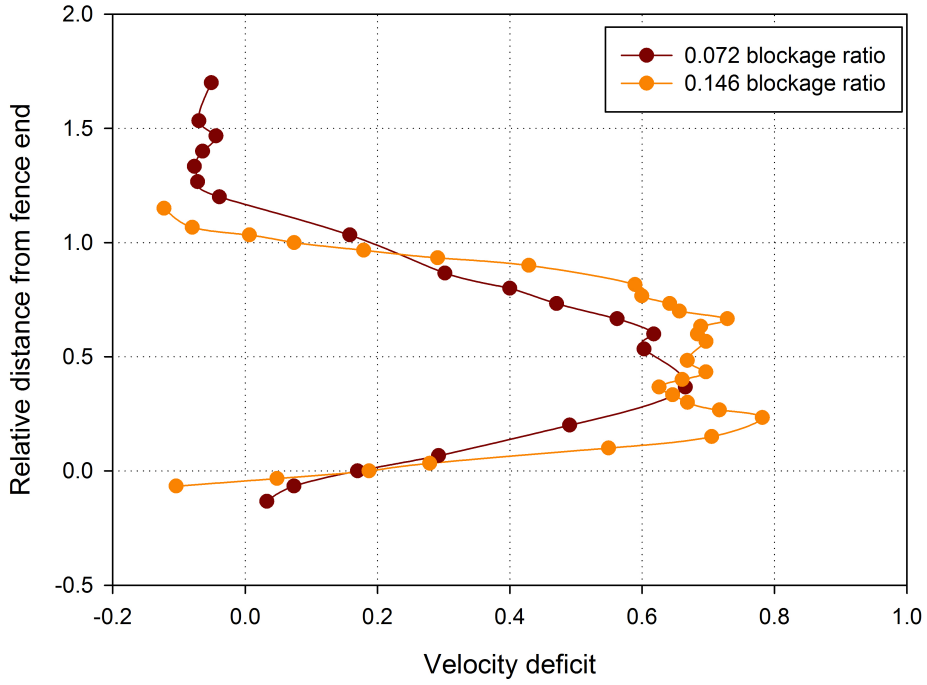

Figure 5.37: Comparison of velocity deficit 5 diameters downstream of 0.072 and 0.146 blockage ratio fences positioned 0.6 diameters from sidewall of flume

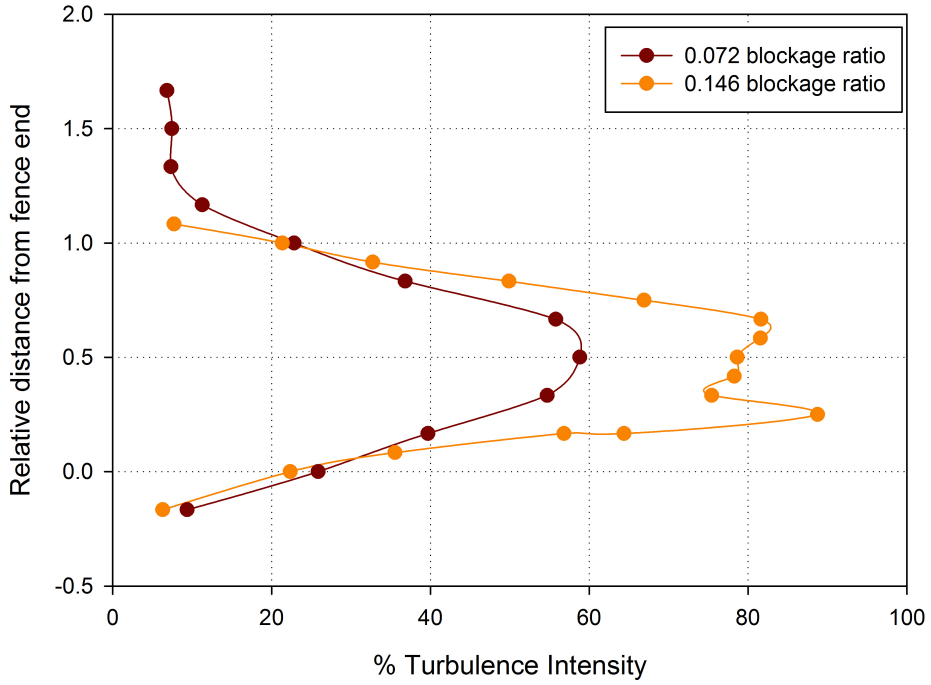

Figure 5.38: Comparison of turbulence intensity 5 diameters downstream of 0.072 and 0.146 blockage ratio fences positioned in centre of flume

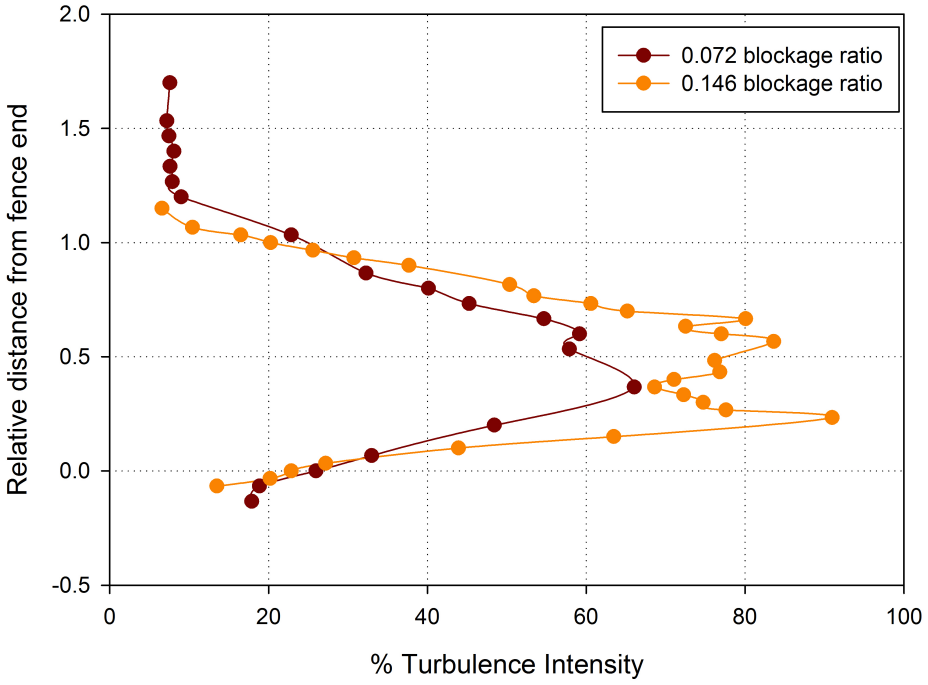

Figure 5.39: Comparison of turbulence intensity 5 diameters downstream of 0.072 and 0.146 blockage ratio fences positioned 0.6 diameters from sidewall of flume

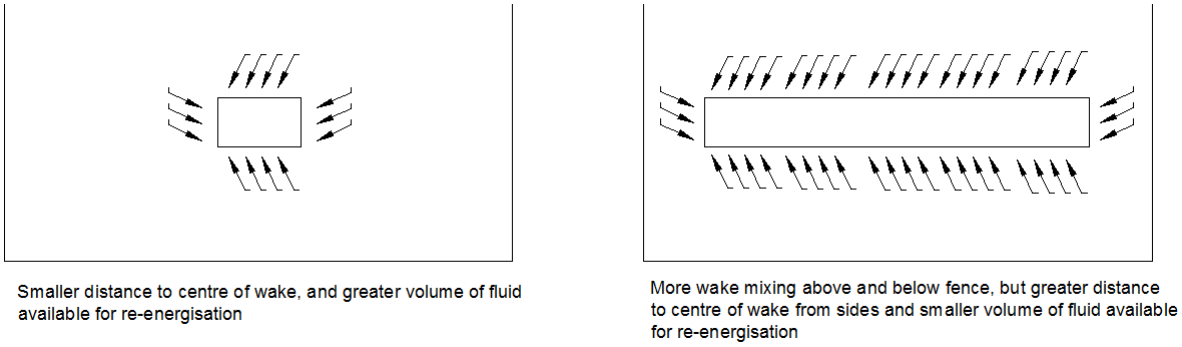

Figure 5.40: Demonstration of differences in wake mixing processes between small and large blockage ratio fences

given by:

$$u_4 = \frac{u_0 - u_3 + \left[\epsilon u_0^2 - 2\epsilon u_0 u_3 + \left(1 - \epsilon + \epsilon^2\right) u_3^2\right]^{\frac{1}{2}}}{1 - \epsilon} \tag{5.2}$$

The assumptions and simplifications made in arriving at these values were:

- The channel in question had a uniform cross sectional area across its entire length.
- The flow velocity upstream of the channel was uniform and had a constant pressure across its width.
- The flow is separated into a streamtube through the turbine or row of turbines with a

Distance from sidewall of bypass measurement	1000mm	450mm
Distance from sidewall of wake measurement	650mm	650mm
U_3	0.093	0.093
Calculated U_4	0.366	0.366
Measured U_4	0.324	0.318
% difference	11.5	13.2

Table 5.6: Results of comparison of measured and theoretical bypass velocity values for 0.072 blockage ratio fence with measurements taken 5 diameters downstream of fence

wake region which has a constant velocity across its width, and two bypass flow regions, with the same bypass flow velocity across their entire width. Both regions also had a constant pressure across their width.

- Pressures upstream and downstream of the turbine or row of turbines was constant across their width.
- Swirling components of the flow were disregarded.

Measured experimental data was entered into the above expression, along with fixed values of upstream flow velocity U_0 and blockage ratio ϵ. The value of upstream flow velocity chosen was 0.326m/s, as calculated in section 4.2. Flow measurements were inserted into the above expression to determine theoretical bypass flow velocities in the following situations:

- A 0.072 blockage ratio fence in the centre of the channel, with flow measurements taken 5 and 9 diameters downstream.
- A 0.146 blockage ratio fence in the centre of the channel with flow measurements taken 9 diameters downstream.

For all of the above scenarios, the wake velocity value used in the theoretical expression was that measured at mid depth in the flow, and also as close as possible to the centre of the wake itself. The resultant theoretical bypass flow velocity was then compared to measured values in the bypass region one either side of the actuator fence. The specific measurement point which theory was compared to was chosen such that it was at centre depth of the flow and as close as possible to the central lateral position of its respective bypass flow region.

The results for 5 diameters downstream of the 0.072 blockage ratio fence are summarised in table 5.6. The results for 9 diameters downstream of the 0.072 blockage ratio fence are summarised in table 5.7, while the results for 5 diameters downstream of the 0.146 blockage ratio fence are summarised in table 5.8.

It is clear that the difference between measured and theoretical values of bypass velocity is dependent on both the distance downstream at which measured values used for comparison are taken and the blockage ratio of the turbines in question. It is argued that this demonstrates that the simplifications made by Garrett and Cummins (2007) mean their theoretical model is unable to predict bypass flow velocities for any tidal turbine array configuration. Looking at the simplifications above, we can firstly see that the uniform flow velocity values

Distance from sidewall of bypass measurement	1035mm	485mm
Distance from sidewall of wake measurement	685mm	685mm
U_3	0.205	0.205
Calculated U_4	0.338	0.338
Measured U_4	0.312	0.309
% difference	7.7	8.6

Table 5.7: Results of comparison of measured and theoretical bypass velocity values for 0.072 blockage ratio fence with measurements taken 9 diameters downstream of fence

Distance from sidewall of bypass measurement	1035mm	285mm
Distance from sidewall of wake measurement	685mm	685mm
U_3	0.096	0.096
Calculated U_4	0.41	0.41
Measured U_4	0.344	0.331
% difference	16	19

Table 5.8: Results of comparison of measured and theoretical bypass velocity values for 0.146 blockage ratio fence with measurements taken 5 diameters downstream of fence

across the channel and in streamtubes, as well as uniform pressures across the turbines, effectively assumes an inviscid flow with no boundary layers or momentum transfer between fluid streamlines. In reality, there is unlikely to be any real tidal site where such an assumption can be valid. The choice of disregarding swirling components of flow is also unlikely to be valid for tidal turbines, mainly due to the swirl effects associated with tip vortices off the turbine blades. Thus the model is not sufficiently capable of estimating exact values for flow velocity in different regions surrounding tidal turbines. As with the other blockage models proposed reviewed in section 2.2.2, the theoretical blockage model of Garrett and Cummins (2007) appears to be most useful in demonstrating the possibility of extracting more power with tidal turbines compared to wind turbines due to the constrained nature of the tidal resource. It has also demonstrated clearly the dependency of power output of turbines on flow velocities in the vicinity of turbines, a conclusion which was one of the main drivers of the work for this thesis.

Chapter 6

Results of analysis of tidal turbine rows in split channels

6.1 Objectives and approach of split channel analysis

The overall objective of the split channel analysis carried out was to examine how influential specific position of rows of turbines and row blockage ratio were on the distribution of volumetric flow rate between sub channels in a split tidal site. Theoretical analysis by Atwater and Lawrence (2010), which was reviewed in section 2.3.2 demonstrated how the distribution of overall flow rate in a split tidal site between sub channels directly affects the potential power which can be extracted by turbines in such a site. It was intended that the results of this analysis would then allow tidal developers interested in split channels to make more informed decisions on where turbines should be placed with respect to flow boundaries, and also on what would be the most efficient and cost effective number of given turbines to install in a site.

The following steps were taken with the aim of fulfilling this objective.

- The values of relevant parameters from the scale channel used in experimentation, such as length of the split mechanism and cross sectional area of both sub channels, were then inserted into the Atwater and Lawrence theoretical model as described in section 3.5. This was to determine the theoretical optimum distribution of volumetric flow rate between both sub channels and the maximum extraction efficiency for the modelled channel.

- Detailed flow velocity measurements were taken throughout a fixed cross sectional area in the split section of the channel domain. The aim of this was to determine the naturally occurring volumetric flow rate distribution between both sub channels with no actuator fences present.

- Actuator fences were then placed in one of the two sub channels in the split channel setup, hereafter referred to as the impeded channel. The position of this fence with respect to the front of the split mechanism was altered, and the flow conditions in the opposite channel, (hereafter referred to as the free channel) were measured. This

process was to examine what if any change in volumetric flow rate distribution occurred with change in fence position.

- The above process was repeated for other blockage ratio fences. Also, for the smallest blockage ratio of 0.146, the lateral position of the fence with respect to impeded channel sidewalls was also examined. This was with the aim of examining what if any changes to flow rate distribution could be attributed to change in lateral position.
- For certain cases where changes in flow rate distribution were found with change in the aforementioned parameters, more detailed flow measurements were carried out to determine the exact % of overall volumetric flow rate in both impeded and free sub channels.
- Detailed flow measurements were also taken for certain cases where multiple fences were placed in the impeded sub channel.
- The choice of the above configurations tested in experimental analysis was made completely independent of the theoretical model of Atwater and Lawrence. The choice of configurations was made purely with the aim of examining quantitatively changes to loads experienced by actuator fences and volumetric flow rate distribution with changes in variables such as specific position and blockage ratio of tidal turbine rows, as per the overall hypothesis of the research in this thesis.
- The results for % flow rate in both channels which were found from detailed flow measurements were compared with the optimum predicted by the theoretical approach suggested by Atwater and Lawrence. As previously mentioned, the values inserted into the model were the modelled scale channel values of the relevant parameters. This was to determine what if any configuration would achieve the theoretical optimum distribution and extraction efficiency, and also to allow some conclusions on the accuracy of the theoretical approach to be made.

More detailed discussion of the approach taken, as well as the results and conclusions of this split channel analysis, can be found in the subsequent sections.

6.2 Application of Atwater and Lawrence theory to set-up in Chilworth flume

When a channel is divided into sub channels, the installation of turbines in one will have an effect on the volumetric flow rate in the other. This is a simple consequence of the continuity principle. If flow in any one part of a system is blocked by any obstruction (in this case tidal turbines), it must be redirected to other areas of the system to maintain the overall mass flow rate. If an insufficient number of turbines were installed in the impeded channel in future, the maximum amount of power would not be extracted. Conversely, if too many turbines were installed, too much flow would be blocked to the impeded channel and the amount of power extracted would be below the maximum available. The theory developed by Atwater

and Lawrence (2010) can be used to calculate the optimum difference in volumetric flow rate between a free and impeded channel, based on the value of parameters such as hydraulic radius and cross sectional area. When the authors applied their model to Current Passage, Johnstone Strait, Canada, they concluded a maximum extraction efficiency of 5.7%, which could be achieved when the distribution of volumetric flow rate was 27% of the total in the impeded channel and 73% in the free channel. However what if any effect both specific position and blockage ratio of tidal turbines in their respective channel had on this imbalance in volumetric flow rate was beyond the scope of this study.

To examine whether any combination of these factors would result in the optimum imbalance being achieved, it was first necessary to apply the model to the split mechanism constructed in the Chilworth channel. Figure 6.1 gives a graphical description of the set-up. In this analysis, the inlet and outlet of the flume were assumed to be the open oceans of the Atwater and Lawrence model. The justification for this assumption is that as with the oceans in the analytical model, these sections do not affect the overall dynamics of the split mechanism. The channel had the following characteristics applicable to the theory:

- L_u= 8.5m
- L_i= L_f= 4m
- L_d= 8.5m
- A_u= $0.411m^2$
- A_i=A_f= $0.20325m^2$
- A_d= $0.411m^2$
- R_{hu}=R_{hd}= 0.2086m
- R_{hi}=R_{hf}= 0.1288m
- Inserting these values into the following equation gave the head loss coefficient for each respective section of the channel:

$$q = \frac{fL}{2R_h g A^2} \tag{6.1}$$

Thereby giving the following q/f values for the various section of split channel setup:

- q_u= 12.29
- q_i= 31.02
- q_d= 12.29
- q_f= 31.02

As with the Atwater and Lawrence model, the bottom roughness coefficient f was assumed constant throughout the domain. This can be justified by examining the changes in the compounds Manning's n between different sections of the channel. As demonstrated in section

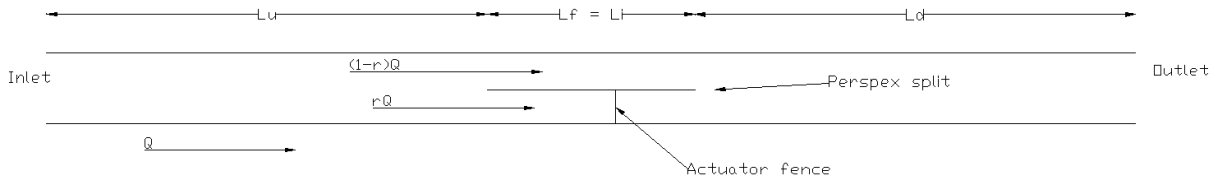

Figure 6.1: Graphical description of set-up for Chilworth split channel experiments

5.2, the regular open channel has a compound Manning's n of 0.0152. When the compound Manning's n calculations of appendix B were applied to each individual sub channel in the split mechanism, a value of 0.014 was found. A difference between these values of 7.9% was considered sufficiently small such as to ensure constant bottom roughness coefficient throughout the flow domain in the Chilworth flume was a reasonable assumption to make.

The theoretical head losses calculated throughout each section of the domain were then used to estimate the values for β and γ.

$$\beta = \frac{q_I}{q_f} \tag{6.2}$$

$$\gamma = \frac{q_u + q_d}{q_f} \tag{6.3}$$

It was found for the Chilworth channel that $\beta = 1$ and $\gamma = 0.793$. Then assuming a number of values for α, given by:

$$\alpha = \frac{q_T}{q_f} \tag{6.4}$$

and inserting the calculated values for β and γ into the following expressions:

$$\eta = \frac{P_{extracted}}{P_{available}} = \frac{\alpha\left(1+\sqrt{\alpha+\beta}\right)^{-3}}{\gamma+\left(1+\sqrt{\beta}\right)^{-2}\beta}\left(\frac{Q}{Q_o}\right)^{-3} \tag{6.5}$$

$$\frac{Q}{Q_o} = \sqrt{\frac{\gamma+\left(1+\sqrt{\beta}\right)^{-2}\beta}{\gamma+\left(1+\sqrt{\alpha+\beta}\right)^{-2}(\alpha+\beta)}} \tag{6.6}$$

$$r = \frac{1}{1+\sqrt{\alpha+\beta}} \tag{6.7}$$

it was possible to determine a graph of r (fraction of overall volumetric flow rate through impeded channel) against extraction efficiency η. This figure is displayed in figure 6.2. This curve is very similar to the curve for Johnstone Strait shown in section 2.5.10. It demonstrates that for the particular channel set-up in the Chilworth flume, the maximum extraction efficiency is 8.44%, which could be achieved when 30% of the volumetric flow rate was directed through the impeded channel and the remaining 70% through the free channel. Figure 6.2 clearly demonstrates the transition between insufficient and excessive blockage ratio. r values from 0.5 to 0.31 show how the number of turbines installed in the impeded channel is insufficient and therefore the maximum amount of power is not being extracted. From r

values of 0.29 onwards, too much of the flow is being blocked by turbines and so there is an insufficient volumetric flow rate in the impeded channel to allow maximum power output. It is at a value for r of 0.3 that the optimum balance between sufficient number of turbines installed and as little diversion as possible of flow into free channels was met.

6.3 Examination of natural distribution in volumetric flow rate

The first requirement for the split channel analysis was to examine the natural imbalance in volumetric flow rate between the two sub channels in the experimental set-up. The application of the Atwater and Lawrence model to the Chilworth flume split channel set-up (presented in the previous section) assumed equal cross sectional area and hydraulic radius in each channel with no turbines present in the system. Therefore the ideal volumetric flow rate distribution was 50% into each channel. Every effort was made to ensure the experimental set-up would have both sub channels in the split channel mechanism with an equal cross sectional area.

The method of examining the volumetric flow rate in the split channel set-up was very similar to that used in section 4, and is displayed in figure 6.3. Flow velocity was measured at a number of lateral positions and throughout the depth of the flow, and each velocity reading was considered to have been taken at the centre of an elemental area. The volumetric flow rate through each element was then summed to give the total volumetric flow rate in the sub channel.

The initial analysis gave an estimate for total volumetric flow rate through the system of approximately $0.12\frac{m^3}{s}$. Of this total, 52% was distributed through the channel into which actuator fences were subsequently placed, and 48% through the free sub channel. Although falling slightly short of the ideal distribution, 52:48 was considered as close as practically achievable within the limits of experimental error.

A source of error inherent in the method used is the assumption of a constant flow velocity over each individual elemental area. Within each elemental area, there will be variation in flow velocity across it, both laterally and vertically. This source of error is likely to be more appreciable with elements located close to boundary layers at the sidewalls and near the bed of the flume. Despite this, this method was still considered the most practical option available for measuring flow rate, with this inherent experimental error described considered acceptable. Other possible methods of measuring volumetric flow rat included installing crump or broad crested weirs, notches or using some material to create a throated flume. However these would have required additional machining and installation, both of which were judged to be very time intensive. Also, these methods would not be without sources of error themselves, and it was not believed these methods would give estimates which were so much more accurate than the method used as to justify the expense and time required to manufacture and install them.

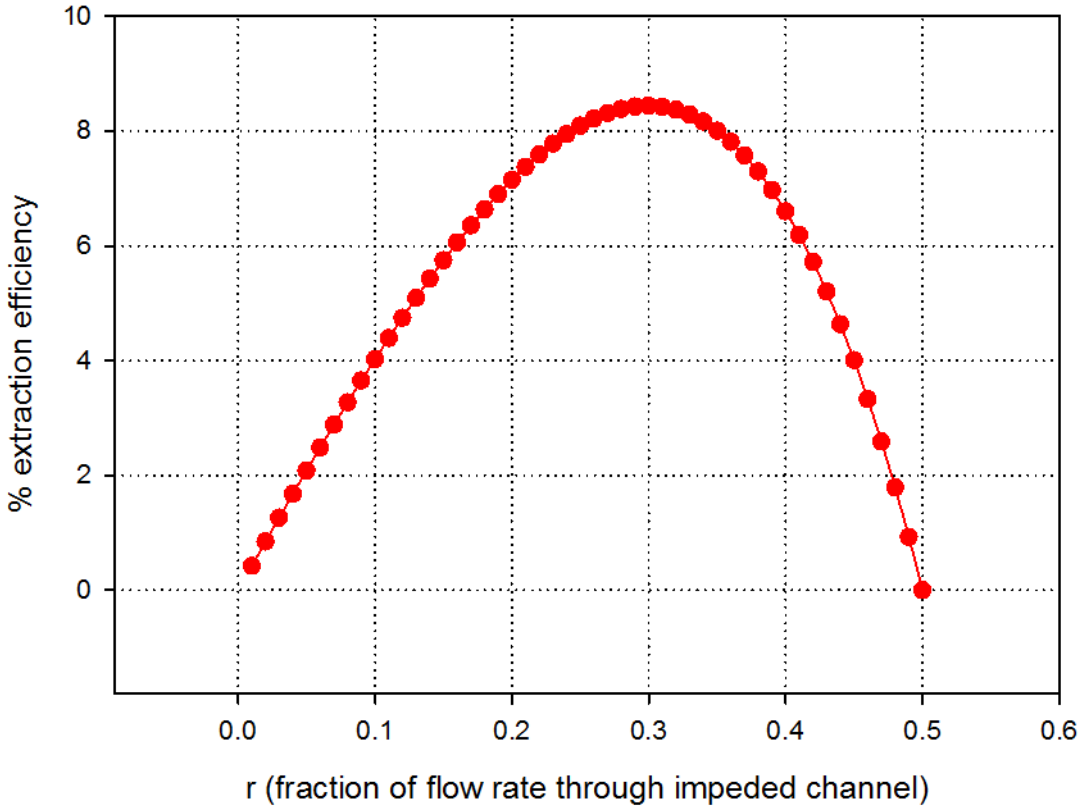

Figure 6.2: Curve of r vs % extraction efficiency of Chilworth channel

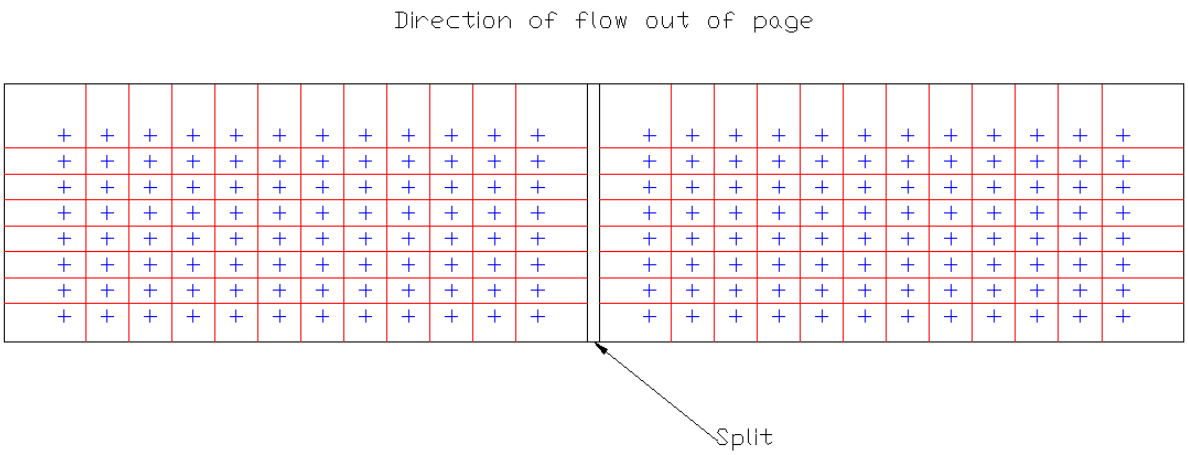

Figure 6.3: Examination of natural imbalance in volumetric flow rate between sub channels in split channel set-up.

6.4 Correction to values for cross sectional area and hydraulic radius

It was decided that this error required a correction to the application of Atwater and Lawrence theory to the experimental setup. It was decided the most appropriate method of doing this would be to correct the values for cross sectional area and hydraulic radius of both sub

channels inserted into the Atwater and Lawrence model. These were replaced with corrected values for channel dimensions which would give a natural flow distribution of 52:48 between the impeded and free sub channels respectively.

The volumetric flow rate was estimated using the aforementioned elemental area method to be $0.12m^3/s$. Over an area of $0.411m^2$, this gives an average flow velocity of 0.292m/s. This was assumed to be the average cross sectional velocity in both sub channels also. The cross sectional areas of both sub channels were amended such as to ensure 52% of the total flow rate ($0.0627m^3/s$) was diverted through the impeded channel, and the remaining 48% ($0.0577m^3/s$) through the free sub channel. The corrected impeded channel area values, and also corrected values for other flow parameters used in equations 6.1 to 2.119 are as follows:

- Impeded channel area = $0.2139m^2$
- Impeded channel width = 0.7056m.
- Impeded channel wetted perimeter = 1.3056m.
- Impeded channel hydraulic radius = 0.1639m.

Similarly for the free sub channel:

- Impeded channel area = $0.197m^2$
- Impeded channel width = 0.649m.
- Impeded channel wetted perimeter = 1.249m.
- Impeded channel hydraulic radius = 0.1577m.

The calculations for correcting these values are outlined in detail in appendix E.

After these corrected values were inserted into equations 6.1 to 2.119, they gave values for $\beta = 0.817$ and $\gamma = 0.73$ (as opposed to $\beta = 1$ and $\gamma = 0.793$ without correction). A split tidal channel setup with these new values for impeded and free channel cross sectional area had a maximum extraction efficiency of 9.04%, achieved with a ratio of volumetric flow rate between impeded and free sub channel of 32:68 (as opposed to 30:70 without correction.). In subsequent analysis, results of flow imbalances are compared to this 32:68 imbalance to examine what if any scenarios achieve this optimum.

6.5 Examination of centre line velocity and thrust coefficient with changes in actuator fence longitudinal position

An initial examination of changes in volumetric flow rate with fence position is displayed graphically in figures 6.4 and 6.5. The split mechanism was a total of 4m (40 actuator fence diameters) long. Both sub channels were approximately 677.5mm (6.77 diameters) wide, and the flow depth was 300mm (3 diameters). A 600mm (6 diameter) wide actuator fence was placed in one sub channel, and was 100mm (1 diameter) deep and placed at the centre depth. This meant that in its respective sub channel, the actuator fence occupied 89% of the width

and 33% of the depth of the channel, hence a total blockage ratio of 0.295. The porosity of the fence was 0.34.

In the impeded sub channel, the fence was placed at four longitudinal positions with respect to the front of the split, 0, 20, 30 and 40 diameters, as shown in figure 6.4. When the fence was placed at each of these points, the ADV recorded velocity measurements in the free unimpeded sub channel. A total of 12 points laterally across the flume at centre depth were recorded. In each case, the stream-wise position of the ADV was 2m from the front of the split mechanism, representing the halfway point along the length of the split in the downstream direction. The purpose of this was to give an initial indication of what changes to the amount of flow diverted into the free sub channel might take place due to change in the position of the tidal array with respect to the front of the split. The results of this particular initial analysis are shown in figure 6.6. The Y axis shows the distance between each particular recorded velocity point and the wall of the split in the free sub channel. As no flow velocity data was recorded in the impeded channel, only the extents of the free channel on the Y axis is shown. This is to avoid any empty spaces in the bottom of the plot which would occur if the entire channel width was included, and to ensure clear trends in flow behaviour can be observed. Ambient conditions are also included.

It was anticipated that boundary layer development laterally across the free channel would be quite different from the boundary layer development off the sidewall of the flume, as shown in figure 3.24. This was because it was anticipated that a combination of a sharp edge at both the front and rear of the split would result in boundary layer separation further downstream. Boundary layer separation is explained by Anderson [2005, pp219 - 221]. At the front of the split, flow is brought to zero velocity at the front edge of the split. From here on, a boundary layer develops normally along the full length of the perspex wall, and velocity gradually increases and hence static pressure decreases. However as flow travels towards the rear of the wall, velocity begins to decrease, and pressure increases, due to another stagnation point at the rear edge of the perspex wall. This results in an adverse pressure gradient, where the imbalance in forces between the high pressure rear edge of the wall and the lower static pressure further upstream in the boundary layer causes retarding

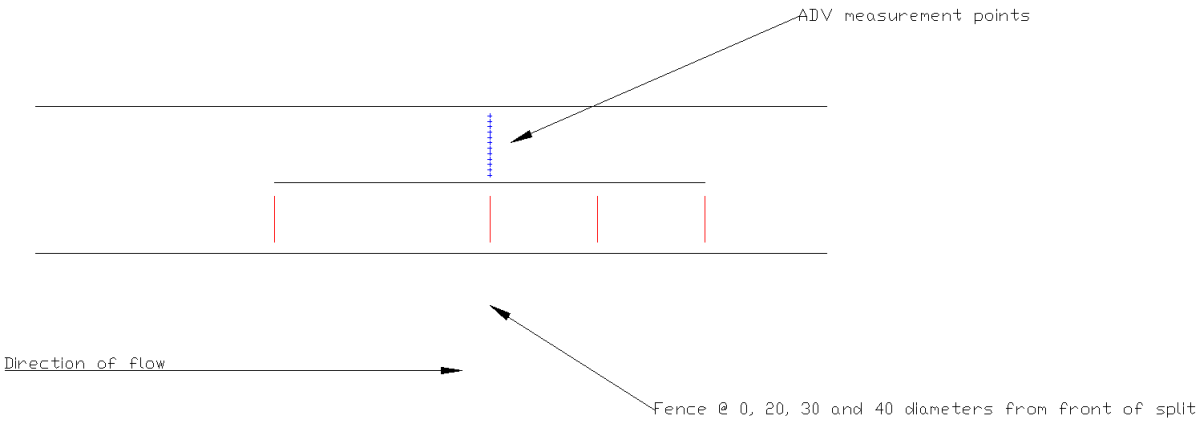

Figure 6.4: Plan view of fence positions and flow measurement points for initial flow distribution analysis

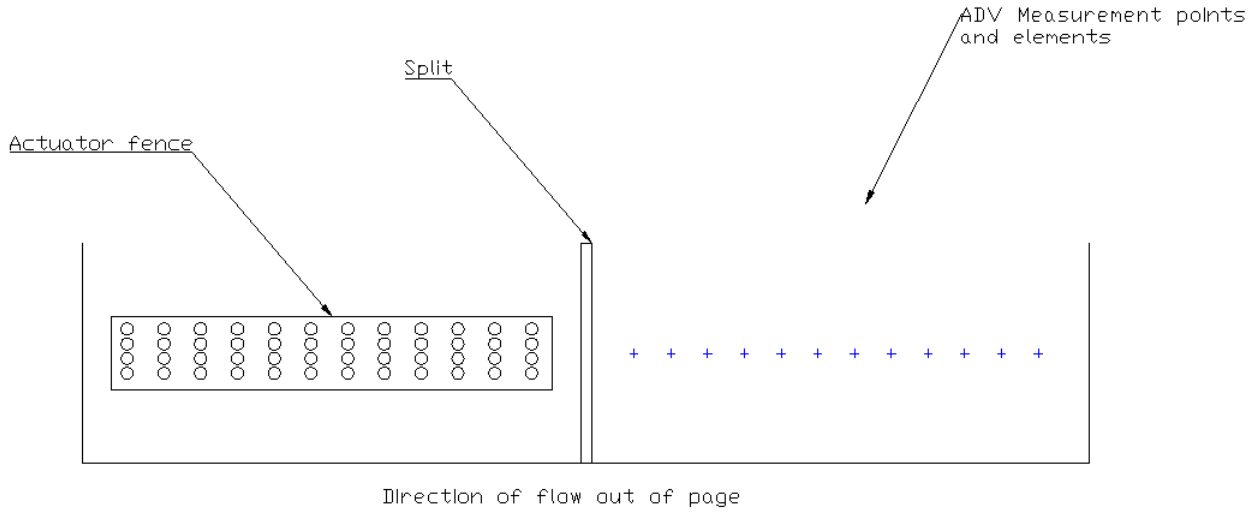

Figure 6.5: Elevation view of fence and flow measurement points for initial flow distribution analysis

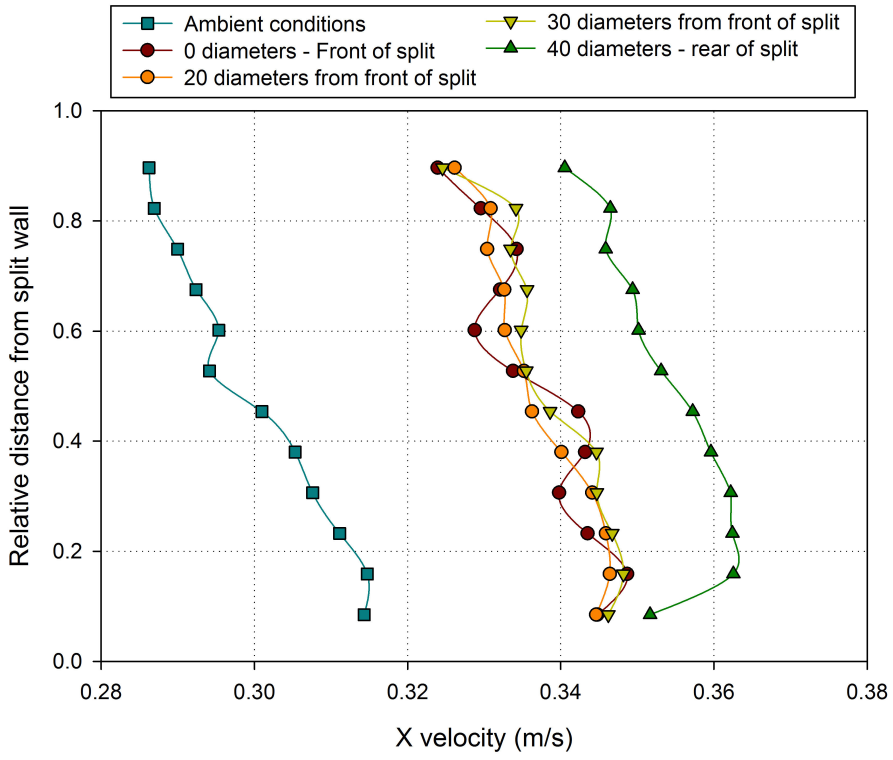

Figure 6.6: Velocity profiles across free sub channel with different actuator fence positions in impeded channel

forces to act on the boundary layer. If sufficiently strong enough, these retarding forces can cause the boundary layer to separate off the perspex wall. This can result in the formation of a strong wake region filled with von Karmen vortices.

The results for the case of ambient flow in figure 6.6 give clear evidence for the flow separation effects which were anticipated. The slower flow velocity towards the centre of

the free sub channel give clear evidence of the effect of retarding forces caused by adverse pressure gradients from the rear edge of the perspex wall. It is also interesting to note that this phenomenon appears to occur consistently across all scenarios with an actuator fence placed in the impeded channel. This demonstrates that increasing the volumetric flow rate in the channel does not cause this flow separation effect to be alleviated.

It is also evident that the increase in volumetric flow rate through the channel due to the presence of the actuator fence in the impeded channel is quite substantial. Comparing the 0 diameter measurements with the ambient measurements, the results show that each particular point has increased in velocity quite substantially. Also, the velocity profiles show that this increase compared to ambient conditions does not appear to change between fences positioned between 0 and 30 diameters, or between 0% and 75% of the distance from the front to the rear of the split. But when the fence was placed at the rear of the split, results suggest the amount of flow diverted into the free sub channel is larger compared to the other 3 examined cases.

Because of the large changes in the flow regime between the 30 and 40 diameter fence positions, it was decided positions within this range should be examined. This would give a greater indication of the precise point at which the amount of flow diverted increased, and whether or not it was a gradual or sudden increase. Additional examination of the exact same ADV measurement points in the free channel was carried out for fence positions in the impeded sub channel of 32, 33, 35, 37 and 39 diameters from the front of the split. The results

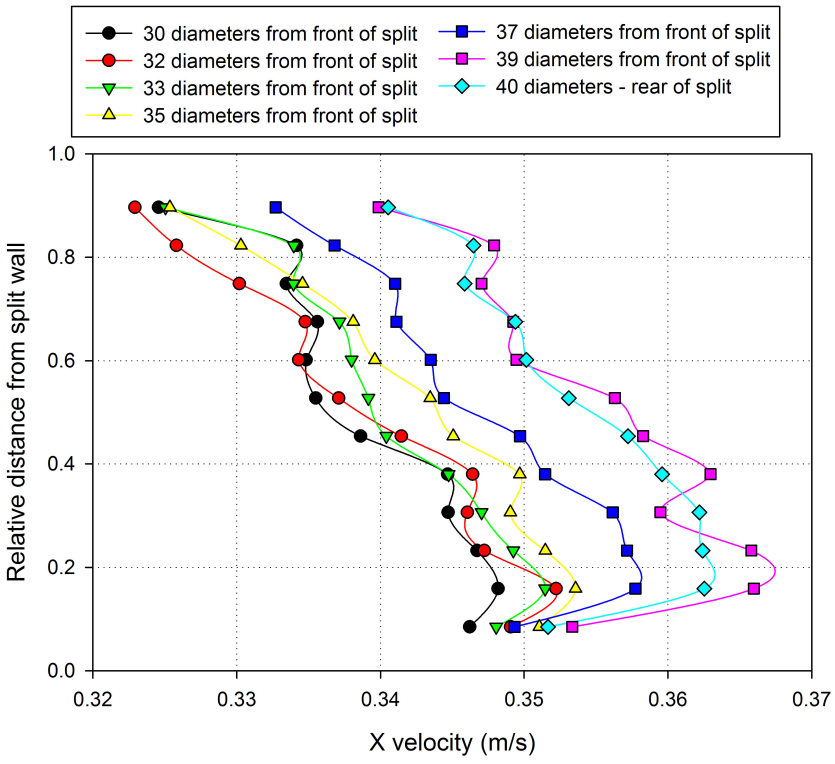

Figure 6.7: Velocity profiles across free sub channel with actuator fence positioned between 30 and 41 diameters from front of split in impeded channel

of this analysis are displayed in figure 6.7. The results appear to show that the increase in flow diversion between fence positions of 30 and 40 diameters from the front of the split is quite gradual from 30 diameters onwards, before achieving a maximum at the rear of the split.

As well as flow velocity changes, changes in thrust coefficient were also examined in this analysis. The method used for measuring thrust and calculating thrust coefficient was exactly as that used in section 5.2. The velocity used in the thrust coefficient calculation was determined by examining the natural flow regime in the flume without actuator fences present. Flow velocity was measured at the centre depth, and at severally points laterally along the width of the channel, for each stream-wise position at which the actuator fence was positioned. Measurements were then used to calculate the average cross sectional velocity at each fence position, and this value was inserted into the thrust coefficient equation along with the thrust forces measured by the load cell. The results of this analysis can be seen in figure 6.8 and table 6.1. This figure clearly shows the correlation between volumetric flow rate in the impeded channel and thrust on the actuator fence. The thrust coefficient is constant up to 3m from the front of the split. However as the fence is positioned further downstream, the reduction in volumetric flow rate causes a corresponding reduction in thrust on the fence.

This shows that longitudinal position of a tidal array with respect to the front of a split mechanism does appear to be a parameter which requires consideration in split tidal channel projects. Before discussing the possible reasons for these particular experimental results, an examination of lateral position is presented in the next section. It will be seen that the results

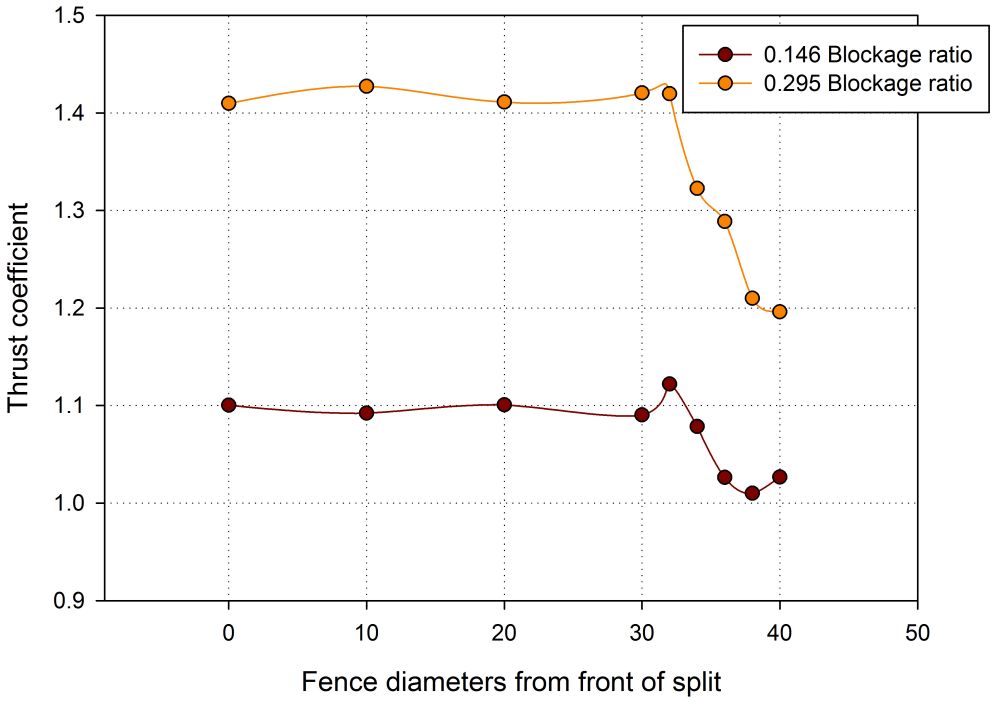

Figure 6.8: Changes to thrust coefficient with actuator fence position in impeded sub channel of split tidal set-up

Diameters from front of split	Thrust coefficient
0	1.41
10	1.43
20	1.41
30	1.42
32	1.42
34	1.32
36	1.29
38	1.21
40	1.2

Table 6.1: Thrust coefficient values for 0.295 blockage ratio fence at varying positions from front of split

of this analysis give a greater insight into why the imbalance in volumetric flow rate changes with change in actuator fence position.

6.6 Examination of centre line velocity and thrust coefficient with changes in actuator fence lateral position

For smaller tidal arrays occupying only a fraction of the width of their respective sub channel, lateral position with respect to the walls of the channel is another variable parameter. How lateral position affects volumetric flow rate in both sub channels is also another question which the reviewed literature did not examine, and to the author's knowledge, currently developed analytical theory is unable to answer this research question.

A 0.146 blockage ratio fence was used for this analysis. This fence was 300mm wide, meaning its width was less than 50% of the 670mm width of the impeded sub channel. It was placed at three lateral positions across the width of the channel which are shown in figures 6.9. This process was carried out at 0 and 40 diameters from the front of the split, the front and rear respectively. As with the examination of longitudinal position, an initial analysis was carried out by examining flow velocity at points in the free sub channel at centre depth and 2m downstream of the front of the split. This was to give an initial indication of changes in the imbalance in volumetric flow rate between the sub channels.

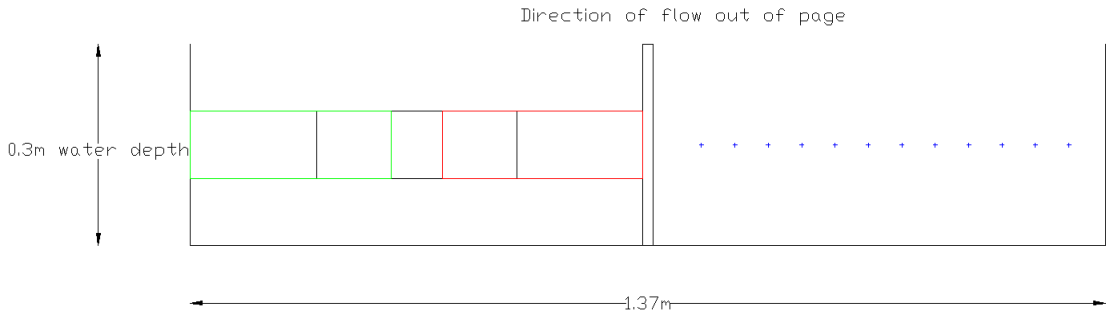

Figure 6.9: Lateral positions of actuator fence and velocity measurement points for examination of changes in volumetric flow rate distribution with changes in lateral position of array.

The results of this analysis can be seen in figure 6.10. Once again ambient conditions have been included for comparison. At 5 of the 6 fence positions, the increase in the flow velocity at the fixed points in the free channel is constant. It is only when the actuator fence is placed right against the wall of the split that a change in the flow velocity is observed. As with the longitudinal position analysis, thrust coefficient was also examined in this analysis, with the results shown in table 6.2. The two sets of results, both volumetric flow rate imbalances and thrust coefficients, also contain one apparent contradiction. Examining firstly the 40 diameter right of centre position, a lower thrust coefficient is observed compared to upstream. As with the longitudinal position analysis in the previous section, this can simply be explained by a smaller volumetric flow rate in the impeded channel at this position. However at the two other lateral positions 40 diameters downstream, a decrease in thrust coefficient compared to upstream conditions occurs, but without a corresponding change in the amount of flow diverted between the free and impeded sub channel.

All of the experimental split channel analysis to date has left the following questions:

- Why is there a gradual change in the amount of flow diverted between sub channels and thrust coefficient on actuator fences as the fence is moved between 30 and 40 diameters downstream of the front of the split mechanism?
- At the rear of the split mechanism, why is there a reduction in thrust coefficient in some lateral positions without any corresponding change in volumetric flow rate distribution between sub channels, as demonstrated by results presented in figure 6.10 and table 6.2.

It is postulated that the observed experimental results are a consequence of both actuator disc theory and Newton's third law.

When fluid passes through the actuator fence, it experiences a change in momentum, and the rate of change of momentum in turn gives the magnitude of the force the fluid exerts on the actuator fence. Newton's third law dictates that the actuator fence must simultaneously apply a force of equal magnitude and opposite direction on the fluid. Some analytical expressions to show how this fundamental physics applies to actuator discs was presented by Burton et al. [2001, pp. 41-46] and was also presented in section 2.5.4. However in the blocked channel case, theory was developed by Garrett and Cummins (2007) which showed thrust on actuator fences to be a function of both wake and bypass velocity values. This theory was presented in section 2.5.5.

In the context of this work on split tidal channels, $(U_4 - U_3)$ is the most important term in the above equations. It is the numerical difference between the bypass velocity of flow surrounding the fence (U_4) and the flow velocity at any arbitrary point in the downstream wake of the fence (U_3). In a normal open tidal channel, the U_3 value at any point in the wake is dictated entirely by wake mixing between the wake fluid streamlines and flow which has bypassed the fence. There is only one source of fast moving fluid surrounding the wake whose faster moving fluid streamlines mix and interact with streamlines in the wake, thereby eventually allowing the entire cross section of the channel to return to the same flow conditions as the undisturbed flow upstream of the actuator fence. When the fence is positioned towards

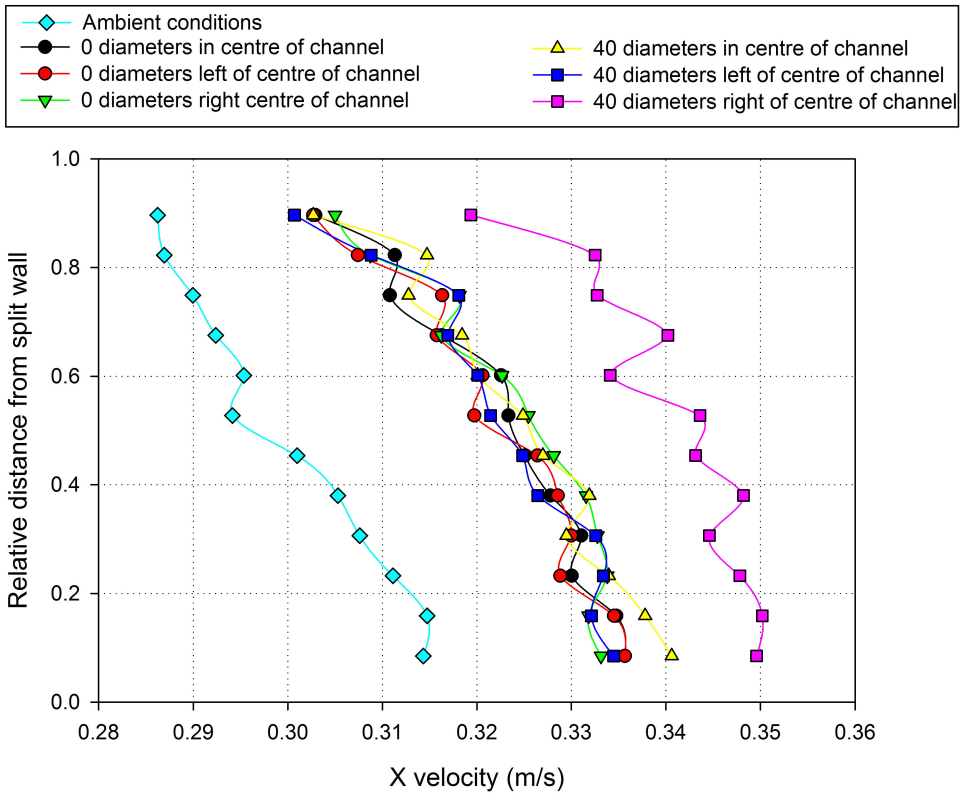

Figure 6.10: Velocity profiles in free sub channel for different actuator fence lateral positions

Fence position	Thrust coefficient
0 diameters left of centre	1.09
0 diameters centre	1.09
0 diameters right of centre	1.09
20 diameters left of centre	1.1
20 diameters centre	1.1
20 diameters right of centre	1.1
40 diameters left of centre	1.03
40 diameters centre	1.03
40 diameters right of centre	0.96

Table 6.2: Thrust coefficient readings for each longitudinal and lateral position of 0.146 blockage ratio fence

the front of the split, wake recovery occurs entirely because of momentum transfer between slow moving flow in the wake and the fast moving bypass flow accelerated around the sides. Therefore the wake recovery process is the very same as in an open channel. Results would suggest that this is the case for fence positions of between 0 and 30 diameters from the front of the split. However as the fence is moved further to the rear of the split mechanism, it is postulated that the fast moving flow, which has bypassed the impeded channel entirely by flowing into the unimpeded sub channel, begins to interact with the wake of the fence as it moves back into the open section of the channel downstream of the end of the split mechanism. Therefore in the experimental analysis, from 30 to about 37 diameters, the wake

is not only re-energised by the flow bypassing around the sides of the fence in the impeded channel, but also by the fast moving flow coming out of the free channel. The fast moving free channel flow therefore acts as a sort of external source of re-energisation for the actuator fence wake. Wake expansion will be considerably reduced. As explained by Burton et al. (2001, p66), wake expansion normally occurs because of flow separation at the edge of the actuator fence. Viscosity dissipates the kinetic energy of flow just around the edge of the fence, and a boundary layer around the edge develops. The flow in this boundary layer does not have sufficient kinetic energy to flow around the fence edge, and so it separates and continues in the stream-wise direction. However in the case of the rear of the split channel, the kinetic energy required to flow around the fence edge, and hence reduce wake expansion, will be provided by momentum transfer from bypass flow from the free channel to flow which has separated from the fence edge.

This is explained graphically in figure 6.11. If the wakes of tidal arrays towards the front and rear of the split are compared, this sudden extra re-energisation of the wake will mean considerable numerical differences in the $(U_4 - U_3)$ term between both. If both U_4 and U_3 are chosen at fixed distances downstream of the fence in both cases, it is clear that the value of $(U_4 - U_3)$ will be much smaller towards the rear of the split channel. U_4will remain constant, but U_3 will be larger due to the transfer of momentum to the wake, not only from flow bypassing the actuator fence, but also from fast moving bypass flow streamlines coming out of the free sub channel, and consequent quicker wake recovery. Looking again at equation 2.5.5, it can be seen that this smaller value of $(U_4 - U_3)$ will mean that the force exerted by the tidal array on the fluid will be smaller. By Newton's third law, this means that the equal and opposite force exerted by the fluid on the fence must also be smaller. The only way this can be done is with a reduction in the mass flow rate inflow to the actuator fence. Therefore the mass flow rate in the impeded channel where a fence is present must reduce, ultimately to ensure Newton's third law is obeyed and the new forces exerted by the fluid and actuator

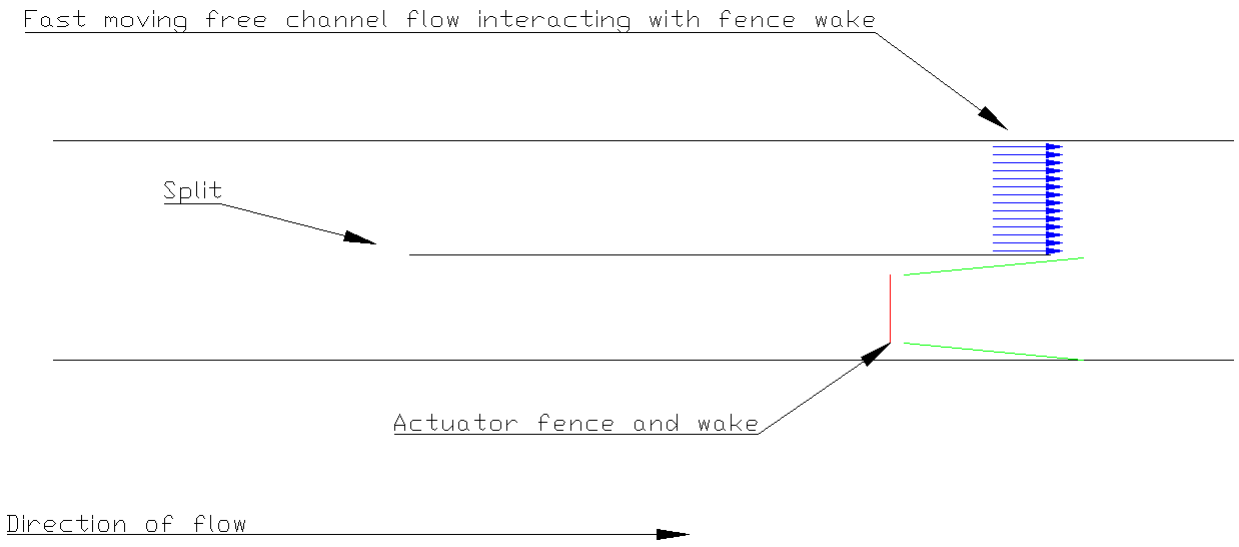

Figure 6.11: Interaction of fast moving free channel flow and actuator fence wake towards rear of split mechanism

fence are equal and opposite. If the mass flow in the impeded channel is reduced, the mass flow rate in the free channel must simultaneously increase to obey conservation of mass and the continuity principle.

It is argued that this postulation can explain both the experimental observations when the longitudinal and lateral position of the actuator fence are altered. Consider firstly changes in longitudinal position and fixed points upstream and downstream of the actuator fences from which to take U_4 and U_3 respectively. As the fence is positioned further towards the rear (and to the fast moving freestream flow), the value of U_3, and hence the value of $(U_4 - U_3)$ will gradually drop due to more re-energisation of the wake by fast moving free channel flow. According to the above postulation, this gradual change in $(U_4 - U_3)$ should be accompanied by a gradual decrease in mass flow rate in the impeded channel. This is exactly what was observed in experiments, and demonstrated by results presented in figures 6.6 and 6.7. There should also be a decrease in the thrust coefficient on the fence due to smaller mass flow rate and smaller equal and opposite forces exerted by the fence and the fluid flow. This was again observed and demonstrated by results in figure 6.1.

Now consider the case of lateral position changes. For fence positions at the very front of the split, and also at 20 diameters downstream of the front, it was observed that there were no changes to volumetric flow rate distribution or thrust coefficient. This is simply because at these positions, wake mixing is dictated by bypass flow around the fence edges, and there is no interaction between the fence wake and fast moving free channel flow. However when the lateral position of the fence is changed at the rear of the split mechanism, the experimental observations are as follows:

- When the fence was positioned against the outer channel wall and also in the middle of the channel, a drop in thrust coefficient compared to upstream was observed. However no change in volumetric flow rate in the impeded channel was observed.
- When the fence was positioned against the split mechanism wall, an even larger decrease in thrust coefficient compared to upstream was observed. There was also an increase in volumetric flow rate in the free channel and a decrease in the impeded channel.

It is argued that this particular set of results gives the greatest support to the postulation put forward. This can be explained with the aid of figure 6.12. When the fence is positioned against the split wall, the wake of the fence is directly adjacent to the fast moving flow coming out of the free channel. This leads to significant wake re-energisation, causing the same dramatic reduction in thrust and impeded channel volumetric flow rate as occurred with changing the longitudinal position of large fences. Some wake re-energisation will also occur at the other lateral positions, but it will not be as dramatic due to the larger lateral distance between fast moving free channel flow and the fence wake. Therefore although there will be a change in the values of U_4 and U_3, the change in the numerical difference between them may not be large enough to warrant an appreciable change in the mass flow rate to the impeded channel. This would explain why there is a difference between the thrust values at lateral positions at the rear of the split, and also why mass flow rate distribution only changes when the fence is such that its wake is directly adjacent to fast moving free channel

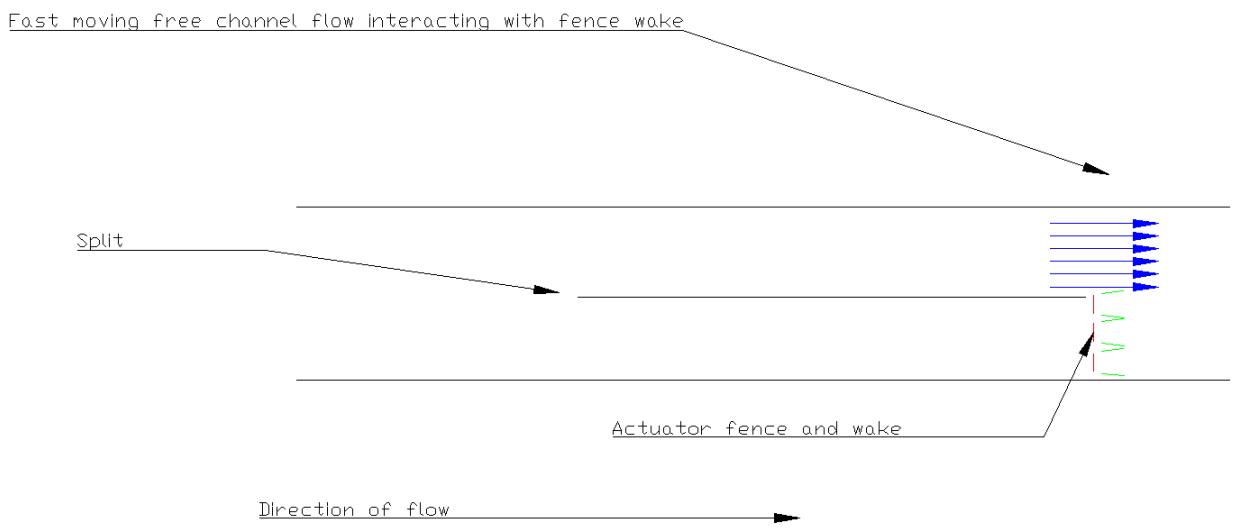

Figure 6.12: Interaction of fast moving free channel flow and actuator fence wake towards rear of split mechanism with changes in fence lateral position

flow.

This analysis has suggested a very significant difference in the behaviour of actuator fence wakes between open and split channels. It has also given strong evidence to support the claim that specific position with respect to flow boundaries plays a big role in determining how much flow is diverted between sub channels in a split tidal site. For tidal developers, this is a very interesting observation, and one which could not have been predicted or observed with the analytical models or site specific numerical models reviewed in chapter 2. The analytical models reviewed examine changes in flow regime in split tidal channels by examining changes to fluid momentum in certain channels which are assumed to occur due to tidal turbines being present. However in these models, increased or decreased power extraction is assumed to be the only parameter affecting momentum changes in an impeded channel, with no consideration to whether changing a row of turbines proximity to natural channel boundaries may affect change in momentum for a given number of turbines with a given blockage ratio. As for the numerical models, changing the position of turbines in a split channel was simply beyond the scope of their investigation. With this in mind, it is now worth using experimental data to examine the limits of one particular analytical model further.

6.7 Testing of Atwater and Lawrence analytical model

The experimental results presented so far have demonstrated that the specific position of a tidal array in a split tidal channel is a parameter which requires consideration in any given tidal array project in a site. The next step in this split channel analysis was to examine more closely how distribution in volumetric flow rate changed with both position and also blockage ratio. The main reason for this analysis was to examine whether any specific arrangement led to the theoretical optimised distribution predicted by the application of the Atwater and Lawrence analytical model. This would also give a greater indication of the applicability of the model itself and the power estimates for split tidal channels predicted by it.

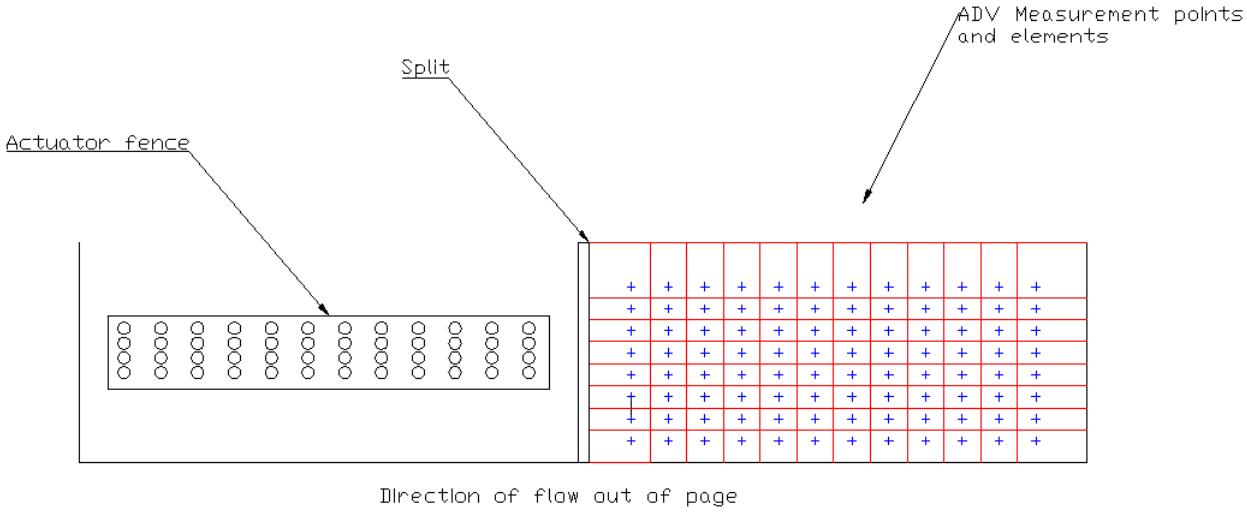

Figure 6.13: Examination of volumetric flow rate in free sub channel of split channel set-up

When corrected for experimental error (as mentioned in section 6.4 and outlined in appendix F), this ideal distribution is 32:68. It is against this distribution between impeded and free channel that the Atwater and Lawrence model is tested against. The total volumetric flow rate through the system for this set of experiments was estimated in section 6.3 as $0.12m^3/s$. The method by which the volumetric flow rate for each case of an actuator fence in the impeded channel is displayed in figure 6.13, and is similar to the method used to examine the natural imbalance in section 6.2. When the approximate volumetric flow rate for the free channel was determined, this value was compared to the overall flow rate of $0.12m^3/s$ to determine what percentage of volumetric flow rate was distributed between the impeded and free sub channels. The following scenarios were initially examined:

- Fences of blockage ratio 0.295, 0.244 and 0.195, all positioned laterally in the centre of the channel, and at distances downstream of the front of the split of 30 and 40 diameters. These two longitudinal positions were examined due to the clear difference in flow rate distribution between them shown in results in section 6.5 and figure 6.6.
- Fences of blockage ratio 0.146 at the rear, but at lateral positions of the centre of the channel and against the right wall of the channel. Examination of both of these positions was due to results presented in section 6.6 and figure 6.10.
- Thrust coefficient values for each of these cases were also recorded.

These positions are explained graphically in figures 6.14 and 6.15, while the results of this analysis are summarised in table 6.3. As with the largest blockage ratio of 0.295, ratios of 0.244 and 0.195 also show more flow diversion into the free channel when the fence is positioned to the rear of the split, and a corresponding decrease in fence thrust coefficient. Similar results can also be seen for the changes in lateral position with the smallest 0.146 blockage ratio fence.

So far results have shown that even the largest sized actuator fences do not achieve the optimum imbalance in volumetric flow rate between sub channels. Therefore, the blockage

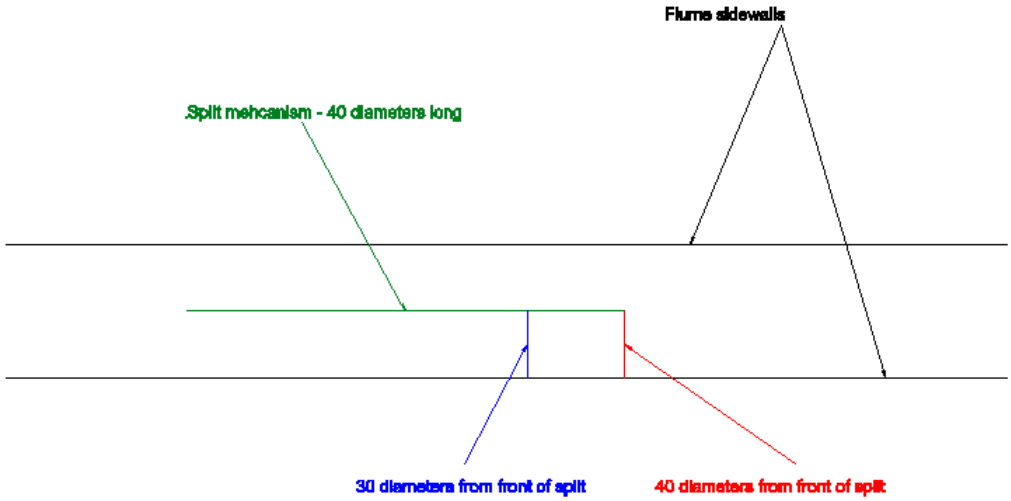

Figure 6.14: Longitudinal positions of 0.295 blockage ratio actuator fences examined for comparison with Atwater and Lawrence model

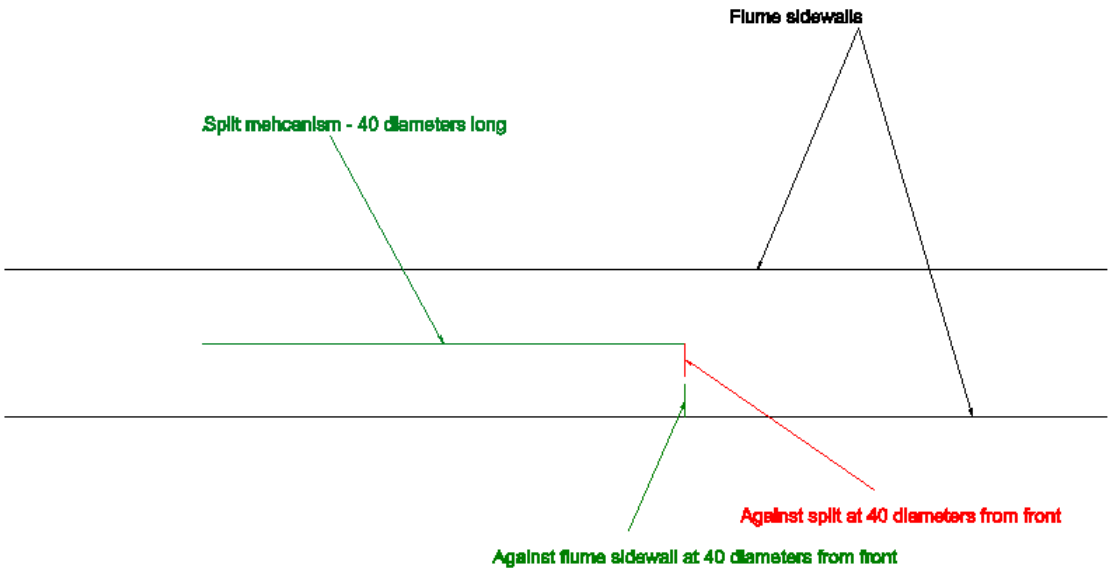

Figure 6.15: Lateral positions of 0.146 blockage ratio actuator fences examined for comparison with Atwater and Lawrence model

Blockage and position	% in impeded channel	% in free channel	C_t
Natural conditions	52	48	-
Optimum	32	68	-
0.295 - 30 diameters	43.8	56.2	1.42
0.295 - 40 diameters	41.8	58.2	1.2
0.244 - 30 diameters	45.4	54.6	1.2
0.244 - 40 diameters	44	56	1.09
0.195 - 30 diameters	47.1	52.9	1.19
0.195 - 40 diameters	44.9	55.1	1
0.146 - 40 diameters - centre	46.8	53.2	1.03
0.146 - 40 diameters - against split	44.8	55.2	0.96

Table 6.3: Distribution of volumetric flow rate between impeded and free sub channels for different blockage ratio actuator fences and fence positions

effect of actuator fences was increased by examining the following scenarios:

- A solid plate of blockage ratio 0.295 positioned at the very rear of the split. Similarly to section 5.2, this solid plate effectively represents a zero blockage ratio actuator fence.
- Two 0.295 blockage ratio fences in the impeded channel, one at the front of the split and one at the rear.
- Three 0.295 blockage ratio fence in the impeded channel, positioned at the front, rear and midpoint of the split.

These results are shown in table 6.4. For the calculation of thrust coefficient, inflow velocity to each fence was recorded by taking flow velocity measurements across the centre depth and laterally at the downstream plane at which the fence was present. Crucially, for the cases of multiple fences, these measurements were taken with the upstream fences in place. This was considered to present a more realistic value for inflow velocity, as opposed to if measurements were taken with no fences in place. Also worth noting is that thrust measurements for the solid plate were not recorded, as there were concerns that its thrust would be in excess of the 10N load cell limit, and thus measuring it would cause irreversible damage to the load cells internal strain gauges.

Also included in table 6.4 is the distribution between channels for a single 0.295 blockage ratio fence. The results do show that the scenario of a solid plate does get very close to achieving the optimum imbalance predicted theoretically. However it must also be remembered that solid plate represents a solid obstruction to the flow, and does not actually represent any practical arrangement of tidal turbines. Its inclusion was purely to test the limits of the theory. It is also clear from results that the addition of more actuator fences increases the amount of flow diverted into the free channel. This is simply because more of the flow is blocked from the impeded channel and hence diverted into the free channel. But it can be seen that the increase in flow diverted to the free channel for the addition of further fences is relatively small. Going from one to two fences increases the percentage of overall flow in the free channel by just 3%, with the addition of a third fence again increasing this figure by only another 2%.

% in impeded channel	% in free channel	Thrust (N)	C_t
Natural conditions			
52	48	-	-
Optimum			
32	68	-	
Fence at front			
41.8	58.2	3.91	1.4
Fence at front and rear			
38.8	61.2	2.97, 2.46	1.06, 1.25
Fence at front, middle and rear			
36.8	63.2	2.77, 2.41, 2.04	0.99, 1.28, 1.32
Solid plate			
35.4	64.6	-	-

Table 6.4: Distribution of volumetric flow rate between impeded and free sub channels for multiple 0.295 blockage ratio fences and solid fence

Assuming this small increase in flow diversion were to continue with the addition of further fences, it would appear that including somewhere between 5 and 7 fences might achieve the imbalance of 32% in the impeded channel and 68% in the free channel. While the model would suggest that this would result in optimum power extraction, this may not necessarily be the case. This is due to the close longitudinal spacing that would be required to fit so many rows of turbines into the one sub channel. As an example, fitting 5 rows into the experimental set-up would require an average longitudinal spacing between each row of 8 turbine diameters. As results for 9 diameters downstream of a turbine have showed in section 5.3.1, the wake of turbines persists at this distance downstream of a row of turbines. This in turn means that subsequent rows of turbines will experience a lower thrust for a given number of turbines and turbine designs due to slower inflow conditions. In any given arrangement of a number of rows, the first row will experience the highest thrust, while the thrust force on each subsequent row will continually reduce. To demonstrate this, for the cases of one, two and three 0.295 blockage ratio fences in the impeded sub channel, thrust measurements were taken on each. Also recorded were the inflow velocity conditions to each fence. In the case of two and three fences, this meant that the flow velocity for the second and third fences were slower than the first fence, as they lay in the wake of an upstream fence. This analysis is presented in table 6.5.

The analytical theory presented in Atwater and Lawrence [2010] and outlined in section 2.5.10 gave an estimate of the flow conditions necessary in a split tidal channel for optimal performance of tidal turbines. It was based on the assumption that the more flow that is directed into an unimpeded channel by tidal turbines in an impeded channel, the greater the power output of the turbines themselves, provided too much flow was not blocked to the impeded channel. Using this theory, an attempt was made to determine the optimum imbalance in overall volumetric flow rate between both sub channels. The experimental analysis presented here suggests that multiple rows of turbines in the sub channel of a split site may result in the theoretical optimum imbalance in volumetric flow rate. However results have also raised doubt as to whether this will actually result in the optimal performance of

Single actuator fence @ 0 diameters		
Fence position	Thrust (N)	Velocity to actuator fence (m/s)
0 diameters	3.906	0.305
Fences @ 0 and 40 diameters		
Fence position	Thrust (N)	Velocity to actuator fence (m/s)
0 diameters	2.965	0.305
40 diameters	2.463	0.256
Fences @ 0, 20 and 40 diameters		
Fence position	Thrust (N)	Velocity to actuator fence (m/s)
0 diameters	2.766	0.305
20 diameters	2.409	0.256
40 diameters	2.04	0.227

Table 6.5: Reduction in power per row of turbines with addition of turbines in impeded channel

turbines. This is because, at present, the model is unable to account for the changing inflow conditions to rows of turbines downstream of an initial row. It has been clearly shown that the inflow conditions to additional rows of turbines are considerably slower due to the wake of an initial array, leading to lower thrust forces on downstream rows of turbines. Interestingly, this observation of diminishing return per row with multiple rows is consistent with results of a theoretical analysis into optimally tuning the flow conditions into tidal turbines by Vennell (2010). The only other alternative, which is also suggested by Vennell (2010), would therefore be if a single row of turbines were sufficiently designed, tuned, and had a sufficient cross sectional blockage ratio, to cause the optimum imbalance predicted by Atwater and Lawrence without the need for additional rows. The possibility of this being achievable has been called into question by the results for the solid actuator fence. Even a solid obstruction occupying 33% of the depth and 89% of the width of the channel has not resulted in the 32:68 optimum imbalance predicted by the Atwater and Lawrence model.

Interesting, the experimental results also suggest a major assumption in the Atwater and Lawrence model may not necessarily be correct. The basis of examining volumetric flow rate distribution between sub channels in the model is that if more flow is being diverted into a free channel, this must be occurring because more turbines are present in the impeded channel. The addition of more turbines is therefore assumed to be the only parameter affecting the amount of flow diverted into the free channel. However the results presented in this analysis suggest that the simple act of changing the position of a row of turbines can increase the amount of flow diverted into unimpeded channel without any change in blockage ratio. Results presented in figure 6.8 also suggest that the smaller amount of flow available in an impeded channel due to this change in fence position can reduce the thrust forces on turbines, again without any change in blockage ratio.

It is therefore very clear that as well as blockage ratio, specific position and the number of rows of turbines are also factors which affect power output and volumetric flow distribution in split tidal channels. All of these have not been accounted for in the currently available Atwater and Lawrence model.

It is freely acknowledged that there a number of variables associated with any real life tidal

turbine projects in split channels which cannot possibly be investigated in a small project with modest resources. These include site bathymetry, specific design of tidal turbine rotors and support structures and sediment transport processes. It is also freely acknowledged that some or all of these parameters may affect the nature of the flow regime resulting from the installation of tidal turbines. However it is believed that this split tidal analysis has revealed some fundamental physics of how flow in split tidal channels behaves, and has therefore added to the knowledge gained from previous work.

Chapter 7

Conclusions and future work

The overall hypothesis which this PhD project aimed to test was that both the specific position and blockage ratio of a row of tidal energy turbines both directly affected both the power performance and hydrodynamic effects associated with tidal power extraction. The four specific effects which were examined were:

- The loading on turbines in both open and split channels.
- The increase in flow velocity compared to ambient conditions in the gaps between the edge of turbines and channel walls in open channels.
- The structure of the far field wake region of the flow downstream of the tidal turbine row in open channels.
- The imbalance in volumetric flow rate between sub channels in a split tidal channel.

The following sections summarise the main conclusions of the experimental analysis carried out, and some suggested future work to examine these effects further.

7.1 Thrust coefficient analysis to examine loading on turbines

The main conclusions from the thrust coefficient analysis are:

- The non-dimensional thrust coefficient of a row of turbines did not change appreciably depending on position with respect to channel walls in an open channel. For the smallest blockage ratio of 0.072, the difference in thrust coefficient between the furthest and closest points to the channel sidewall was found to be approximately 2.5%. For the largest blockage ratio of 0.146, this figure was 2.3%.
- In an open channel, positioning a row of turbines closer to a channel wall led to smaller thrust forces (and hence power output) compared to when turbines are positioned away from the wall. For the smallest fence of 0.072 blockage, thrust was found to be 15% higher at the furthest point from the wall compared to the closest point. For the 0.146 blockage ration fence, thrust was 9% higher further from the channel wall.

- Positioning closer to an open channel wall led to greater variability in the thrust experienced between individual turbines within a row. Positioned close to the channel wall, a difference between consecutive thrust measurements of up to 7.7% was observed, while the highest difference between consecutive measurements found when positioned further away from the channel wall was 1.31%.

- The lower thrust and greater variability close to channel sidewalls are believed to be due to the boundary layer off the channel sidewall. The boundary layer means lower velocity and hence thrust in this region. It also means different inflow conditions between individual turbines within a row. These different inflow conditions are not present in the centre of the channel where flow conditions are less variable.

The variability of thrust identified when a row of turbines is positioned closer to channel walls is worthy of further investigation. It would be of great benefit to tidal developers to better understand the possible implications of varying inflow conditions to different turbines within an row. One possible method of examining this experimentally would be to use a series of relatively thin strips of actuator fence material to represent a row of turbines and measure the thrust readings on these strips individually using several load cells. The lateral position of these could then be altered, and the results could examine how the difference in thrust experienced by each individual strip changes as the row position is changed.

It is also worth noting that the examination carried out which identified this variability was only carried out with attention paid to ensuring subcritical Froude number. However one uncertainty which remains after this analysis is whether the same variability observed would also occur with different flow Reynolds numbers. The Reynolds number is the ratio of inertial to viscous forces, and it is these viscous forces which control the development of the boundary layer off the sidewall of the channel, which is postulated to be the reason behind the variability of thrust close to the channel wall. It is therefore worth investigating, in future work, the variability at different flow Reynolds numbers. This could help determine whether the variability effects are more or less pronounced for different Reynolds numbers in the subcritical Froude number region.

7.2 Flow constraining analysis

The results of the flow constraining analysis lead to the following conclusions:

- Positioning rows of turbines closer to channel boundaries initially resulted in a linear increase in flow velocity compared to ambient conditions. The largest increase was approximately 30% for a 0.146 blockage ratio fence and 20% for a 0.072 blockage fence. This increased up to the point at which flow was not constrained and the localised volumetric flow rate through the gap between turbines and the channel wall remained constant.

- Positioning a row of turbines within the boundary layer off the channel sidewall led to a sudden reduction in flow velocity of up to 70% compared to ambient conditions, even before the fence was touching the channel wall. This is postulated to occur due to the

high velocity gradients and viscous forces, which divert fluid streamlines away from the gap between turbines and the wall.

- The position at which this reduction in flow velocity occurs is the same irrespective of the number of turbines within a row or the blockage ratio, 1 diameter from the sidewall.
- This position where this reduction occurred was found to be 1.2 diameters on the opposite side of the experimental flume. This was postulated to be due to a different local Reynolds number and hence different boundary layer formation at this side of the channel.

The final point suggests that, as with thrust coefficient analysis, the influence of Reynolds number on the position at which the observed reduction in flow velocity occurs should be investigated further. While the specific point at which this occurs is likely to be dependent on channel geometry, this analysis has clearly showed it to also be dependent on viscous effects associated with different flow conditions, even with the same flow depth and Froude number. Future analysis could examine whether this onset of reduction in flow velocity occurs closer or further away from the channel wall with increasing or decreasing local Reynolds number.

This area of research could also be expanded on by examining flow constraining effects with multiple rows of turbines in a channel. As an example, it would be interesting to examine if placing another row of turbines in the same lateral plane as that closest to the sidewall leads shows any different increase or decrease in flow compared to ambient conditions. It would also be interesting to examine rows of turbines downstream of the first row. In particular, experimental analysis could determine to what extent increases in velocity identified in this work lead to increase in thrust experienced by downstream rows. This research could aid tidal developers with determining the layout of large tidal turbine rows. It would shed light on how they could strategically position turbines to extract maximum power at any given time in the spring-neap cycle.

7.3 Wake analysis

In the wake analysis in this research, the wake characteristics of two blockage ratio actuator fences were examined: The results of this analysis gave the following conclusions:

- For the smaller blockage ratio examined, positioning a row of turbines closer to channel sidewalls lead to increased velocity deficit, lower lateral Reynolds stresses and higher turbulence intensity at the side of the wake closest to the channel wall. Velocity deficit increases from approximately -0.1 to 0.35. Reynolds shear stress decreased from approximately 1.5 to 0.25 N/m^2, and turbulence intensity increased from approximately 58% to 68%.
- Conditions in the remainder of the wake remained broadly similar irrespective of proximity to channel sidewall.
- The lower lateral Reynolds stresses when positioning close to the channel wall were accompanied by higher shear stresses in the other planes of flow. This suggests that

fluid streamlines diverted away from the gap between the row of turbines and sidewall due to viscous forces are directed above and below the turbines, as opposed to directly through them.

- This postulation is supported by the observation in the thrust analysis of no increase in thrust close to a channel wall.
- When the larger blockage ratio was examined, similar changes were observed in wake characteristics around the side of the fence closest to the channel wall when moved closer to the wall.
- Some fundamental differences in wake characteristics were also observed however. The centre of the wake was no longer the point of highest velocity deficit or turbulence intensity. Additional regions of wake mixing with freestream fluid streamlines were also identified. The wake of the larger blockage ratio row of turbines also had a more asymmetrical profile.
- A comparison of the wakes of both blockage ratios showed that a larger blockage ratio had higher velocity deficit, lower absolute values for lateral Reynolds shear stress and higher turbulence intensity. The maximum velocity deficit was approximately 0.78 for the larger fence compared to 0.6 for the smaller fence. Reynolds shear stress was $1.5N/m^2$ for the smaller fence compared to 1 N/m^2 for the larger fence. Finally, turbulence intensity was 85% for the larger fence compared to 60% for the smaller fence.This was despite the additional regions of wake mixing with freestream fluid streamlines identified.

For future work, it would be very interesting to examine the effects of wake changes further. If the smaller 0.072 blockage ratio case is examined first, the most interesting investigation would be to compare the point of recovery to freestream conditions between different proximity. Following this analysis, it does now appear to be the case that closer proximity to channel boundaries causes less wake mixing in the region around the side of the row closest to the boundary. How this might translate in a delay in complete wake recovery would be very interesting to examine. It would also give tidal developers a greater knowledge to decide whether or not the possible advantages of positioning close to boundaries might be offset by slower flow velocity to other downstream turbines, as well as the associated environmental impacts of wake changes.

There is also large potential scope for examining in more depth the changes to downstream wake conditions associated with changes to row blockage ratio. The analysis presented in this thesis has only assumed two sized fences, with one twice the blockage ratio of the other. More blockage ratios in between these values could be examined. As well as comparing the magnitudes of the wake parameters investigated in this analysis, it would be of great interest to compare the downstream distance required for recovery to ambient conditions. An investigation such as this could be carried out in the Chilworth flume with all the experimental equipment used in this analysis. The results would also allow tidal developers to make a more informed choice in deciding the size of any given proposed tidal turbine row.

While the wake changes observed in this analysis have potentially far reaching effects, the use of highly simplified and idealised porous fences means a certain level of uncertainty remains. While these simplified fences were considered the ideal starting point for examining the relationship between channel boundary proximity and wake parameters, a natural advancement of this would be to repeat the analysis with groups of individual actuator discs, with a lateral spacing between each that would ensure full merging of individual disc wakes. If findings of this proposed analysis were found to be similar to those presented in this thesis, a further investigation could then examine if the conclusions of the inter-device spacing studies by authors such as Stallard et al. [2013] would also hold for groups of individual turbines positioned close to channel boundaries as well as towards the centre of their respective channel. Small scale rotor wake testing is also possible. It would be interesting to observe if the introduction of the blade tip vortices associated with rotors to the flow would still result in the changes in wake parameters observed when turbines are positioned closer to channel walls.

Finally, it is worth noting that the wake analysis carried out in this thesis was with the actuator fence present in the centre depth of the flow, where turbulence conditions, in particular turbulence intensity, were found to be reasonably uniform. However an examination of natural conditions in the experimental facilities showed much more non-uniform flow towards the bed of the channel due to the boundary layer formation. Turbulence intensity values, which previous work by authors such as Maganga et al. (2010) and Blackmore et al. (2014) has shown to be a major influencing factor in wake recovery. It would be useful to examine the effect of changing proximity of tidal turbines to channel boundaries when turbines are positioned deeper in the flow, to determine whether similar changes in wake properties found from this analysis are also observed. This would be of particular interest to tidal developers wishing to place turbines in shallower channels where the influence of viscous forces from the bed of the channel are likely to propagate through a greater relative proportion of the flow depth.

7.4 Split tidal analysis

The main conclusions of the split channel analysis are:

- Both specific position and blockage ratio were found to affect the amount of flow distributed between sub channels in a split tidal channel. For the largest blockage ratio of 0.295, the volumetric flow rate in the undisturbed channel was 58.2% of the total when positioned at the rear of the split, and 56.2% when positioned towards the front of the split. When comparing blockage ratios, with fences positioned towards the front of the split, a blockage of 0.295 resulted in 56.2% of the flow rate in the free channel, compared with 52.9% with the smaller 0.146 blockage ratio fence.

- Specific position was also found to affect the thrust coefficient on an actuator fence. A decrease in thrust on fences was observed when they were positioned such that their wake interacts with fast moving flow coming out of the rear of an unoccupied sub channel. The largest fence had a thrust coefficient of approximately 1.4 when positioned

towards the front of the split, but this dropped to 1.2 when positioned towards the rear of the split. For the smaller blockage ratio fence, the drop was from 1.1 to 1.0. This drop is considered to be a direct consequence of the changes in imbalance in volumetric flow rate between channels associated with changing position of fences with respect to the front of the split.

- The analytical model of Atwater and Lawrence (2010) estimated an optimum imbalance in volumetric flow rate of 32% in the impeded channel and 68% in the free channel. It was found that neither a single nor multiple fences of the largest blockage ratio reached this imbalance. The closest configuration to achieve this was three 0.295 blockage ratio fences, positioned at the front, rear and middle of the split, which resulted in 36.8% in the impeded channel and 63.2% in the free channel.

- A solid plate of 0.295 blockage ratio, despite not representing any real tidal turbine configuration, was tested to examine the limits of theory. This resulted in 35.4% in the impeded channel and 64.6% in the free channel.

The postulation of interaction between fast moving free sub channel flow and tidal turbine wake could be scrutinised further in future work. This could be done firstly by carrying out extensive flow measurements of the actuator fence wake at numerous distances from the front of the split mechanism used. This date could then be used to examine the interaction between the wake of the actuator fence and the fast moving flow coming out of the free channel. Comparing the wakes of actuator fences at different longitudinal and lateral positions would give a greater insight into whether the postulated effect of interaction between wake and free channel flow is responsible for the changes in flow diversion observed. The wake and free channel flow postulation could also be further examined by repeating the analysis in this project with longer split mechanisms. Finally, if the wake and free channel flow postulation was supported further by future experiments, the effect of the depth of immersion of a row of turbines could be examined. Previous work by Myers and Bahaj [2010] has shown deeper immersion of tidal turbines to lead to a slower wake at a fixed distance downstream of a row of tidal turbines. Based on both this, and the conclusions of the analysis presented in this thesis, it is possible that at any distance downstream of the front of a split, increasing the depth at which turbines are installed may lead to a change in volumetric flow rate in both sub channels, with a corresponding change in the power output of a row of turbines.

7.5 Implications of results for tidal turbine developers

7.5.1 Flow constraining analysis

The flow constraining analysis has shown that positioning closer to channel boundaries can lead to increases in local flow velocity magnitude at certain points in the flow regime surrounding a row of tidal turbines. The analysis has shown also that there is a certain proximity at which the flow between the channel and edge of the row of turbines is blocked, reducing the local volumetric flow rate in that area and diverting flow away from the channel boundary. There also appears to be no definite proximity at which this occurs, and it appears to be

dependent on the Reynolds number of the flow and the associated strength of viscous forces in the boundary layer off the channel wall.

Increased flow velocity magnitude is likely to be of interest to tidal developers due to the cubic relationship between power output and flow velocity. Therefore increases in flow velocity of up to 20% found in the analysis presented suggest that there is scope for positioning multiple tidal turbines strategically closer to channel boundaries such as to avail of this increase, thereby improving overall tidal farm performance. This will also have a positive effect on the economics of the project. It has also been shown however that tidal developers will only be able to avail of this increase up to a certain proximity where blockage effects divert flow away from the sides of the channel. It has also been demonstrated that this "tipping point" at where reduction in flow velocity occurs is dependent on the local Reynolds number in that region of the flow and the corresponding strength of viscous forces off the channel sidewalls. There will also be other site specific factors, which cannot be accounted for in an idealised scaled down experimental channel, which will affect the proximity of this tipping point. Some examples include:

- The rock and sand formation on the bed of the channel, which influences the turbulence of the flow.
- The shape of the channel bed towards its wall. As opposed to the simplified rectangular shape of the experimental facility, real channels are likely to have much more irregular shapes. These will mean more uncertainty in the estimation of crucial channel parameters such as hydraulic radius, Manning's n and the effective channel cross sectional area.

For these reasons, tidal developers wishing to avoid the occurrence of this reduction in velocity would be advised to carry out some site specific studies using field data, similar to that of Blunden and Bahaj (2007), to determine the proximity between tidal turbines and channel boundaries at any specific site at which the diversion of flow away from the local flow region near the channel wall is likely to occur.b

As well as the implications for tidal turbine performance, the flow constraining effects observed are also likely to have implications for natural processes, in particular sediment transport. Higher velocity could potentially lead to a greater ability of the flow to erode shorelines and carry sediment, which may have unpredictable negative effects on wildlife and residents living locally to a tidal turbine installation. These negative effects could potentially outweigh the positives associated with the potential improved performance of tidal turbines. Thus tidal developers would be advised to recognise and be aware of the potential environmental impact of the flow velocity changes which accompany positioning closer to channel boundaries, thus ensuring their installation can be safely considered socially as well as environmentally sustainable.

7.5.2 Thrust analysis

The purpose of the thrust and thrust coefficient analysis in section 5.2 was to examine whether position and blockage ratio changes affected the power output of tidal turbine rows. For

reasons already mentioned in this section, it is difficult to get an indication of power output itself from actuator fences due to the fundamental difference in how they dissipate energy in the flow. However changes to the fluid forces acting on an actuator fence, and the non-dimensionalising of these forces, can give a good indication of how the performance of a row of turbines might change.

The results of this analysis clearly indicate that specific position with respect to channel walls is a factor in the amount of thrust experienced by turbines. The thrust experienced by a row appears to be much higher when it is positioned away from channel walls. In a channel bounded on both sides, such as a river channel, the very centre of the channel appears to give highest thrust on turbines. This is postulated to be a simple consequence of cross channel flow variation due to boundary layers off the channel walls, and the square relationship between thrust and velocity. However it can also be seen that when non-dimensionalising thrust against in the inflow velocity to turbines, specific position does not show turbines to produce more power per unit flow velocity or turbine swept area. It is also very interesting to observe that the flow constraining phenomenon experienced positioning close to channel boundaries does not result in more flow diverted directly through the row of turbines for power production. All of the flow which can no longer divert around the sides of the fence can only be diverted either above or below the fence. This means that reduced cabling is the only gain which tidal developers will make from positioning close to shorelines, and this gain will have to be balanced against any environmental problems associated with increased scour and sediment mobilisation.

One other interesting observation from experimentation is the more variable nature of thrust forces when positioning an array closer to channel sidewalls. This is postulated to be as a result of the varying inflow velocity to individual turbines, and the greater turbulence intensity which is present in the boundary layer off the channel sidewall. Positioning a tidal turbine row away from the wall boundary layer will mean relatively little difference in the flow velocity to each individual turbine in a row. Hence the power output and loads experienced by the whole row are fairly constant and predictable. However positioning any given sized row closer to channel boundaries will mean a much greater difference in the local flow velocity experienced by turbines on either side of the row. Some of the possible implications of this include:

- The overall power output from the entire row at any given time instant during the spring-neap tidal cycle may be more variable.

- Varying velocity will also mean the loads experienced by turbines may be different between turbines within the row at any instant during the spring-neap tidal cycle.

- If the loading experienced by individual turbines within an row differs, the design of individual turbines within an row may need to be altered. Some turbines which experience higher loads than others may require stronger blades, rotor hubs or support structures than other turbines. This is likely to impact greatly on the overall project economics.

7.5.3 Wake analysis

The purpose of the wake analysis was to determine the potential impact of changing specific position and blockage ratio of a tidal turbine row on the flow conditions downstream of a row of turbines. This would be of interest to tidal developers who may wish to install other turbines downstream of each other. Changes to the surrounding hydrodynamic environment would also be of interest in examining the environmental impact of tidal turbines.

The results of this analysis appears to suggest that changing the position of a row does change wake structure to some extent. However results suggest that these changes appear to be confined to the region of the wake around the sides of the fence closest to the channel wall. Positioning closer to a channel wall leads to less freestream fluid available for mixing into the wake around the side of the row nearest to the channel wall, leading to considerable changes in wake development. This results in higher velocity deficit, lower horizontal Reynolds shear stresses, higher shear stresses and higher turbulence intensities towards the channel wall as the row is moved closer to it. However in the remaining regions of the wake, in the centre of the wake and around the side closest to the centre of the channel, there is insufficient evidence to conclude that proximity has any effect on wake properties. It is clear from these results that if tidal developers wish to take advantage of lower cable cost by positioning rows closer to shorelines or channel walls, the implications of the associated wake changes found from this analysis will need to be examined. They may result in changes to the power output of downstream turbines, depending on their specific location with respect to channel walls. They may also result in different environmental effects, such as changes in the build up of sediment over long periods of time, or possible changes to fish migration patterns. It is however worth noting just how close to channel walls rows need to be positioned before these changes are observed. Beyond a distance of 1.2 diameters between the edge of a row and a channel wall, no changes in any wake properties are observed in this analysis. For tidal developers, this means that in the vast majority of the lateral space available for positioning rows, the downstream wake conditions will not be any different.

When examining larger blockage ratio fences, results again showed similar changes to wake properties around the side of the row of turbines close to the channel wall. But results also suggest some very fundamental differences in how the wakes of larger blockage ratio rows recover to freestream conditions. Larger blockage ratios display much higher vertical shear stresses and lower horizontal shear stresses, showing that they entrain more freestream fluid above and below the fence . This appears to result in the centre of the wake becoming re-energised faster than the sides of the wake, and hence peak values for velocity deficit and turbulence intensity no longer occurring directly in the centre of the wake. There is also a more asymmetrical shape to the wakes of larger blockage ratio fences when positioned closer to channel boundaries, with peak values for velocity deficit and turbulence intensity being lower on the side of the row towards the centre of the channel. This is postulated to be due to viscous forces forcing fluid streamlines away from the gap between the row and the channel wall, with the direction in which they are diverted being a consequence of Bernoulli's principle. For tidal developers, these particular results give clear evidence that the structure of a wake downstream of a row of turbines can be dependent on blockage ratio. This will

have significant implications in the context of further turbines downstream. Fundamental differences in downstream conditions, such as the location of peak turbulence intensity values, may mean the configuration of downstream rows would have to be tailored differently for different blockage ratios to ensure optimum performance of downstream turbines.

One of the main areas of uncertainty which remains due to the idealisations in the experimental analysis is the effects of the flow between multiple single devices, and the different wake structures associated with these. The use of porous actuator fences carries with it an implicit assumption that the wakes of all individual turbines in the simulated row merge together to form one wake, and the results of this analysis can be considered valid for this instance. However it is not clear if the overall flow regime effects observed in this analysis would also hold for a row of turbines where inter-device spacing means the idealised merged single wake no longer occurs. It is possible that jets of flow through gaps between turbines might result in very different effects associated with changing the overall proximity of the row of turbines to neighbouring channel boundaries. This is an effect which tidal developers must be aware of with their specific installation. A step forward from this research would be to carry out an examination of overall flow conditions downstream of a row of individual porous discs, followed by an examination of these downstream conditions when this row of discs was moved closer to channel walls. This could be carried out for both constant and varying inter device spacing.

It is also important for tidal developers to examine the inflow turbulence conditions to the specific location where turbines are proposed to be installed. The cross sectional area where analysis was carried out for this research had a maximum variation in turbulence intensity of 2%. Were specific sites found to have greater variation at different proximities from the channel boundary, caused possibly by upstream obstructions or changes in bed material or formation, these will also have a major bearing on the different downstream flow conditions associated with installation of turbines. The work of Blackmore et al. (2014) has also shown turbulence length scale to be another parameter which might affect wake conditions, and so different turbulence length scales at different proximities to channel boundaries is also a possibility tidal developers would need to be aware of.

7.5.4 Split tidal channels

Literature reviewed for this project showed a relative lack of previous work on generic split tidal channels. While a number of site specific studies using modelling techniques have been carried, only two analytical models have been developed, compared to numerous models for open channels. Prior to this research, there was also a clear lack of experimentation on split channels. As a result, it was unclear what if any effect changing specific row position with respect to flow boundaries or blockage ratio had on power available and the surrounding hydrodynamic environment. One of the two analytical models reviewed by Atwater and Lawrence [2010] had demonstrated how the distribution of volumetric flow rate between sub channels affected the power available to turbines installed in one of these sub channels. The purpose of the split channel analysis in this project was to examine this imbalance in volumetric flow rate further, and to examine what if any effect specific position and blockage

ratio had on this imbalance. The analysis also aimed to examine what if any combination of these factors achieved the theoretical optimum volumetric flow rate imbalance predicted by the Atwater and Lawrence model.

Experimental results suggest that changing specific position of a row of turbines with respect to flow boundaries can change the amount of flow diverted. In the case of large blockage ratio rows spanning more than half the width of their respective sub channel, changing location from the front to the rear of impenetrable land masses leads to an increase in the volume of flow diverted into empty sub channels. The corresponding decrease in flow in the impeded channel leads to a very substantial decrease in power output of any given tidal fence. In the case of smaller rows spanning less than half the width of a sub channel, lateral position of a row with respect to channel sidewalls does not change the volumetric flow rate imbalance between sub channels towards the front of the split. However towards the rear of the split mechanism, more flow is diverted into unimpeded channels if the row is located closer to the side of the impenetrable land mass. Again, the consequent reduction in volumetric flow rate results in a smaller power output of this row. The postulation put forward to explain these effects were that they were due to interaction between the wake of a row of turbines and fast moving flow coming out of the unimpeded sub channel.

The results have also allowed some conclusions to be made on the analytical model developed by Atwater and Lawrence [2010]. Numerical manipulation of this model allowed the optimum imbalance in volumetric flow rate between sub channels in a split channel to be calculated. Subsequent calculations also allowed an estimate of the maximum available power in a split channel to be calculated. The analysis presented in this thesis suggest that while the theory of this model may be sound, the necessary optimum conditions in a split channel it predicts may be difficult or impossible to achieve with only a single row of turbines. The optimum imbalance for the experimental set-up used in this analysis was predicted by Atwater and Lawrence to be 30% of the overall volumetric flow rate in the impeded channel and 70% in the free channel. Results do suggest that multiple rows of turbines may be achieve this imbalance. However due to the slower inflow conditions to rows downstream, which will be in the wake of an initial row, these additional rows will generate less power than the initial row. As well as slower flow, the greater turbulence of inflow conditions to downstream rows will lead to more uneven loading, which may reduce service life of turbines. For tidal developers, this means that the power output estimates found by applying this model to split tidal sites (such as the 112.575MW figure for Johnstone Strait, Canada) are likely to represent only a theoretical upper limit. The actual amount which any practically achievable tidal turbine row might be able to extract may be considerably less. This must be accounted for when examining the economic viability of a tidal project in split channels.

There are a number of potential split tidal channel sites around the world which the findings of this research are relevant to. In the UK, many areas of the Pentland Firth would fall into the split channel category. One good example which is currently the subject of a major tidal energy project is the area surrounding the Island of Stroma. The Meygen consortium is currently in the process of installing multiple tidal turbines with a combined capacity of 400MW in the Inner Sound of Stroma (pictured in figure 7.1). In this split

channel, the island of Stroma represents the impenetrable landmass splitting a channel into two sub channels. While this site will have the wakes of turbines and freestream flow as in the experimental analysis for this research, an additional consideration will be the wake of the island itself. It was found in the experimental analysis that interaction between tidal turbine wakes and fast moving freestream flow caused a change in the amount of flow diverted between sub channels. While this would suggest avoiding the rear of a split mechanism on either the spring or neap cycle, the wake of the island in the case of Stroma may make this unnecessary. If the slow moving wake of the row of tidal turbines only interacts with the wake of the island, as opposed to the fast moving flow from the free channel, the major change in volumetric flow rate distribution, and hence reduction in tidal turbine power output, may be avoided. This would mean tidal developers in this site may have more flexibility in positioning rows of turbines than in other sites where such large wakes off impenetrable land masses are experienced. Is it likely however that there may still be some limitations. If tidal turbines were positioned at the very rear of the split, it is possible that there may be a complete

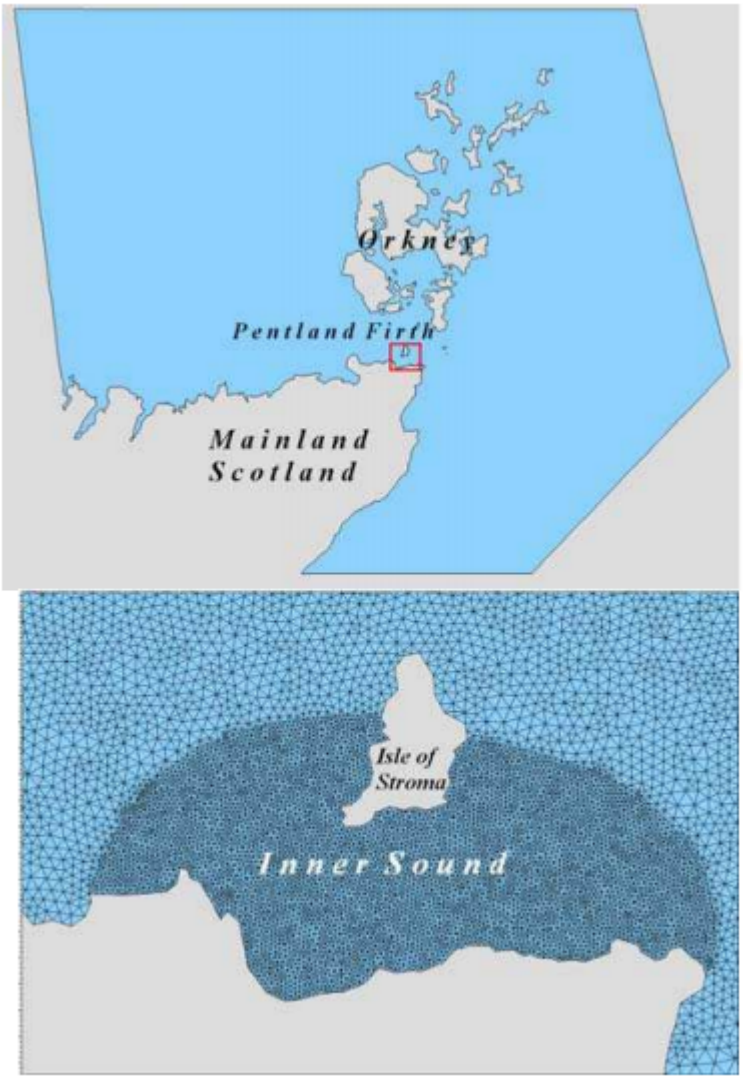

Figure 7.1: Map of Stroma, Inner Sound and surrounding areas from Easton (2010)

merging of the wake of the turbines and the land mass. This large merged wake may then interact with fast moving flow from the free channel, with a resulting drop in turbine power output as suggested by experimental results.

A map of the area surrounding Johnstone Strait in Canada, which was examined by Atwater and Lawrence (2010) is shown in figure 7.2. The complex topography of this site clearly demonstrates the importance, and potential far reaching consequences, of the flow interaction results found from this analysis. Multiple potential tidal energy sites lie in this region, and it is quite clear that the installation of turbines in multiple locations will affect the hydrodynamics, and tidal resource, available in the entire region. A change in the amount of flow diverted between sub channels in any one of these locations will inevitably have an impact on power output of other tidal turbines in other locations. The numerous land masses which lie in this region, and the wakes which are likely to be present off these, complicate the problem of optimal location of turbines even further. It is clear from this research that for any tidal turbine projects in Vancouver Island, the specific location of a row of turbines with respect to flow boundaries is a parameter which requires very careful scrutiny. Failure to do carry out a comprehensive analysis of the effects of changing this parameter could lead to sub-optimal performance of turbines or major differences in volumetric flow rate distribution between channels between the spring and neap cycle.

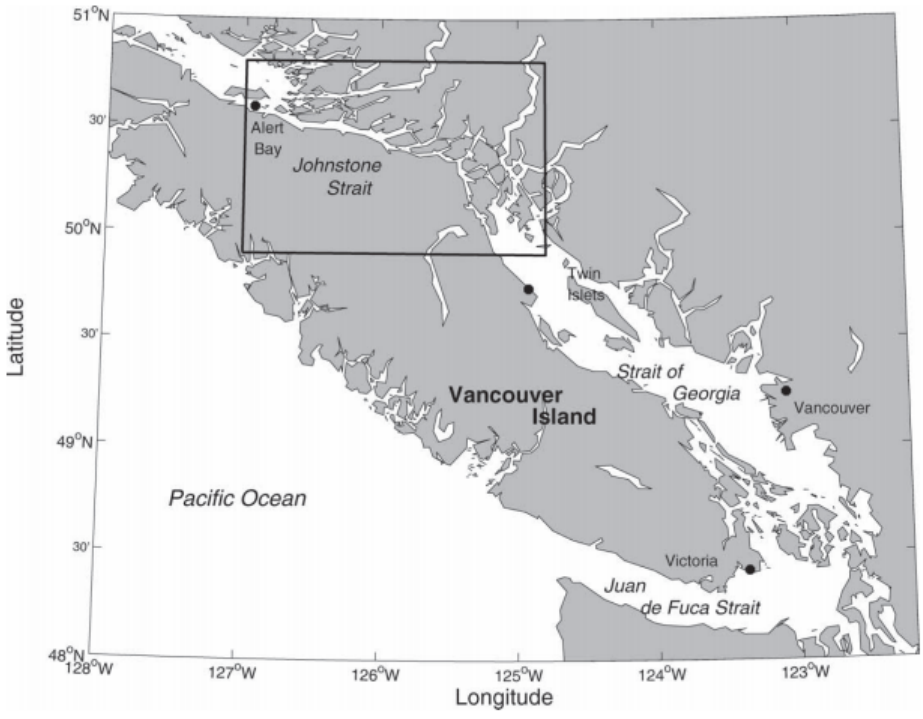

Figure 7.2: Map of area of Vancouver Island, Canada from Sutherland et al. [2007]

Bibliography

R. Ahmadian, R. Falconer, and B. Bockelmann-Evans. Far-field modelling of the hydro-environmental impact of tidal stream turbines. *Renewable Energy*, 38:107–116, 2012.

J.D. Anderson. *Introduction to Flight*. McGraw-Hill, New York, USA., - 5th edition edition, 2005.

J. F. Atwater and G. A. Lawrence. Power potential of a split tidal channel. *Renewable Energy*, 35 (2):329–332, 2010.

A. Betz. Das maximum der theoretisch moglichen ausnutzung des windes durch windmotoren. *Zeitschrift fur das gesamte Turbinenwesen*, 26:307–309, 1920.

Black and Veatch. Tidal stream energy resource and technology summary report. Technical report, The Carbon Trust, Middlesex, UK, 2005.

T. Blackmore, W.M.J. Batten, and A.S. Bahaj. Influence of turbulence on the wake of a marine current turbine simulator. *Philosophical transactions of the Royal Society A: Mathematical, Physical and Engineering Sciences*, 470:107 – 116, 2014.

L. S. Blunden and A. S. Bahaj. Initial evaluation of tidal stream energy resources at portland bill, uk. *Renewable Energy*, 31 (2):121–132, 2006.

L.S. Blunden and A. S. Bahaj. Effects of tidal energy extraction at portland bill, southern uk predicted from a numerical model. In *European Wave and Tidal Energy Conference*, Porto, Portugal, 11th -13th September 2007.

I. G. Bryden, T. Grinsted, and G. T. Melville. Assessing the potential of a simple tidal channel to deliver useful energy. *Applied Ocean Research*, 26 (5):198–204, 2004.

T. Burton, D. Sharpe, N. Jenkins, and E. Bossanyi. *Wind energy handbook*. John Wiley & sons ltd., Chichester, United Kingdom, 2001.

L. Cea, J. Puertas, and L. Pena. Velocity measurements on highly turbulent free surface flow using adv. *Experiments in Fluids*, 42 (3):333–348, 2007.

J.R. Connel and R.L. George. The wake of the mod-0a1 wind turbine at two rotor diameters downwind on 3 december 1981. Technical report, United States Department of Energy, 1981.

European Renewable Energy Council. Renewable energy technology roadmap: 20 Technical report, European Renewable Energy Council, Brussels, Belguim., 2008.

P. Cummins. The extractable power from a split tidal channel: An equivalent circuit analysis. *Renewable Energy*, 50:395–401, 2013.

R.C Dorf and J.A. Svoboda. *Introduction to electric circuits*. John Wiley & sons ltd, New York, USA, 3rd edition, 1996.

K.R. Dyer. *Coastal and Estuarine Sediment Dynamics*. John Wiley & sons ltd., Chichester, UK, 1986.

M. Easton. An operational hydrodynamic model of a key tidal-energy site: Inner sound of stroma, pentland firth (scotland, uk). In *International Conference on Ocean Energy*, Bilbao, Spain, 6th - 8th October 2010.

P.A. Fraenkel. Marine current turbines: pioneering the development of marine kinetic energy converters. *Proceedings of the Institution of Mechanical Engineers, Part A: Journal of Power and Energy*, 221 (2):159 – 169, 2007.

C. Garrett and P. Cummins. The power potential of tidal currents in channels. *Proceedings of the Royal Society A: Mathematical, Physical and Engineering Science*, 461 (2060):2563–2572, 2005.

C. Garrett and P. Cummins. The efficiency of a turbine in a tidal channel. *Journal of Fluid Mechanics*, 588:243–251, 2007.

H. Glauert. The analysis of experimental results in the windmill brake and vortex ring states of an airscrew. Technical report, His majesty's stationery office, 1926.

L. Hamill. *Understanding hydraulics*. Palgrave MacMillan, Basingstoke, United Kingdom, 3rd edition, 2011.

M. E. Harrison, W. M. J. Batten, L. E. Myers, and A. S. Bahaj. Comparison between cfd simulations and experiments for predicting the far wake of horizontal axis tidal turbines. *IET Renewable Power Generation*, 4:613–627, 2010.

M.E. Harrison, W.M.J. Batten, L. S. Blunden, L.E. Myers, and A. S. Bahaj. Comparisons of a large tidal turbine array using the boundary layer and field wake interaction models. In *International Conference on Ocean Energy*, Brest, France, 15-17 October 2008.

D. Hasegawa, J. Sheng, D. A. Greenberg, and K. R. Thompson. Far-field effects of tidal energy extraction in the minas passage on tidal circulation in the bay of fundy and gulf of maine using a nested-grid coastal circulation model. *Ocean Dynamics*, 61(11):1845–1868, 2011.

Sustainable Energy Ireland. Tidal and current energy resources in ireland. Technical report, Sustainable Energy Ireland, 2006.

A.S. Iyer, S.J. Couch, J.P. Harrison, and A.R. Wallace. Analysis and comparisons of tidal datasets. In *European Wave and Tidal Energy Conference*, Uppsala, Sweden, 7th - 10th September 2009.

M.J. Kaiser and B. Snyder. Offshore wind capital cost estimation in the u.s. outer continental shelf - a reference class approach. *Marine Policy*, 36(5):1112–1122, 2012.

F. Lanchester. A contribution to the theory of propulsion and the screw propeller. *Journal of the American Society for Naval Engineers*, 27(2):509–510, 1915.

L.B. Leopald and M.G. Wolman. River channel patterns: braided, meandering, and straight. Technical report, US Government Printing Office, 1957.

J.T. Limerinos. Determination of the manning coefficient from measured bed roughness in natural channels. Technical report, United States department of the interios, 1970.

D. MacKay. *Sustainable Energy - Without the hot air*. UIT Cambridge Ltd, Cambridge, United Kingdom., 2008.

F. Maganga, G. Germain, J. King, G. Pinon, and E. Rivoalen. Experimental characterisation of flow effects on marine current turbine behaviour and on its wake properties. *IET Renewable Power Generation*, 4 (6):498–509, 2010.

B. Massey and J. Ward-Smith. *Mechanics of fluids*. Stanley Thornes publishers, Cheltenham, United Kingdom, 8th edition, 2006.

I. Masters, R. Malki, A.J. Williams, and T.N. Croft. The influence of flow acceleration on tidal stream turbine wake dynamics: A numerical study using a coupled bem cfd model. *Applied Mathematical Modelling*, 37(2013):7905 – 7918, 2013.

J. McNaughton, S. Rolfo, D. Apsley, T. Stallard, and P. Stansby. Cfd power and load prediction on a 1mw tidal stream turbine with typical velocity profiles from the emec test site. In *European Wave and Tidal Energy Conference*, Aalborg, Denmark, 2 - 5 September 2013.

L. Myers and A. S. Bahaj. Scale reproduction of the flow field for tidal energy converters. In *10th World Renewable Energy Congress, 19 - 25 July*, Brest, France, 19-25 July 2008.

L. E. Myers and A. S. Bahaj. Experimental analysis of the flow field around horizontal axis tidal turbines by use of scale mesh disk rotor simulators. *Ocean Engineering*, 37 (2-3): 218–227, 2010.

L.E. Myers and A. S. Bahaj. Wake studies of a 1/30th scale horizontal axis marine current turbine. *Ocean Engineering*, 34 (5-6):758–762, 2007.

L.E. Myers and A.S. Bahaj. An experimental investigation simulating flow effects in first generation marine current energy converter arrays. *Renewable Energy*, 37:28–36, 2012.

L.E. Myers and A.S. Bahaj. Shaping array design of marine current energy converters through scaled experimental analysis. *Energy*, 59:83–94, 2013.

L.E. Myers, A.S. Bahaj, G. Germain, and J. Giles. Flow boundary interaction effects for marine current energy conversion devices. In *World Renewable Energy Congress X*, Glasgow, UK., July 2008 2008.

T. Nishino and R.H.J Willden. The efficiency of an array of tidal turbines partially blocking a wide channel. *Journal of Fluid Mechanics*, 708:596 – 606, 2012.

C.M. Poindexter, P.J. Rusello, and E.A. Variano. Acoustic doppler velocimeter-induced acoustic streaming and its implications for measurement. *Experiments in Fluids*, 50 (5): 1429 – 1442, 2011.

B. Polagye, P. Malte, M. Kawase, and D. Durran. Effect of large-scale kinetic power extraction on time-dependent estuaries. *Proceedings of the Institution of Mechanical Engineers, Part A: Journal of Power and Energy*, 222 (5):471–484, 2008.

B. Polagye, M. Kawase, and P. Malte. In-stream tidal energy potential of puget sound, washington. *Proceedings of the Institution of Mechanical Engineers, Part A: Journal of Power and Energy*, 223 (5):571–587, 2009.

S.B. Pope. *Turbulent flows*. Cambridge University Press, Cambridge, United Kingdom., 2000.

L.F. Richardson. *Weather prediction by numerical process*. Cambridge University Press, Cambridge, United Kingdom., 1922.

J. Rosen and L. Quinn-Gothard. *Encyclopedia of Physical Science (Facts on File Science Library) Volume 1*. Infobase Publishing, New York, USA., 2009.

P.J. Rusello, A. Lohrmann, E. Siegel, and T. Maddux. Improvements in acoust doppler velocimetry. In *Proceedings of the 7th International Conference on HydroScience and Engineering, 10 - 13 September*, Philidelphia, USA, 10 - 13 September 2006.

P.M. Sforza, P Sheerin, and M. Smorto. Three-dimensional wakes of simulated wind turbines. *American Institute of Aeronautics and Astronautics Journal*, 19:1101–1107, 1981.

R.K. Shah and D.P. Sekulic. *Fundamentals of Heat Exchanger Design*. John Wiley & sons ltd, 2003.

H. Snodin. Scotlands renewable resource 2001 volume 1: The analysis. Technical Report 2850/GR/02, Scottish Executive, 2001.

G.L. Squires. *Practical Physics*. Cambridge University Press, Cambridge, United Kingdom, 4th edition, 2001.

T. Stallard, R. Collings, T. Feng, and J. Whelan. Interactions between tidal turbine wakes: experimental study of a group of 3-bladed rotors. *Philosophical Transactions of the Royal Society A: Mathematical, Physical and Engineering Sciences*, 871:13, 2013.

G. Sutherland, M. Foreman, and C. Garrett. Tidal current energy assessment for johnstone strait, vancouver island. *Proceedings of the Institution of Mechanical Engineers, Part A: Journal of Power and Energy*, 221 (2):147–157, 2007.

Ross Vennell. Tuning turbines in a tidal channel. *Journal of Fluid Mechanics*, 663:253–267, 2010.

G. Voulgaris and J.H. Trowbridge. Evaluation of the acoustic doppler velocimeter (adv) for turbulence measurements. *Journal of Atmospheric and Ocean Technology*, 15:272–289, 1998.

Jo I. Whelan, J. M. R. Graham, and J. Peiro. A free-surface and blockage correction for tidal turbines. *Journal of Fluid Mechanics*, 624:281–291, 2009.

Appendix A

Engineering drawing of load cell rig

A fully dimensioned engineering drawing of the load cell rig mechanism is presented in this appendix. This purpose built load cell rig was used to measure the forces exerted on actuator fences under flow conditions in the Chilworth flume.

The load cell rig consists of rectangular plates, which are joined together with 4 threaded bars and which are screwed into concentric holes drilled into both plates. The bottom plate additionally consists of a low friction mechanical rolling pivot, which can freely rotate, and is supported by two low density polyethylene supports on either side of the plate. Through this rolling pivot is a hollow through which a support stem can fit through, and this support stem has the actuator fence attached to it at the bottom. When the force of water acts on the actuator fence, the stem moves due to the freely rotating pivot which it is secured into. At the top plate, the stem pushes against a strategically placed load cell, which reads the output voltage of the excited signal caused by the force of the combined actuator fence and support stem pushing against it.

To convert the voltage of the excited signal to the force acting on the actuator fence in the water, two steps are necessary.

- The voltage reading is converted to a force reading using the calibration curve techniques outlined in 3.2.

- Due to the pivot mechanism setup, the force read by the load cell is actually the force exerted on the fence amplified by the ratio of two distances, and it is necessary to multiply the force by this ratio. These distances are:

1. The distance from the pivot point to the position of the load cell on the top plate.

2. The distance from the centre of the actuator fence to the centre of the pivot point.

These distances can be altered, depending on the expected force on the load cell, by adjusting the position of the top plate on the threaded bars, or by altering the position of the actuator fence support stem using a 3mm grub screw in the freely rolling pivot of the rig. Adjustment of these heights was necessary, in particular for the highest blockage ratio fences tested during experiments, due to the fact that the maximum capacity of the load cell is 10 Newtons, and

any forces beyond this were likely to permanently damage the load cell's internal strain gauges.

The first drawing gives a general outline of the entire rig, while the second drawing gives closer detail of the mechanical rolling pivot in the rig. All dimensions are in millimetres with a tolerance of +/- 0.01mm. All parts are constructed from stainless steel, with the exception of the rolling pivot supports on the bottom plate, which are constructed of low density polyethylene.

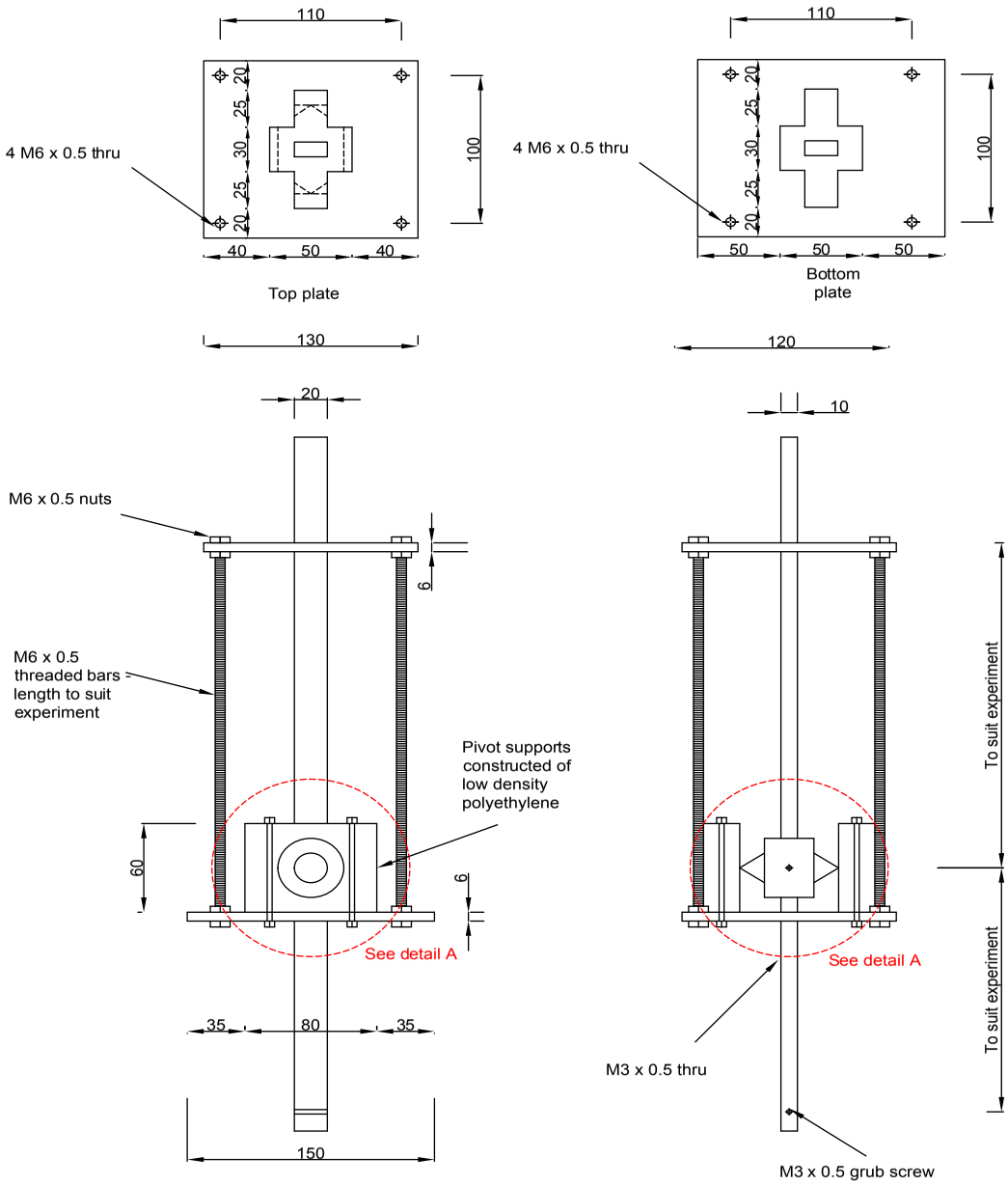

Tim Daly
University of Southampton
23/10/2014
Chilworth load cell rig
All dimensions in mm
Tolerance +/- 0.01mm
All parts constructed of stainless steel unless otherwise specified

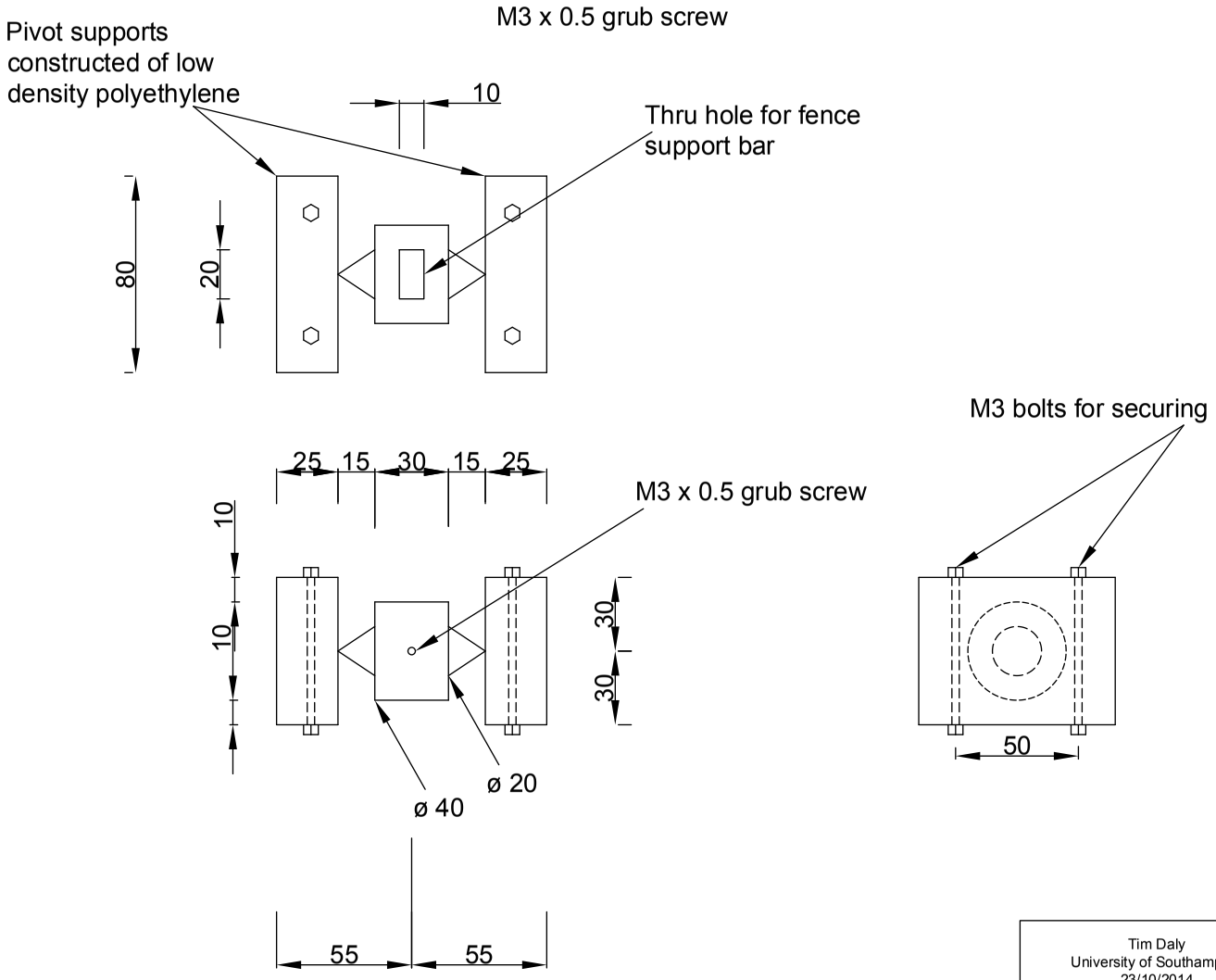

Tim Daly
University of Southampton
23/10/2014
Chilworth load cell rig detail A
All dimensions in mm
Tolerance +/- 0.01mm
All parts constructed of stainless steel unless otherwise specified

Appendix B

Physics of syphons

Syphonic action is a method by which fluid can travel through a pipe which rises above the level of the fluid, despite the forces of gravity. This syphonic action is simply a consequence of the Bernoulli's principle, and is widely used in practical engineering applications, such as for the transfer of water uphill to reservoirs. Three conditions which are necessary for syphonic action to take place are:

- The entire pipe needs to be initially full of fluid so that no air bubbles are present in the pipe transferring water upwards.
- If one end of a pipe is immersed in the fluid, the other end of the pipe at the end of the syphon must be at a level lower than the water level. The necessity for this will be demonstrated by some of the mathematics which follows.
- Syphonic action is only possible when the crest of the syphon (as marked point 2 in figure B.1) is less than 7.5m above the water level. At this point air locks begin to emerge and syphoning is no longer possible (Hamill [2011, p. 166]).

Syphonic action was used in the analysis for measuring possible head losses outlined in section 3.6. Figure B.1 gives a graphical description of the pipe and cylinders used to measure the possible head losses downstream of the actuator fence in the channel. As already stated, one of the conditions for a syphon to begin working is that fluid must fill the entire tube and no air blocks must be present. This required initially a strong negative pressure to be applied to the end of the tube which were later attached to the cylinders, so that the water could be sucked through the entire tube. This was carried out using a small water pump.

The explanation given for syphonic action presented here is similar to an explanation for syphoning given in Hamill [2011, pp.110-111]. Bernoulli's equation can be used to demonstrate how and why a syphon work. A reminder that the Bernoulli equation (assuming no energy losses throughout the system) is given by:

$$\frac{P_1}{\rho g} + z_1 + \frac{U_1^2}{2g} = \frac{P_2}{\rho g} + z_2 + \frac{U_2^2}{2g} = \frac{P_3}{\rho g} + z_3 + \frac{U_3^2}{2g} \tag{B.1}$$

The points marked 1, 2 and 3 in figure B.1 represent the water level, the crest of the pipe travelling over the side of the Chilworth channel and the end of the pipe attached to the

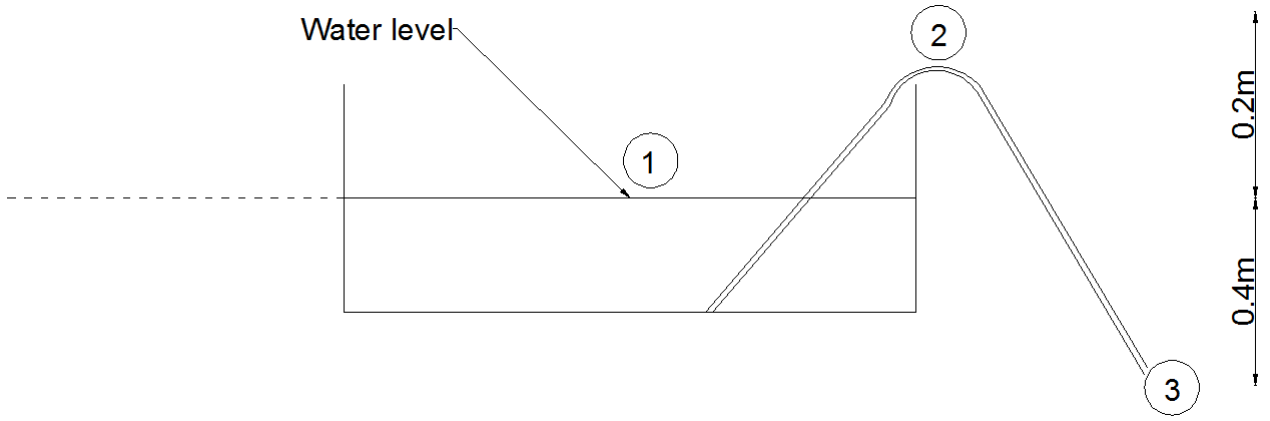

Figure B.1: Graphical description of syphon used to measure reduction in water surface elevations across actuator fences

measurement cylinders. The dotted line indicates the point of the assumed elevation datum, the top of the water level in the channel. In this analysis the following assumptions are made:

- Energy losses in the tube connecting the bed of the flume to the measuring cylinders are negligible.
- Atmospheric pressure is assumed the datum pressure. As a consequence all subsequent pressures are in gauge pressure head.

At point 1 in figure B.1, the pressure head, velocity head and elevation head are given by:

- $P_1 = 0$ (as pressure is atmospheric)
- $V_1 = 0$
- $Z_1 = 0$

The pressure and velocity head at point 2 are unknown, however it is known that:

- $Z_2 = 0.2m$

At point 3 the velocity is unknown, however it is known that:

- $P_3 = 0$
- $Z_3 = -0.4m$

Applying the Bernoulli equation between points 1 and 3 can give the flow velocity of the water as it flows through the pipe:

$$0 + 0 + 0 = 0 - 0.4 + \frac{V_3^2}{2g}$$

After numerical manipulation this gives:

$$V_3 = 2.8m/s$$

As the cross sectional area of the tube is constant, continuity means:

$$V_2 = 2.8m/s$$

The above expressions demonstrate the necessity for the end of the tube attached to the cylinders to be at an elevation below the water level. Were it to be above water level, the above expressions would calculate a negative velocity head. This would simply result in the flow of water in the tube not initiating.

The only unknown left is the pressure head at the crest of the tube reaching over the top of the sidewall of the channel, which can now be determined by applying Bernoulli's equation to points 1 and 2:

$$0 + 0 + 0 = \frac{P_2}{\rho g} + 0.2 + \frac{(2.8)^2}{2g}$$

Numerical manipulation of this expression gives the pressure head at the crest of the syphon as:

$$\frac{P_2}{\rho g} = -0.6m$$

This means that the pressure head at the crest of the syphon is below atmospheric pressure, and there is therefore a partial vacuum. This imbalance in pressure head between the water surface and the crest of the syphon causes the water to flow up from the end of the pipe immersed in the water, while the force of gravity draws it downwards to the end of the tube. It is this other end that is attached to the measurement cylinders displayed in section 3.6. Provided this end of the pipe stays below the water level of the channel, the water will continually syphon and flow through into the cylinders. Water will continually flow until the water level in the cylinders is the exact same as the water level in the channel, and therefore the sum of pressure, velocity and elevation head (0) at both points is the same.

By placing tubes both upstream and downstream of the actuator fence, and examining the water levels in both, it was possible to examine what if any reduction in water surface elevation occurred due to the presence of the actuator fence. Carrying out this analysis in the Chilworth flume showed that even for the largest sized actuator fence, no measurable reduction in water surface elevations were observed. This meant that the constraining of flow observed in results presented in section 5.1 were entirely the result of changes in both the blockage ratio of the actuator fence and the changes in position of the fence with respect to the channel sidewall.

Appendix C

Energy coefficient

Much of the theory used to examine open channels assumes uniform distribution of velocity across a given channel cross section. Exact uniformity is in practice impossible due to flow turbulence and viscous action of fluid, both between fluid streamlines and between fluid and channel boundaries. To account for this non-uniformity, some open channel hydraulics theory includes certain coefficients into their equations. An example of such a coefficient is an energy coefficient, or velocity distribution coefficient, discussed briefly by Hamill [2011, pp113 - 114]. This is given the symbol α and is used in the following expression for specific energy of a flow as a function of depth.

$$E = h + \frac{\alpha Q^2}{2g\left(Bh\right)^2} \tag{C.1}$$

The above expression was used to develop the graph of specific energy vs critical depth for the Chilworth flume, displayed in figure 4.2 in section 3.6. In many flows, the assumption of uniformity can be assumed with negligible error, and so α can be assumed equal to 1. However experimental data was available which allowed the validity of this assumption to be examined.

Hamill [2011, p.114] gave the following expression for energy coefficient. The cross sectional area of a channel is assumed to consist of discrete elemental areas of area dA and velocity u, while the overall area and average flow velocity are A and U respectively. The energy coefficient is given by:

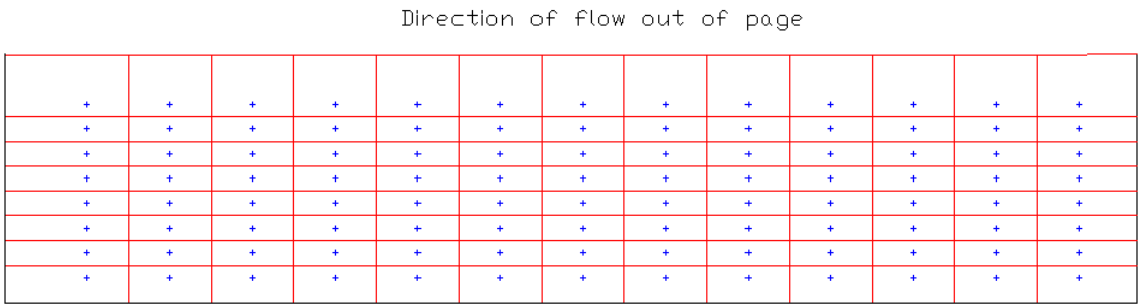

Figure C.1: Flume cross section divided into element areas (red) to estimate energy coefficient using ambient flow measurements (blue)

$$\alpha = \frac{\sum \left(u^3 dA\right)}{U^3 A} \tag{C.2}$$

In section 4, a number of flow velocity measurements were used, along with the splitting of the flume cross sectional area into discrete elemental areas (Figure C.1) to estimate the volumetric flow rate through the channel. These same velocity readings and elemental areas were entered into equation C.2 to determine the energy coefficient for this flow. The resulting value from this expression was 1.015. This demonstrated that the error in assuming uniform flow when determining the specific energy vs depth graph for the Chilworth flume in figure 4.2 were negligible.

Appendix D

Calculations for correction to Chilworth channel dimensions included in Atwater and Lawrence model calculations

In section 6, split tidal channels were examined experimentally, to determine what if any effect specific position and blockage ratio had on the distribution of volumetric flow rate between sub channels. Theory developed by Atwater and Lawrence (2010) could be used to show that this distribution between channels effected the maximum amount of power which could be extracted from these sites. It could also be shown that there was a certain optimum distribution which would allow maximum power extraction. To examine what if any specific position and blockage combination might achieve this optimum distribution, a split tidal channel was set up in th Chilworth hydraulics laboratory, and the Atwater and Lawrence model was applied to its geometry.

The split tidal channel set-up in the Chilworth flume was with the aim of both sub channels having an equal cross sectional area and hydraulic radius. This would mean that the natural flow conditions should have 50% of the flow through both sub channels. The approximate dimensions of the channel set-up, as applied to the Atwater and Lawrence model, were as follows:

- L_u= 8.5m (length of upstream channel before split)
- L_i= L_f= 4m (length of impeded and free sub channels)
- L_d= 8.5m (length of downstream channel after split)
- A_u= $0.411m^2$(cross sectional area of upstream channel)
- The width of the free and impeded sub channels is 0.6775m. This is determined by the width of the entire channel (1.37m) minus the width of the split mechanism (0.015m).
- The wetted perimeter of both the free and impeded sub channel is 1.2775m (the width of each channel plus 0.3m flow depth along either sidewall).

- A_i=A_f= 0.20325m^2(cross sectional area of impeded and free sub channels)
- A_d= 0.411m^2(area of downstream channel after split)
- R_{hu}=R_{hd}= 0.2086m (hydraulic radius of upstream and downstream channels)
- R_{hi}=R_{hf}= 0.1288m (hydraulic radius of impeded and free sub channels)

Inserting these values into the Atwater and Lawrence theory gave values for $\beta = 1$ and $\gamma = 0.793$, and an optimum volumetric flow rate distribution (with tidal turbines operating) of 30% in the impeded channel and 70% in the unoccupied channel.

However this optimum distribution is based on both sub channels having equal areas and hydraulic radii, and hence equal volumetric flow rate under natural conditions. When flow measurements to estimate natural flow distribution in the experimental set-up were taken, this was found not to be the case. It was found that of the overall flow rate of $0.12m^3/s$, 52% was flowing through the channel where an actuator fence was to be place, and 48% through the channel which was to be left free. Therefore, it was decided that to determine the real optimum conditions for the experimental set-up, the areas and hydraulic radii inserted into the analytical model needed to account for this 52:48 distribution.

The steps involved in this correction are as follows:

- Upstream of the split mechanism, a volumetric flow rate of $0.1205m^3/s$ was flowing through a cross sectional of $0.411m^2$(1.37m channel width and 0.3m flow depth). This gave an average velocity across the channel of 0.292m/s.
- It was assumed that this was also the flow velocity in both the impeded and free sub channels.
- Using this assumption, and the recorded flow rates in both channels, it was possible to determine corrected values for cross sectional area for both channels.
- The flow rate through the impeded channel was $0.0627m^3/s$. Using the assumption of 0.292m/s velocity, this gives a corrected value for the impeded channel cross sectional area of $0.2139m^2$. With a flow depth of 0.3m, this gives an adjusted channel width of 0.7056m, an adjusted wetted perimeter of 1.3056m and an adjusted hydraulic radius of 0.1639m.
- Similarly for the free sub channel, there was a volumetric flow rate of $0.0577m^3/s$. When adjusted assuming 0.292m/s velocity, the corrected values were cross sectional area of $0.197m^2$, an adjusted channel width of 0.649m, an adjusted wetted perimeter of 1.249m and an adjusted hydraulic radius of 0.1577m.

Inserting these new adjusted values for cross sectional area and hydraulic radius for both sub channels gave values for $\beta = 0.819$ and $\gamma = 0.729$. Applying all of these new derived values into the analytical model gave a new maximum extraction efficiency of 9.04%, achieved when 32% of the flow is directed through the channel with turbines present, and 68% through the channel with no turbines present.